PNNL-39257

FAST-1.2.2: Integral Assessment

Developed under NQA-1-2017

May 2026

KJ Geelhood, PNNL
DF Wray, PNNL
JJ Whitman, NRC
CE Goodson, PNNL
WG Luscher, PNNL
DV Colameco, PNNL
J Corson, NRC

Prepared for the U.S. Nuclear Regulatory Commission
Office of Nuclear Regulatory Research
Under contract DE-AC05-76RL01830
Interagency Agreement A2307-031-089-048662
Task Order Number: 31310024S0022

DISCLAIMER

This report was prepared as an account of work sponsored by an agency of the United States Government. Neither the United States Government nor any agency thereof, nor Battelle Memorial Institute, nor any of their employees, makes **any warranty, express or implied, or assumes any legal liability or responsibility for the accuracy, completeness, or usefulness of any information, apparatus, product, or process disclosed, or represents that its use would not infringe privately owned rights.** Reference herein to any specific commercial product, process, or service by trade name, trademark, manufacturer, or otherwise does not necessarily constitute or imply its endorsement, recommendation, or favoring by the United States Government or any agency thereof, or Battelle Memorial Institute. The views and opinions of authors expressed herein do not necessarily state or reflect those of the United States Government or any agency thereof.

PACIFIC NORTHWEST NATIONAL LABORATORY
operated by
BATTELLE
for the
UNITED STATES DEPARTMENT OF ENERGY
under Contract DE-AC05-76RL01830

Printed in the United States of America

Available to DOE and DOE contractors from
the Office of Scientific and Technical Information,
P.O. Box 62, Oak Ridge, TN 37831-0062
www.osti.gov
ph: (865) 576-8401
fax: (865) 576-5728
email: reports@osti.gov

Available to the public from the National Technical Information Service
5301 Shawnee Rd., Alexandria, VA 22312
ph: (800) 553-NTIS (6847)
or (703) 605-6000
email: info@ntis.gov
Online ordering: http://www.ntis.gov

PNNL-39257

FAST-1.2.2: Integral Assessment

Developed under NQA-1-2017

May 2026

KJ Geelhood, PNNL
DV Colameco, PNNL
WG Luscher, PNNL
JJ Whitman, NRC
CE Goodson, PNNL
DF Wray, PNNL
J Corson, NRC

Prepared for the U.S. Nuclear Regulatory Commission
Office of Nuclear Regulatory Research
Under Contract DE-AC05-76RL01830
Interagency Agreement A2307-031-089-048662
Task Order Number: 31310024S0022

Pacific Northwest National Laboratory
Richland, Washington 99352

Project Summary and Document Characteristics

Project Name	FAST Fuel Performance Code Development and Assessment
Project No.	83915 Task 31310024S0022
Product Management Office No. / Organization	PM053 / Nuclear Science and Legacy Waste

Approvals

Role	Name	Signature	Date
Code Custodian	David Colameco	David V Colameco Digitally signed by David V Colameco Date: 2026.07.01 00:07:02 -07'00'	
Lead Software Developer	Ken Geelhood	Kenneth J (Ken) Geelhood Digitally signed by Kenneth J (Ken) Geelhood Date: 2026.07.01 11:19:11 -07'00'	
Project Manager	Katie Wagner	Katie A Wagner Digitally signed by Katie A Wagner Date: 2026.07.01 14:52:12 -07'00'	

Revision History

Revision	Date	Comments
0	May 2026	Initial Release

Abstract

This integral assessment quantifies the predictive capabilities of Fuel Analysis under Steady-state and Transients (FAST), a thermal-mechanical nuclear fuel performance code designed to analyze fuel behavior from beginning of life to burnup levels allowed by the U.S. Nuclear Regulatory Commission. FAST code calculations are shown to compare satisfactorily to a pre-selected set of experimental data with both steady-state (including anticipated operating occurrence) operating conditions and design basis accident transient operating conditions.

This document describes the assessment of FAST-1.2.2, the latest version of FAST, released May 2026.

This page intentionally blank.

Foreword

The ability to accurately calculate the performance of light water reactor (LWR) fuel rods under high burnup conditions is a major objective of the reactor safety research program being conducted by the U.S. Nuclear Regulatory Commission (NRC). To achieve this objective, the NRC has sponsored an extensive program of analytical computer code development. One product of this program is NRC's FAST code, which provides the ability to accurately calculate the high burnup response of LWR fuel rods.

The NRC also continues to sponsor both in-pile and out-of-pile experiments to benchmark and assess the analytical code capabilities. 348 assessment cases use data from recent integral irradiation experiments and post-irradiation examination programs which provided valuable information on modern cladding materials and high burnup fuel behavior.

This report documents an integral assessment performed using the latest version of FAST, FAST-1.2.2, to demonstrate the code's ability to accurately calculate the performance of newer fuel designs and operating conditions.

This page intentionally blank.

Executive Summary

This document is Volume 2 of a three volume series that describes the Fuel Analysis under Steady-state and Transients (FAST) code and its assessment. Volume 1 (Geelhood, Colameco, et al. 2026) describes the FAST code along with input instructions. Volume 2 (this document) describes the integral code assessment, done by comparing the code predictions for fuel temperatures, fission gas release (FGR), rod internal void volume, fuel swelling, cladding creep/-growth, cladding corrosion, and hoop strain to data from integral irradiation experiments and post-irradiation examination (PIE) programs. Volume 3 (Geelhood, Luscher, et al. 2026) describes the Material Library used by FAST. The cases used for code assessment were selected based on the following criteria:

- Well-characterized design and operational data were provided.
- The reported results spanned ranges of interest for both design and operating parameters.

Thus, the fuel rod cases were selected to represent both boiling water reactor (BWR) and pressurized water reactor (PWR) fuel types, with pellet-to-cladding gap sizes within, above, and below the normal range for power reactor rods. The fill gas is pure helium in most cases, but cases are included for which helium-xenon fill gas mixtures were used to assess the gap conductance model. The linear heat generation rates at beginning of life (BOL) range up to 60 kW/m (18 kW/ft), and during end of life (EOL) power ramps, they range up to 47 kW/m (14 kW/ft). The rod-average fuel burnups range up to 99 GWd/MTU, but only up to 76 GWd/MTU for power ramp cases. However, the code is only considered validated to rod-average burnup of 62 GWd/MTU. The EOL FGR ranges from less than 1% to greater than 50% of the produced quantity.

The primary code assessment database (used also for benchmarking the thermal and FGR models) consists of 227 well-characterized fuel rods. These include 132 “steady-state” rods, 45 test rods that experienced end of life power ramps, and 50 test rods for transient experiments:

- 13 steady-state rods for BOL temperature predictions
- 33 steady-state rods for temperature predictions as a function of burnup
- 4 steady-state rods for metallic fuel redistribution predictions
- 117 steady-state, power-ramped, or transient rods for FGR predictions
- 29 steady-state rods for EOL void volume predictions
- 32 steady-state rods for cladding waterside oxidation predictions
- 6 steady-state rods for metallic fuel-cladding chemical interaction (FCCI) predictions
- 58 power-ramped or transient rods for hoop strain predictions
- 32 transient rods for reactivity-initiated accident failure predictions

- 18 transient rods for loss-of-coolant accident failure predictions

Predictions were evaluated against a wide set of conditions, fuel types, and cladding types. Uranium dioxide (UO_2), mixed oxide (MOX), urania-gadolinia (UO_2-Gd_2O_3), and metallic fuels are included as well as BWR Zircaloy-2; PWR Zircaloy-4, low tin Zircaloy-4, ZIRLO®,[1], Optimized ZIRLO™, and M5™,[2]; and SFR stainless steel cladding.

The following conclusions about FAST were made as a result of this assessment:

- ***Thermal***: Comparisons were made for BOL UO_2 temperature measurements and UO_2, MOX, and UO_2-Gd_2O_3 temperature measurements as a function of burnup. Overall, FAST gave reasonable predictions of fuel centerline temperature for fuel rods with UO_2, MOX, and UO_2-Gd_2O_3 fuel (standard error of less than 6%).
- ***Fission Gas Release***: Comparisons were made for the UO_2 and MOX FGR measurements for rods with widely varying power levels and burnups. Overall, FAST gave reasonable predictions (about 5.5% FGR absolute) of fission gas release for fuel rods with UO_2 and MOX fuel. For the transient cases, FAST predicted FGR with a 7.6% (FGR absolute) standard error.
- ***Constituent Redistribution***: Comparisons were made for constituent redistribution of U-Zr and U-Pu-Zr metallic fuels. The predictions for the U-Zr cases showed good agreement with the experimental data. The U-Pu-Zr case predictions showed good agreement with the experimental data, but with both under-prediction and over-prediction for the zirconium atom fractions in each phase for two cases.
- ***Internal Void Volume***: Comparisons were made to data from 26 commercial reactor and three test reactor fuel rods. The code predicted void volume with a standard error of 14.8%.
- ***Cladding Corrosion***: Comparisons were made to data from two commercial BWR rods with Zircaloy-2 cladding, four commercial PWR rods with Zircaloy-4 cladding, two commercial PWR rods with low tin Zircaloy-4 cladding, 14 commercial PWR rods with ZIRLO cladding, and 10 commercial PWR rods with M5 cladding. The oxide corrosion predictions were very good and tend to bracket the data.
- ***Fuel-Cladding Chemical Interaction***: Comparisons were made to data from six metallic fuel rods with stainless steel cladding. For the two non-failed rods, FAST bounded FCCI well.
- ***Cladding Hoop Strain***: Comparisons were made to data available up to a burnup of around 76 GWd/MTU and demonstrated that, on average, FAST slightly over-predicts cladding hoop strain by 0.07% strain.
- ***Reactivity-Initiated Accidents***: Comparisons were made to data from 32 refabricated, irradiated rods with burnup levels between 26 and 75 GWd/MTU, representing a large range of rod designs and reactor conditions. The residual hoop strain predictions were reasonable for cases with less than 2.2% strain; for cases with greater than 2.2% measured strain, strain was

1. Optimized ZIRLO and ZIRLO are trademarks or registered trademarks of Westinghouse Electric Company LLC, its affiliates and/or its subsidiaries in the United States and may be registered in other countries throughout the world.
2. M5 is a registered trademark of Framatome or its affiliates in the USA or other countries.

slightly under-predicted. Maximum fuel enthalpies and fission gas releases were predicted well.

- ***Loss-of-Coolant Accidents***: Comparisons were made to data from 18 test cases from re-fabricated rods with burnup levels between 0 and 83 GWd/MTU. In general FAST predicts failure well for these tests, with a 34% (relative) standard deviation for predicted rupture time and prediction of failure in only three cases when none was observed. FAST both over- and under-predicts cladding hoop strain after a LOCA.

This page intentionally blank.

Acronyms and Abbreviations

ADU	ammonium diuranate
AOO	anticipated operating occurrence
ATR	Advanced Test Reactor
AUC	ammonium uranyl carbonate
BNFL	British Nuclear Fuels, Ltd.
BOL	beginning of life
BWR	boiling water reactor
DNB	departure from nucleate boiling
EBR-II	Experimental Breeder Reactor II
EOL	end of life
EPMA	electron probe microanalysis
FCCI	fuel-cladding chemical interaction
FFTF	Fast Flux Test Facility
FGR	fission gas release
FIPD	Metallic Fuels Irradiation & Physics Database
GNF	Global Nuclear Fuel
HBEP	High Burnup Effects Program
HBWR	heavy boiling water reactor
HUHB	Halden Ultra High Burnup
ISFSI	integrated spent fuel storage installation
KKL	Kernkraftwerk Leibstadt
LHGR	linear heat generation rate
LOCA	loss-of-coolant accident
LWR	light water reactor
MIMAS	micronized master blend
NRC	U.S. Nuclear Regulatory Commission
ORNL	Oak Ridge National Laboratory
PBF	Power Burst Facility
PCMI	Pellet/Cladding Mechanical Interaction
PIE	post-irradiation examination
PNNL	Pacific Northwest National Laboratory
PWR	pressurized water reactor
SBR	short binderless route
SCIP	Studsvik Cladding Integrity Program
SFR	sodium-cooled fast reactor
SNF	spent nuclear fuel
SPND	self-powered neutron detector
TCD	thermal conductivity degradation
TD	theoretical density

TREAT	Transient Reactor Test Facility

Contents

Abstract v

Foreword vii

Executive Summary ix

Acronyms and Abbreviations xiii

Contents xv

Figures xxi

Tables xxix

1.0 Introduction 1

2.0 Assessment Data Description 3

2.1 Description of the Steady-State Cases 6

2.2 Description of the Power-Ramp Cases 16

2.3 Description of the Transient Cases 20

3.0 Thermal Behavior Assessment 27

3.1 Temperature Predictions 27

3.1.1 UO_2 Temperature Predictions 27

3.2 Assessment of Temperature Predictions as a Function of Burnup 28

3.2.1 UO_2 Centerline Temperature Predictions as a Function of Burnup . . . 28

3.2.2 MOX Centerline Temperature Predictions as a Function of Burnup . . 42

3.2.3 UO_2-Gd_2O_3 Centerline Temperature Predictions as a Function of Burnup 56

3.3 Constituent Redistribution 65

4.0 Fission Gas Release Assessment 69

4.1 Assessment of Steady-State FGR Predictions 69

4.1.1 UO_2 Steady-State FGR Predictions 69

4.1.2 MOX Steady-State FGR Predictions 72

4.1.3 UO_2-Gd_2O_3 Steady-State FGR Predictions 75
4.2 Assessment of Power-Ramped FGR Predictions 76
4.2.1 UO_2 Power-Ramped FGR Predictions 76
4.2.2 MOX Power-Ramped FGR Predictions 78

5.0 Internal Rod Void Volume Assessment 81
5.1 Fuel Rod Void Volume 81

6.0 Cladding Corrosion Assessment 83
6.1 BWR Cladding Corrosion 83
6.1.1 Zircaloy-2 Corrosion 83
6.2 PWR Cladding Corrosion 84
6.2.1 Zircaloy-4 Corrosion 84
6.2.2 Low Tin Zircaloy-4 Corrosion 86
6.2.3 ZIRLO Corrosion 88
6.2.4 M5 Corrosion 95
6.3 Fuel-Cladding Chemical Interaction 101

7.0 Cladding Hoop Strain During Power Ramps 105
7.1 Assessment Cases 105
7.2 Comparisons vs. Ramp Terminal Level 106
7.3 Comparisons vs. Burnup 107

8.0 Reactivity Initiated Accident Assessment 109
8.1 Cladding Hoop Strain Predictions 109
8.2 Cladding Failure Predictions 111
8.3 Fission Gas Release Predictions 113

9.0 Loss-of-Coolant Accident Assessments 115
9.1 Cladding Ballooning, Failure, and Pressure Predictions 115

9.2 Residual Hoop Strain Predictions 119

9.3 Fission Gas Release Predictions 120

10.0 Conclusions 123

11.0 References 125

Appendix A Description of Assessment Cases A.1

A.1 Steady-State Assessment Cases A.1

A.1.1 Halden IFA-432 Rods A.1

A.1.2 Halden IFA-513 Rods A.1

A.1.3 Halden IFA-633 Rods A.2

A.1.4 Halden IFA-677.1 Rods A.2

A.1.5 Halden IFA-562 Rod A.2

A.1.6 Halden IFA-597.3 Rod A.3

A.1.7 Halden IFA-515.10 Rods A.3

A.1.8 Halden IFA-681 Rods A.4

A.1.9 Halden IFA-558 Rods A.4

A.1.10 Halden IFA-629.1 Rods A.5

A.1.11 Halden IFA-610 Rods A.5

A.1.12 Halden IFA-648.1 Rods A.6

A.1.13 Halden IFA-629.3 Rods A.6

A.1.14 Halden IFA-606 Rod A.6

A.1.15 Halden IFA-636 Rods A.7

A.1.16 BR-3 Rods A.7

A.1.17 Zorita Rod A.8

A.1.18 BNFL BR-3 Rods A.8

A.1.19 DR-3 Rods A.8

A.1.20 NRX Rods A.8

A.1.21 EL-3 Rods A.9
A.1.22 FUMEX 6f and 6s Rods A.9
A.1.23 Halden IFA-429 Rod A.9
A.1.24 Arkansas Nuclear One Unit 2 PWR Rod A.10
A.1.25 Oconee PWR Rod A.10
A.1.26 Halden IFA-651 Rods A.11
A.1.27 Advanced Test Reactor WG-MOX Rods A.11
A.1.28 Gravelines-4 PWR Rods A.11
A.1.29 Beznau-1 M504 Rods A.12
A.1.30 Beznau-1 M308 Rod A.12
A.1.31 Halden IFA-597.4/.5/.6/.7 Rods A.12
A.1.32 FUGEN Rods A.13
A.1.33 Monticello BWR Rod A.13
A.1.34 TVO-1 BWR Rod A.13
A.1.35 Vandellos PWR ZIRLO Rods A.14
A.1.36 Gravelines-5 PWR M5 Rod A.14
A.1.37 GAIN UO_2-Gd_2O_3 Rods A.14
A.1.38 North Anna Sibling Rods A.14
A.2 Power-Ramp Assessment Cases A.15
A.2.1 Ramped HBEP Obrigheim/Petten Rods A.15
A.2.2 Super-Ramp Rods A.15
A.2.3 Inter-Ramp Rods A.16
A.2.4 Ramped Halden/DR-2 Rods A.16
A.2.5 Risø-3 Ramped Rods A.17
A.2.6 B&W Rods Ramped at Studsvik A.17
A.2.7 Regate Rod A.18
A.2.8 Beznau-1 M501 Rods A.18

A.2.9 Studsvik Cladding Integrity Project Ramped Rods A.18

A.3 Transient Assessment Cases A.19

A.3.1 Reactivity Insertion Accident Assessment Cases A.19

A.3.2 Loss-of-Coolant Accident Assessment Cases A.22

This page intentionally blank.

Figures

2-1 Rod-average LHGR vs. rod-average burnup for temperature assessment cases . . . 4

2-2 Rod-average LHGR vs. rod-average burnup for fission gas release assessment cases 5

2-3 Rod-average LHGR vs. rod-average burnup for hoop strain assessment cases 5

3-1 Measured and predicted centerline temperature for the first ramp to power for 13 assessment cases 28

3-2 Measured and predicted centerline temperature for the UO_2 assessment cases throughout life 29

3-3 Predicted minus measured divided by measured centerline temperature for the UO_2 assessment cases as a function of burnup 30

3-4 Measured and predicted centerline temperature for IFA-432 rod 1 UO_2 lower thermocouple (burnup = 45 GWd/MTU, as-fabricated radial gap = 114 µm) 31

3-5 Measured and predicted centerline temperature for IFA-432 rod 3 UO_2 lower thermocouple (burnup = 45 GWd/MTU, as-fabricated radial gap = 38 µm) 32

3-6 Measured and predicted centerline temperature for IFA-513 rod 1 UO_2 upper thermocouple (burnup=10 GWd/MTU, as-fabricated radial gap=108 µm) 33

3-7 Measured and predicted centerline temperature for IFA-513 rod 1 UO_2 lower thermocouple (burnup=10 GWd/MTU, as-fabricated radial gap=108 µm) 33

3-8 Measured and predicted centerline temperature for IFA-513 rod 6 UO_2 upper thermocouple (burnup=10 GWd/MTU, as-fabricated radial gap=108 µm) 34

3-9 Measured and predicted centerline temperature for IFA-513 rod 6 UO_2 lower thermocouple (burnup=10 GWd/MTU, as-fabricated radial gap=108 µm) 35

3-10 Measured and predicted rod-average centerline temperature for IFA-562 rod 18 UO_2 (burnup = 76 GWd/MTU, as-fabricated radial gap = 50 µm) 36

3-11 Measured and predicted centerline temperature for IFA-597 rod 8 (starting burnup = 68 GWd/MTU, ending burnup=71 GWd/MTU, as-fabricated radial gap=105 µm) . . 37

3-12 Measured and predicted centerline temperature for IFA-515.10 rod A1 (UO_2) (burnup = 80 GWd/MTU, as-fabricated radial gap=25 µm) 38

3-13 Measured and predicted centerline temperature for IFA-515.10 rod B1 (UO_2) (burnup = 80 GWd/MTU, as-fabricated radial gap = 25 µm) 38

3-14 Measured and predicted centerline temperature for IFA-681 rod 1 UO_2 (burnup = 33 GWd/MTU, as-fabricated radial gap = 85 µm) 39

3-15 Measured and predicted centerline temperature for IFA-681 rod 5 UO_2 (burnup = 32 GWd/MTU, as-fabricated radial gap = 85 μm) 40

3-16 Measured and predicted centerline temperature for IFA-677.1 rod 2 UO_2 (burnup = 32 GWd/MTU, as-fabricated radial gap = 85 μm) 41

3-17 Measured and predicted centerline temperature for IFA-558 rod 6 UO_2 (burnup = 41 GWd/MTU, as-fabricated radial gap = 95 μm) 42

3-18 Measured and predicted centerline temperature for the MOX assessment cases throughout life 43

3-19 Predicted minus measured divided by measured centerline temperature for the MOX assessment cases as a function of burnup 44

3-20 Measured and predicted centerline temperature for IFA-629.1 rod 1 (MOX) (starting burnup = 27 GWd/MTU, ending burnup=33 GWd/MTU, as-fabricated radial gap = 84 μm) 45

3-21 Measured and predicted centerline temperature for IFA-629.1 rod 2 (starting burnup = 29 GWd/MTU, ending burnup = 40 GWd/MTU, as-fabricated radial gap = 84 μm) 45

3-22 Measured and predicted centerline temperature for IFA-610.2 (MOX) (starting burnup = 55 GWd/MTU, ending burnup = 56 GWd/MTU, as-fabricated radial gap = 84 μm) 46

3-23 Measured and predicted centerline temperature for IFA-610.4 (MOX) (starting burnup = 56 GWd/MTU, ending burnup = 57 GWd/MTU, as-fabricated radial gap = 84 μm) 47

3-24 Measured and predicted centerline temperature for IFA-648.1 rod 1 (MOX) (starting burnup = 55 GWd/MTU, ending burnup = 62 GWd/MTU, as-fabricated radial gap = 84 μm) 48

3-25 Measured and predicted centerline temperature for IFA-648.1 rod 2 (MOX) (starting burnup = 55 GWd/MTU, ending burnup = 62 GWd/MTU, as-fabricated radial gap = 84 μm) 48

3-26 Measured and predicted centerline temperature for IFA-629.3 rod 5 (MOX) (starting burnup = 62 GWd/MTU, ending burnup = 72 GWd/MTU, as-fabricated radial gap = 84 μm) 49

3-27 Measured and predicted centerline temperature for IFA-629.3 rod 6 (MOX) (starting burnup = 62 GWd/MTU, ending burnup = 68 GWd/MTU, as-fabricated radial gap = 84 μm) 50

3-28 Measured and predicted centerline temperature for IFA-606 Phase 2 (MOX) (starting burnup = 49 GWd/MTU, as-fabricated radial gap = 94 μm) 51

3-29 Measured and predicted centerline temperature for IFA-633-1 rod 6 (MOX) (burnup = 32 GWd/MTU, as-fabricated radial gap= 104 μm) 52

3-30 Measured and predicted centerline temperature for IFA-597.4, .5, .6, .7 rod 10 (MOX) (burnup = 36 GWd/MTU as-fabricated radial gap = 95 μm) 53

3-31 Measured and predicted centerline temperature for IFA-597.4, .5, .6, .7 rod 11 (MOX) (burnup = 37 GWd/MTU as-fabricated radial gap = 95 μm) 53

3-32 Measured and predicted centerline temperature for IFA-651.1 rod 1 (MOX) (burnup = 22 GWd/MTU as-fabricated radial gap = 79 μm) 54

3-33 Measured and predicted centerline temperature for IFA-651.1 rod 3 (MOX) (burnup = 22 GWd/MTU as-fabricated radial gap = 79 μm) 55

3-34 Measured and predicted centerline temperature for IFA-651.1 rod 6 (MOX) (burnup = 20 GWd/MTU as-fabricated radial gap = 81 μm) 55

3-35 Measured and predicted centerline temperature for the UO_2-Gd_2O_3 assessment cases throughout Life 56

3-36 Predicted minus measured divided by measured centerline temperature for the UO_2-Gd_2O_3 assessment cases as a function of burnup 57

3-37 Measured and predicted centerline temperature for IFA-515.10 rods A1 (UO_2) and A2 (UO_2-8% Gd_2O_3) (burnup=80 GWd/MTU, as-fabricated radial gap=25 μm) . . . 58

3-38 Measured and predicted centerline temperature for IFA-515.10 rods B1 (UO_2) and B2 (UO_2-8% Gd_2O_3) (burnup=80 GWd/MTU, as-fabricated radial gap=25 μm) . . . 59

3-39 Measured and predicted centerline temperature for IFA-636 rod 2 (UO_2-8% Gd_2O_3) (burnup=25 GWd/MTU, as-fabricated radial gap=77 μm) 60

3-40 Measured and predicted centerline temperature for IFA-636 rod 4 (UO_2-8% Gd_2O_3) (burnup = 25 GWd/MTU, as-fabricated radial gap = 77 μm) 61

3-41 Measured and predicted centerline temperature for IFA-681 rod 1 (UO_2) (burnup = 24 GWd/MTU, as-fabricated radial gap = 85 μm) 62

3-42 Measured and predicted centerline temperature for IFA-681 rod 2 (UO_2-2% Gd_2O_3) (burnup = 23 GWd/MTU, as-fabricated radial gap = 85 μm) 62

3-43 Measured and predicted centerline temperature for IFA-681 rod 3 (UO_2-8% Gd_2O_3) (burnup = 12 GWd/MTU, as-fabricated radial gap=85 μm) 63

3-44 Measured and predicted centerline temperature for IFA-681 rod 4 (UO_2-2% Gd_2O_3) (burnup = 22 GWd/MTU, as-fabricated radial gap = 85 μm) 63

3-45 Measured and predicted centerline temperature for IFA-681 rod 5 (UO_2) (burnup = 23 GWd/MTU, as-fabricated radial gap = 85 μm) 64

3-46 Measured and predicted centerline temperature for IFA-681 rod 6 (UO_2-8% Gd_2O_3) (burnup = 13 GWd/MTU, as-fabricated radial gap = 85 μm) 64

3-47 Measured and predicted zirconium distribution for EBR-II Rod DP-11 (U-10Zr, burnup = 7.7 at.%) . . . 65

3-48 Measured and predicted zirconium distribution for EBR-II Rod DP-81 (U-10Zr, burnup = 3.5 at.%) . . . 66

3-49 Measured and predicted zirconium distribution for EBR-II Rod DP-16 (U-19Pu-10Zr, burnup = 10.0 at.%) . . . 66

3-50 Measured and predicted zirconium distribution for EBR-II Rod T-179 (U-19Pu-10Zr, burnup = 1.9 at.%) . . . 67

4-1 Comparison of FAST predictions to measured FGR data for the UO_2 steady-state assessment cases . . . 70

4-2 Predicted minus measured FGR versus rod-average burnup for the UO_2 steady-state assessment cases . . . 70

4-3 Comparison of FAST predictions to measured FGR data for the MOX steady-state assessment cases . . . 73

4-4 Predicted minus measured FGR versus rod-average burnup for the MOX steady-state assessment cases . . . 73

4-5 Comparison of FAST predictions to measured FGR data for the UO_2 power-ramped assessment cases . . . 76

4-6 Predicted minus measured FGR Versus rod-average burnup for the UO_2 power-ramped assessment cases . . . 77

4-7 Comparison of FAST predictions to measured FGR data for the MOX power-ramped assessment cases . . . 79

4-8 Predicted minus measured FGR Versus rod-average burnup for the MOX power-ramped assessment cases . . . 80

6-1 Measured and predicted corrosion layer thickness as a function of axial position for Oconee 5-cycle PWR Zircaloy-4 Rod 15309, 49.5 GWd/MTU (rod-average) . . . 84

6-2 Measured and predicted corrosion layer thickness as a function of axial position for ANO-2 5-cycle PWR Zircaloy-4 Rod TSQ002, 53 GWd/MTU (rod-average) . . . 85

6-3 Measured and predicted corrosion layer thickness as a function of axial position for North Anna 4-cycle PWR Zircaloy-4 Rod F35P17, 60 GWd/MTU (rod-average) . . . 85

6-4 Measured and predicted corrosion layer thickness as a function of axial position for North Anna 4-cycle PWR Zircaloy-4 Rod F35K13, 59 GWd/MTU (rod-average) . . . 86

6-5 Measured and predicted corrosion layer thickness as a function of axial position for North Anna 3-cycle PWR low tin Zircaloy-4 Rod 3A1B16, 48 GWd/MTU (rod-average) . . . 87

6-6 Measured and predicted corrosion layer thickness as a function of axial position for North Anna 3-cycle PWR low tin Zircaloy-4 Rod 3A1F05, 51 GWd/MTU (rod-average) 87

6-7 Measured and predicted corrosion layer thickness as a function of axial position for Gravelines 5-Cycle PWR ZIRLO Rod A06, 65.9 GWd/MTU (rod-average) 88

6-8 Measured and predicted corrosion layer thickness as a function of axial position for Gravelines 5-Cycle PWR ZIRLO Rod A12, 66.4 GWd/MTU (rod-average) 89

6-9 Measured and predicted corrosion layer thickness as a function of axial position for North Anna 3-Cycle PWR ZIRLO Rod 6U3I07, 54 GWd/MTU (rod-average) 89

6-10 Measured and predicted corrosion layer thickness as a function of axial position for North Anna 3-Cycle PWR ZIRLO Rod 6U3M09, 55 GWd/MTU (rod-average) . . . 90

6-11 Measured and predicted corrosion layer thickness as a function of axial position for North Anna 3-Cycle PWR ZIRLO Rod 6U3K09, 54 GWd/MTU (rod-average) . . . 90

6-12 Measured and predicted corrosion layer thickness as a function of axial position for North Anna 3-Cycle PWR ZIRLO Rod 6U3L08, 55 GWd/MTU (rod-average) 91

6-13 Measured and predicted corrosion layer thickness as a function of axial position for North Anna 3-Cycle PWR ZIRLO Rod 6U3O05, 58 GWd/MTU (rod-average) . . . 91

6-14 Measured and predicted corrosion layer thickness as a function of axial position for North Anna 3-Cycle PWR ZIRLO Rod 6U3M03, 57 GWd/MTU (rod-average) . . . 92

6-15 Measured and predicted corrosion layer thickness as a function of axial position for North Anna 3-Cycle PWR ZIRLO Rod 6U3P16, 50 GWd/MTU (rod-average) . . . 92

6-16 Measured and predicted corrosion layer thickness as a function of axial position for North Anna 3-Cycle PWR ZIRLO Rod 3F9N05, 54 GWd/MTU (rod-average) . . . 93

6-17 Measured and predicted corrosion layer thickness as a function of axial position for North Anna 3-Cycle PWR ZIRLO Rod 3F9D07, 52 GWd/MTU (rod-average) . . . 93

6-18 Measured and predicted corrosion layer thickness as a function of axial position for North Anna 3-Cycle PWR ZIRLO Rod 3F9P02, 49 GWd/MTU (rod-average) 94

6-19 Measured and predicted corrosion layer thickness as a function of axial position for North Anna 3-Cycle PWR ZIRLO Rod 3D8E14, 59 GWd/MTU (rod-average) . . . 94

6-20 Measured and predicted corrosion layer thickness as a function of axial position for North Anna 3-Cycle PWR ZIRLO Rod 3D8B02, 50 GWd/MTU (rod-average) . . . 95

6-21 Measured and predicted corrosion layer thickness as a function of axial position for Gravelines 5-Cycle PWR M5 Rod N05, 68.1 GWd/MTU (rod-average) 96

6-22 Measured and predicted corrosion layer thickness as a function of axial position for North Anna 3-Cycle PWR M5 Rod 30AG09, 54 GWd/MTU (rod-average) 96

6-23 Measured and predicted corrosion layer thickness as a function of axial position for North Anna 3-Cycle PWR M5 Rod 30AK09, 53 GWd/MTU (rod-average) 97

6-24 Measured and predicted corrosion layer thickness as a function of axial position for North Anna 3-Cycle PWR M5 Rod 30AD05, 54 GWd/MTU (rod-average) 97

6-25 Measured and predicted corrosion layer thickness as a function of axial position for North Anna 3-Cycle PWR M5 Rod 30AE14, 54 GWd/MTU (rod-average) 98

6-26 Measured and predicted corrosion layer thickness as a function of axial position for North Anna 3-Cycle PWR M5 Rod 30AP02, 49 GWd/MTU (rod-average) 98

6-27 Measured and predicted corrosion layer thickness as a function of axial position for North Anna 3-Cycle PWR M5 Rod 5K7P02, 51 GWd/MTU (rod-average) 99

6-28 Measured and predicted corrosion layer thickness as a function of axial position for North Anna 3-Cycle PWR M5 Rod 5K7C05, 57 GWd/MTU (rod-average) 99

6-29 Measured and predicted corrosion layer thickness as a function of axial position for North Anna 3-Cycle PWR M5 Rod 5K7K09, 54 GWd/MTU (rod-average) 100

6-30 Measured and predicted corrosion layer thickness as a function of axial position for North Anna 3-Cycle PWR M5 Rod 5K7O14, 53 GWd/MTU (rod-average) 100

6-31 Measured and predicted FCCI penetration depth vs. height for EBR-II fuel rod cases (burnups = ~10 at.%) 101

6-32 Measured and predicted FCCI penetration depth vs. height for FFTF fuel rod 193045 from MFF-3 (burnup = 12.8 at.%) 102

6-33 Measured and predicted FCCI penetration depth vs. height for FFTF fuel rod 195011 from MFF-5 (burnup = 10.4 at.%) 103

7-1 Measured and predicted rod-average permanent hoop strain for first half of the assessment database 105

7-2 Measured and predicted peak node permanent hoop strain for second half of the assessment database 106

7-3 Predicted minus measured permanent hoop strain as a function of ramp terminal power level 107

7-4 Predicted minus measured permanent hoop strain as a function of burnup 108

8-1 FAST-1.2.2 predictions of residual cladding hoop strain for CABRI and NSRR UO_2 and MOX rods 109

8-2 FAST-1.2.2 Predictions of RIA FGR for CABRI and NSRR UO_2 Rods 113

9-1 Relative difference in predicted and measured ([P-M]/M) rupture time, after start of transient, vs. average burnup for the tests where FAST predicted failure correctly; the FRF-2 measured rupture times were provided as a range. 116

9-2 FAST-1.2.2 predicted internal pressure for LOC-11C rods. FAST predicted failure for rods 2 and 3. None of the rods were measured to fail and rod internal pressure history was not available for these rods. 117

9-3 FAST-1.2.2 predicted and measured rod internal pressure for TREAT FRF-2 rods. Solid lines show pressure for two rods. Dashed line shows failure time range for all 7 rods. 117

9-4 FAST-1.2.2 predicted and measured rod internal pressure for IFA-650.5 118

9-5 FAST-1.2.2 predicted and measured rod internal pressure for IFA-650.6 118

9-6 FAST-1.2.2 predicted and measured rod internal pressure for IFA-650.7 119

9-7 Absolute difference in predicted and measured (P-M) hoop strain vs. average burnup; the FRF-2 measured hoop strains were provided as a range. 120

9-8 Absolute difference in predicted and measured (P-M) FGR vs. average burnup . . . 121

This page intentionally blank.

Tables

2-1 Steady-state fuel rod data cases used for FAST integral assessment 7

2-2 Power-ramped fuel rod data cases used for FAST integral assessment 17

2-3 Fuel rod cases used for FAST-1.2.2 transient integral assessment 21

4-1 Steady-state UO_2 FGR assessment cases 71

4-2 Steady-state MOX FGR assessment cases 74

4-3 Steady-State UO_2-Gd_2O_3 FGR Assessment Cases 76

4-4 Power-ramped UO_2 FGR assessment cases 78

4-5 Power-ramped MOX FGR assessment cases 80

5-1 Measured and calculated void volume for high-burnup fuels rods 81

5-1 Measured and calculated void volume for high-burnup fuels rods (continued) 82

6-1 Peak oxide measured and calculated for two high burnup BWR fuel rods 84

8-1 FAST-1.2.2 predictions of residual cladding hoop strain for CABRI and NSRR UO_2 and MOX rods 110

8-2 FAST-1.2.2 failure and enthalpy predictions for RIA assessment cases 111

8-3 FAST-1.2.2 predictions of RIA FGR for CABRI and NSRR UO_2 rods 114

9-1 FAST-1.2.2 predicted and measured peak cladding residual strain following LOCA tests 120

This page intentionally blank.

1.0 Introduction

This report is Volume 2 of a three volume series that describes the Fuel Analysis under Steady-state and Transients (FAST) code and its assessment. Volume 1 (Geelhood, Colameco, et al. 2026) describes the FAST code. This document describes the assessment of the integral performance of FAST.

This report provides the results of the assessment of the integral code predictions to measured data for fuel temperatures, fission gas release (FGR), internal void volume, cladding deformation, oxidation, and hydriding. The benchmark datasets are described in Section 2.0. Appendix A describes each set of benchmark data and gives the code input for each data comparison. The benchmark data are drawn from a wide range of burnup levels and operating conditions that are relevant to commercial operations. Experimental fuel rods with linear heat generation rates (LHGRs) at or near the maxima for commercial fuel operations were selected because the U.S. Nuclear Regulatory Commission (NRC) licenses fuel to the most limiting rod in the core. Not all the data selected are at limiting conditions. Some of the cases involve commercial fuel rods that operated at normal commercial operating conditions, which are significantly less severe than the limiting conditions. Also, it is noted that most of the thermal and FGR benchmark cases are drawn from experimental programs that involved numerous fuel rods, of which only a few were selected as benchmark cases. This was either because the rods in a given group were all irradiated under similar conditions and had similar FGR or because only rods with design parameters and operating conditions similar to current commercial practice were selected.

The integral code assessments include comparisons to fuel temperature data in Chapter 3.0 and FGR data in Section 4.0. Comparisons of code predictions to internal void volume, cladding corrosion and hydriding, and hoop strain data are given in Chapters 5.0, 6.0, and 7.0 respectively. Chapter 8.0 describes the reactivity-initiated accident (RIA) assessment cases and Chapter 9.0 describes the loss-of-coolant accident (LOCA) assessment cases. A summary and conclusions are found in Chapter 10.0.

This page intentionally blank.

2.0 Assessment Data Description

A total of 339 benchmark cases from 227 fuel rods were selected for the FAST integral assessment. These include 132 fuel rods with steady-state irradiations covering a wide range of burnup, 45 fuel rods with steady-state irradiations followed by an end of life (EOL) power ramp, and 50 fuel rods with steady-state irradiations (or no irradiation) followed by transient testing. The code assessment compares the code against a limited set of well-qualified data spanning the range of limiting operational conditions for commercial light water reactors (LWRs) to verify the code adequately predicts the integral data. An additional seven cases compare the code against experimental data from fuel rods irradiated in sodium-cooled fast reactors (SFRs).

The integral data of interest for LWRs were fuel temperatures, FGR, corrosion, void volumes, and cladding deformation. For the SFR cases, code predictions of constituent redistribution and fuel-cladding chemical interaction were assessed. The cases in this relatively limited group were selected using criteria regarding the completeness and the quality of the rod performance data, as follows:

- The cases should all provide pre-irradiation characterization with well-qualified fuel rod powers, and some data should include PIE data of interest (e.g., FGR, cladding dimensional changes, etc.).
- Cases for temperature assessment should provide well-qualified fuel centerline temperature data as a function of time or burnup to verify fuel temperature predictions.
- Cases ranging from low to high fuel burnup, as well as low to high (limiting) LHGR, should be provided to cover the operating ranges for reactor operation for each fuel performance issue of interest (e.g., fuel temperature, FGR, deformation).
- Cases should provide cladding oxidation, hydriding, and deformation under prototypical pressurized water reactor (PWR), boiling water reactor (BWR), and SFR conditions, as appropriate.
- Cases should demonstrate the effects (FGR and cladding deformation) of normal operational transients and overpower transients including anticipated operational occurrences (AOOs) at low and high burnup.
- Transient cases should include both failed and non-failed rods in order to assess the cladding failure predictions in FAST.

The selected cases fulfill the above criteria, and they provide a mix of well-qualified test reactor data and less qualified (where fuel rod power uncertainties are generally greater) commercial power reactor rod data.

Figures 2-1, 2-2, and 2-3 show the rod-average LHGRs as a function of rod-average burnup (from full power histories of all the rods) for the rods in the temperature, FGR, and hoop strain assessment databases, respectively. These figures demonstrate the range of burnup and LHGRs to which the FAST predictions have been qualified for each of these integral code predictions. For the code prediction of cladding corrosion, the predictions are a function of time, power level, and coolant

temperature. FAST has been qualified to predict cladding corrosion of Zircaloy-2 under BWR conditions beyond a rod-average burnup of 62 GWd/MTU, and Zircaloy-4, ZIRLO, and M5 under PWR conditions beyond a rod-average burnup of 70 GWd/MTU for 12 ft cores. The outlet temperature of 14 ft reactor cores may be higher than has been assessed for FAST, and the corrosion predictions at these temperatures have not been assessed.

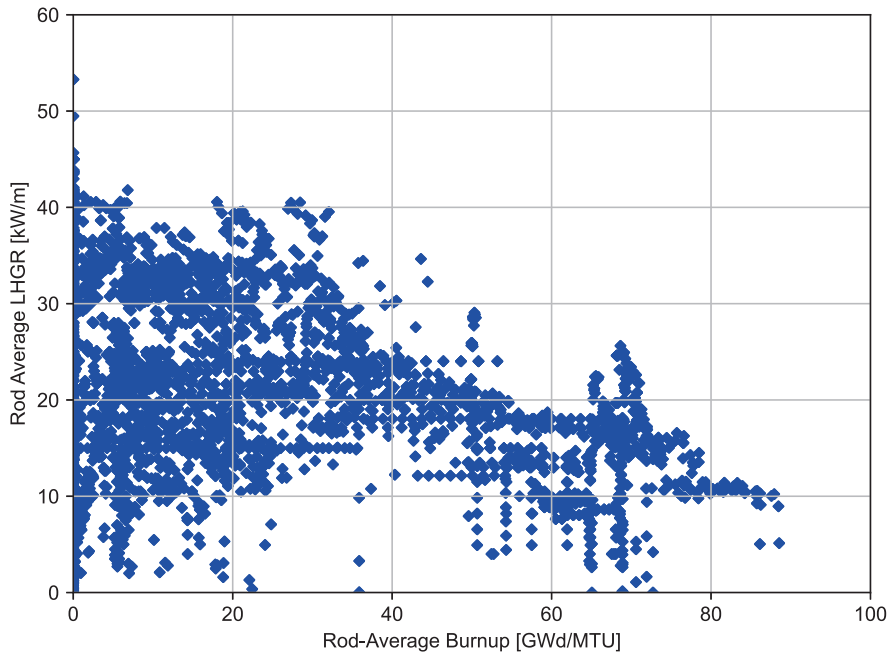

Figure 2-1. Rod-average LHGR vs. rod-average burnup for temperature assessment cases

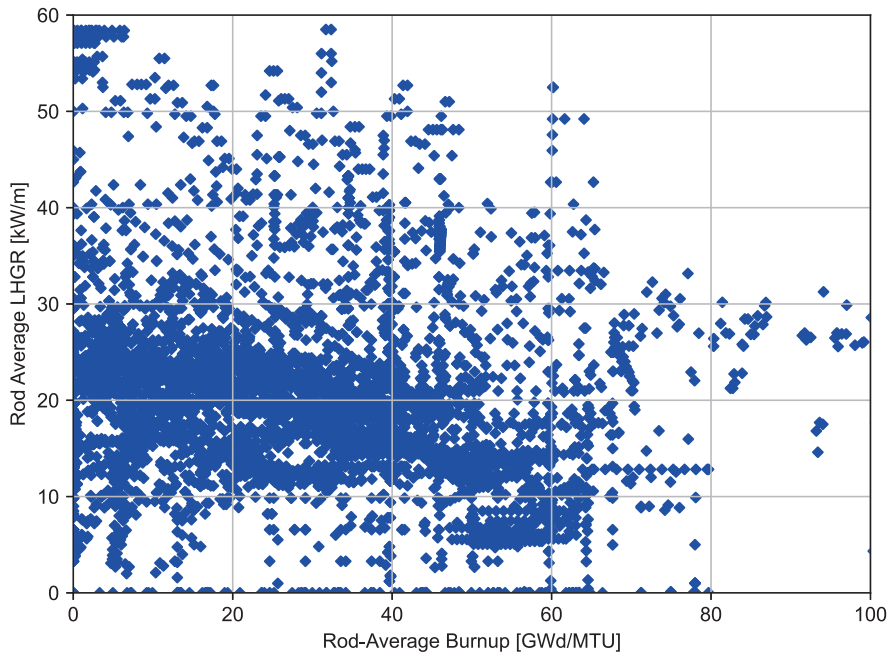

Figure 2-2. Rod-average LHGR vs. rod-average burnup for fission gas release assessment cases

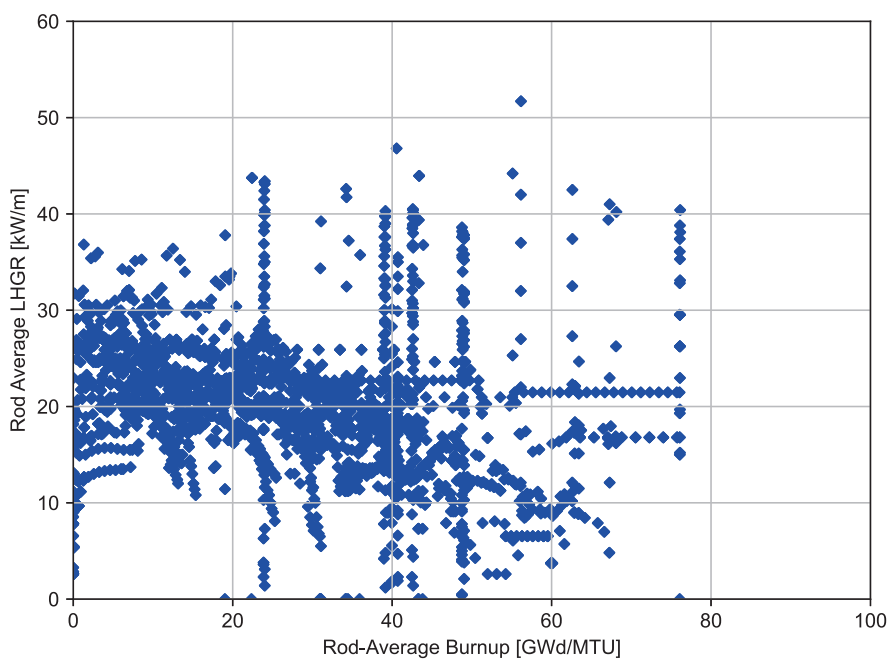

Figure 2-3. Rod-average LHGR vs. rod-average burnup for hoop strain assessment cases

2.1 Description of the Steady-State Cases

The steady-state assessment cases are listed in Table 2-1 and the EOL burnup and fuel type are given for each rod. This table presents the steady-state fuel behavior phenomena that are assessed in this report and indicates which rod are used for that assessment. An “X” in a table cell indicates that the corresponding data comparison was performed for a particular rod to assess code predictions.

Detailed information for each rod is found in Appendix A.1.

Table 2-1. Steady-state fuel rod data cases used for FAST integral assessment

Reactor	Reference	Rod	Fuel Type	Rod-Average Burnup (GWd/MTU)	Thermal vs. Burnup	BOL Thermal	FGR	Void Volume	Corrosion	Redistribution	FCCI
Halden (HBWR)	Lanning 1986	IFA-432 Rod 1	UO_2	45	X	X	–	–	–	–	–
		IFA-432 Rod 2	UO_2	30	–	X	–	–	–	–	–
		IFA-432 Rod 3	UO_2	45	X	X	–	–	–	–	–
Halden (HBWR)	Bradley et al. 1981	IFA-513 Rod 1	UO_2	12	X	X	–	–	–	–	–
		IFA-513 Rod 6	UO_2	12	X	X	–	–	–	–	–
Halden (HBWR)	Rø and Rossiter 2005	IFA-633 Rod 1	UO_2	40	–	X	–	–	–	–	–
		IFA-633 Rod 3	UO_2	40	–	X	–	–	–	–	–
		IFA-633 Rod 5	UO_2	40	–	X	–	–	–	–	–
Halden (HBWR)	Thérache 2005 Jošek 2008b	IFA-677.1 Rod 2	UO_2	32	X	X	–	–	–	–	–
		IFA-677.1 Rod 3	UO_2	6	–	X	–	–	–	–	–
		IFA-677.1 Rod 4	UO_2	6	–	X	–	–	–	–	–
		IFA-677.1 Rod 6	UO_2	7	–	X	–	–	–	–	–
Halden (HBWR)	Wiesenack 1992	IFA-562 Rod 18	UO_2	76	X	–	–	–	–	–	–
Halden (HBWR)	Matsson and Turnbull 1998	IFA-597 Rod 8	UO_2	71	X	–	X	–	–	–	–

Table continued on next page

Table 2-1. Steady-state fuel rod data cases used for FAST integral assessment (continued)

Reactor (Type)	Reference	Rod	Fuel Type	Rod-Average Burnup (GWd/MTU)	Thermal vs. Burnup	BOL Thermal	FGR	Void Volume	Corrosion	Redistribution	FCCI
Halden (HBWR)	Tvergerg and Amaya 2001	IFA-515.10 Rod A1	UO_2	80	X	–	–	–	–	–	–
		IFA-515.10 Rod A2	UO_2-Gd_2O_3	80	X	–	–	–	–	–	–
		IFA-515.10 Rod B1	UO_2	80	X	–	–	–	–	–	–
		IFA-515.10 Rod B2	UO_2-Gd_2O_3	80	X	–	–	–	–	–	–
Halden (HBWR)	Klecha 2006	IFA-681 Rod 1	UO_2	33	X	X	–	–	–	–	–
		IFA-681 Rod 2	UO_2-Gd_2O_3	23	X	–	–	–	–	–	–
		IFA-681 Rod 3	UO_2-Gd_2O_3	12	X	–	–	–	–	–	–
		IFA-681 Rod 4	UO_2-Gd_2O_3	22	X	–	–	–	–	–	–
		IFA-681 Rod 5	UO_2	32	X	–	–	–	–	–	–
		IFA-681 Rod 6	UO_2-Gd_2O_3	13	X	–	–	–	–	–	–
Halden (HBWR)	Turnbull and White 2002	IFA-558 Rod 6	UO_2	41	X	–	–	–	–	–	–
Halden (HBWR)	White 1999	IFA-629-1 Rod 1	MOX	33	X	–	–	–	–	–	–
		IFA-629-1 Rod 2	MOX	29 (FGR) 40 (Thermal)	X	–	X	–	–	–	–

Table continued on next page

Table 2-1. Steady-state fuel rod data cases used for FAST integral assessment (continued)

Reactor (Type)	Reference	Rod	Fuel Type	Rod-Average Burnup (GWd/MTU)	Thermal vs. Burnup	BOL Thermal	FGR	Void Volume	Corrosion	Redistribution	FCCI
Halden (HBWR)	Beguin 1999 Fujii and Claudel 2001	IFA-610.2	MOX	56	X	–	–	–	–	–	–
		IFA-610.4	MOX	57	X	–	–	–	–	–	–
Halden (HBWR)	Claudel and Huet 2001	IFA-648.1 Rod 1	MOX	62	X	–	–	–	–	–	–
		IFA-648.1 Rod 2	MOX	62	X	–	–	–	–	–	–
Halden (HBWR)	Petiprez 2002	IFA-629.3 Rod 5	MOX	72	X	–	X	–	–	–	–
		IFA-629.3 Rod 6	MOX	68	X	–	X	–	–	–	–
Beznau-1 / Halden (HBWR)	Mertens et al. 1998 Mertens and Lippens 2001	IFA-606 Phase 2	MOX	49	X	–	X	–	–	–	–
Halden (HBWR)	Tverberg et al. 2005	IFA-636 Rod 2	UO_2-Gd_2O_3	25	X	–	–	–	–	–	–
		IFA-636 Rod 4	UO_2-Gd_2O_3	25	X	–	–	–	–	–	–
BR-3 (PWR)	Balfour 1982 Balfour et al. 1982	24-I-6	UO_2	60.1	–	–	X	X	–	–	–
		36-I-8	UO_2	61.5	–	–	X	X	–	–	–
		111-I-5	UO_2	48.6	–	–	X	X	–	–	–
		28-I-6	UO_2	53.3	–	–	X	–	–	–	–
		30-I-8	UO_2	57.85	–	–	X	–	–	–	–
DR-3 (PWR)	Bagger et al. 1978	M2-2C	UO_2	43.75	–	–	X	–	–	–	–
		PA29-4	UO_2	47.39	–	–	X	–	—	–	–

Table continued on next page

Table 2-1. Steady-state fuel rod data cases used for FAST integral assessment (continued)

Reactor (Type)	Reference	Rod	Fuel Type	Rod-Average Burnup (GWd/MTU)	Thermal vs. Burnup	BOL Thermal	FGR	Void Volume	Corrosion	Redistribution	FCCI
BR-3 (PWR)	Lanning et al. 1987	HBEP BNFL 373-5-DH	UO_2	42	–	–	X	–	–	–	–
BR-3 (PWR)	Barner et al. 1990	HBEP BNFL 366-DE	UO_2	33.9	–	–	X	–	–	–	–
NRX (HWR)	Meulemeester et al. 1973	EPL-4	UO_2	10.4	–	–	X	–	–	–	–
NRX (HWR)	Notley et al. 1967 Notley and MacEwan 1965	CBR	UO_2	2.7	–	–	X	–	–	–	–
		CBY	UO_2	2.65	–	–	X	–	–	–	–
		LFF	UO_2	3.29	–	–	X	–	–	–	–
		CBP	UO_2	2.61	–	–	X	–	–	–	–
EL-3 (PWR)	Janvier et al. 1967	4110-AE2	UO_2	6.2	–	–	X	–	–	–	–
		4110-BE2	UO_2	6.6	–	–	X	–	–	–	–
Zorita (PWR)	Balfour et al. 1982	332	UO_2	56.8	–	–	X	–	–	–	–
Halden (HBWR)	Chantoin et al. 1997	FUMEX 6f	UO_2	55.45	–	–	X	–	–	–	–
		FUMEX 6s	UO_2	55.45	–	–	X	–	–	–	–
Halden (HBWR)	Turnbull 2001	IFA-429 Rod DH	UO_2	98.9	–	–	X	–	–	–	–
ANO-2 (PWR)	Smith et al. 1994	TSQ002	UO_2	53.2	–	–	X	X	X	–	–
Oconee (PWR)	Newman 1986	15309	UO_2	50	–	–	X	X	X	–	–

Table continued on next page

Table 2-1. Steady-state fuel rod data cases used for FAST integral assessment (continued)

Reactor (Type)	Reference	Rod	Fuel Type	Rod-Average Burnup (GWd/MTU)	Thermal vs. Burnup	BOL Thermal	FGR	Void Volume	Corrosion	Redistribution	FCCI
Halden (HBWR)	Blair and Wright 2004	IFA-651.1 Rod 1	MOX	22.41	X	–	X	–	–	–	–
		IFA-651.1 Rod 3	MOX	21.73	X	–	X	–	–	–	–
		IFA-651.1 Rod 6	MOX	20.27	X	–	X	–	–	–	–
ATR	Morris et al. 2000 Morris et al. 2001 Morris et al. 2005 Hodge et al. 2002 Hodge et al. 2003	Phase II, Capsule 2, Pin 5	MOX	21	–	–	X	–	–	–	–
		Phase III, Capsule 3, Pin 6	MOX	30	–	–	X	–	–	–	–
		Phase III, Capsule 10, Pin 13	MOX	30	–	–	X	–	–	–	–
		Phase IV, Capsule 4, Pin 7	MOX	40	–	–	X	–	–	–	–
		Phase IV, Capsule 5, Pin 8	MOX	50	–	–	X	–	–	–	–
		Phase IV, Capsule 6, Pin 9	MOX	50	–	–	X	–	–	–	–
		Phase IV, Capsule 12, Pin 15	MOX	50	–	–	X	–	–	–	–

Table continued on next page

Table 2-1. Steady-state fuel rod data cases used for FAST integral assessment (continued)

Reactor (Type)	Reference	Rod	Fuel Type	Rod-Average Burnup (GWd/MTU)	Thermal vs. Burnup	BOL Thermal	FGR	Void Volume	Corrosion	Redistribution	FCCI
Gravelines-4 (PWR)	Beguin 1999 Fujii and Claudel 2001 Claudel and Huet 2001 Petiprez 2002	N06	MOX	48	–	–	X	–	–	–	–
		N12	MOX	57	–	–	X	–	–	–	–
		P16	MOX	53	–	–	X	–	–	–	–
Halden (HBWR)	Wright 2004	IFA 633.1r6	MOX	32	X	–	X	–	–	–	–
Beznau-1 (PWR)	Cook et al. 2003 Cook et al. 2004	M504 H8	MOX	37.5	–	–	X	–	–	–	–
		M504 I2	MOX	43	–	–	X	–	–	–	–
		M504 K9	MOX	42.5	–	–	X	–	–	–	–
		M504 M9	MOX	44.2	–	–	X	–	–	–	–
Beznau-1 (PWR)	Boulanger et al. 2004	M308 Segment 2	MOX	57.5	–	–	X	–	–	–	–
Halden (HBWR)	Koike 2004	IFA-597.4/.5/.6/.7 Rod 10	MOX	35.7	X	–	X	–	–	–	–
		IFA-597.4/.5/.6/.7 Rod 11	MOX	36.8	X	–	X	–	–	–	–
Fugen (HBWR)	Ozawa 2004	E09 Inner Rods	MOX	29.6	–	–	X	–	–	–	–
		E09 Inter-mediate Rods	MOX	39.3	–	–	X	–	–	–	–
		E09 Outer Rods	MOX	42	–	–	X	–	–	–	–
Monticello (BWR)	Baumgartner 1984	MTB99 Rod A1	UO_2	45	–	–	–	–	X	–	–
TVO-1 (BWR)	Barner et al. 1990	HBEP Rod H8/36-6	UO_2	51.4	–	–	–	–	X	–	–

Table continued on next page

Table 2-1. Steady-state fuel rod data cases used for FAST integral assessment (continued)

Reactor (Type)	Reference	Rod	Fuel Type	Rod-Average Burnup (GWd/MTU)	Thermal vs. Burnup	BOL Thermal	FGR	Void Volume	Corrosion	Redistribution	FCCI
Vandellos-2 (PWR)	CSN and ENUSA 2002	A06	UO_2	68	–	–	–	–	X	–	–
		A12	UO_2	68	–	–	–	–	X	–	–
Vandellos-2 (PWR)	Segura and Bernaudat 2002	N05	UO_2	70	–	–	–	–	X	–	–
BR-3/BR-2 (PWR)	Hoffmann and Kraus 1984 Manley et al. 1989 Reindl et al. 1991	GAIN Rod 301	UO_2-Gd_2O_3	38.8	–	–	X	–	–	–	–
		GAIN Rod 302	UO_2-Gd_2O_3	37.79	–	–	X	–	–	–	–
		GAIN Rod 701	UO_2-Gd_2O_3	38.9	–	–	X	–	–	–	–
		GAIN Rod 702	UO_2-Gd_2O_3	38.9	–	–	X	–	–	–	–
Ringhals-3 (PWR)	Schrire 2018	R3-2AH3-D12	UO_2	33.3	–	–	–	X	–	–	–
		R3-0AH5-E14	UO_2	57.82	–	–	–	X	–	–	–
		R3-2AH3-D15	UO_2	34.1	–	–	–	X	–	–	–
Ringhals-2 (PWR)	Schrire 2018	R2-AL06-D6	UO_2	27.97	–	–	–	X	–	–	–
		R2-AD23-D5	UO_2	62.95	–	–	–	X	–	–	–
		07R2D5	UO_2	62.0	–	–	–	X	–	–	–

Table continued on next page

Table 2-1. Steady-state fuel rod data cases used for FAST integral assessment (continued)

Reactor (Type)	Reference	Rod	Fuel Type	Rod-Average Burnup (GWd/MTU)	Thermal vs. Burnup	BOL Thermal	FGR	Void Volume	Corrosion	Redistribution	FCCI
North Anna (PWR)	Montgomery et al. 2018 Shimskey et al. 2019 Montgomery and Bevard 2023	30AG09	UO_2	54	–	–	–	–	X	–	–
		30AK09	UO_2	53	–	–	X	X	X	–	–
		30AD05	UO_2	54	–	–	X	X	X	–	–
		30AE14	UO_2	54	–	–	X	X	X	–	–
		30AP02	UO_2	49	–	–	X	X	X	–	–
		5K7P02	UO_2	51	–	–	X	X	X	–	–
		5K7C05	UO_2	57	–	–	X	X	X	–	–
		5K7K09	UO_2	54	–	–	X	X	X	–	–
		5K7O14	UO_2	53	–	–	–	–	X	–	–
		6U3I07	UO_2	54	–	–	–	–	X	–	–
		6U3M09	UO_2	55	–	–	–	–	X	–	–
		6U3K09	UO_2	55	–	–	X	X	X	–	–
		6U3L08	UO_2	55	–	–	X	X	X	–	–
		6U3O05	UO_2	58	–	–	X	X	X	–	–
		6U3M03	UO_2	57	–	–	X	X	X	–	–
		6U3P16	UO_2	50	–	–	X	X	X	–	–
		3F9N05	UO_2	54	–	–	X	X	X	–	–
		3F9D07	UO_2	52	–	–	–	–	X	–	–
		3F9P02	UO_2	49	–	–	X	X	X	–	–
		3D8E14	UO_2	59	–	–	X	X	X	–	–
		3D8B02	UO_2	50	–	–	–	–	X	–	–
		3A1B16	UO_2	48	–	–	–	–	X	–	–
		3A1F05	UO_2	51	–	–	X	X	X	–	–
		F35P17	UO_2	60	–	–	X	X	X	–	–
		F35K13	UO_2	59	–	–	X	X	X	–	–

Table continued on next page

Table 2-1. Steady-state fuel rod data cases used for FAST integral assessment (continued)

Reactor (Type)	Reference	Rod	Fuel Type	Rod-Average Burnup (GWd/MTU)	Thermal vs. Burnup	BOL Thermal	FGR	Void Volume	Corrosion	Redistribution	FCCI
EBR-II (SFR)	Galloway et al. 2015 Hirschhorn et al. 2021 Carmack 2012 Matthews et al. 2017 Yacout et al. 2021	DP-11	U-10Zr	7.7 at.%	–	–	–	–	–	X	X
		DP-81	U-10Zr	3.6 at.%	–	–	–	–	–	X	–
		DP-16	U-19Pu-10Zr	10.0 at.%	–	–	–	–	–	X	–
		T-179	U-19Pu-10Zr	1.9 at.%	–	–	–	–	–	X	–
		DP-04	U-10Zr	~10 at.%	–	–	–	–	–	–	X
		DP-70	U-10Zr	~10 at.%	–	–	–	–	–	–	X
		DP-75	U-10Zr	~10 at.%	–	–	–	–	–	–	X
FFTF (SFR)	Carmack 2012 Matthews et al. 2017 Yacout et al. 2021	193045	U-10Zr	12.8 at.%	–	–	–	–	–	–	X
		195011	U-10Zr	10.4 at.%	–	–	–	–	–	–	X

Table continued on next page

2.2 Description of the Power-Ramp Cases

The power-ramp assessment cases are listed in Table 2-2, and the EOL burnup, fuel type, ramp terminal power level, and hold time are given for each rod. This table presents the power-ramp fuel behavior phenomena that are assessed in this report and indicates which rods are used for that assessment. An “X” in a table cell indicates that the corresponding data comparison was performed for a particular rod to assess code predictions.

Detailed information for each rod is found in Appendix A.2.

Table 2-2. Power-ramped fuel rod data cases used for FAST integral assessment

Base Irradiation/Ramp Testing	Reference	Rod	Fuel Type	Rod-Average Burnup (GWd/MTU)	Ramp Terminal Level (kW/m)	Ramp Hold Time	FGR	Hoop Strain
Obrigheim/Petten	Barner et al. 1990	HBEP D200	UO_2	25	45.3	2.4 days	X	–
		HBEP D226	UO_2	44	45.0	2.6 days	X	–
Obrigheim/Studsvik R-2	Djurle 1985	PK1/1	UO_2	35.4	37.2	12 hr	–	X
		PK1/3	UO_2	35.2	42.6	12 hr	–	X
		PK2/1	UO_2	45.2	36.8	12 hr	–	X
		PK2/3	UO_2	44.6	44.0	12 hr	–	X
		PK2/S	UO_2	43.4	44.0	12 hr	–	X
		PK4/1	UO_2	33.7	34.3	12 hr	–	X
		PK4/2	UO_2	33.8	39.2	12 hr	–	X
		PK6/1	UO_2	36.7	43.7	1 hr	–	X
		PK6/2	UO_2	36.8	35.7	12 hr	X	X
		PK6/3	UO_2	36.5	43.3	12 hr	X	–
		PK6/S	UO_2	35.9	41.0	12 hr	X	–
Studsvik	Mogard et al. 1979 Lysell and Birath 1979	Inter-Ramp Rod 16	UO_2	21	43.8	24 hr	X	X
		Inter-Ramp Rod 18	UO_2	18	37.7	24 hr	X	X
Halden/DR-2	Knudsen et al. 1983	Risø F14-6	UO_2	27	28.7	3 days	X	–
		Risø F7-3	UO_2	35	30.2	17 hr	X	–
		Risø F9-3	UO_2	33	29.7	30 hr	X	–

Table continued on next page

Table 2-2. Power-ramped fuel rod data cases used for FAST integral assessment (continued)

Base Irradiation/Ramp Testing	Reference	Rod	Fuel Type	Rod-Average Burnup (GWd/MTU)	Ramp Terminal Level (kW/m)	Ramp Hold Time	FGR	Hoop Strain
Quad Cities 1 & Millstone 1 / DR-3	Chantoin et al. 1997	Risø GE-2	UO_2	41.9	41.9	38 hr	X	X
		Risø GE-4	UO_2	24.0	24.0	34 hr	X	X
		Risø GE-6	UO_2	42.3	38.1	5 days	X	X
		Risø GE-7	UO_2	41	35.5	4 hr	X	X
ANO-1/Studsvik R-2	Wesley et al. 1994	B&W Rod 1	UO_2	62.3	22.1	12 hr	X	X
		B&W Rod 3	UO_2	62.1	24.7	12 hr	X	X
Biblis A/DR-3	Chantoin et al. 1997	Risø AN-1	UO_2	41.3	40.3	3 days	X	X
		Risø AN-8	UO_2	40.3	30.1	12 hr	X	X
Gravelines-5/SILOE	Struzik 2004	Regate	UO_2	50.2	38.5	1.5 hr	X	–
Beznau-1/Petten	White et al. 2001 Cook et al. 2000 Cook et al. 2003 Cook et al. 2004	M501 HR-1	MOX	37	38.1	12 hr	X	
		M501 HR-2	MOX	37	35.7	12 hr	X	–
		M501 HR-3	MOX	37	46.2	12 hr	X	–
		M501 HR-4	MOX	36	47.0	12 hr	X	–
		M501 MR-1	MOX	34	38.1	12 hr	X	–
		M501 MR-2	MOX	34	41.9	12 hr	X	–
		M501 MR-3	MOX	34	40.5	12 hr	X	–
		M501 MR-4	MOX	33	41.7	20 min	X	–

Table continued on next page

Table 2-2. Power-ramped fuel rod data cases used for FAST integral assessment (continued)

Base Irradiation/Ramp Testing	Reference	Rod	Fuel Type	Rod-Average Burnup (GWd/MTU)	Ramp Terminal Level (kW/m)	Ramp Hold Time	FGR	Hoop Strain
Leibstadt/Studsvik	Kallstrom 2005	KKL-1	UO_2	63	42.5	40 min	X	–
		KKL-2	UO_2	67	41	30 s	–	X
		KKL-3	UO_2	56	52	12 hr	–	X
		KKL-4	UO_2	40	45	5 s	–	X
Ringhals-4/Studsvik	Kallstrom 2005	M5-H1	UO_2	67	40	5 s	–	X
		M5-H2	UO_2	68	40	12 hr	–	X
Oskarshamn-2/Studsvik	Kallstrom 2005	O2	UO_2	55	40	30 s	–	X
Vandellos/Studsvik	Kallstrom 2005	Z-2	UO_2	76	40	6 hr	–	X
North Anna/Studsvik	Kallstrom 2005	Z-3	UO_2	76	40	<1 s*	–	X
		Z-4	UO_2	76	38	6 hr	–	X

* Rod failed during ramp to power

2.3 Description of the Transient Cases

A listing of the selected integral assessment cases is provided in Table 2-3. More information is provided in Appendix A.3.

During the assessment, errors in the FAST coding were identified and corrected. However, FAST was not “tuned” to provide agreement with the assessment cases. For cases where cladding temperature data were available, the FAST runs were made so that the calculated cladding temperatures matched the data; this was done to eliminate the effect of the thermal-hydraulic models in evaluating the performance of the fuel and cladding behavior models. Although FAST-1.2.2 does contain a robust suite of thermal-hydraulic correlations, FAST is not intended to be used primarily for predicting thermal-hydraulic performance because other codes have been developed for that purpose. The primary purpose of FAST is to predict the thermal response of the fuel and its impact on the mechanical response of the cladding. The approach to assigning cladding temperatures for each case is provided in Appendix A.3.

Because FAST-1.2.2 can predict fuel rod behavior under steady-state and transient conditions, the code is used both to simulate the steady-state irradiation prior to the transient as well as any fuel rod refabrication that may have occurred and the transient itself. Correctly modeling the steady-state irradiation defines burnup-dependent parameters such as radial dimensions, gas composition and pressure, and radial power and burnup profiles.

Table 2-3. Fuel rod cases used for FAST-1.2.2 transient integral assessment

Base Irradiation	Transient Reactor	Rod	Reference	Fuel Type	Rod Type	Rod- or Rodlet-Average Burnup (GWd/MTU)	Other Comments
Reactivity Insertion Accidents							
Gravelines-5	CABRI	NA1	Papin et al. 2003	UO_2	PWR 17×17	64	113.7 cal/g, 9.5 ms, failed
	CABRI	NA3		UO_2	PWR 17×17	53.8	123.5 cal/g, 9.5 ms, ε_{hoop} =2.2 %
	CABRI	NA4		UO_2	PWR 17×17	62	85 cal/g, 76.4 ms, ε_{hoop} =0.4 %
	CABRI	NA5		UO_2	PWR 17×17	64	108 cal/g, 8.8 ms, ε_{hoop} =1.1 %
	CABRI	NA8		UO_2	PWR 17×17	60	98 cal/g, 75 ms, failed
BR-3	CABRI	NA2	Papin et al. 2003	UO_2	BR-3	66	199 cal/g, 9.6 ms, ε_{hoop} =3.5 %
St. Laurent B2	CABRI	NA6	Papin et al. 2003	MOX	PWR 17×17	47	133 cal/g, 32 ms, ε_{hoop} =2.6 %
Gravelines-4	CABRI	NA7	Papin et al. 2003	MOX	PWR 17×17	55	138 cal/g, 40 ms, failed
Gravelines-3 and -2	CABRI	NA10	Papin et al. 2003	UO_2	PWR 17×17	63	98 cal/g, 31 ms, failed
Vandellos-2	CABRI	CIP0-1	Georgenthum 2009 Jeury et al. 2003 Jeury et al. 2004	UO_2	PWR 17×17	74.8	98 cal/g, 32 ms, ε_{hoop} =0.5 %
Fukushima-Daiichi-3	NSRR	FK-1	Nakamura et al. 2000	UO_2	BWR 10×10	45.3	125 cal/g, 4.5 ms, ε_{hoop} =0.9 %

Table continued on next page

Table 2-3. Fuel rod cases used for FAST-1.2.2 transient integral assessment (continued)

Base Irradiation	Transient Reactor	Rod	Reference	Fuel Type	Rod Type	Rod- or Rodlet-Average Burnup (GWd/MTU)	Other Comments
Genkai-1	NSRR	GK-1	Fuketa et al. 1997	UO_2	PWR 14×14	42.1	121 cal/g, 4.4 ms, ε_{hoop} =2.5 %
Ohi-1	NSRR	HBO-1	Fuketa et al. 1997	UO_2	PWR 17×17	50.4	93 cal/g, 4.4 ms, failed
	NSRR	HBO-5		UO_2	PWR 17×17	44	100 cal/g, 4.4 ms, failed
	NSRR	HBO-6		UO_2	PWR 17×17	49	100 cal/g, 4.4 ms, ε_{hoop} =1.2 %
Mihama-2	NSRR	MH-3	Fuketa et al. 1997	UO_2	PWR 14×14	38.9	87 cal/g, 4.5 ms, ε_{hoop} =1.6 %
Ohi-2	NSRR	OI-2	Fuketa et al. 1997	UO_2	PWR 17×17	39.2	136 cal/g, 4.4 ms, ε_{hoop} =4.8 %
Tsuruga-1	NSRR	TS-5	Nakamura et al. 1994	UO_2	BWR 7×7	26.6	104 cal/g, 4.6 ms, ε_{hoop} =0 %
Vandellos-2	NSRR	VA-1	Georgenthum 2009 Sugiyama 2009	UO_2	PWR 17×17	71	142 cal/g, 4.4 ms, failed
	NSRR	VA-3		UO_2	PWR 17×17	72	114 cal/g, 4.4 ms, failed

Table continued on next page

Table 2-3. Fuel rod cases used for FAST-1.2.2 transient integral assessment (continued)

Base Irradiation	Transient Reactor	Rod	Reference	Fuel Type	Rod Type	Rod- or Rodlet-Average Burnup (GWd/MTU)	Other Comments
Novovoronezh	BIGR	RT-1	Yegorova et al. 2005a Yegorova et al. 2005b	UO_2	VVER-1000	48.3	142 cal/g, 3 ms
	BIGR	RT-2		UO_2	VVER-1000	48.0	115 cal/g, 3 ms
	BIGR	RT-3		UO_2	VVER-1000	47.5	138 cal/g, 3 ms
	BIGR	RT-5		UO_2	VVER-1000	48.6	146 cal/g, 3 ms
	BIGR	RT-6		UO_2	VVER-1000	47.8	153 cal/g, 3 ms
	BIGR	RT-10		UO_2	VVER-1000	46.9	164 cal/g, 3 ms
	BIGR	RT-11		UO_2	VVER-1000	47.2	188 cal/g, 3 ms, failed
	BIGR	RT-12		UO_2	VVER-1000	47.3	155 cal/g, 3 ms, failed
Kola	BIGR	RT-4	Yegorova et al. 2005a Yegorova et al. 2005b	UO_2	VVER-440	60.1	125 cal/g, 3 ms
	BIGR	RT-7		UO_2	VVER-440	60.5	134 cal/g, 3 ms
	BIGR	RT-8		UO_2	VVER-440	60.0	164 cal/g, 3 ms, failed
	BIGR	RT-9		UO_2	VVER-440	59.8	165 cal/g, 3 ms, failed
Loss-of-Coolant Accidents							
None	PBF	LOC-11C R1 and R4	Buckland et al. 1978 Larson et al. 1979 Larson et al. 1978	UO_2	PWR 15×15	0	Scram plus LOCA
	PBF	LOC-11C R2		UO_2	PWR 15×15	0	Scram plus LOCA

Table continued on next page

Table 2-3. Fuel rod cases used for FAST-1.2.2 transient integral assessment (continued)

Base Irradiation	Transient Reactor	Rod	Reference	Fuel Type	Rod Type	Rod- or Rodlet-Average Burnup (GWd/MTU)	Other Comments
	PBF	LOC-11C R3		UO_2	PWR 15×15	0	Scram plus LOCA
None	TREAT	FRF-2	Lorenz and Parker 1972	UO_2	BWR 7×7	0	Power ramp, adiabatic heatup
Commercial PWR	Halden	IFA-650.5	Kekkonen 2007a	UO_2	PWR 15×15	83	LOCA
Loviisa	Halden	IFA-650.6	Kekkonen 2007b	UO_2	VVER-1000	56	LOCA
Commercial BWR	Halden	IFA-650.7	Jošek 2008b	UO_2	BWR 10×10	44	LOCA
Vandellos-2	Studsvik	SCIP III 09-VUL2	Mileshina and Magnusson 2019 Zwicky and Magnusson 2019	UO_2	PWR 17×17	74	LOCA
Olkiluoto-1	Studsvik	SCIP III 09-OL1L04	Magnusson et al. 2019 Tejland and Sheng 2019b	UO_2	BWR 10×10	60	Overheating
Ringhals-1	Studsvik	SCIP III 12-R1E10	Tejland and Sheng 2019c Tejland and Sheng 2019a	UO_2	BWR 10×10	56	Overheating
Liebstadt	Halden	IFA-650.14	Tradotti 2014 Wiesenack 2015 Oberländer and Jenssen 2014	UO_2	BWR	71	Balloon without Burst
Loviisa-1	Studsvik	SCIP IV 18-L1M7	Magnusson and Tejland 2023	UO_2 (annular)	VVER	61	LOCA
Oskarshamn-3	Studsvik	SCIP IV 10-O3C1	Andersson and Tejland 2022	UO_2 (ADOPT)	BWR	62	LOCA

Table continued on next page

Table 2-3. Fuel rod cases used for FAST-1.2.2 transient integral assessment (continued)

Base Irradiation	Transient Reactor	Rod	Reference	Fuel Type	Rod Type	Rod- or Rodlet-Average Burnup (GWd/MTU)	Other Comments
Ringhals-2	Studsvik	SCIP IV 07-R2RUP2	Tejland et al. 2022	UO_2	PWR	56	LOCA
	Studsvik	SCIP IV 10-R2L15	Zwicky and Tejland 2022	UO_2	PWR	53	LOCA
Vandellos-2	Studsvik	SCIP IV 09-VUD1	Zwicky 2024a	UO_2	PWR	64	LOCA
	Studsvik	SCIP IV 09-VUL1	Zwicky 2024b	UO_2	PWR	72	LOCA
	Studsvik	SCIP IV 09-VUR1-LOCA3	Jädernaäs 2023	UO_2	PWR	64	LOCA (small plenum)

This page intentionally blank.

3.0 Thermal Behavior Assessment

Thermal predictions are important for calculating initial fuel stored energy, which is used as input to loss-of-coolant accident (LOCA) analyses. The fuel temperatures are also used to calculate FGRs and EOL rod pressures and to verify no fuel has melted. In general, PWR LOCA and fuel melt analyses are calculated with FAST to be more limiting at burnups between 25 and 35 GWd/MTU, while the same analyses for BWRs are generally more limiting at burnups between 15 and 25 GWd/MTU.

Comparisons of predicted and measured fuel centerline temperatures from instrumented Halden reactor test assemblies have been used to evaluate the code's ability to predict BOL temperatures and through-life temperature histories (i.e., rod power vs. burnup). The BOL and through-life temperature comparisons are separated because they have different biases and uncertainties (based on standard deviation) in the code thermal predictions. The through-life temperature history comparisons will be used to bound the uncertainties on PWR and BWR LOCA initialization and fuel melting analyses. The BOL temperature database includes not only rods with helium-filled gaps, but also rods with xenon- and xenon-helium-filled gaps and rods with pellet/cladding gap sizes both larger and smaller than typically used in commercial fuel designs. These variations in gap size and fill gas indicate that the code can properly account for the thermal resistance across the fuel cladding gap as a function of gap size and gas composition and is not just tuned to provide good results for typical LWR commercial fuel designs.

The comparisons of measured and predicted through-life fuel center temperature histories were done with two goals in mind. The first was to determine if the code properly accounts for the fuel thermal conductivity degradation (TCD) with burnup. The second goal was to determine if the code properly predicts the effect of thermal feedback on fuel temperature caused by gas release and consequent contamination of the initial helium fill gas with lower conductivity fission gas. It should be noted that in many cases the cycle outages at Halden are not modeled in FAST; the corresponding drop in temperature seen in the data is not reflected in the FAST predictions. The purpose of these comparisons is to show the temperature predictions relative to data when the reactor is at power.

The BOL and through-life code-to-data comparisons are discussed separately in the following sections.

3.1 Temperature Predictions

The BOL fuel centerline temperature predictions are assessed against centerline temperature measurements taken during the first ramp to power. This power ramp occurs during the first 1 to 2 days of operation. Because of this, the initial fuel rod dimensions apply and there is no time for phenomena such as FGR, fuel densification and swelling, cladding creep, or cladding corrosion.

3.1.1 UO_2 Temperature Predictions

FAST was assessed against BOL temperature measurements taken during the first ramp to power. Thirteen rods are used to assess the performance of FAST at BOL: IFA-432 rod 1, IFA-432 rod 2, IFA-432 rod 3, IFA-513 rod 1, IFA-513 rod 6, IFA-681 rod 1, IFA-633 rod 1, IFA-633 rod 3, IFA-633 rod 5, IFA-677.1 rod 2, IFA-677.1 rod 3, IFA-677.1 rod 4, and IFA-677.1 rod 6. Figure 3-1 shows

the predicted vs. measured temperature for the BOL ramp up to power for the 13 assessment cases.

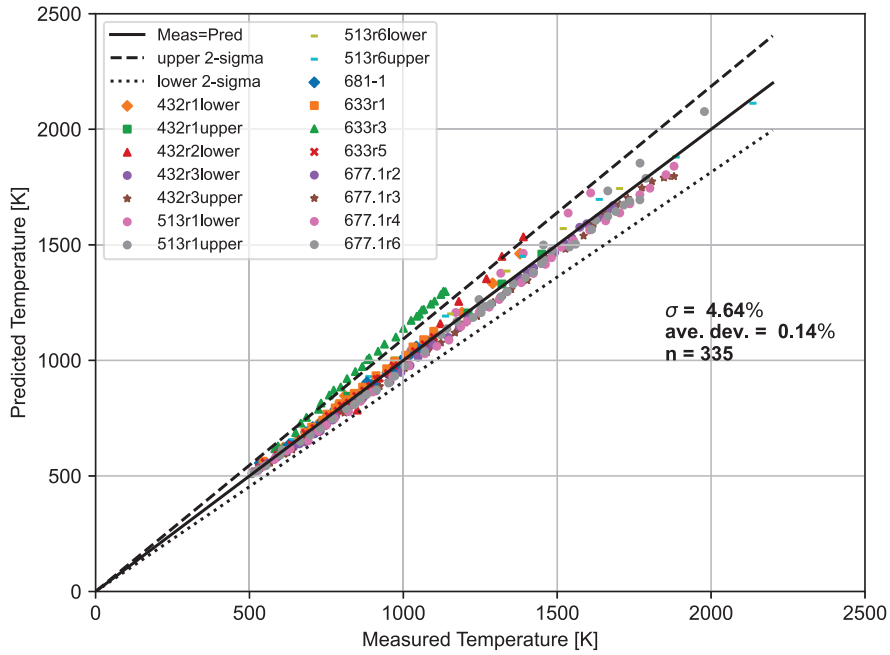

Figure 3-1. Measured and predicted centerline temperature for the first ramp to power for 13 assessment cases

This figure shows that FAST predicts these centerline temperatures within a standard error of 4.6% of the measured centerline temperature and no bias (and an average deviation $\frac{\sum(P-M)/M}{n}$ of +0.14%). A standard error of 4.6% is reasonable given the uncertainty in the thermocouple data and the calculated rod power. The BOL fuel temperature assessment is an improvement over the FRAPCON predictions due to the incorporation of a new fuel relocation model in FAST.

3.2 Assessment of Temperature Predictions as a Function of Burnup

3.2.1 UO_2 Centerline Temperature Predictions as a Function of Burnup

The assessment of FAST UO_2 temperature predictions was performed using the same cases that were used for the BOL assessment, with the following differences.

1. IFA-432 rod 2 has been removed as an assessment of FAST as a function of burnup, as the test is not prototypical of current fuel designs due to its large gap, and a small over-prediction in FGR can result in a large temperature over-prediction.

2. IFA-633 rods 1, 3, and 5 and IFA-677.1 rods 3, 4, and 6 originally only had BOL temperature reported and only recently had measured temperature as a function of burnup reported. Therefore, these rods are not included in this assessment.

3. IFA-562 rod 18, IFA-597 rod 8, IFA-515.10 rods A1 and B1, IFA-681 rod 5, and IFA-558 rod 6 have been added in addition to the BOL assessment cases.

The following figures show measured and predicted fuel centerline temperatures from rods with centerline temperature measurements. Individual rod predictions may demonstrate a systematic error (bias) that may be due to thermocouple decalibration or a systematic error in the power history or axial power shape (power at thermocouple location) provided due to decalibration in or with the neutron detectors. However, when all the comparisons are examined, it is found that there is no overall systematic error (bias) in the prediction of UO_2 fuel temperature throughout life, as can be seen in Figure 3-2. For all the cases, a standard error of 6.0% on the centerline temperature was calculated.

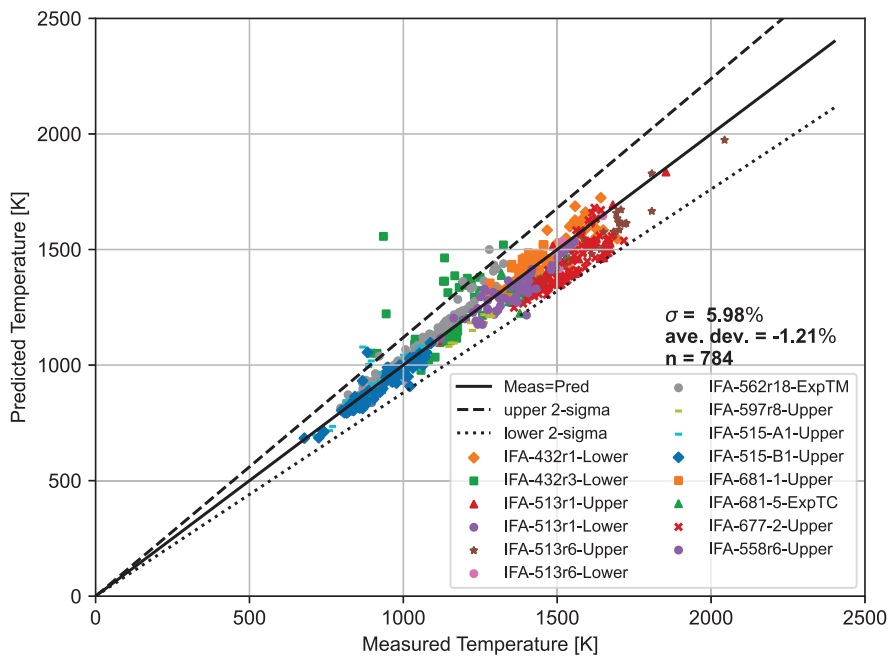

Figure 3-2. Measured and predicted centerline temperature for the UO_2 assessment cases throughout life

These data are also shown in terms of relative bias in Figure 3-3 as a function of burnup. There appears to be an under-predictive bias of 1.2% , on average, early in life between 2 and 16 GWd/MTU. However, there appears to be no systematic bias in the predictions with increasing burnup.

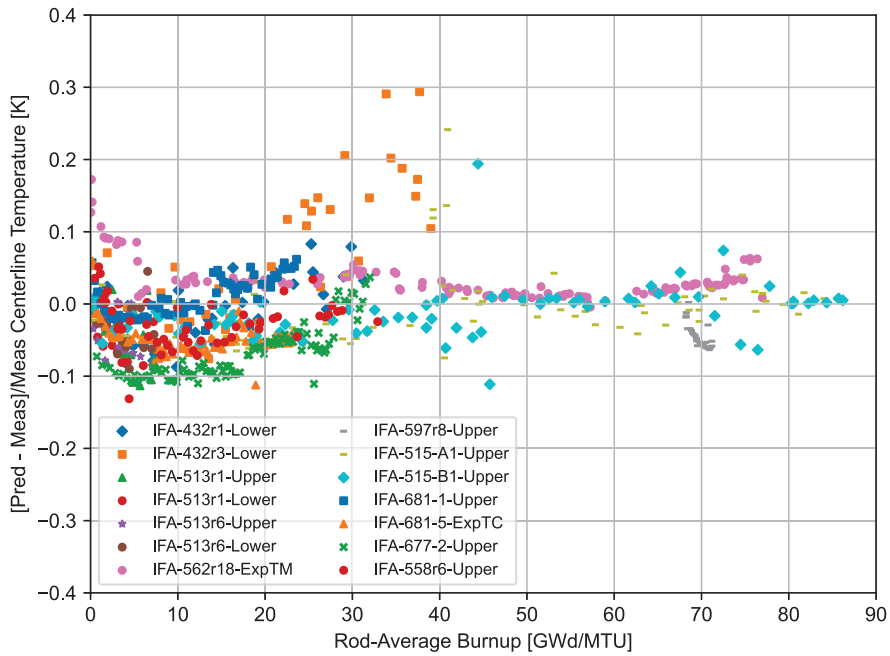

Figure 3-3. Predicted minus measured divided by measured centerline temperature for the UO_2 assessment cases as a function of burnup

Figure 3-4 shows the measured and predicted centerline temperature for IFA-432r1. This figure contains data from the lower thermocouple. This rod also contained an upper thermocouple, but it failed after 150 days. The comparisons to the upper thermocouple data are similar to the lower thermocouple. This figure shows excellent agreement between the FAST predictions and the data.

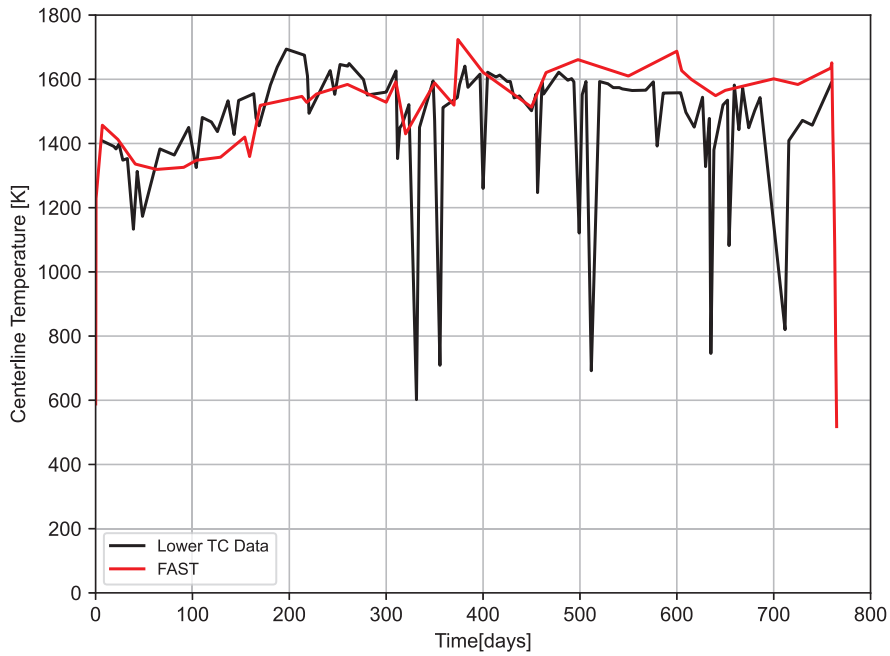

Figure 3-4. Measured and predicted centerline temperature for IFA-432 rod 1 UO_2 lower thermocouple (burnup = 45 GWd/MTU, as-fabricated radial gap = 114 μm)

Figure 3-5 shows the measured and predicted centerline temperature for IFA-432r3. This figure contains data from the lower thermocouple. This rod also contained an upper thermocouple, but it failed after 550 days. The comparisons to the upper thermocouple data are similar to the lower thermocouple. This figure shows excellent agreement between the FAST predictions and the data at BOL, and an over-prediction of about 100 K (7% relative) at EOL. This over-prediction may be due to FAST over-predicting the gas release, leading to higher predicted temperatures. As noted earlier, over-prediction of gas release leads to lower gap conductivity and results in higher fuel temperature predictions. It should also be noted that some of the helium fill and fission gases were found to have leaked out of these IFA-432 rods based on rod puncture data (i.e., the leak was theorized to have occurred around the thermocouple penetrations through the end caps).

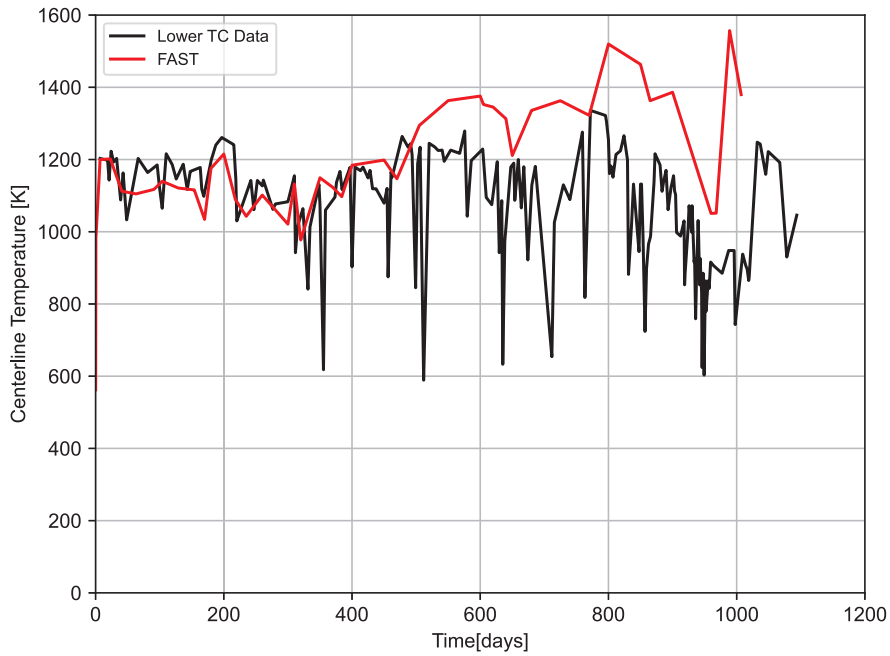

Figure 3-5. Measured and predicted centerline temperature for IFA-432 rod 3 UO_2 lower thermocouple (burnup = 45 GWd/MTU, as-fabricated radial gap = 38 μm)

Figures 3-6 and 3-7 show the measured and predicted centerline temperature for IFA-513r1. These figures contain data from the upper and lower thermocouples and show reasonable agreement between the FAST predictions and the data.

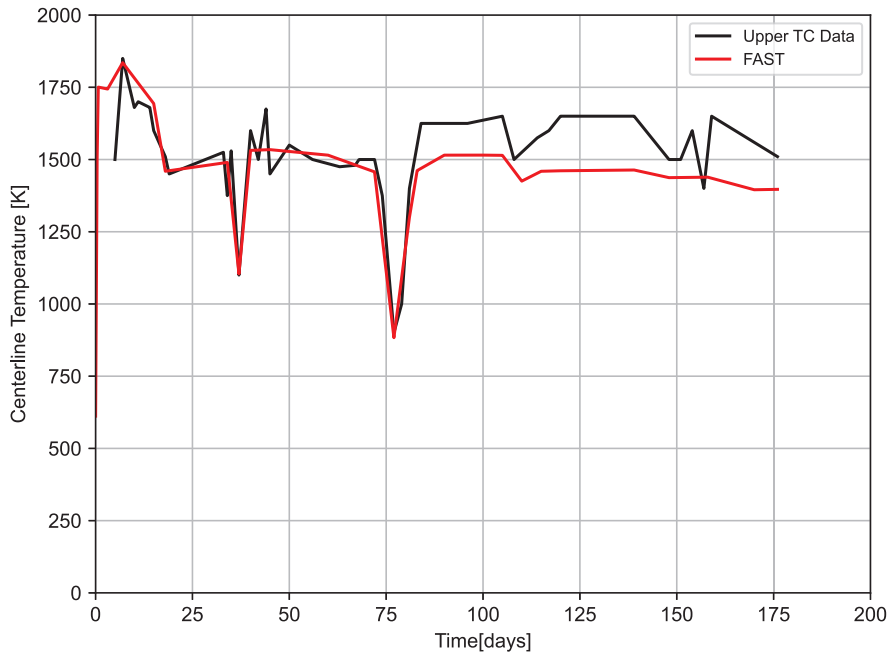

Figure 3-6. Measured and predicted centerline temperature for IFA-513 rod 1 UO_2 upper thermocouple (burnup=10 GWd/MTU, as-fabricated radial gap=108 μm)

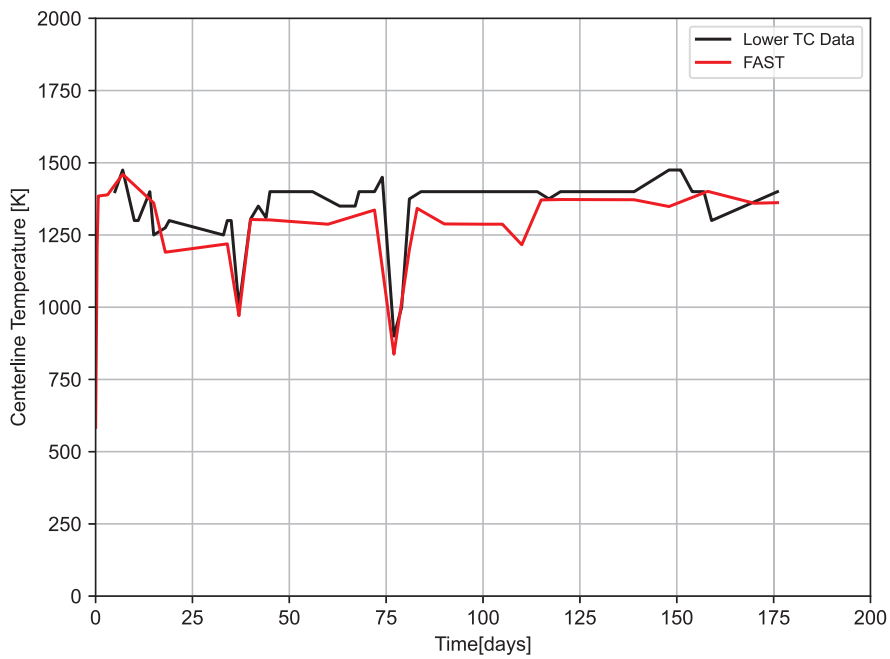

Figure 3-7. Measured and predicted centerline temperature for IFA-513 rod 1 UO_2 lower thermocouple (burnup=10 GWd/MTU, as-fabricated radial gap=108 μm)

Figures 3-8 and 3-9 show the measured and predicted centerline temperature for IFA-513r6. These figures contain data from the upper and lower thermocouples and show reasonable agreement between the FAST predictions and the data.

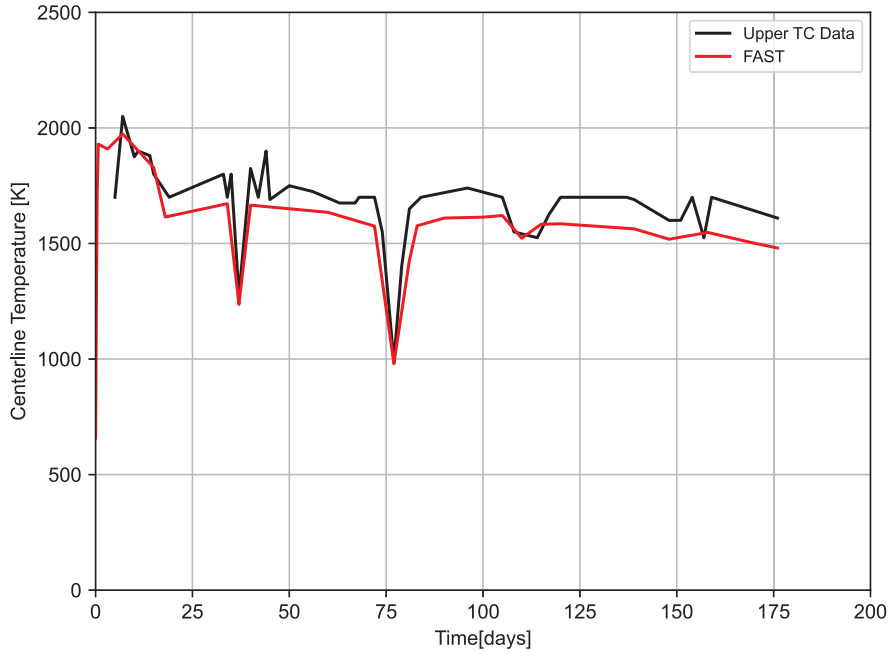

Figure 3-8. Measured and predicted centerline temperature for IFA-513 rod 6 UO_2 upper thermocouple (burnup=10 GWd/MTU, as-fabricated radial gap=108 μm)

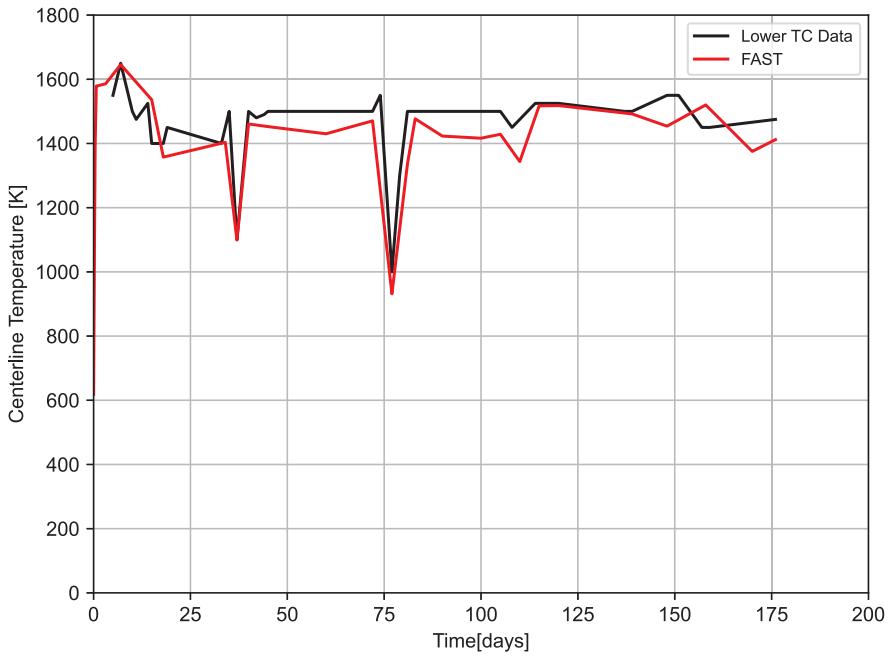

Figure 3-9. Measured and predicted centerline temperature for IFA-513 rod 6 UO_2 lower thermocouple (burnup=10 GWd/MTU, as-fabricated radial gap=108 μm)

Figure 3-10 shows the measured and predicted centerline temperature for IFA-562r18. This figure contains rod axial-averaged temperature data from the expansion thermometer. This figure shows excellent agreement between the FAST predictions and the data.

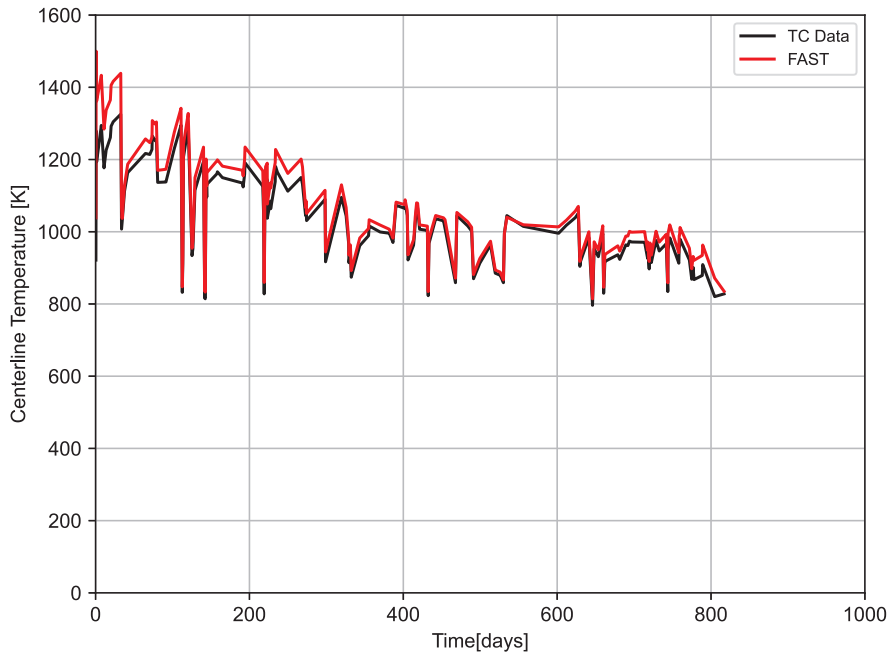

Figure 3-10. Measured and predicted rod-average centerline temperature for IFA-562 rod 18 UO_2 (burnup = 76 GWd/MTU, as-fabricated radial gap = 50 μm)

Figure 3-11 shows the measured and predicted centerline temperature for IFA-597r8. This rod was refabricated from a commercial rod that was irradiated to 68 GWd/MTU. This figure contains upper thermocouple data and shows reasonable agreement between the FAST predictions and the data (±75 K, 6% relative).

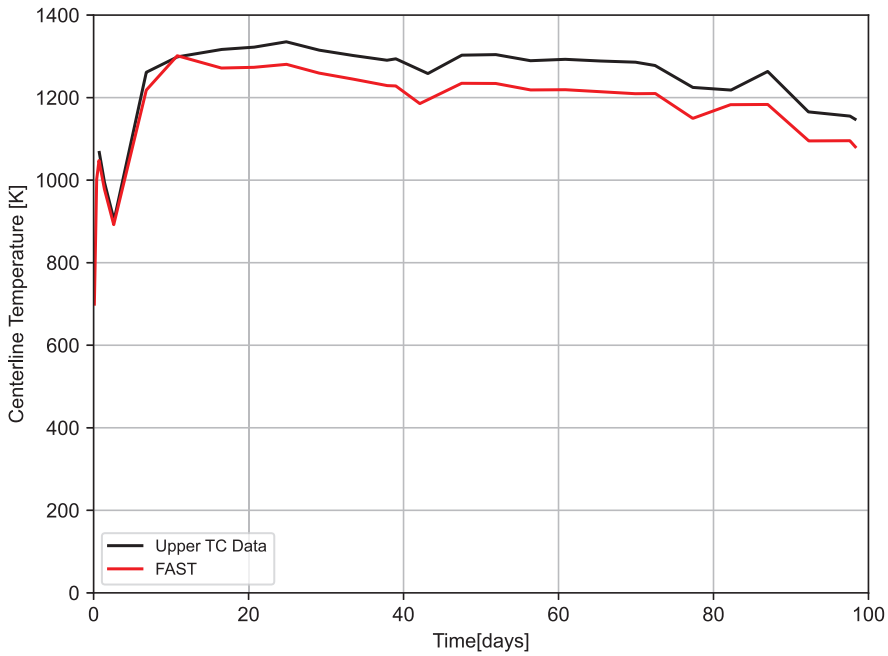

Figure 3-11. Measured and predicted centerline temperature for IFA-597 rod 8 (starting burnup = 68 GWd/MTU, ending burnup=71 GWd/MTU, as-fabricated radial gap=105 µm)

Figures 3-12 and 3-13 show the measured and predicted centerline temperature for IFA-515.10 rods A1 and B1. These figures contain upper thermocouple data and show reasonable agreement between the FAST predictions and the data (±50 K, 6% relative). In these figures, the vertical line denotes where the thermocouple failed. The data reported after the failure are not valid.

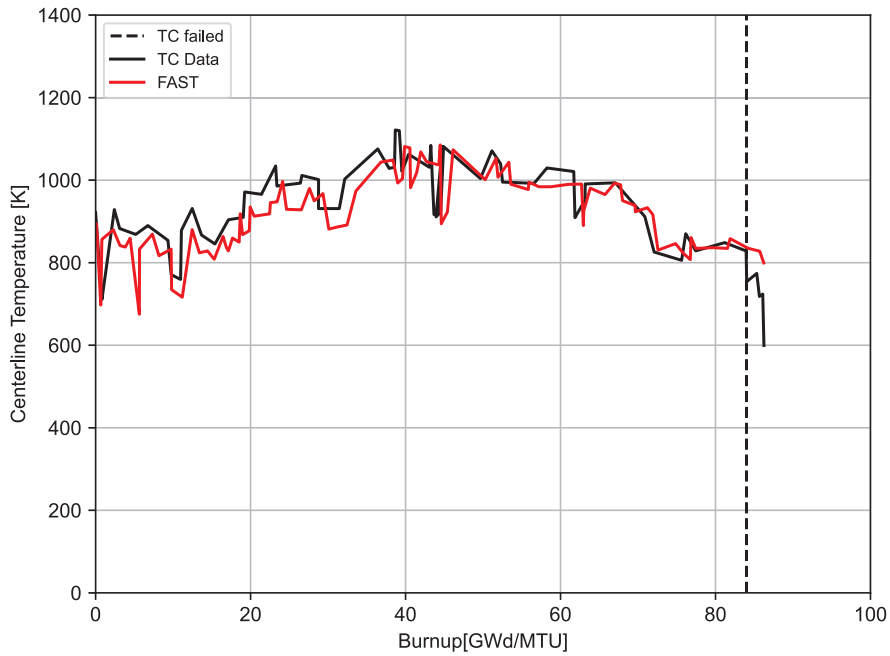

Figure 3-12. Measured and predicted centerline temperature for IFA-515.10 rod A1 (UO_2) (burnup = 80 GWd/MTU, as-fabricated radial gap=25 µm)

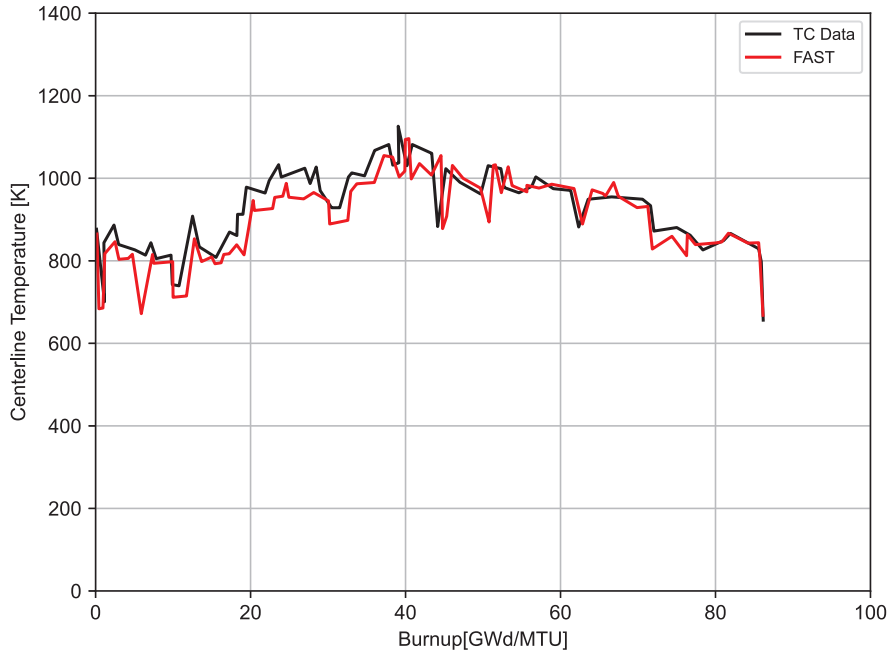

Figure 3-13. Measured and predicted centerline temperature for IFA-515.10 rod B1 (UO_2) (burnup = 80 GWd/MTU, as-fabricated radial gap = 25 µm)

Figures 3-14 and 3-15 show the measured and predicted centerline temperature for IFA-681 rods

1 and 5. These figures contain upper thermocouple data (rod 1) and expansion thermometer data (rod 5). These figures show reasonable agreement between the FAST predictions and the data (±30 K, 2% relative).

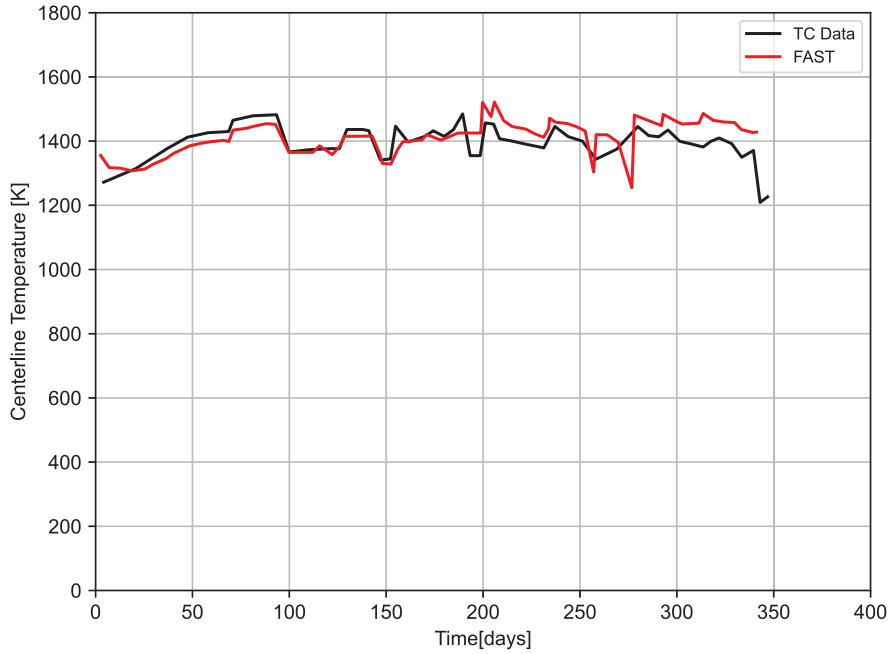

Figure 3-14. Measured and predicted centerline temperature for IFA-681 rod 1 UO_2 (burnup = 33 GWd/MTU, as-fabricated radial gap = 85 µm)

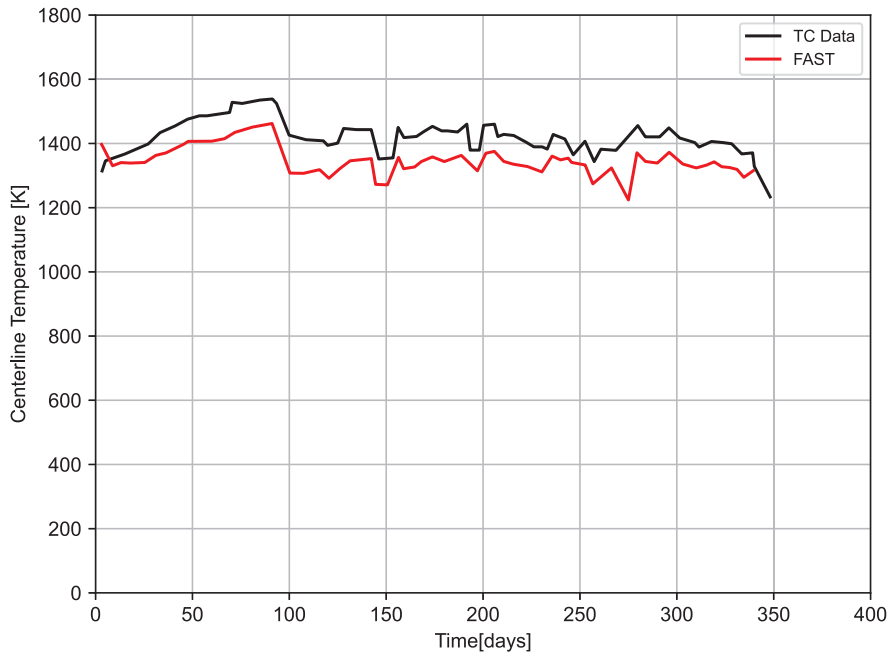

Figure 3-15. Measured and predicted centerline temperature for IFA-681 rod 5 UO_2 (burnup = 32 GWd/MTU, as-fabricated radial gap = 85 µm)

Figure 3-16 shows the measured and predicted centerline temperature for IFA-677 rod 2. This figure contains upper thermocouple data and shows significant under-prediction of the FAST predictions relative to the data at BOL of up to 150 K (11% relative). However, by 300 days, the under-prediction has been reduced to a more reasonable level of 75 K (5% relative) or less. This rod (Figure 3-16) had similar LHGR and burnup and the same gap size as IFA-681 rod 5 (Figure 3-15) but significantly higher fuel centerline temperatures (~130 °C, 10% relative) at low burnups.

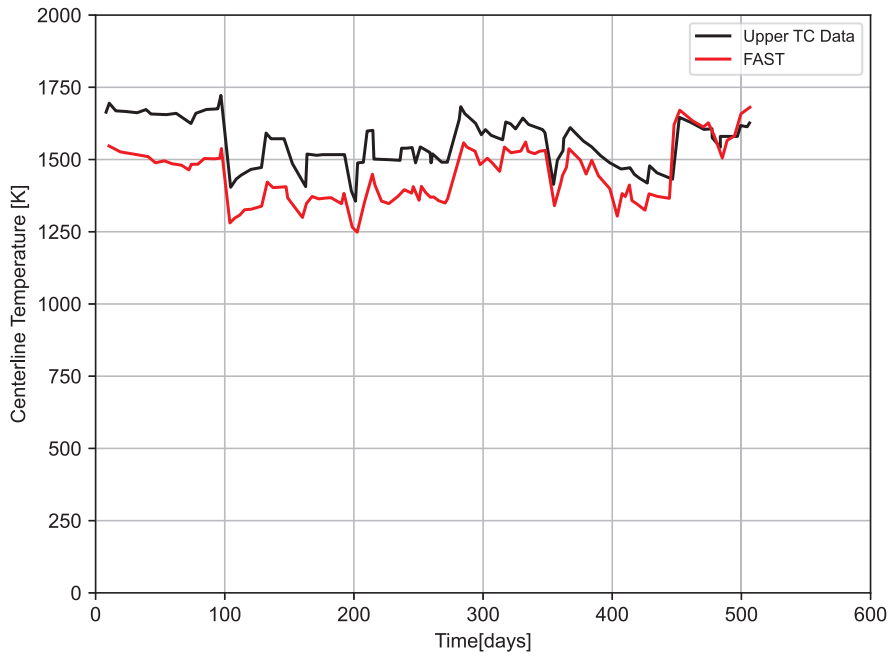

Figure 3-16. Measured and predicted centerline temperature for IFA-677.1 rod 2 UO_2 (burnup = 32 GWd/MTU, as-fabricated radial gap = 85 µm)

Figure 3-17 shows the measured and predicted centerline temperature for IFA-558 rod 6. This figure contains upper thermocouple data and shows reasonable agreement between the FAST predictions and the data (±50-75 K, 4-6% relative), except at burnups between 25.5 and 28 GWd/MTU, where temperatures are under-predicted by up to 120 K (10% relative) but then start to provide good agreement at 29 GWd/MTU.

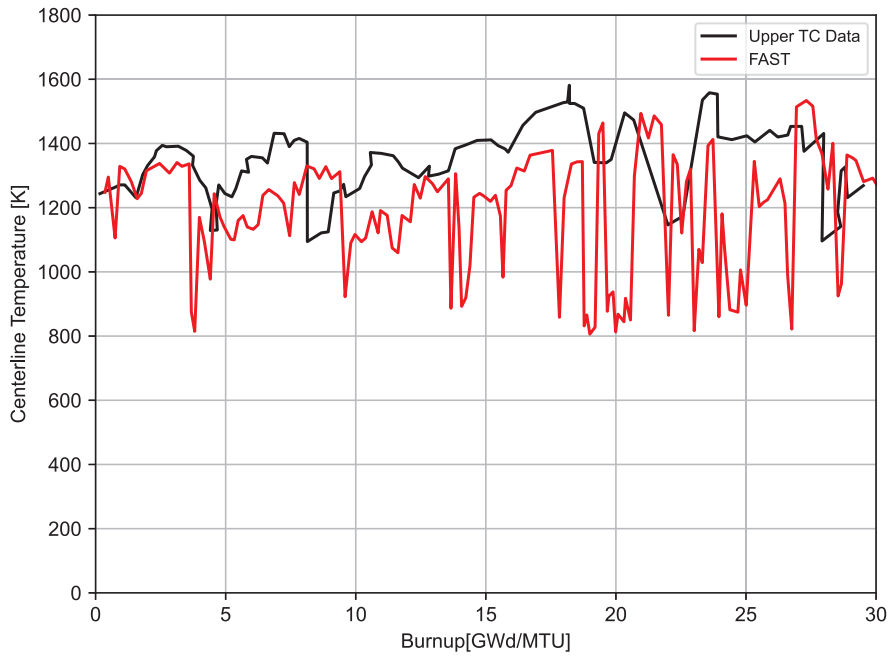

Figure 3-17. Measured and predicted centerline temperature for IFA-558 rod 6 UO_2 (burnup = 41 GWd/MTU, as-fabricated radial gap = 95 µm)

This section demonstrates that FAST continues to provide a best-estimate prediction of centerline temperature for UO_2 rods to within a standard error of 4.7% for recent experimental data (see Figure 3-2). The largest deviation was for IFA-677 rod 2 (Figure 3-16), which shows a 150 K (11% relative) under-prediction at BOL that decreases to less than 75 K (6% relative) by 300 days. All the IFA-677 rods were also slightly under-predicted in the BOL temperature section, perhaps demonstrating a bias in this data, particularly compared with rods of similar power, burnup levels, and gap size that demonstrate better agreement with the code.

It is noted that in some of these cases the temperatures are predicted well throughout life, while in other cases there is a deviation with time, and in others there is a consistent bias throughout life. The cases with a deviation with time are likely due to a small difference in FGR predictions that affect the calculated centerline temperature or a drift in neutron detectors with time that affects measured rod powers. In some cases, the neutron detectors are recalibrated between reactor cycles such that at a given burnup or time the predicted and measured temperatures begin to agree better or deviate. The cases with a constant bias throughout life are likely due to a bias in the predictions, the reported rod power, or the measured temperature.

3.2.2 MOX Centerline Temperature Predictions as a Function of Burnup

FAST predictions have been benchmarked against centerline temperatures taken from eight Halden tests with instrumented fuel assemblies containing 15 MOX fuel rods. The results of these comparisons are provided in this section.

The following figures show measured and predicted fuel centerline temperatures from rods with

centerline temperature measurements. Individual rod predictions may demonstrate a systematic error (bias) that may be due to thermocouple decalibration or a systematic error in the power history or axial power shape (power at thermocouple location) provided due to decalibration in or with the neutron detectors. However, when all the comparisons are examined, no overall systematic error (bias) is found in the prediction of MOX fuel temperature, as can be seen in Figure 3-18. For all the cases, a standard error of 4.7% on the centerline temperature was calculated.

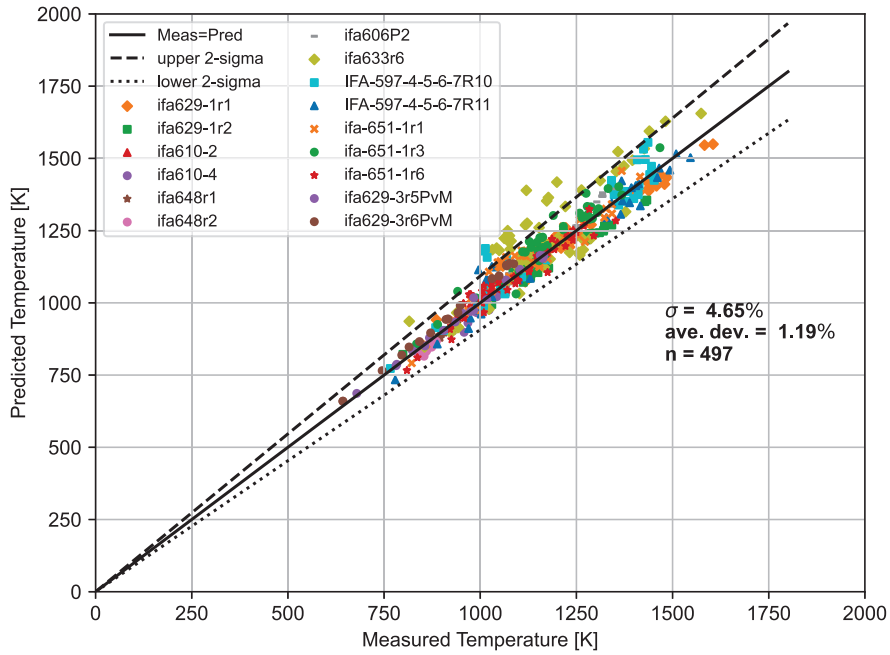

Figure 3-18. Measured and predicted centerline temperature for the MOX assessment cases throughout life

These data are also shown in terms of relative bias in Figure 3-19 as a function of burnup. There appears to be no systematic bias in the predictions with increasing burnup.

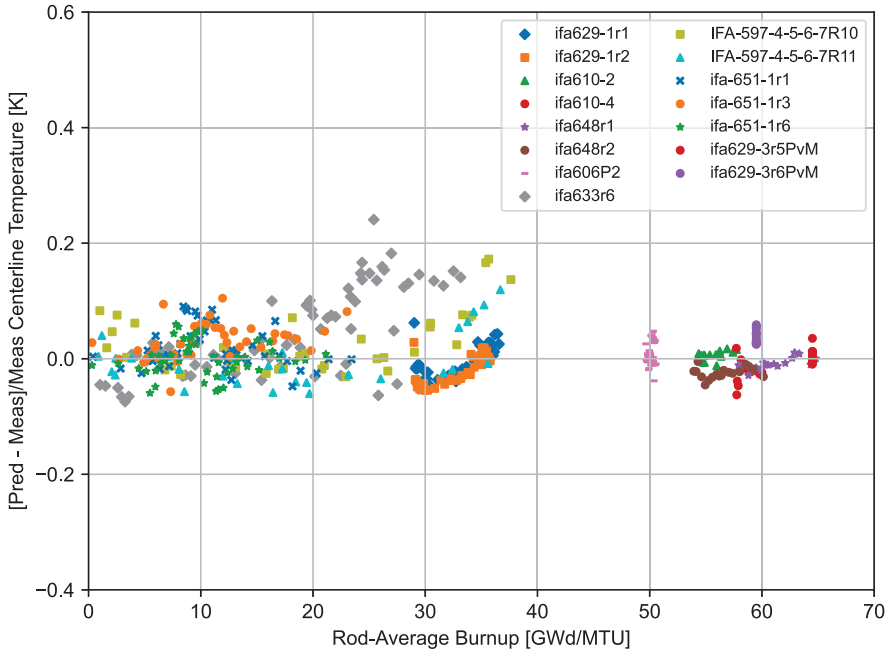

Figure 3-19. Predicted minus measured divided by measured centerline temperature for the MOX assessment cases as a function of burnup

Figures 3-20 and 3-21 show the measured and predicted centerline temperatures for IFA-629.1 rods 1 and 2. These figures show good agreement between the FAST predictions and the data. The slight offset during parts of the irradiation could be due to power or thermocouple calibration changes at the end of each cycle.

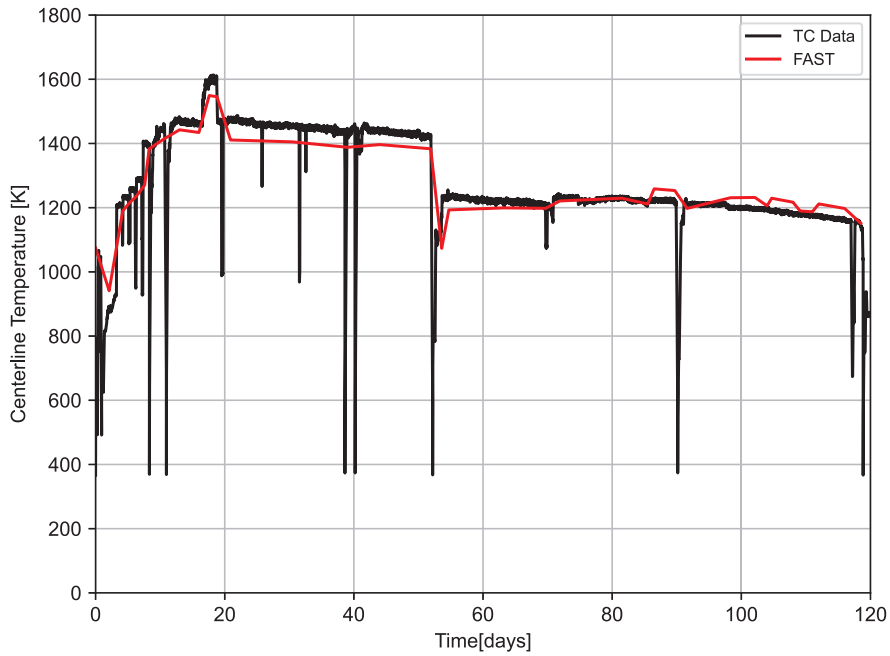

Figure 3-20. Measured and predicted centerline temperature for IFA-629.1 rod 1 (MOX) (starting burnup = 27 GWd/MTU, ending burnup=33 GWd/MTU, as-fabricated radial gap = 84 μm)

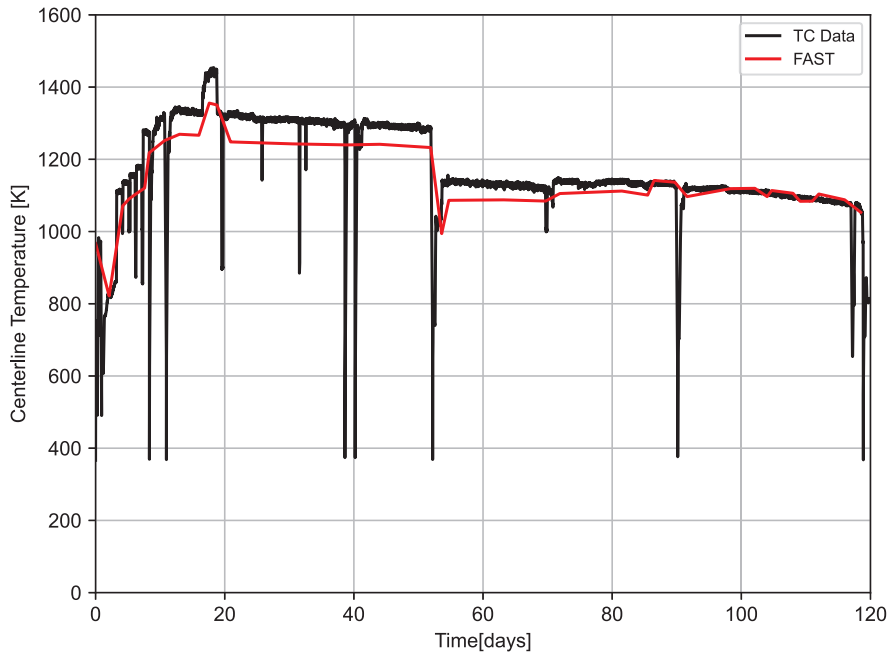

Figure 3-21. Measured and predicted centerline temperature for IFA-629.1 rod 2 (starting burnup = 29 GWd/MTU, ending burnup = 40 GWd/MTU, as-fabricated radial gap = 84 μm)

Figures 3-22 and 3-23 show the measured and predicted centerline temperature for IFA-610.2 and IFA-610.4. These figures show excellent agreement between the FAST predictions and the data.

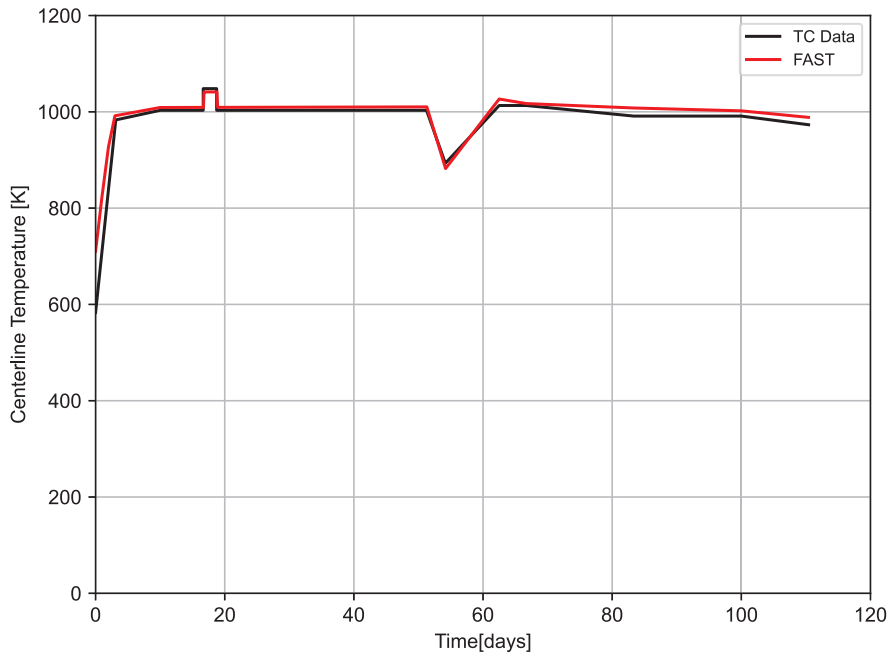

Figure 3-22. Measured and predicted centerline temperature for IFA-610.2 (MOX) (starting burnup = 55 GWd/MTU, ending burnup = 56 GWd/MTU, as-fabricated radial gap = 84 μm)

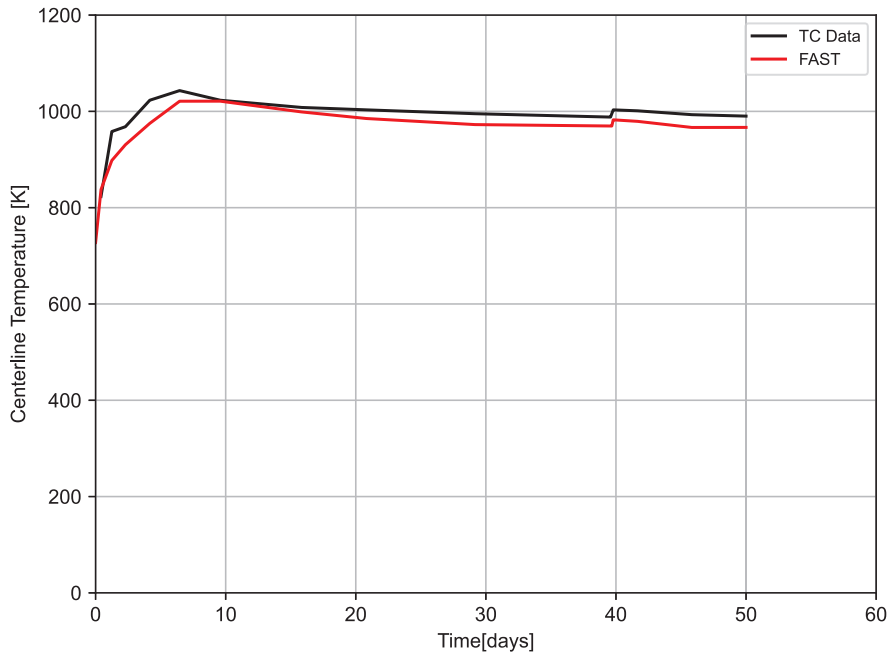

Figure 3-23. Measured and predicted centerline temperature for IFA-610.4 (MOX) (starting burnup = 56 GWd/MTU, ending burnup = 57 GWd/MTU, as-fabricated radial gap = 84 μm)

Figures 3-24 and 3-25 show the measured and predicted centerline temperature for IFA-648.1 rods 1 and 2. These figures show excellent agreement between the FAST predictions and the data.

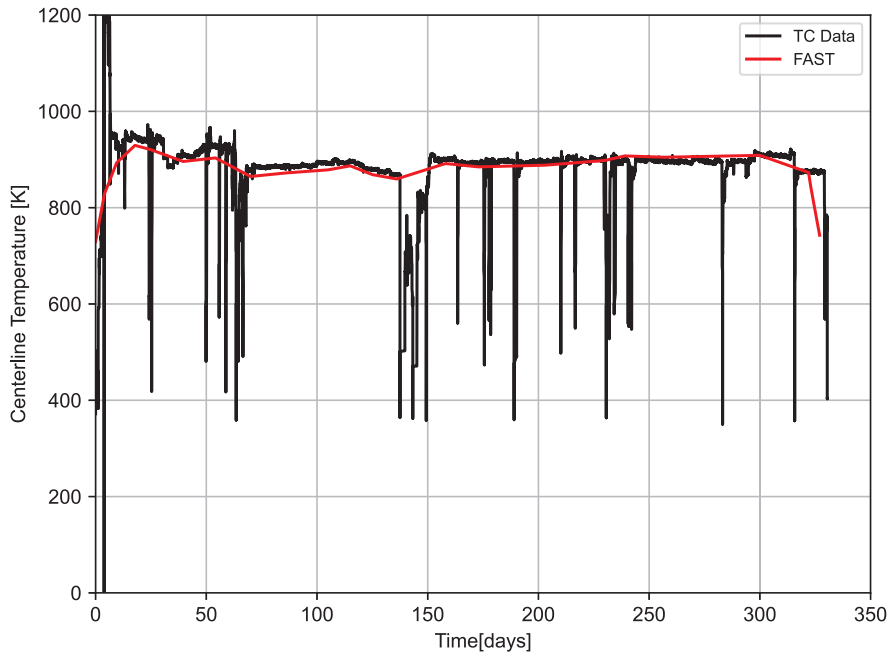

Figure 3-24. Measured and predicted centerline temperature for IFA-648.1 rod 1 (MOX) (starting burnup = 55 GWd/MTU, ending burnup = 62 GWd/MTU, as-fabricated radial gap = 84 μm)

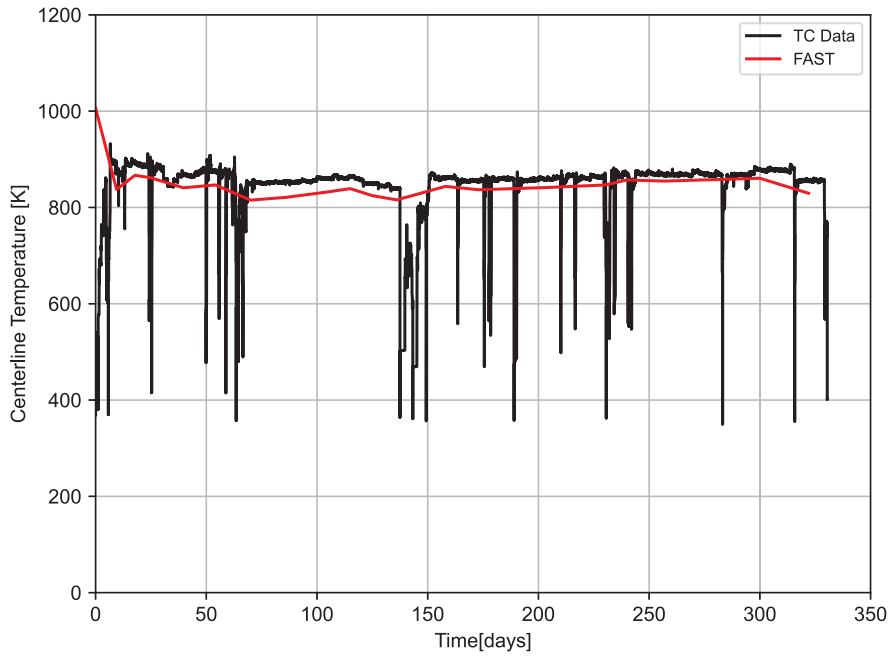

Figure 3-25. Measured and predicted centerline temperature for IFA-648.1 rod 2 (MOX) (starting burnup = 55 GWd/MTU, ending burnup = 62 GWd/MTU, as-fabricated radial gap = 84 μm)

Figures 3-26 and 3-27 show the measured and predicted centerline temperature for IFA-629.3 rods 5 and 6. These figures show excellent agreement between the FAST predictions and the data.

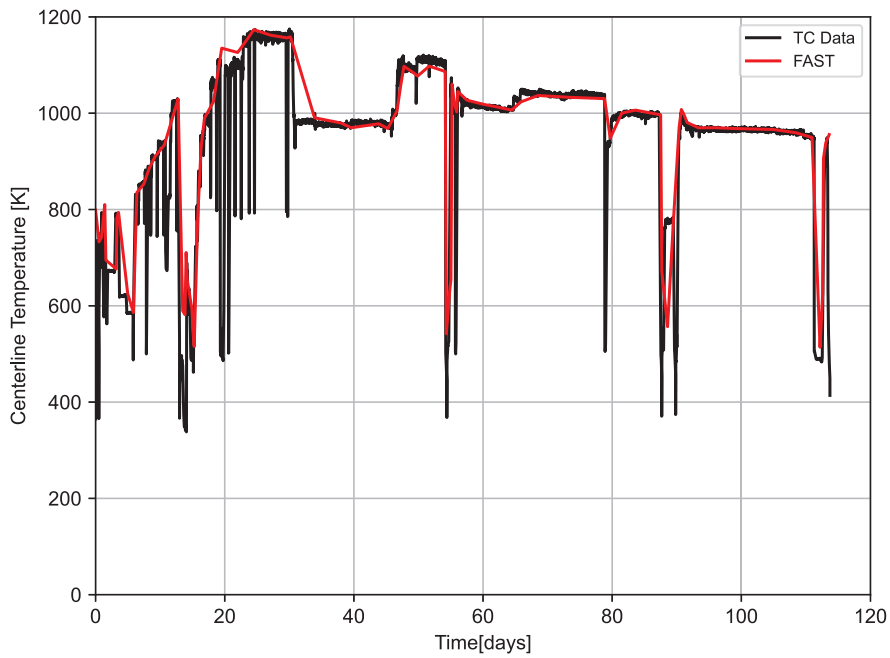

Figure 3-26. Measured and predicted centerline temperature for IFA-629.3 rod 5 (MOX) (starting burnup = 62 GWd/MTU, ending burnup = 72 GWd/MTU, as-fabricated radial gap = 84 μm)

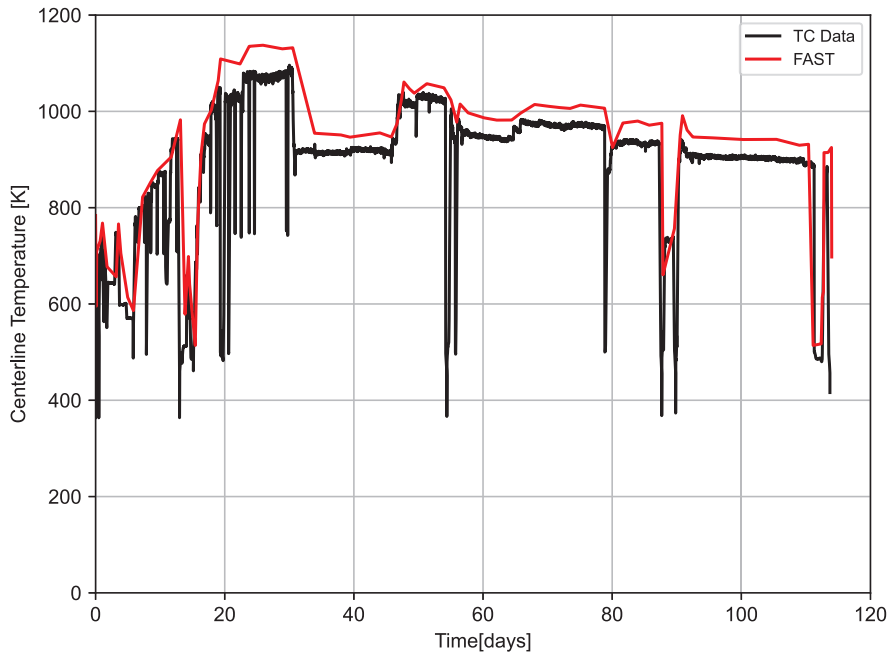

Figure 3-27. Measured and predicted centerline temperature for IFA-629.3 rod 6 (MOX) (starting burnup = 62 GWd/MTU, ending burnup = 68 GWd/MTU, as-fabricated radial gap = 84 μm)

Figure 3-28 shows the measured and predicted centerline temperature for IFA-606 Phase 2. This figure shows reasonable agreement between the FAST predictions and the data (within ±75 K, 7% relative).

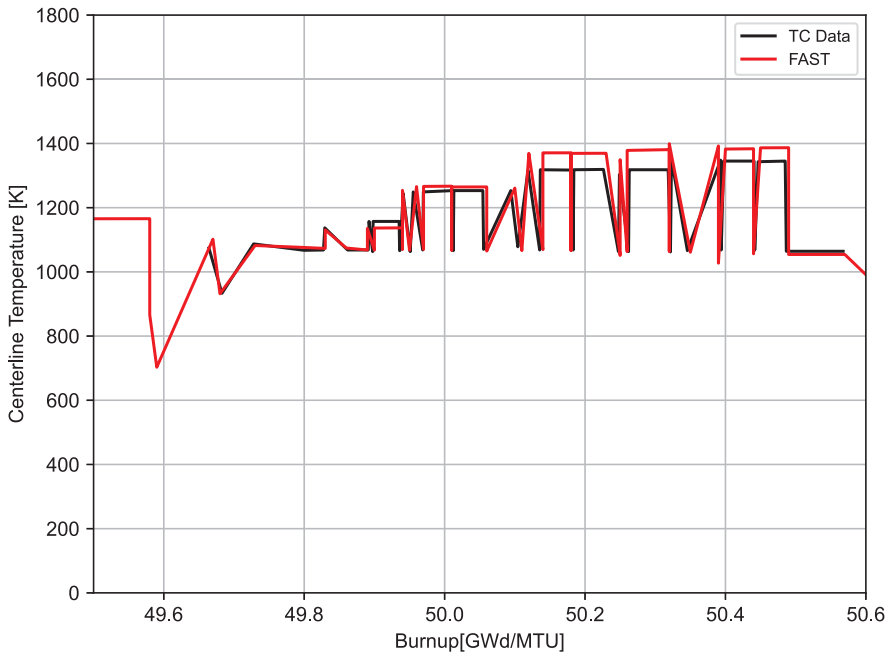

Figure 3-28. Measured and predicted centerline temperature for IFA-606 Phase 2 (MOX) (starting burnup = 49 GWd/MTU, as-fabricated radial gap = 94 μm)

Figure 3-29 shows the measured and predicted centerline temperature for IFA-633-1 rod 6. This figure shows reasonable agreement between the FAST predictions and the data (within ±75 K, 5% relative) until about 26 GWd/MTU, when FAST over-predicts the data by about 125 to 150K (13% relative). This may be because FAST over-predicts the FGR (measured FGR=6% , predicted=13%) for this rod, which will lead to increased fuel temperatures.

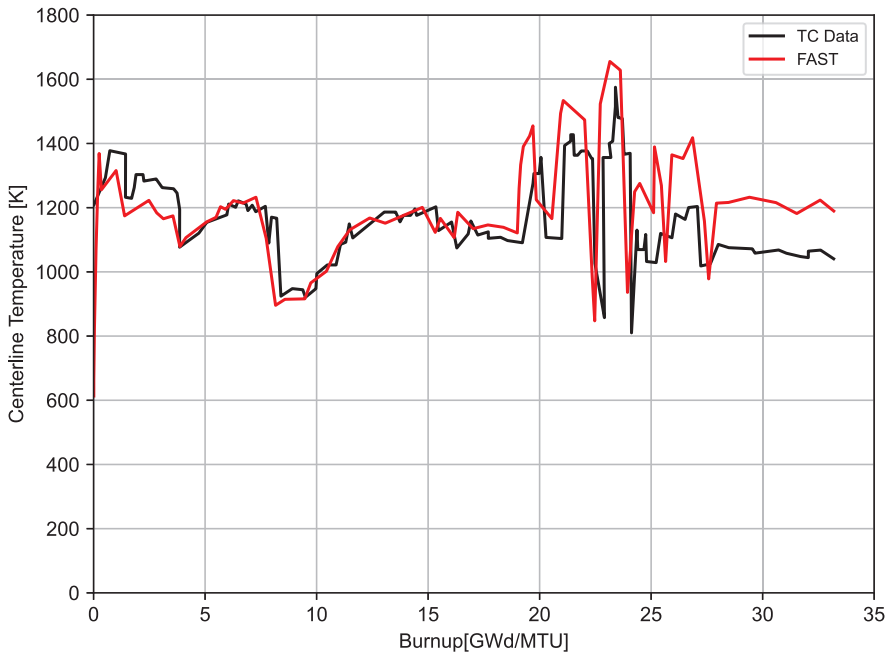

Figure 3-29. Measured and predicted centerline temperature for IFA-633-1 rod 6 (MOX) (burnup = 32 GWd/MTU, as-fabricated radial gap= 104 μm)

Figures 3-30 and 3-31 show the measured and predicted centerline temperature for IFA-597.4, .5, .6, .7 rods 10 and 11. These figures show excellent agreement between the FAST predictions and the data up to 25 GWd/MTU, when the code begins to over-predict the data by up to 100 K (7% relative).

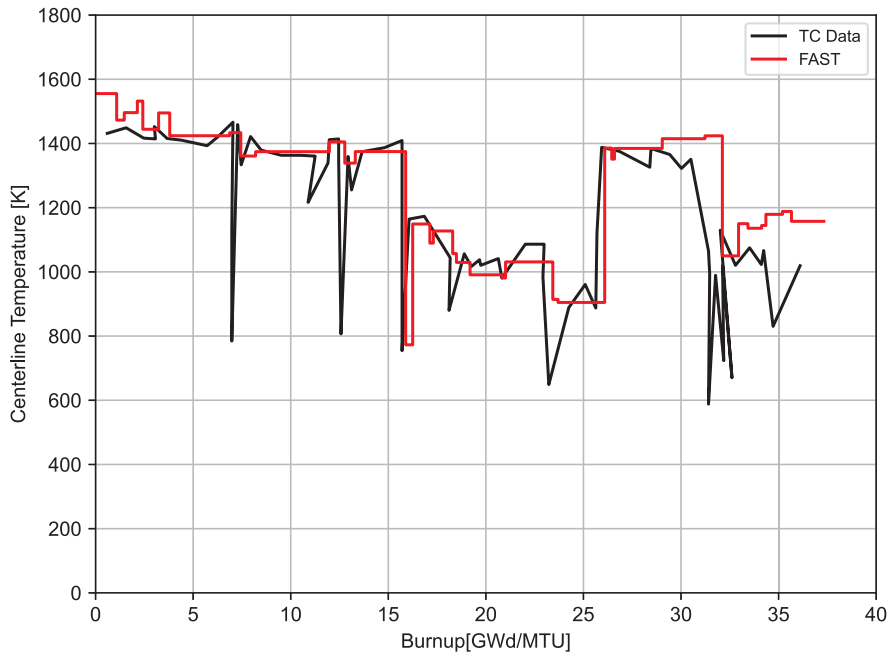

Figure 3-30. Measured and predicted centerline temperature for IFA-597.4, .5, .6, .7 rod 10 (MOX) (burnup = 36 GWd/MTU as-fabricated radial gap = 95 μm)

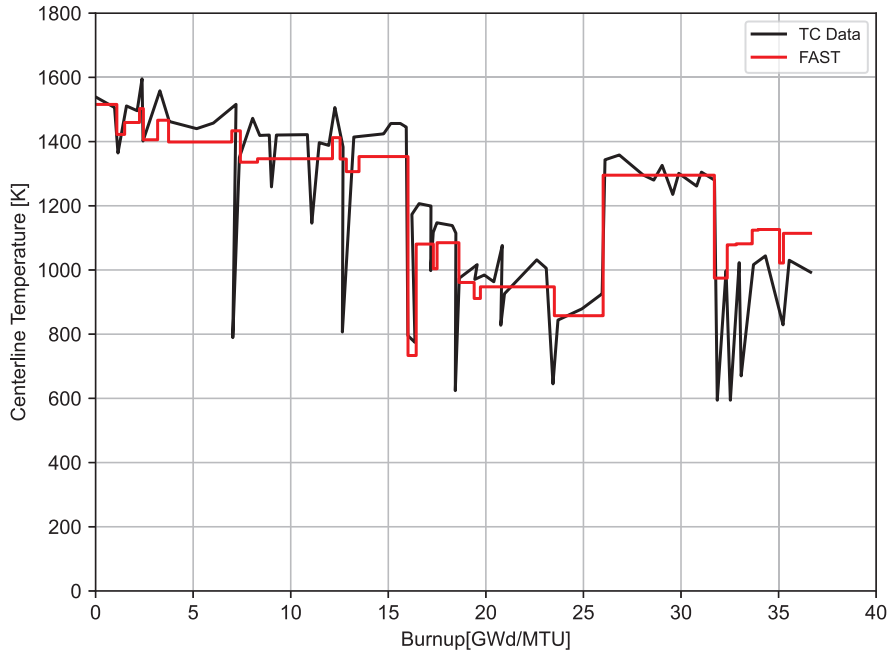

Figure 3-31. Measured and predicted centerline temperature for IFA-597.4, .5, .6, .7 rod 11 (MOX) (burnup = 37 GWd/MTU as-fabricated radial gap = 95 μm)

Figures 3-32, 3-33, and 3-34 show the measured and predicted centerline temperature for IFA-

651.1 rods 1, 3, and 6. These figures show excellent agreement between the FAST predictions and the data from rods 1 and 6 that were instrumented with centerline thermocouple, and reasonable agreement (±50 K, 5% relative) with the data from rod 3 that was instrumented with an expansion thermometer.

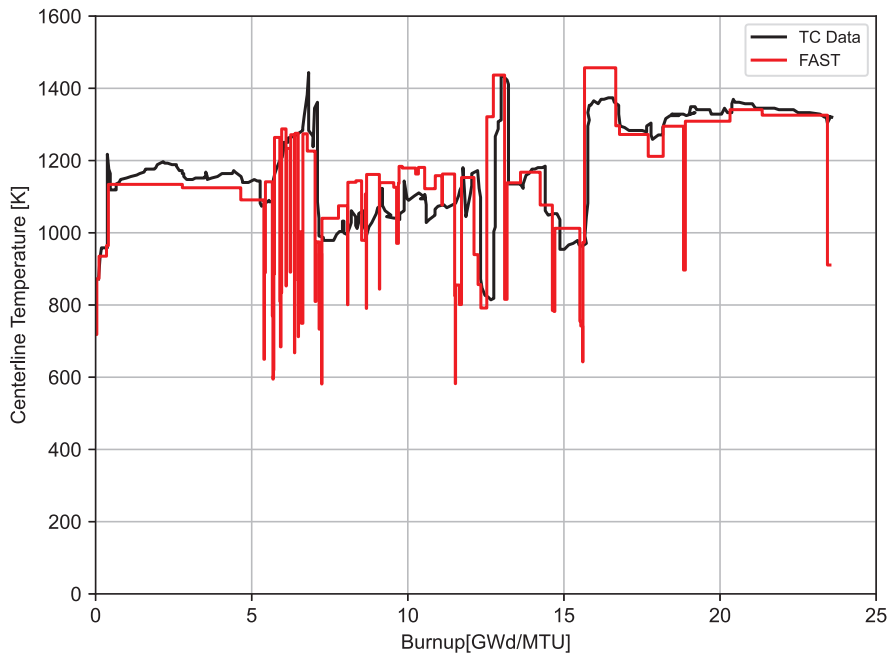

Figure 3-32. Measured and predicted centerline temperature for IFA-651.1 rod 1 (MOX) (burnup = 22 GWd/MTU as-fabricated radial gap = 79 μm)

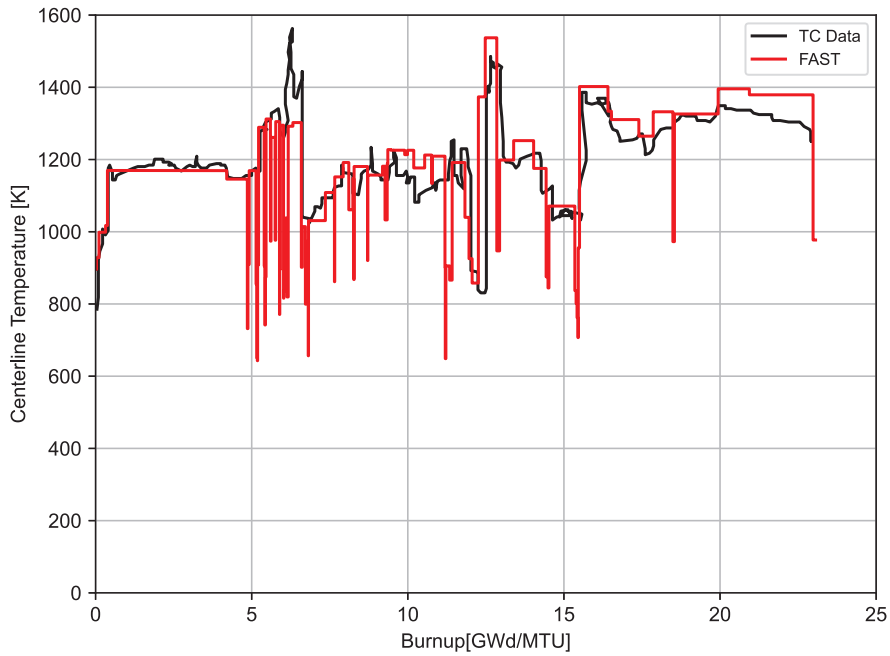

Figure 3-33. Measured and predicted centerline temperature for IFA-651.1 rod 3 (MOX) (burnup = 22 GWd/MTU as-fabricated radial gap = 79 µm)

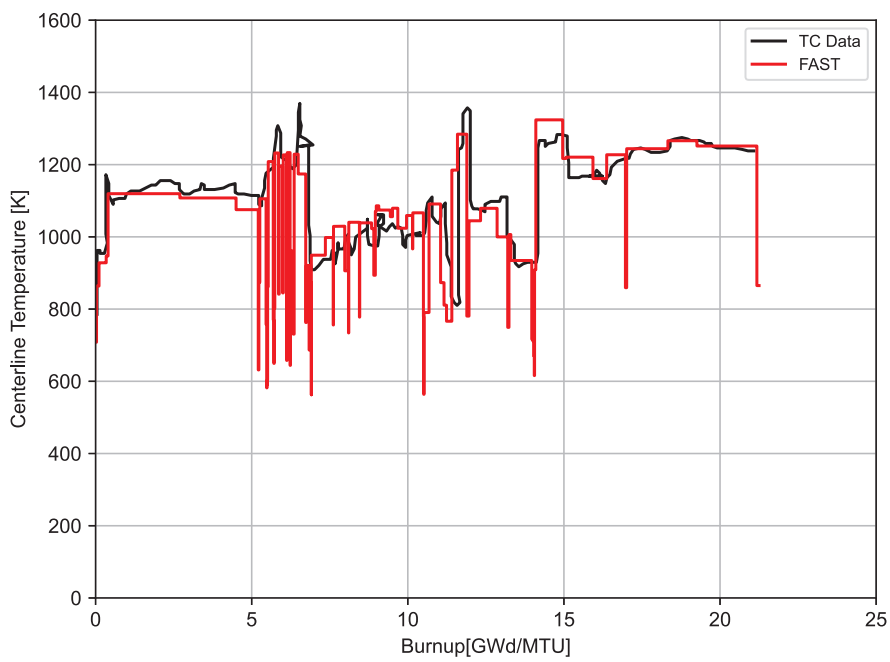

Figure 3-34. Measured and predicted centerline temperature for IFA-651.1 rod 6 (MOX) (burnup = 20 GWd/MTU as-fabricated radial gap = 81 µm)

This section demonstrates that FAST continues to provide a best-estimate prediction of centerline

temperature for MOX rods to within a standard error of 4.7% . The largest deviation was for IFA-633.1 rod 6 (Figure 3-29), which shows up to a 150 K (13% relative) over-prediction at higher burnup. This may be due to over-predicting the FGR for this rod.

3.2.3 UO_2-Gd_2O_3 Centerline Temperature Predictions as a Function of Burnup

The adjustment for gadolinia in the thermal conductivity model has been assessed against centerline temperature predictions from three instrumented fuel assemblies irradiated at the Halden reactor. The results of these comparisons are provided in this section.

The following figures show measured and predicted fuel centerline temperatures from rods with centerline temperature measurements. Individual rod predictions may demonstrate a systematic error (bias) that may be due to thermocouple decalibration or a systematic error in the power history or axial power shape (power at thermocouple location) provided due to decalibration in or with the neutron detectors with time. However, when all the comparisons are examined, no overall systematic error (bias) is found in the prediction of UO_2-Gd_2O_3 temperature throughout life, as can be seen in Figure 3-35. For all the cases, a standard error of 5.76% on the centerline temperature was calculated.

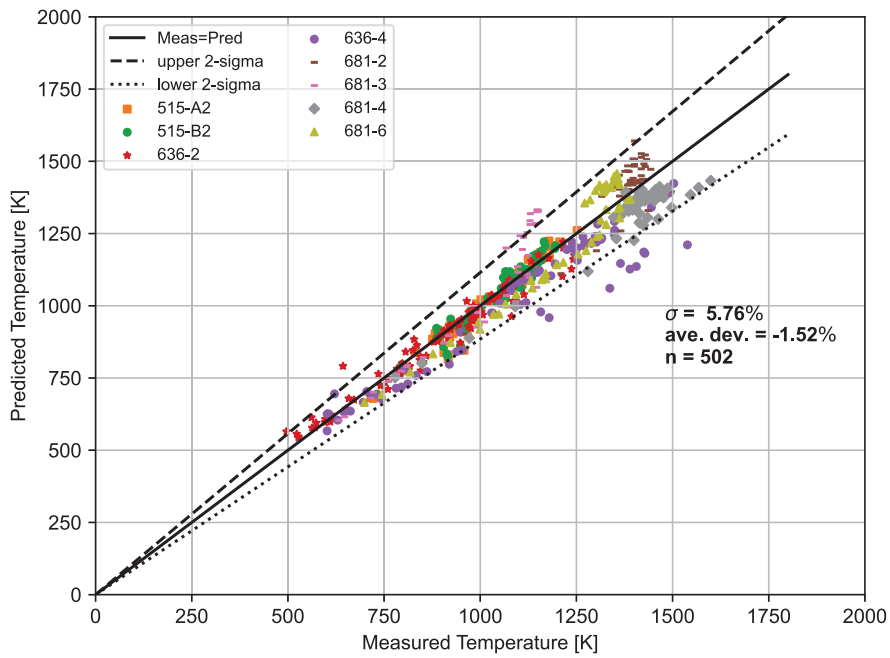

Figure 3-35. Measured and predicted centerline temperature for the UO_2-Gd_2O_3 assessment cases throughout Life

These data are also shown in terms of relative bias in Figure 3-36 as a function of burnup. It can be seen that there appears to be no systematic bias in the predictions with increasing burnup.

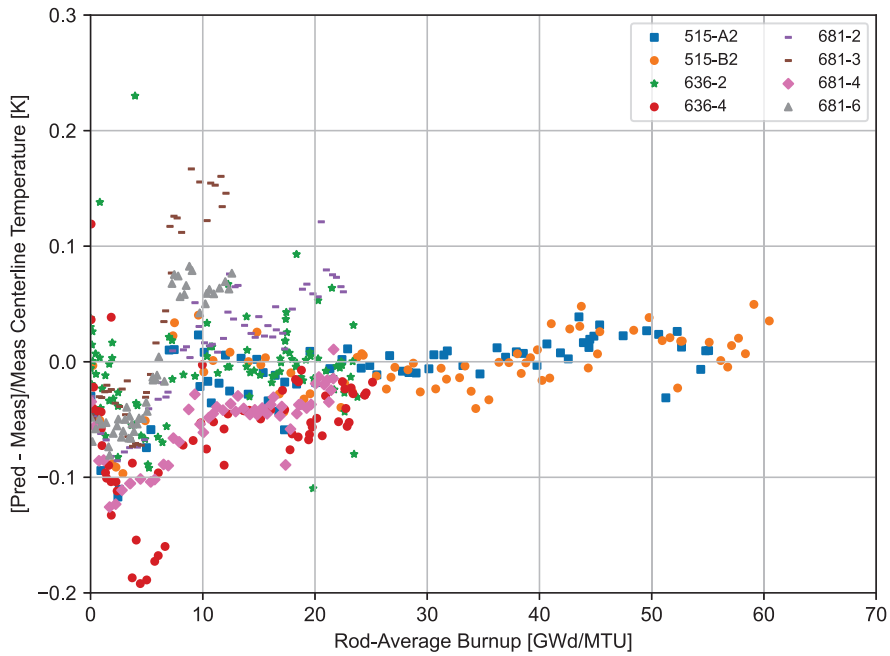

Figure 3-36. Predicted minus measured divided by measured centerline temperature for the $UO_2Gd_2O_3$ assessment cases as a function of burnup

Figures 3-37 and 3-38 show the measured and predicted centerline temperature for IFA-515.10 rods A1, A2, B1, and B2. Rods A1 and B1 (Figures 37(a) and 38(a)) are UO_2 rods and rods A2 and B2 (Figures 37(b) and 38(b)) are UO_2-Gd_2O_3 rods with depleted gadolinium that did not contain any ^{155}Gd or ^{157}Gd. There are two factors that influence the centerline temperature for UO_2-Gd_2O_3 rods relative to UO_2 rods: 1) TCD due to Gd addition and 2) radial power profile due to the neutron absorption of ^{155}Gd and ^{157}Gd. These rods were meant to show the difference only due to the TCD from gadolinia (Gd_2O_3), not due to the difference in radial power profile. A modified version of FAST that uses the UO_2 radial power profile model (TUBRNP) for UO_2-Gd_2O_3 rods (A2 and B2) was used to perform these calculations. These figures show that FAST predicts the centerline temperatures for UO_2-Gd_2O_3 rods as well as for UO_2 rods. In these figures, the vertical line denotes where the thermocouple failed. The data reported after the failure are not valid.

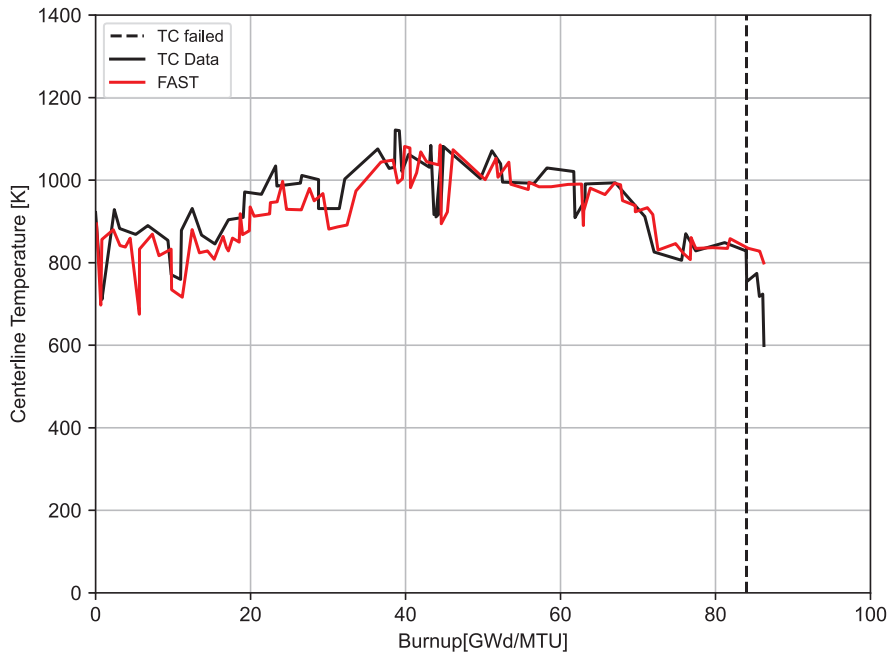

(a) Rod A1

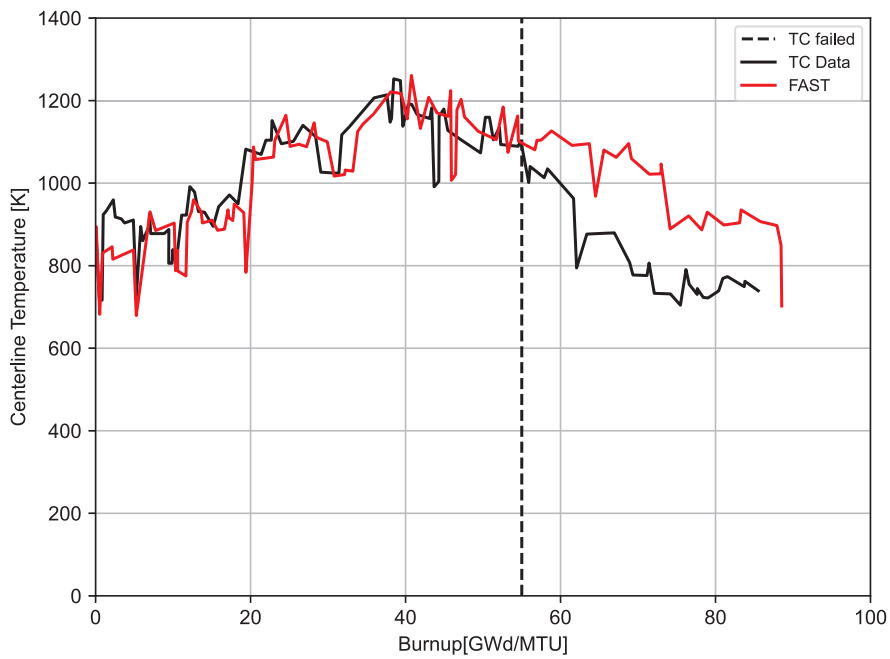

(b) Rod A2

Figure 3-37. Measured and predicted centerline temperature for IFA-515.10 rods A1 (UO_2) and A2 (UO_2-8% Gd_2O_3) (burnup=80 GWd/MTU, as-fabricated radial gap=25 μm)

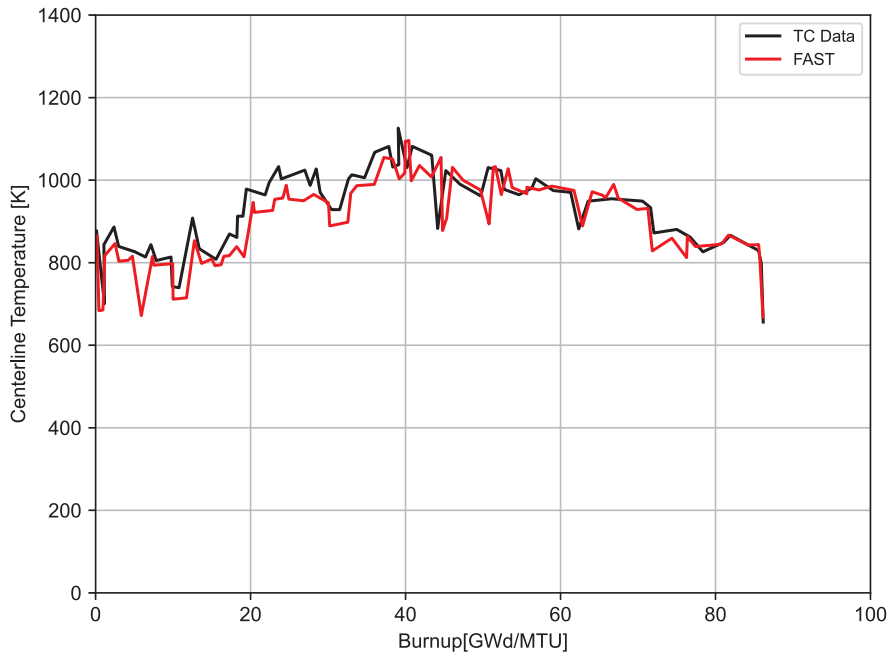

(a) Rod B1

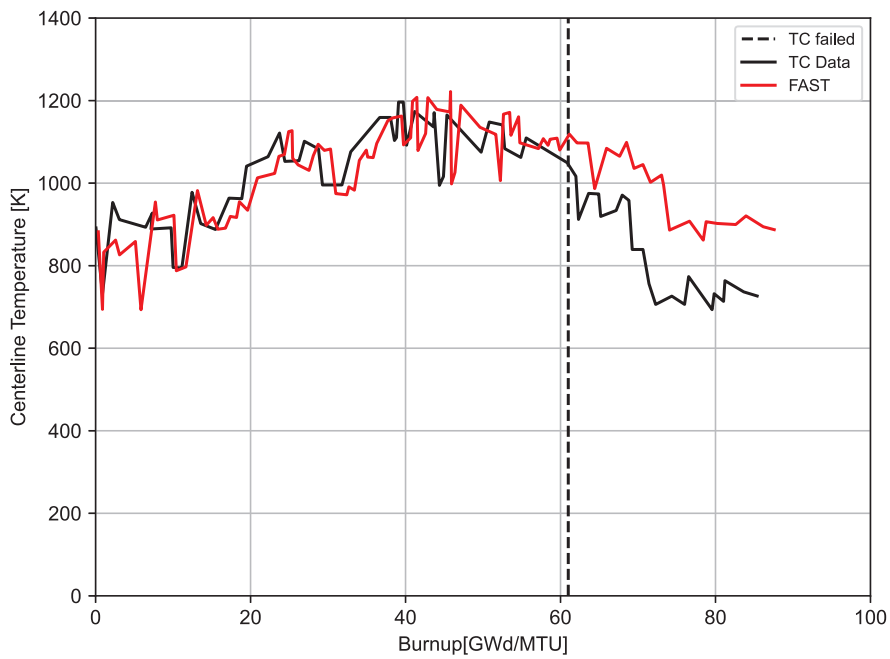

(b) Rod B2

Figure 3-38. Measured and predicted centerline temperature for IFA-515.10 rods B1 (UO_2) and B2 (UO_2-8% Gd_2O_3) (burnup=80 GWd/MTU, as-fabricated radial gap=25 µm)

Figures 3-39 and 3-40 show the measured and predicted centerline temperature for IFA-636 rods 2 and 4. These rods contain standard Gd (no Gd depletion like IFA-515.10), so the release version

of FAST could be used. Rod 2 was equipped with a centerline thermocouple, and the data from this thermocouple is shown in Figure 3-39. Rod 4 contains solid pellets, and the data shown in Figure 3-40 is estimated from rod 2. Because rod 4 does not have a direct measurement of temperature (no thermocouple), there is more uncertainty in the data because this is estimated by Halden using the rod 2 temperature data and correcting for no thermocouple hole. In addition, as the Gd is burning out during the first rise to power, there is a high level of uncertainty on the reported rod power. Because of this, FAST may not predict the centerline temperature well during this period. These figures show excellent agreement between the FAST predictions and the data for rod 2 and significant under-prediction (175 K, 15% relative) between 4 and 10 GWd/MTU and reasonable agreement above 10 GWd/MTU for rod 4, which has greater uncertainty.

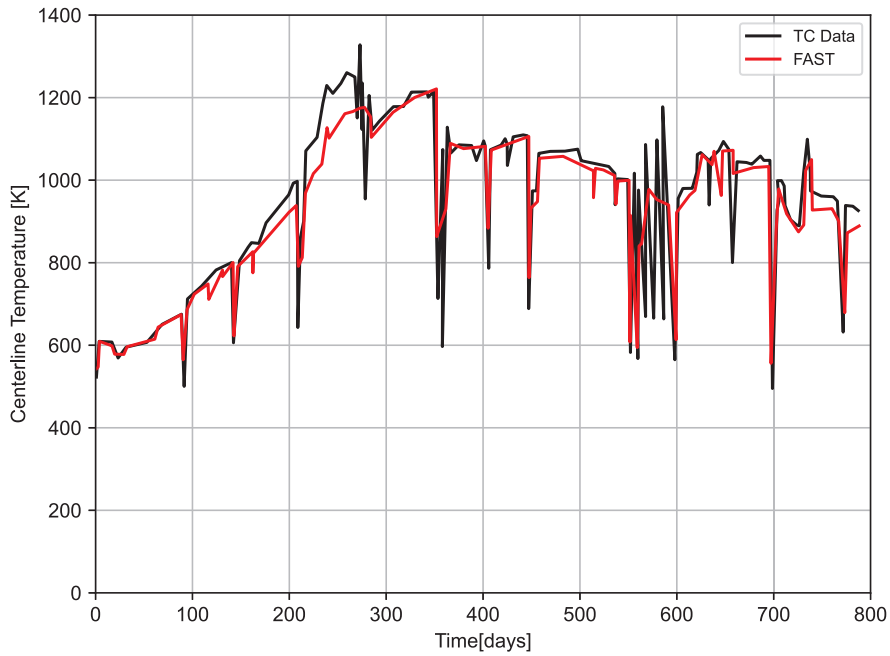

Figure 3-39. Measured and predicted centerline temperature for IFA-636 rod 2 (UO_2-8% Gd_2O_3) (burnup=25 GWd/MTU, as-fabricated radial gap=77 μm)

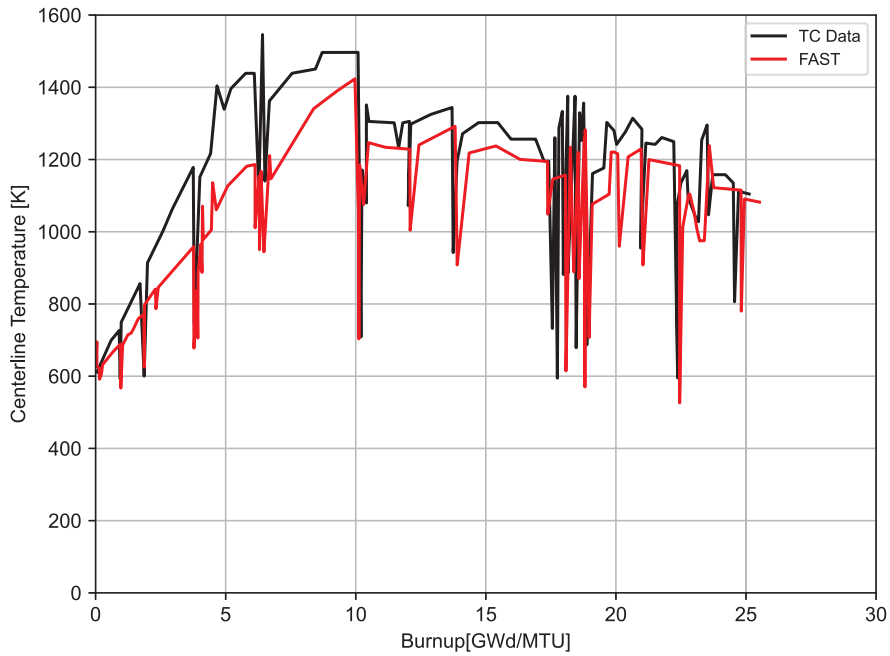

Figure 3-40. Measured and predicted centerline temperature for IFA-636 rod 4 (UO_2-8% Gd_2O_3) (burnup = 25 GWd/MTU, as-fabricated radial gap = 77 μm)

Figures 3-41 through 3-46 show the measured and predicted centerline temperature for IFA-681 rods 1, 2, and 3 with centerline thermocouples and rods 4, 5, and 6 with hollow pellets and expansion thermometers. Rods 1 and 5 are UO_2 rods; rods 2 and 4 contain standard Gd with 2 wt% Gd_2O_3; rods 3 and 6 contain standard Gd with 8 wt% Gd_2O_3. Since these rods contain standard Gd, the release version of FAST could be used. During the first rise to power, as the Gd is burning out, there is a high level of uncertainty on the reported rod power. Because of this, FAST may not predict the centerline temperature well during this period. This does not significantly affect future predictions because power levels while the Gd is burning out are low and will not cause significant FGR that will affect future temperature predictions.

These figures show excellent agreement between the FAST predictions and the data for rod 1 (UO_2, Figure 3-41) and 2 (2 wt% Gd_2O_3, Figure 3-42). For rod 3 (8 wt% Gd_2O_3, Figure 3-43), the FAST predictions are in excellent agreement with the data for the first 200 days. After this, FAST over-predicts the data by up to 120 K (13% relative). The reason for this is not clear, as both the power and the FAST temperature prediction increase during this time period, but the measured temperature does not increase with increasing power. For the hollow pellet rods, the 2 wt% Gd_2O_3 rods (IFA-681 rod 4 in Figure 3-44 and rod 5 in Figure 3-45) is uniformly under-predicted by about 50-90 K (4-7% relative) while the 8 wt% Gd_2O_3 rod (IFA-681 rod 6, Figure 3-46) is predicted well. These differences are well within the uncertainty of temperature measurement and power levels.

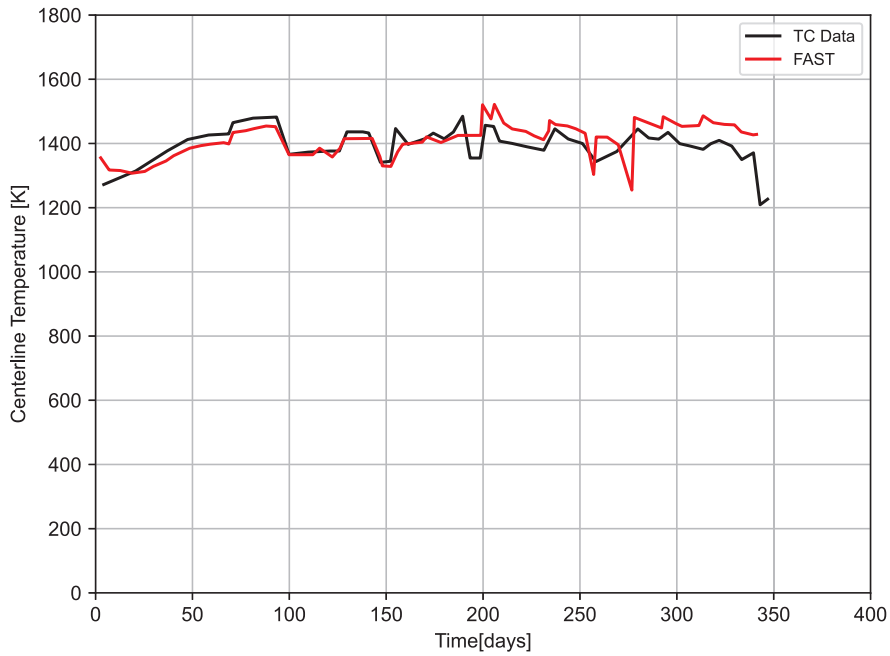

Figure 3-41. Measured and predicted centerline temperature for IFA-681 rod 1 (UO_2) (burnup = 24 GWd/MTU, as-fabricated radial gap = 85 µm)

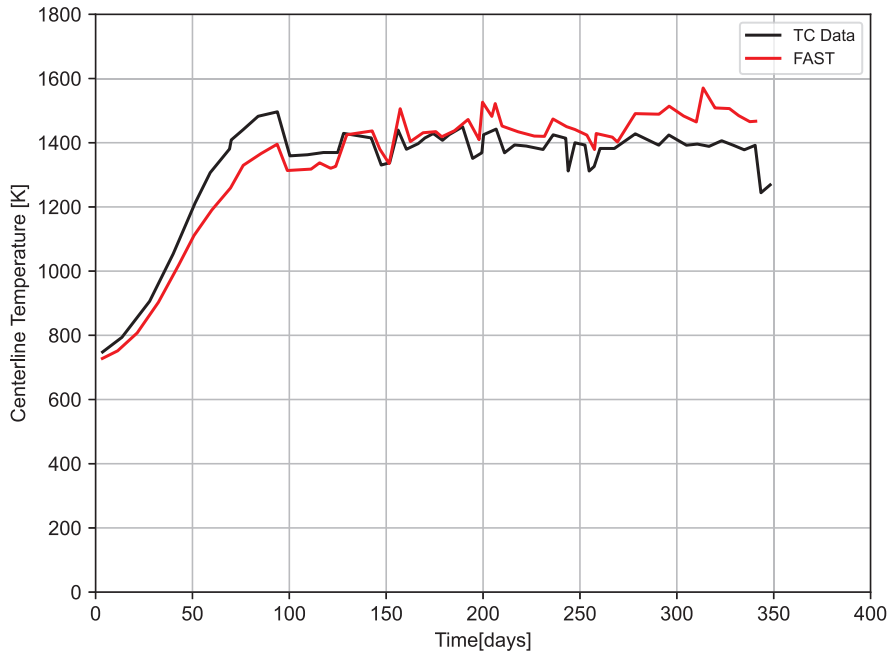

Figure 3-42. Measured and predicted centerline temperature for IFA-681 rod 2 (UO_2-2% Gd_2O_3) (burnup = 23 GWd/MTU, as-fabricated radial gap = 85 µm)

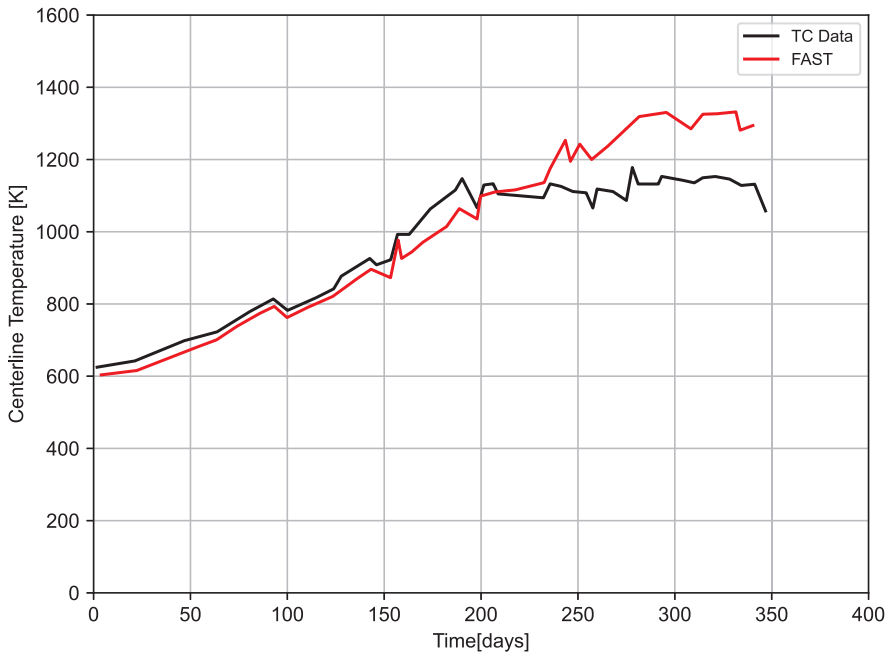

Figure 3-43. Measured and predicted centerline temperature for IFA-681 rod 3 (UO_2-8% Gd_2O_3) (burnup = 12 GWd/MTU, as-fabricated radial gap=85 µm)

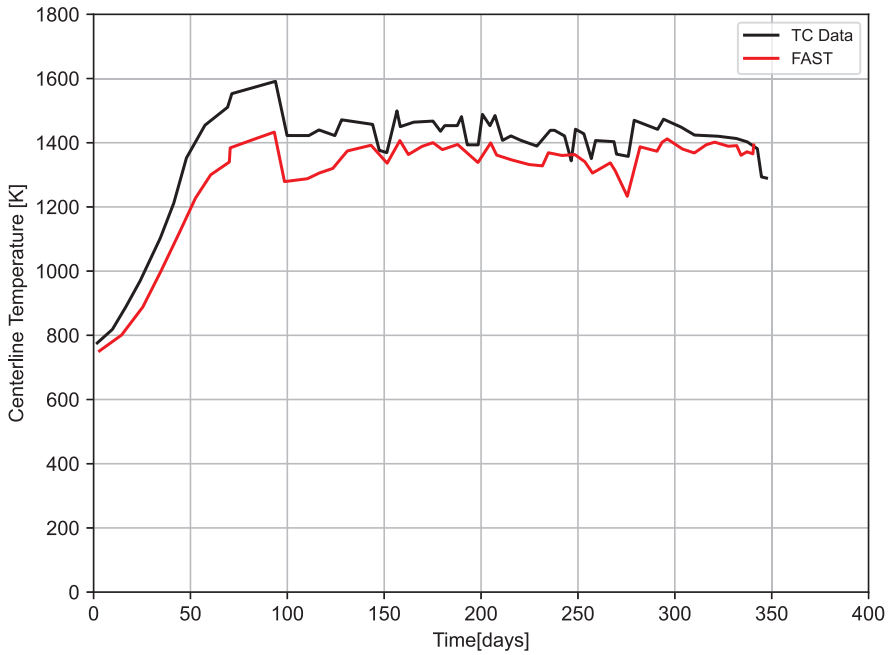

Figure 3-44. Measured and predicted centerline temperature for IFA-681 rod 4 (UO_2-2% Gd_2O_3) (burnup = 22 GWd/MTU, as-fabricated radial gap = 85 µm)

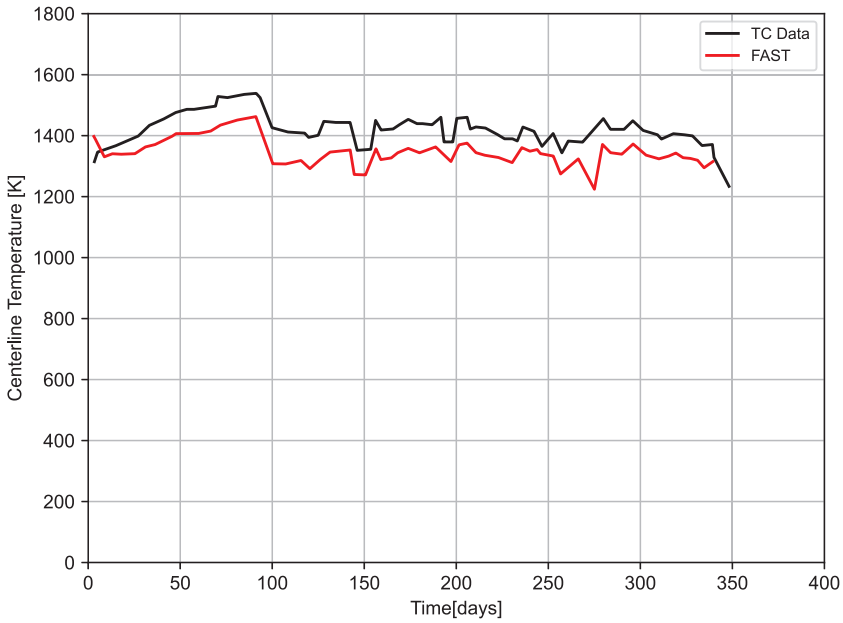

Figure 3-45. Measured and predicted centerline temperature for IFA-681 rod 5 (UO_2) (burnup = 23 GWd/MTU, as-fabricated radial gap = 85 µm)

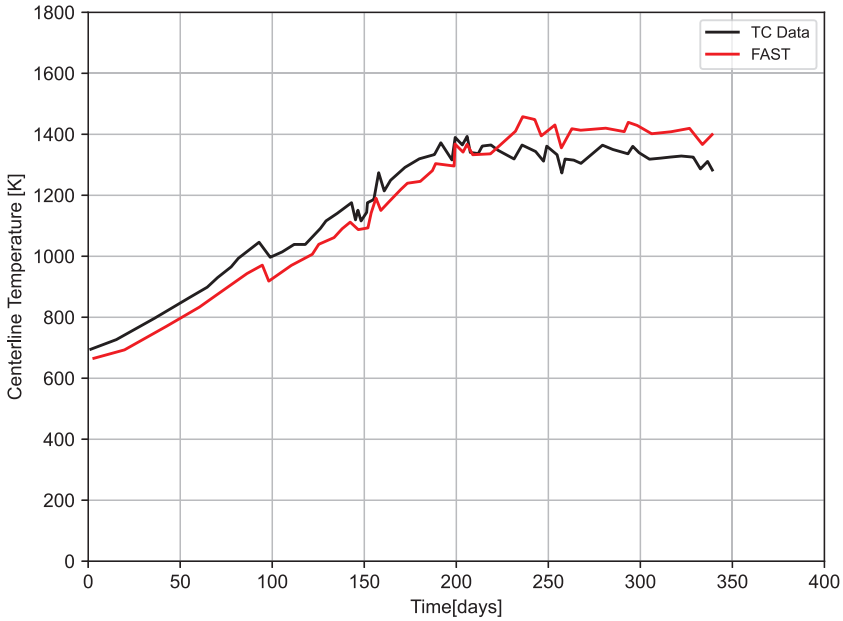

Figure 3-46. Measured and predicted centerline temperature for IFA-681 rod 6 (UO_2-8% Gd_2O_3) (burnup = 13 GWd/MTU, as-fabricated radial gap = 85 µm)

This section demonstrates that FAST continues to provide a best-estimate prediction of centerline temperature for UO_2-Gd_2O_3 rods to within a standard error of 5.8% for recent experimental data.

3.3 Constituent Redistribution

Experimental data from electron probe microanalysis (EPMA) of metal U-Pu-Zr rods irradiated in the Experimental Breeder Reactor II (EBR-II) are available for use in the assessment for constituent redistribution, and power history data is available for these rods from the Metallic Fuels Irradiation & Physics Database (FIPD) (Galloway et al. 2015; Hirschhorn et al. 2021; Yacout et al. 2021). This data takes the form of the zirconium mass fraction and radius for each reading. A set of four fuel rod cases are assessed to cover both binary and ternary cases for a range of burnups:

1. EBR-II fuel rod DP-11: U-10Zr fuel with 7.7 at.% burnup.
2. EBR-II fuel rod DP-81: U-10Zr fuel with 3.6 at.% burnup.
3. EBR-II fuel rod DP-16: U-19Pu-10Zr fuel with 10.0 at.% burnup.
4. EBR-II fuel rod T-179: U-19Pu-10Zr fuel with 1.9 at.% burnup.

Figures 3-47 through 3-50 show the comparison between the experimental data and the FAST model for these four rods, respectively.

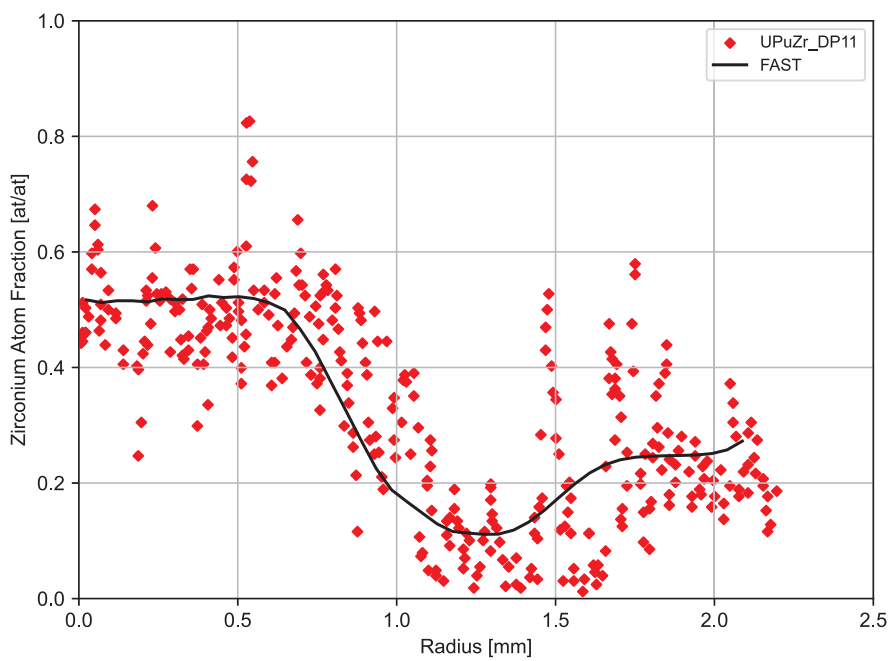

Figure 3-47. Measured and predicted zirconium distribution for EBR-II Rod DP-11 (U-10Zr, burnup = 7.7 at.%)

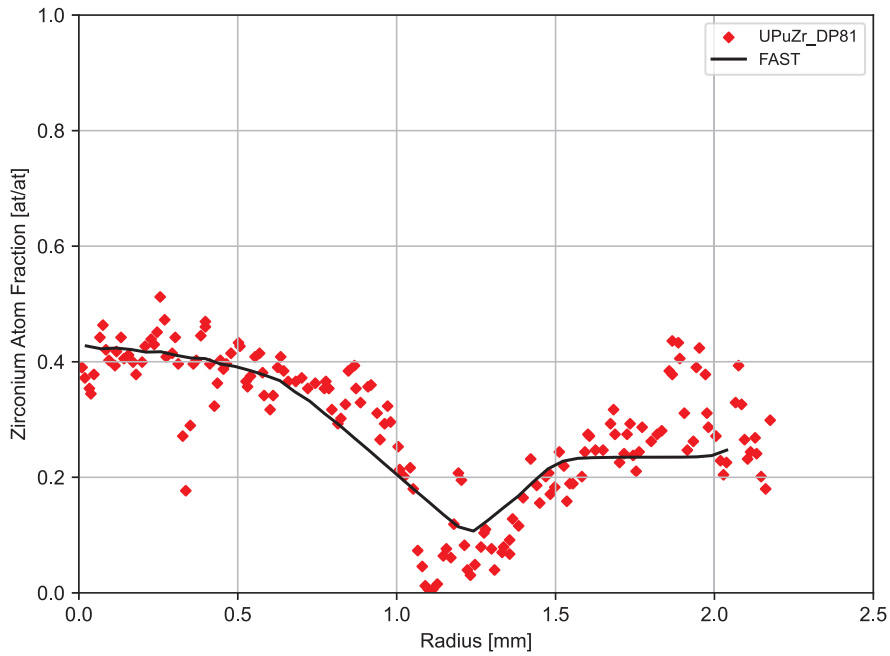

Figure 3-48. Measured and predicted zirconium distribution for EBR-II Rod DP-81 (U-10Zr, burnup = 3.5 at.%)

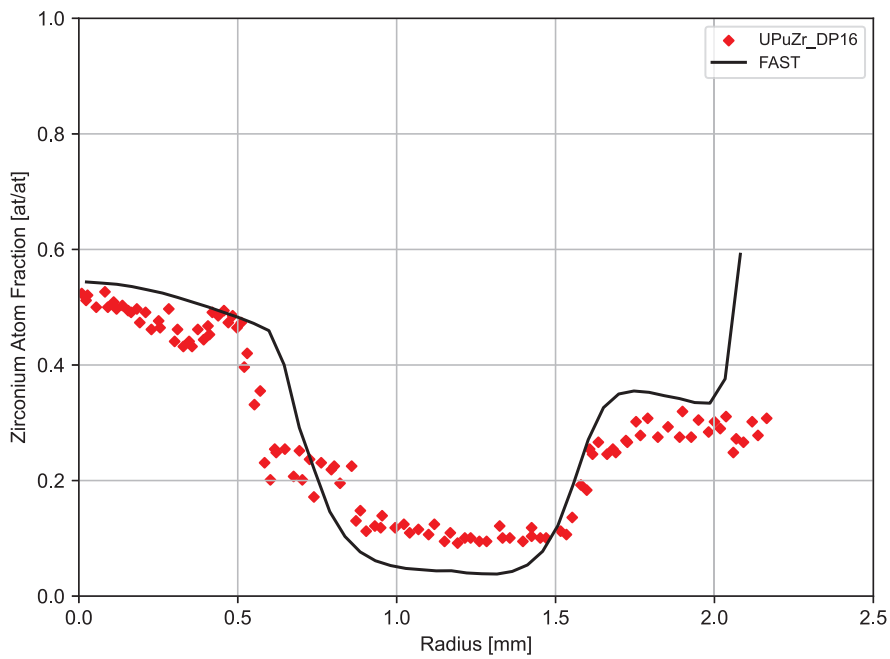

Figure 3-49. Measured and predicted zirconium distribution for EBR-II Rod DP-16 (U-19Pu-10Zr, burnup = 10.0 at.%)

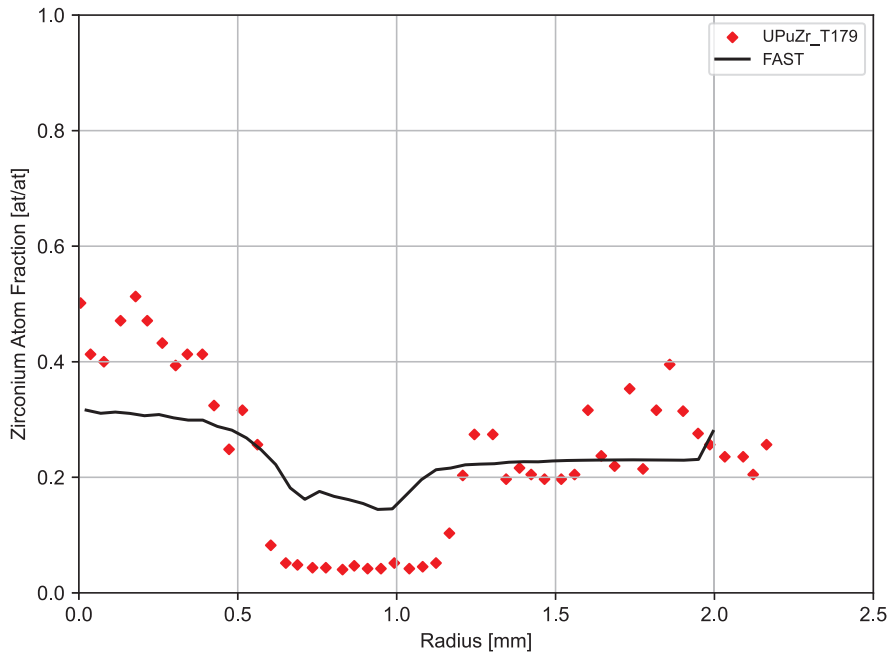

Figure 3-50. Measured and predicted zirconium distribution for EBR-II Rod T-179 (U-19Pu-10Zr, burnup = 1.9 at.%)

The binary fuel cases DP-11 and DP-81 show good agreement between the experimental data and the FAST model as the model predictions fall within the data distribution for most radii. The ternary fuel cases show good agreement between the experimental data and the FAST model for the phase boundaries but show some deviations for the Zr atom fractions in each phase, with the model tending to underestimate the degree of redistribution for the low burnup T-179 case and overestimate the degree of redistribution for the high burnup DP-16 case.

This page intentionally blank.

4.0 Fission Gas Release Assessment

4.1 Assessment of Steady-State FGR Predictions

An accurate prediction of FGR is important for two reasons: 1) it has a significant impact on the prediction of gap conductance and, therefore, fuel temperatures (e.g., as demonstrated in Section 3.2, an over-prediction of FGR can result in an over-prediction of fuel temperatures, and the converse is also true), and 2) it is necessary for the calculation of rod internal pressures that affect LOCA analyses and EOL rod pressures. In many cases, for current operating plants, the limits on and analyses of EOL rod pressures determine the LHGR limits for commercial fuel at burnups greater than 30 GWd/MTU. In addition, the NRC requires that these EOL rod pressure analyses include bounding normal operation transients (e.g., xenon transients lasting several hours) and AOOs (e.g., overpower transients lasting several minutes to hours). Therefore, the accurate prediction of transient FGR under conditions of power increases above steady-state operation is important for licensing analyses.

The code's ability to predict FGR in UO_2 fuel has been assessed based on comparisons to FGR data from 41 UO_2 fuel rods with power histories that are relatively steady-state through the rod's irradiation life and 19 UO_2 rods with power bumping (increase in rod power) at EOL to simulate an overpower AOO or normal operational transients. The code's ability to predict FGR in MOX fuel has been assessed based on comparisons to FGR data from 34 MOX fuel rods with power histories that are relatively steady-state through the rod's irradiation life and 8 MOX rods with power bumping (increase in rod power) at EOL to simulate an overpower AOO or normal operational transients. The fuel rods with greater than 5% FGR were selected because the limiting rods in terms of EOL rod pressure in today's plants (particularly for power uprated plants) have releases above 10% FGR.

Four fuel rods with UO_2-Gd_2O_3 fuel were available for assessment of the code's ability to predict FGR in UO_2-Gd_2O_3 fuel. This is not a large database, but these comparisons seem to indicate that FAST will predict FGR from UO_2-Gd_2O_3 fuel well. This is consistent with the observation that the measured FGR from UO_2-Gd_2O_3 rods is similar to the FGR from UO_2 rods with the same power history (Hirai et al. 1995).

The assessment in this section has used the default FGR model in the MASSIH subroutine in the code that is based on a modified release model proposed by (Forsberg and Massih 1985). This release model is described in Volume 1 of this report (Geelhood, Colameco, et al. 2026). The other FGR models in FAST (i.e., ANS-5.4 and FRAPFGR) provide reasonable predictions of FGR for fuel rods with steady-state power histories, but on average under-predicted FGR for fuel rods with power bumping for a few hours duration.

The following discussions are divided into comparisons of the code predictions to steady-state FGR data and to power bumping (transient) FGR data.

4.1.1 UO_2 Steady-State FGR Predictions

Figure 4-1 shows the predicted FGR as a function of measured FGR for the steady-state UO_2 rods. Figure 4-2 shows the predicted minus measured FGR as a function of burnup for the steady-state

UO_2 rods.

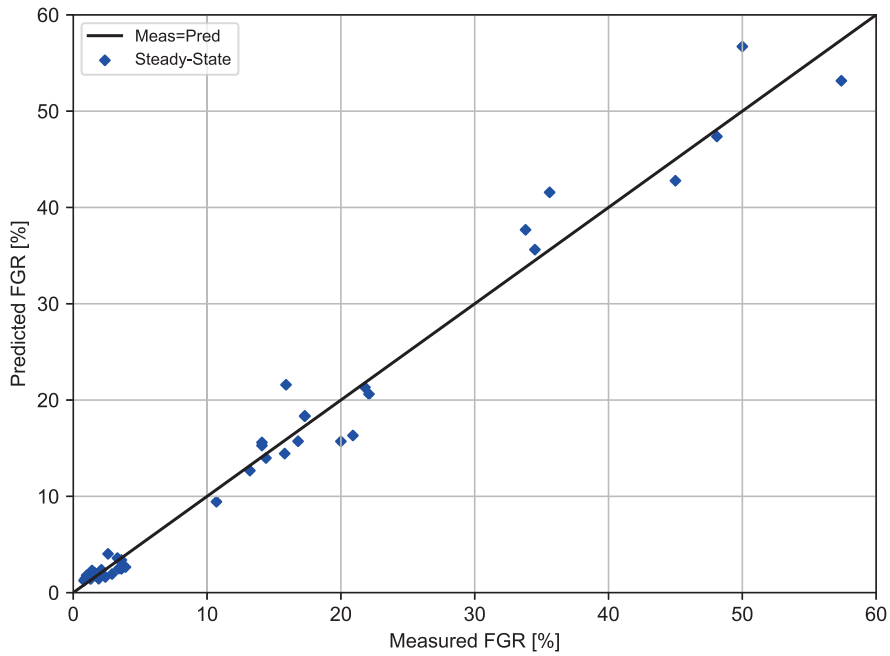

Figure 4-1. Comparison of FAST predictions to measured FGR data for the UO_2 steady-state assessment cases

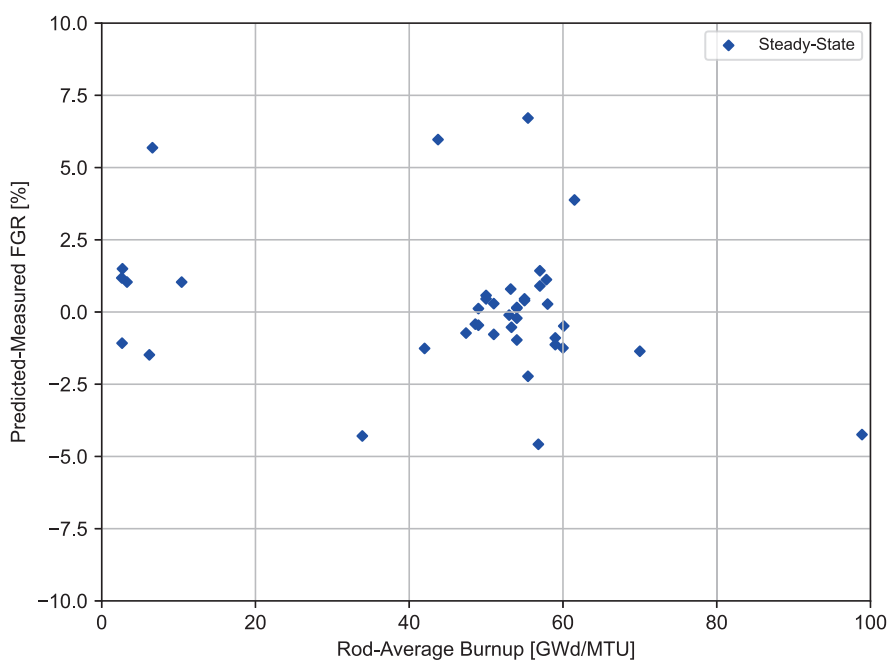

Figure 4-2. Predicted minus measured FGR versus rod-average burnup for the UO_2 steady-state assessment cases

The steady-state UO_2 cases with measured and predicted FGRs are shown in Table 4-1. The standard error for the steady-state predictions is 2.32% absolute FGR up to 70 GWd/MTU. These figures demonstrate that FAST provides a best-estimate calculation of fission gas over a wide range of gas release levels up to a rod-average burnup of 62 GWd/MTU. There are a few cases at higher burnup, but these cases indicated that FAST may begin to under-predict FGR at burnup levels beyond 62 GWd/MTU (Figure 4-2).

Table 4-1. Steady-state UO_2 FGR assessment cases

Rod	Rod-Average Burnup (GWd/MTU)	Measured FGR (%)	FAST-1.2.2 Predicted FGR (%)
24-I-6	60.1	21.8	21.31
36-I-8	61.5	33.8	37.68
111-I-5	48.6	14.4	13.98
28-I-6	53.3	13.2	12.67
HBEP BNFL-DE	42	10.7	9.44
LFF	3.29	17.3	18.34
CBP	2.61	14.1	15.28
4110-AE2	6.2	22.1	20.62
4110-BE2	6.6	15.9	21.59
332	56.8	20.9	16.32
EPL-4	10.4	17.3	18.33
CBR	2.7	14.1	15.60
CBY	2.65	16.8	15.72
HBEP BNFL5-DH	33.9	20	15.71
FUMEX 6f	55.45	45±5.00	42.77
FUMEX 6s	55.45	50±5.00	56.71
IFA 597.3	70	15.8	14.44
IFA429DH	98.9	57.4	53.16
ANO TSQ002	53.2	1	1.79
Oconee 15309	50	0.8	1.25
30-I-8	57.85	34.5	35.62
M2-2C	43.75	35.6	41.57
PA29-4	47.39	48.1	47.37
30AK09	53	1.9	1.79
30AD05	54	1.8	1.93
30AE14	54	1.8	1.96
30AP02	49	1.9	1.44
5K7P02	51	2.4	1.63

Table continued on next page

Table 4-1. Steady-state UO_2 FGR assessment cases (continued)

Rod	Rod-Average Burnup (GWd/MTU)	Measured FGR (%)	FAST-1.2.2 Predicted FGR (%)
5K7C05	57	2.6	4.03
5K7K09	54	2.9	1.93
6U3K09	55	1.6	2.00
6U3L08	55	1.6	2.05
6U3O05	58	2.1	2.37
6U3M03	57	1.4	2.30
6U3P16	50	0.9	1.47
3F9N05	54	3.6	3.39
3F9P02	49	1.3	1.42
3D8E14	59	3.6	2.47
3A1F05	51	3.3	3.59
F35P17	60	3.9	2.65
F35K13	59	3.4	2.50

4.1.2 MOX Steady-State FGR Predictions

Figure 4-3 shows the predicted FGR as a function of measured FGR for the steady-state MOX rods. Figure 4-4 shows the predicted minus measured FGR as a function of burnup for the steady-state MOX rods.

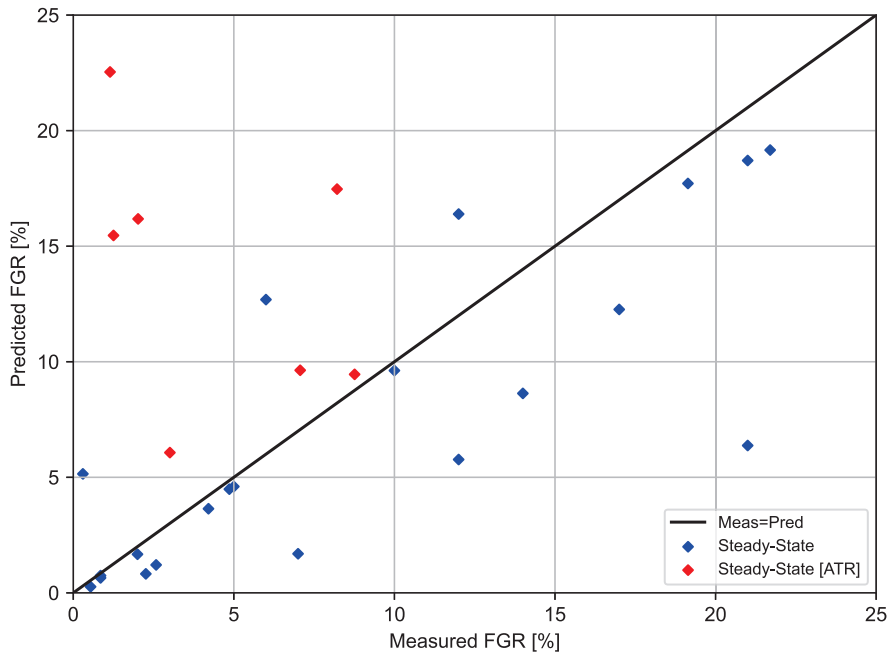

Figure 4-3. Comparison of FAST predictions to measured FGR data for the MOX steady-state assessment cases

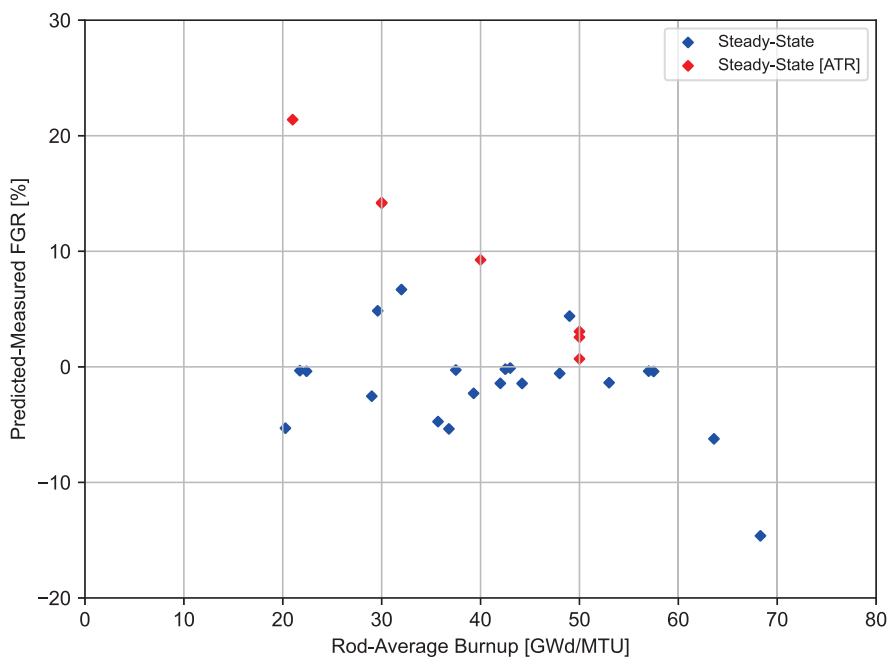

Figure 4-4. Predicted minus measured FGR versus rod-average burnup for the MOX steady-state assessment cases

The steady-state MOX cases with measured and predicted FGRs are shown in Table 4-2. The

standard error for the steady-state predictions is 6.5% FGR. It is noted that some of these MOX rods are from the Advanced Test Reactor (ATR) at Idaho National Laboratory and are subject to large radial flux profiles. Because of this, it is difficult to estimate the rod-average power. If the ATR rods are removed from the calculation of standard error, a standard error of 4.3% absolute FGR is calculated. These figures demonstrate that FAST provides a best-estimate calculation of fission gas over a wide range of gas release levels up to a rod-average burnup of 62 GWd/MTU. There are a few cases at higher burnup, but these cases indicated that FAST may begin to under-predict FGR at burnup levels beyond 62 GWd/MTU (Figure 4-4).

Table 4-2. Steady-state MOX FGR assessment cases

Rod	Rod-Average Burnup (GWd/MTU)	Measured FGR (%)	FAST-1.2.2 Predicted FGR (%)
IFA-651.1r1	22.41	10*	9.62
IFA-651.1r3	21.73	2*	1.67
IFA-651.1r6	20.27	7*	1.69
ATR PII C2 P5	21.00	1.146	21.75
ATR PIII C3 P6	30.00	1.253	15.46
ATR PIII C10 P13	30.00	2.019	16.43
ATR PIV C4 P7	40.00	8.214	17.47
ATR PIV C5 P8	50.00	3.009	6.07
ATR PIV C6 P9	50.00	7.066	9.63
ATR PIV C12 P15	50.00	8.761	9.49
Gravelines N06	48.00	4.210	3.64
Gravelines N12	57.00	4.860	4.49
Gravelines P16	53.00	2.580	1.21
IFA-629.1	29.00	21.700	19.16
IFA-606 Phase 2	49.00	12.000	16.39
IFA 633.1r6	32.00	6.000	12.69
M504 H8	37.50	0.540	0.26
M504 I2	43.00	0.850	0.75
M504 K9	42.50	0.850	0.65
M504 M9	44.20	2.260	0.82
M308 Segment 2	57.50	5.000	4.60
IFA-597.4/.5/.6/.7r10	35.70	17.000	12.26
IFA-597.4/.5/.6/.7r11	36.80	14.000	8.63
IFA-629.3r5	68.30	21.000	6.38

* EOL FGR estimated from rod pressure data (larger error than data from puncture)

Table continued on next page

Table 4-2. Steady-state MOX FGR assessment cases (continued)

Rod	Rod-Average Burnup (GWd/MTU)	Measured FGR (%)	FAST-1.2.2 Predicted FGR (%)
IFA-629.3r6	63.60	12.000	5.77
E09 Rods Inner	29.60	0.200	5.15
E09 Rods Inner	29.60	0.400	5.15
E09 Rods Intermediate	39.30	21.000	18.71
E09 Rods Intermediate	39.30	21.000	18.71
E09 Rods Outer	42.00	19.500	17.71
E09 Rods Outer	42.00	18.200	17.71
E09 Rods Outer	42.00	19.500	17.71
E09 Rods Outer	42.00	18.900	17.71
E09 Rods Outer	42.00	19.600	17.71

4.1.3 UO_2-Gd_2O_3 Steady-State FGR Predictions

The four steady-state UO_2-Gd_2O_3 cases with measured and predicted FGRs are shown in Table 4-3. The standard error for these four predictions is 0.32% absolute FGR. Based on this comparison, it appears that the modified Massih model employed by FAST to describe FGR for UO_2 fuels can provide reasonable predictions for FGR from UO_2-Gd_2O_3 fuel. It is noted that the burnup range is limited (37-39 GWd/MTU) and the gas release values are small. Therefore, it cannot be fully confirmed that this conclusion will hold for high burnup. However, this observation is consistent with previous studies conducted by (Delorme et al. 2012) and (Arana et al. 2012). Delorme studied an irradiated M5-clad fuel rod containing UO_2 doped with 8 wt% Gd. The rod average burnup was 39.2 GWd/MTU and exhibited 0.51% FGR. Although an enhanced high burnup structure was observed and attributed to the chemical effect of Gd additions, the FGR data was consistent with UO_2 rods irradiated to similar levels of burnup, although the measured FGR values are very low. Arana characterized the FGR from fuel rods subjected to high duty conditions in Vandellos II as part of a High Burnup Program (PAQ). Gd-doped rods containing 2 and 8 wt% Gd were irradiated to $\sim$50 and 55 MWd/kgU under high power and high burnup conditions, respectively. The FGR data from these rods were consistent with the FGR data measured from UO_2 pellets under similar power levels.

Table 4-3. Steady-State UO_2-Gd_2O_3 FGR Assessment Cases

Rod	Rod-Average Burnup (GWd/MTU)	Measured FGR (%)	FAST-1.2.2 Predicted FGR (%)
GAIN 301	38.8	0.23	0.56
GAIN 302	37.9	0.19	0.39
GAIN 701	38.9	0.98	0.75
GAIN 701	38.9	0.66	0.35

4.2 Assessment of Power-Ramped FGR Predictions

4.2.1 UO_2 Power-Ramped FGR Predictions

Figure 4-5 shows the predicted FGR as a function of measured FGR for the power-ramped UO_2 rods.

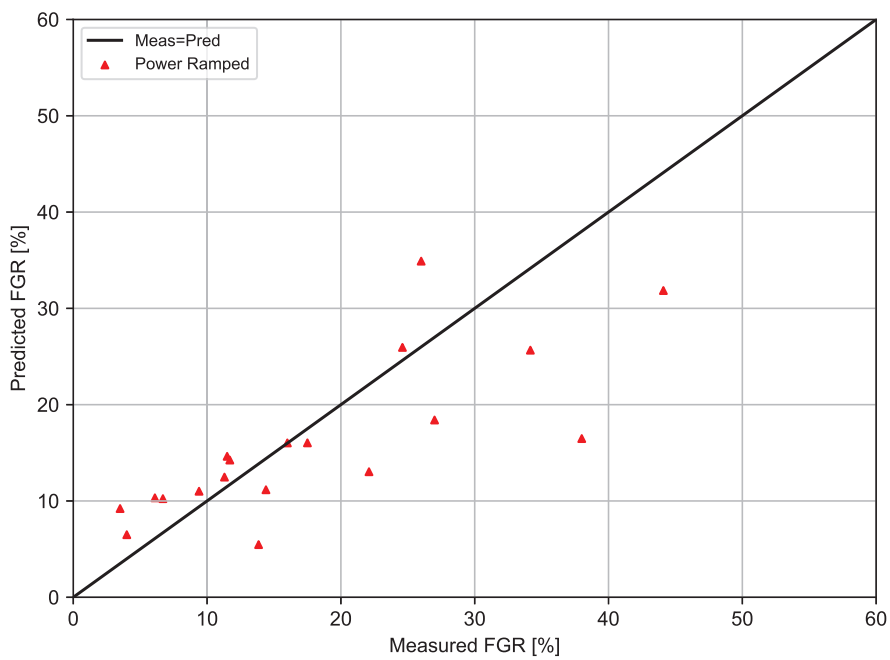

Figure 4-5. Comparison of FAST predictions to measured FGR data for the UO_2 power-ramped assessment cases

Figure 4-6 shows the predicted minus measured FGR as a function of burnup for the power-ramped UO_2 rods.

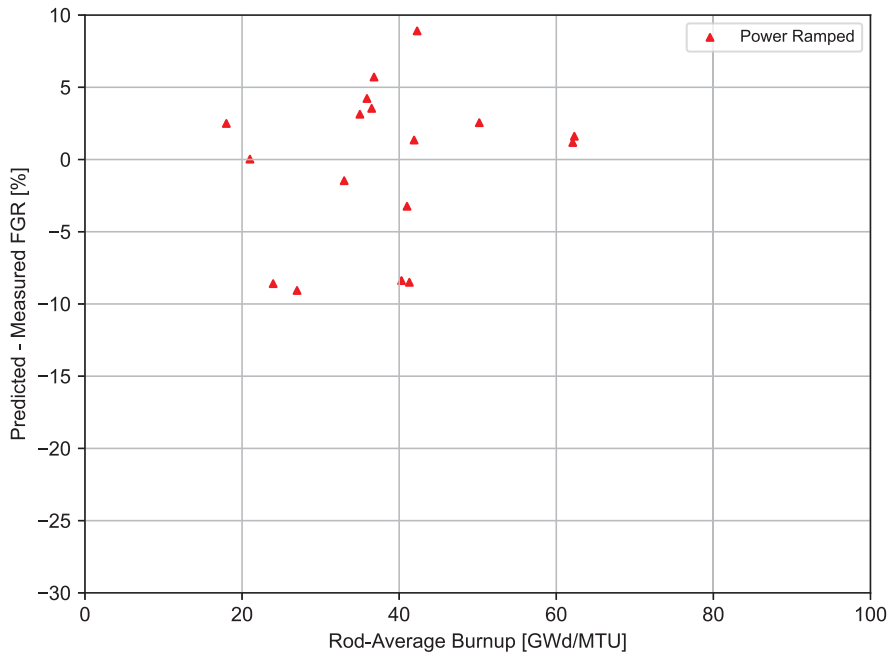

Figure 4-6. Predicted minus measured FGR Versus rod-average burnup for the UO_2 power-ramped assessment cases

The power-ramped UO_2 cases with measured and predicted FGRs are shown in Table 4-4. These comparisons show that the code provides a good prediction of the transient FGR data except for the two High Burnup Effects Program (HBEP) rods, D200 and D226, which are under-predicted by 21.5% and 12.2% release, respectively. The fuel in both of these rods is considered atypical of today's fuel used in commercial rods because it is prone to significant fuel densification ($>$2.5% theoretical density (TD)), unlike the less densification prone (stable) fuel ($<$1.5% TD) of current fuel designs. In addition, there is evidence that fuel with significant densification releases more fission gas than current stable fuel. The standard deviation for the power-ramped predictions without D200 and D226 is 5.5% absolute FGR. These figures demonstrate that FAST provides a best-estimate calculation of fission gas over a wide range of gas release levels up to a rod-average burnup of 62 GWd/MTU.

Table 4-4. Power-ramped UO_2 FGR assessment cases

Rod	Rod-Average Burnup (GWd/MTU)	Measured FGR (%)	FAST-1.2.2 Predicted FGR (%)
HBEP D200	25.00	38.00	16.48
HBEP D226	44.00	44.10	31.85
pk6-2	36.80	3.50	9.21
pk6-3	36.50	6.70	10.24
pk6-S	35.90	6.10	10.33
Inter Ramp Rod 16	21.00	16.00	16.03
Inter Ramp Rod 18	18.00	4.00	6.50
RISØ f14-6.in	27.00	22.10	13.04
RISØ f7-3.in	35.00	11.50	14.64
RISØ f9-3.in	33.00	17.50	16.04
RISØ ge2	41.90	24.60	25.95
RISØ ge4	23.96	27.00	18.41
RISØ ge6	42.29	26.00	34.91
RISØ ge7	41.00	14.40	11.16
B&W Studsvik R1	62.30	9.40	11.01
B&W Studsvik R3	62.10	11.30	12.48
RISØ AN1	41.30	34.16	25.66
RISØ AN8	40.30	13.85	5.47
regate	50.20	11.70	14.25

Normal operational transients typically last between 4 and 12 hours, while AOO power transients last less than 30 minutes. Because both of these types of transients can lead to FGR, the NRC requires that both be included in the rod internal pressure analyses to demonstrate that they meet the no cladding liftoff criterion for establishing a rod pressure limit. In general, the short hold time AOO transient results in the lower FGR. However, the burst release typically seen in transients on the order of less than 30 minutes appears to be increasing with increasing burnups, particularly above 62 GWd/MTU, such that the code may be under-predicting release for short time period transients at high burnup. Future code verification will examine FGR data with power ramps of short duration.

4.2.2 MOX Power-Ramped FGR Predictions

Figure 4-7 shows the predicted FGR as a function of measured FGR for the power-ramped MOX rods.

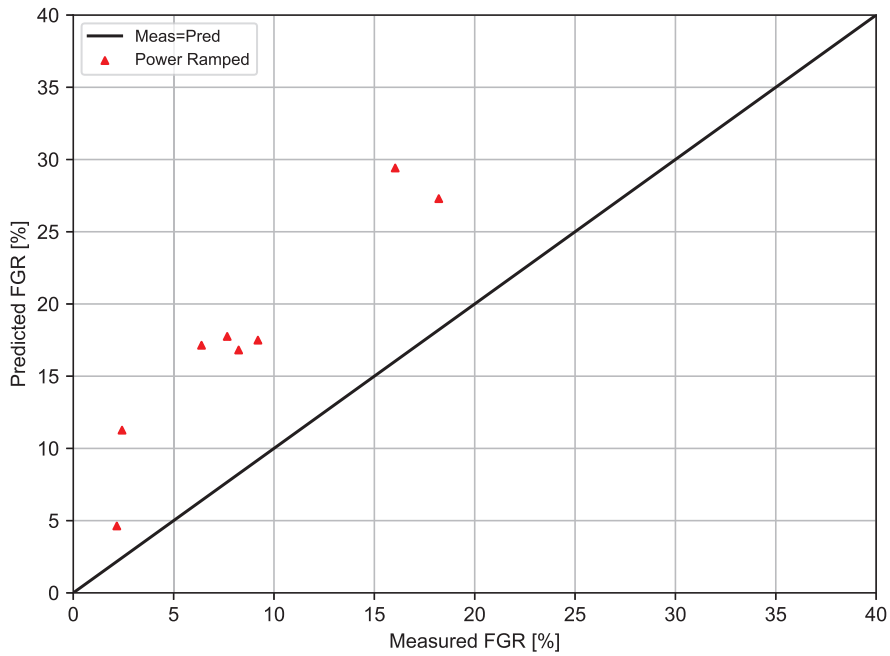

Figure 4-7. Comparison of FAST predictions to measured FGR data for the MOX power-ramped assessment cases

Figure 4-8 shows the predicted minus measured FGR as a function of burnup for the power-ramped MOX rods.

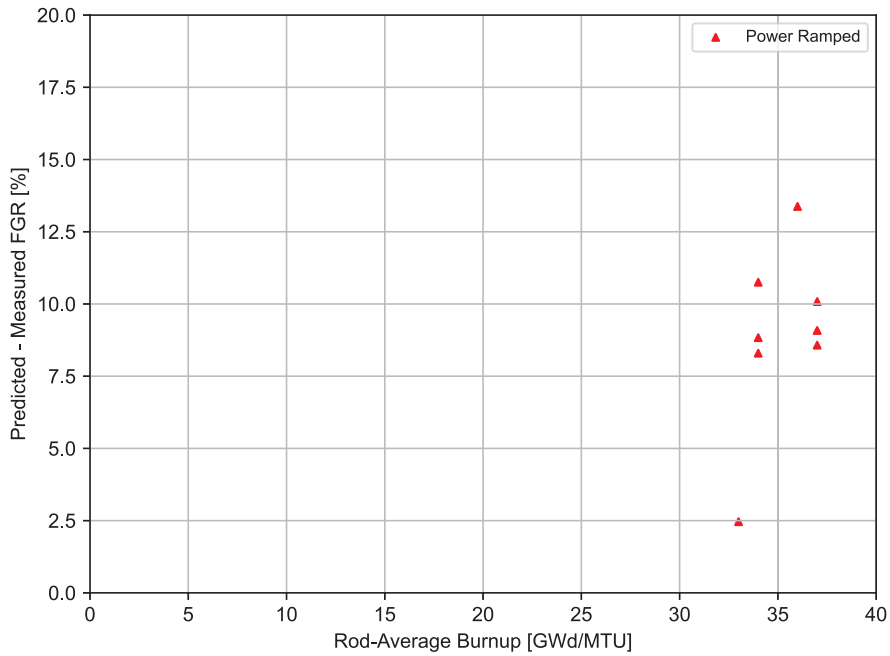

Figure 4-8. Predicted minus measured FGR Versus rod-average burnup for the MOX power-ramped assessment cases

The power-ramped MOX cases with measured and predicted FGRs are shown in Table 4-5. The standard error for the power-ramped predictions is 10.0% absolute FGR and the average deviation (bias) is 8.9% absolute FGR. These figures demonstrate that FAST tends to over-predict the gas release measurement for power-ramped MOX rods. However, it is noted that a limited number of power-ramped rods from only one experimental program are represented here. In addition, it is conservative to over-predict FGR during a power ramp.

Table 4-5. Power-ramped MOX FGR assessment cases

Rod	Rod-average burnup (GWd/MTU)	Measured FGR (%)	FAST-1.2.2 Predicted FGR (%)
M501 HR-1	37	7.67	17.75
M501 HR-2	37	8.24	16.81
M501 HR-3	37	18.21	27.29
M501 HR-4	36	16.04	29.42
M501 MR-1	34	2.43	11.27
M501 MR-2	34	9.20	17.50
M501 MR-3	34	6.39	17.14
M501 MR-4	33	2.17	4.63

5.0 Internal Rod Void Volume Assessment

5.1 Fuel Rod Void Volume

An accurate prediction of the internal void volume of a fuel rod is important in the calculation of the internal rod pressures along with the FGR prediction. The change in the fuel rod void volume with burnup is primarily due to the combined effects of cladding creep, fuel swelling, and axial cladding growth. Nine well characterized fuel rods were selected to assess the capability of FAST to accurately calculate fuel rod void volumes for high burnup. The cases selected include 26 full-length rods (rod TSQ002 from ANO-2; rod 15309 from Oconee; rods 2AH3-D15, 2AH3-D12, 0AH5-E14, 07R2D5, AL06-D6, and AD23-D5 from Ringhals 2 and 3; and 18 rods from North Anna) and three short (44 in long) rods (36-I-8, 111-I-5, and 24-I-6) that were irradiated in the BR-3 reactor. The Ringhals 3 rods were clad in Optimized ZIRLO; rods 6U3-, 3F9-, and 3D8- from North Anna were clad in ZIRLO; the Ringhals 2 rods and the 30A- and 5K7- rods from North Anna were clad in M5; rod 3A1F05 was clad in low tin Zircaloy-4; and the remaining rods were clad with standard Zircaloy-4. All are PWR rods. The burnup levels achieved on these rods range from 33.3 to 62.95 GWd/MTU.

Table 5-1 presents the measured and FAST-calculated void volume at both BOL and EOL for the eleven fuel rods. The calculations were made at 25 °C (77 °F) and atmospheric pressure, which should be reasonably close to the temperature at which the data were collected. A range of values for void volume is provided for Oconee rod 15309 because this is the range of void volumes measured from 16 sibling fuel rods from the same assembly–including the representative rod 15309. All 16 rods have very similar EOL burnups and similar power histories. Therefore, the void volume range includes representative uncertainty in the fabricated void volumes, measured rod power histories, and burnup.

Table 5-1. Measured and calculated void volume for high-burnup fuels rods

Reactor	Rod	Burnup (GWd/MTU)	BOL Measured (in^3)	BOL Calculated (in^3)	EOL Measured (in^3)	EOL Calculated (in^3)
BR-3	36-I-8	61.5	NA	0.639	0.508	0.656
BR-3	111-I-5	48.6	NA	0.642	0.516	0.582
BR-3	24-I-6	60.1	NA	0.640	0.491	0.593
ANO-2	TSQ002	53.0	1.55	1.528	1.0876	1.126
Oconee	15309	49.5 to 49.9	2.14	2.119	1.600 - 1.700	1.546
Ringhals 3	2AH3-D15	34.1	NA	1.228	0.946	0.916
Ringhals 3	2AH3-D12	33.3	NA	1.691	1.080	1.240
Ringhals 3	0AH5-E14	57.82	NA	1.276	0.946	0.943
Ringhals 2	07R2D5	62.0	NA	1.283	0.793	0.960
Ringhals 2	AL06-D6	27.97	NA	1.487	1.220	1.180
Ringhals 2	AD23-D5	62.95	NA	1.444	1.080	0.986

Table continued on next page

Table 5-1. Measured and calculated void volume for high-burnup fuels rods (continued)

Reactor	Rod	Burnup (GWd/MTU)	BOL Measured (in^3)	BOL Calculated (in^3)	EOL Measured (in^3)	EOL Calculated (in^3)
North Anna	30AK09	53	NA	1.157	0.604	0.786
North Anna	30AD05	54	NA	1.157	0.649	0.800
North Anna	30AE14	54	NA	1.157	0.671	0.801
North Anna	30AP02	49	NA	1.157	0.659	0.763
North Anna	5K7P02	51	NA	1.157	0.683	0.800
North Anna	5K7C05	57	NA	1.157	0.592	0.871
North Anna	5K7K09	54	NA	1.157	0.641	0.831
North Anna	6U3K09	55	NA	1.208	0.719	0.798
North Anna	6U3L08	55	NA	1.208	0.757	0.800
North Anna	6U3O05	58	NA	1.208	0.775	0.809
North Anna	6U3M03	57	NA	1.208	0.726	0.807
North Anna	6U3P16	50	NA	1.208	0.799	0.785
North Anna	3F9N05	54	NA	1.208	0.777	0.881
North Anna	3F9P02	49	NA	1.208	0.781	0.804
North Anna	3D8E14	59	NA	1.208	0.716	0.913
North Anna	3A1F05	51	NA	1.216	0.790	0.996
North Anna	F35P17	60	NA	1.164	0.813	0.863
North Anna	F35K13	59	NA	1.164	0.769	0.855

FAST predicts EOL void volume with a standard error of 14.8%, with an average over-prediction of 0.085 in^3.

6.0 Cladding Corrosion Assessment

Thirty-two well characterized fuel rods were selected to demonstrate the capability of FAST to accurately calculate fuel rod waterside oxidation for high burnup. The cases selected include thirty-two full-length rods (rod TSQ002 from ANO-2; rod 15309 from Oconee; rod A1 from bundle MTB99; rod H8/36-6 from TVO-1; rods A06, A12, and N05 from Vandellos II; and all rods from North Anna). The set includes both PWR and BWR fuel rods that are standard Zircaloy-4, low tin Zircaloy-4, ZIRLO, or M5 in PWRs and Zircaloy-2 in BWRs. (All but low tin Zircaloy-4 are cladding alloys currently modeled in FAST.) The rod-average burnup levels achieved on these rods range from 45 to 60 GWd/MTU. The corrosion and hydrogen pickup models in FAST have been compared to significantly more separate effects data (Geelhood and Beyer 2008, 2011) to demonstrate good predictions, but these cases are those with reported power histories and end-of-life measured oxide thickness.

FAST-calculated peak oxide layer thicknesses are bracketed by the choice of crud layer thickness for the PWR rods and are in good agreement for the two BWR rods. The purpose of these code-data comparisons is to demonstrate similar predictions as with standalone versions of the corrosion/hydriding models. The BWR peak corrosion values are fairly well matched by the FAST predictions, and these predictions are not as sensitive to the crud layer input because of the relatively lower heat fluxes and lower operating temperatures.

The conclusion is that the modeling of waterside oxidation is sufficient in FAST for best-estimate analyses. Using integral effect and separate effect data the following standard deviations for each alloy has been calculated or estimated as shown in (Geelhood and Beyer 2008).

- Zircaloy-2: σ =7.6 µm
- Zircaloy-4: σ =15.3 µm
- ZIRLO: σ =15 µm
- M5: σ =5 µm

6.1 BWR Cladding Corrosion

The only alloy currently used in the United States for BWR conditions is Zircaloy-2. The following assessment shows the FAST predictions of cladding corrosion for two commercial rods with Zircaloy-2.

6.1.1 Zircaloy-2 Corrosion

Table 6-1 shows the measured and FAST calculated peak oxide layer thickness for the two selected high burnup BWR rods.

Table 6-1. Peak oxide measured and calculated for two high burnup BWR fuel rods

Reactor	Rod	Burnup (GWd/MTU)	Measured (μm)	Calculated (μm)
Monticello	MTB99 rod A1	45.0	25	8
TVO-1	H8/36-6	51.4	28	22

These comparisons show FAST predicts peak cladding waterside oxidation under BWR conditions with a standard error of 18 μm and an average under-prediction of 11.5 μm.

6.2 PWR Cladding Corrosion

The alloys currently used in the United States for PWR conditions are Zircaloy-4, low-tin Zircaloy-4, ZIRLO, Optimized ZIRLO and M5. The following assessment shows the FAST predictions of cladding corrosion for four commercial rods with Zircaloy-4, two commercial rods with low tin Zircaloy-4, 14 commercial rods with ZIRLO, and 10 commercial rods with M5.

6.2.1 Zircaloy-4 Corrosion

Figures 6-1 through 6-4 show the measured and predicted corrosion layer thicknesses as a function of axial position along the rod for the four PWR rods with Zircaloy-4 cladding.

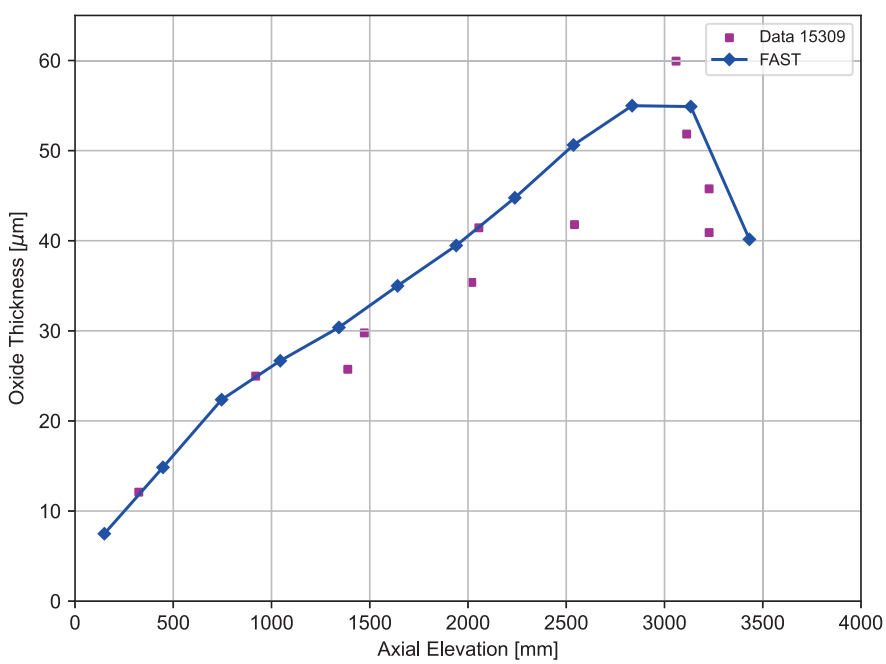

Figure 6-1. Measured and predicted corrosion layer thickness as a function of axial position for Oconee 5-cycle PWR Zircaloy-4 Rod 15309, 49.5 GWd/MTU (rod-average)

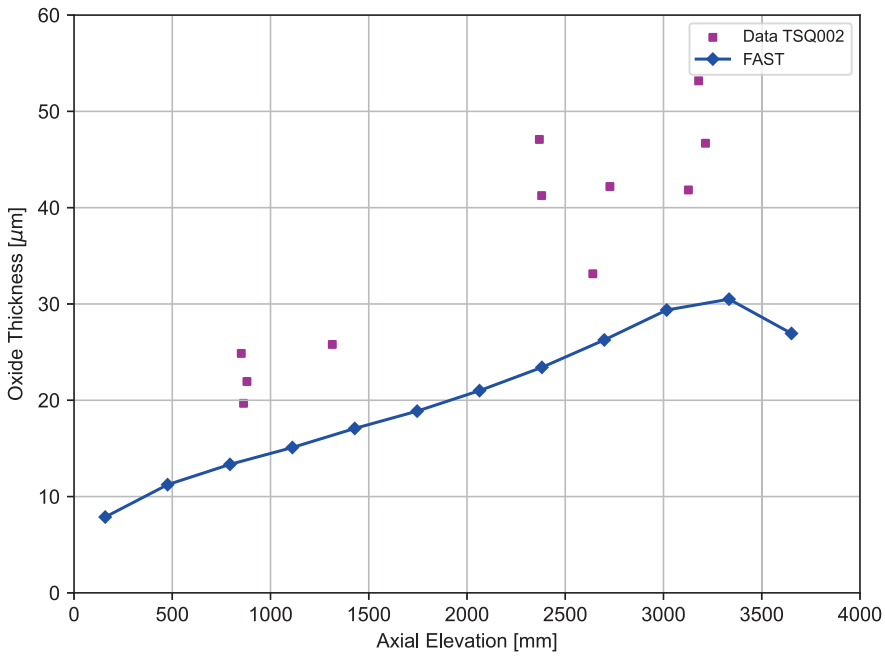

Figure 6-2. Measured and predicted corrosion layer thickness as a function of axial position for ANO-2 5-cycle PWR Zircaloy-4 Rod TSQ002, 53 GWd/MTU (rod-average)

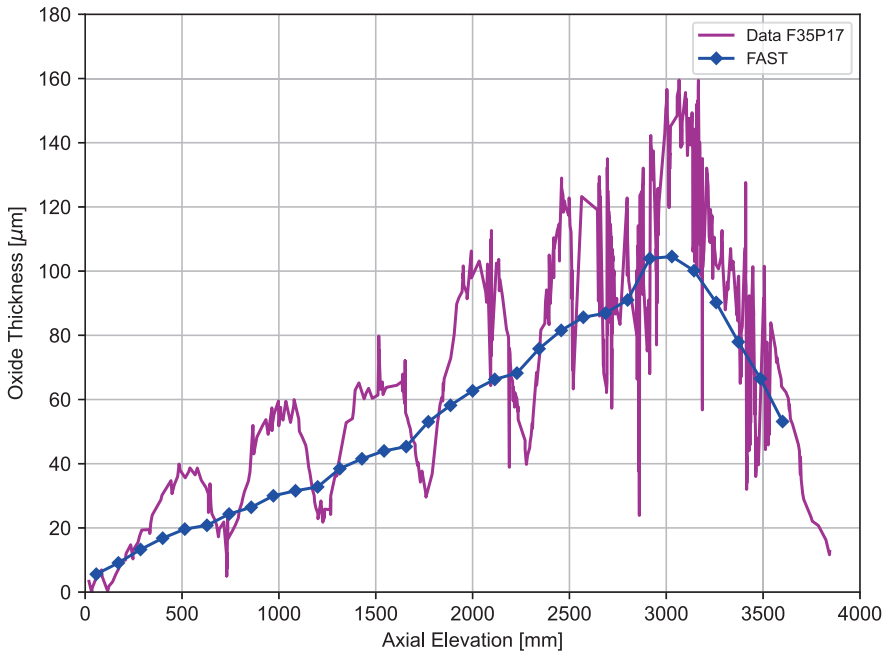

Figure 6-3. Measured and predicted corrosion layer thickness as a function of axial position for North Anna 4-cycle PWR Zircaloy-4 Rod F35P17, 60 GWd/MTU (rod-average)

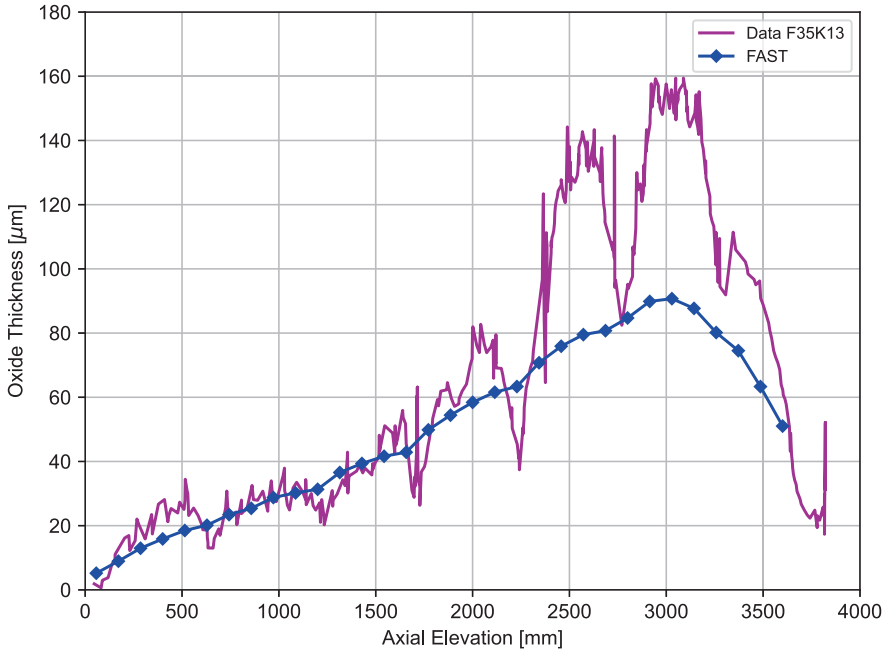

Figure 6-4. Measured and predicted corrosion layer thickness as a function of axial position for North Anna 4-cycle PWR Zircaloy-4 Rod F35K13, 59 GWd/MTU (rod-average)

FAST predicts peak cladding waterside oxidation of Zircaloy-4 under PWR conditions with a standard error of 52 µm and an average under-prediction of 38 µm.

6.2.2 Low Tin Zircaloy-4 Corrosion

Figures 6-5 and 6-6 show the measured and predicted corrosion layer thicknesses as a function of axial position along the rod for the two PWR rods with low tin Zircaloy-4 cladding.

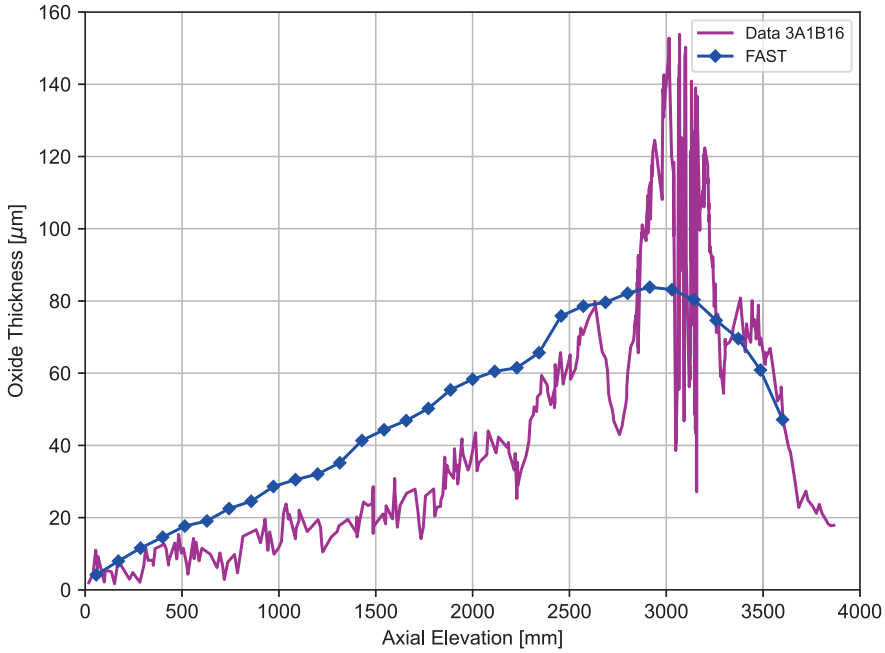

Figure 6-5. Measured and predicted corrosion layer thickness as a function of axial position for North Anna 3-cycle PWR low tin Zircaloy-4 Rod 3A1B16, 48 GWd/MTU (rod-average)

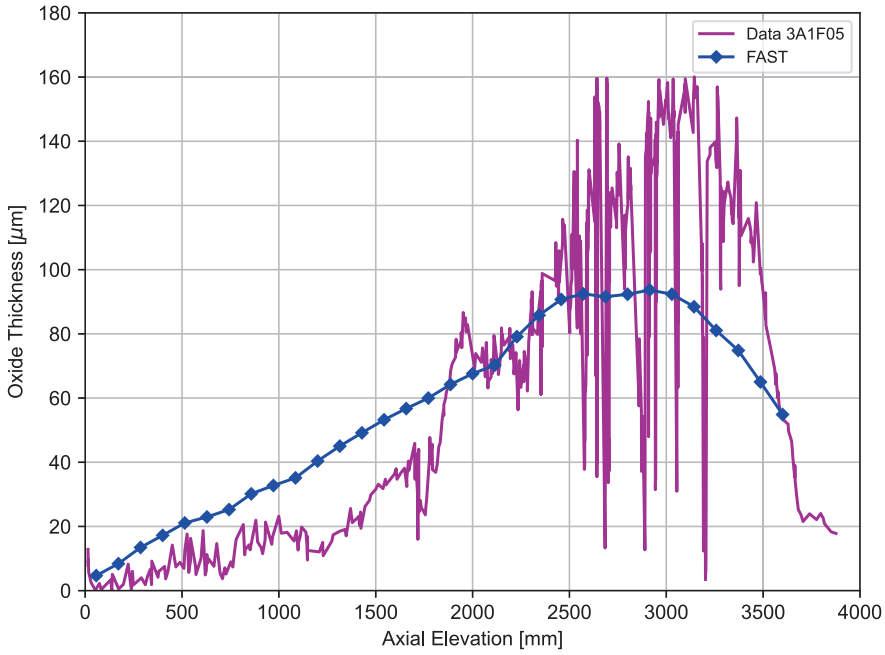

Figure 6-6. Measured and predicted corrosion layer thickness as a function of axial position for North Anna 3-cycle PWR low tin Zircaloy-4 Rod 3A1F05, 51 GWd/MTU (rod-average)

FAST predicts peak cladding waterside oxidation of low-tin Zircaloy-4 under PWR conditions with a standard error of 96 µm and an average under-prediction of 68 µm.

6.2.3 ZIRLO Corrosion

Figures 6-7 through 6-20 show the measured and predicted corrosion layer thicknesses as a function of axial position along the rod for the 14 PWR rods with ZIRLO cladding.

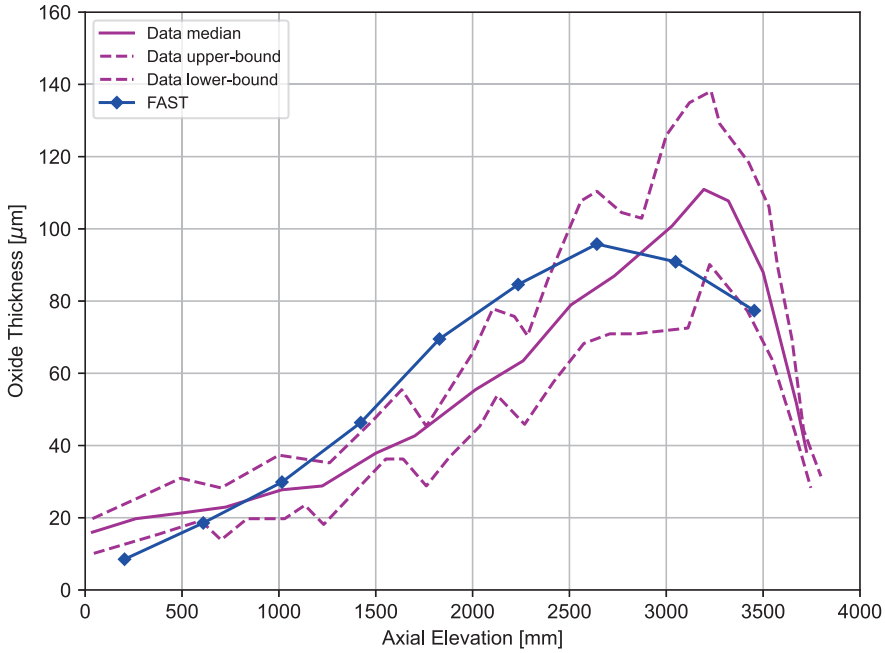

Figure 6-7. Measured and predicted corrosion layer thickness as a function of axial position for Gravelines 5-Cycle PWR ZIRLO Rod A06, 65.9 GWd/MTU (rod-average)

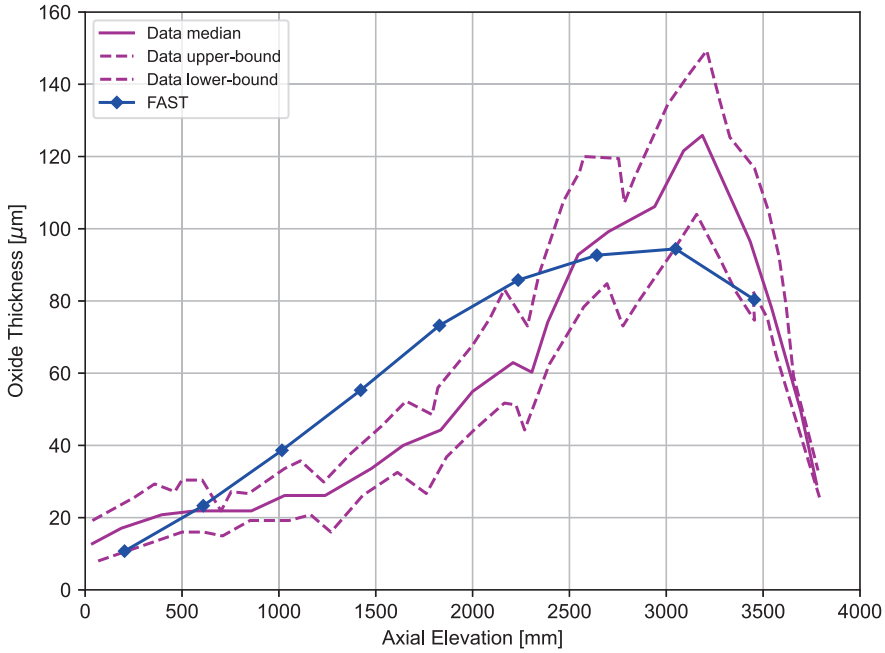

Figure 6-8. Measured and predicted corrosion layer thickness as a function of axial position for Gravelines 5-Cycle PWR ZIRLO Rod A12, 66.4 GWd/MTU (rod-average)

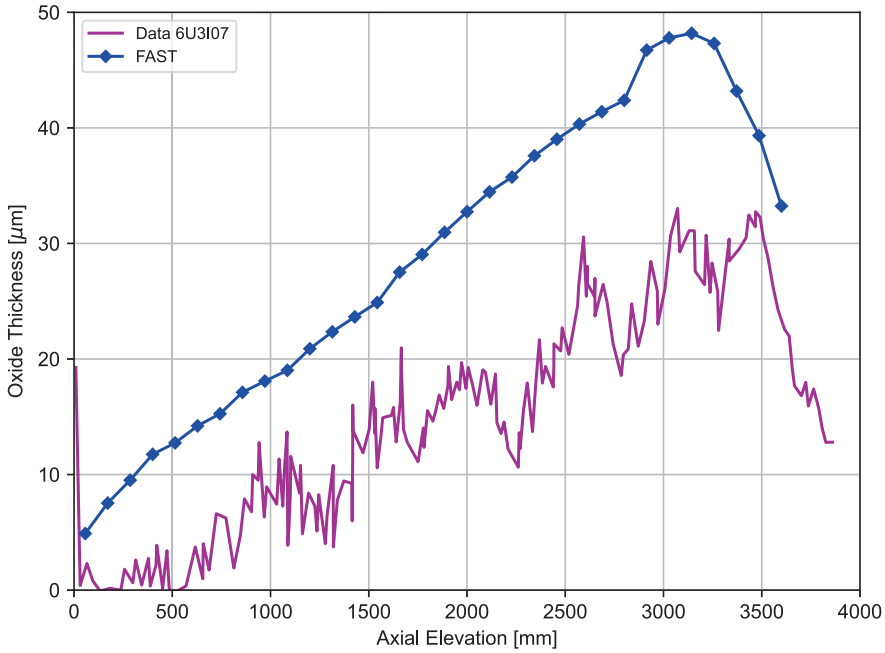

Figure 6-9. Measured and predicted corrosion layer thickness as a function of axial position for North Anna 3-Cycle PWR ZIRLO Rod 6U3I07, 54 GWd/MTU (rod-average)

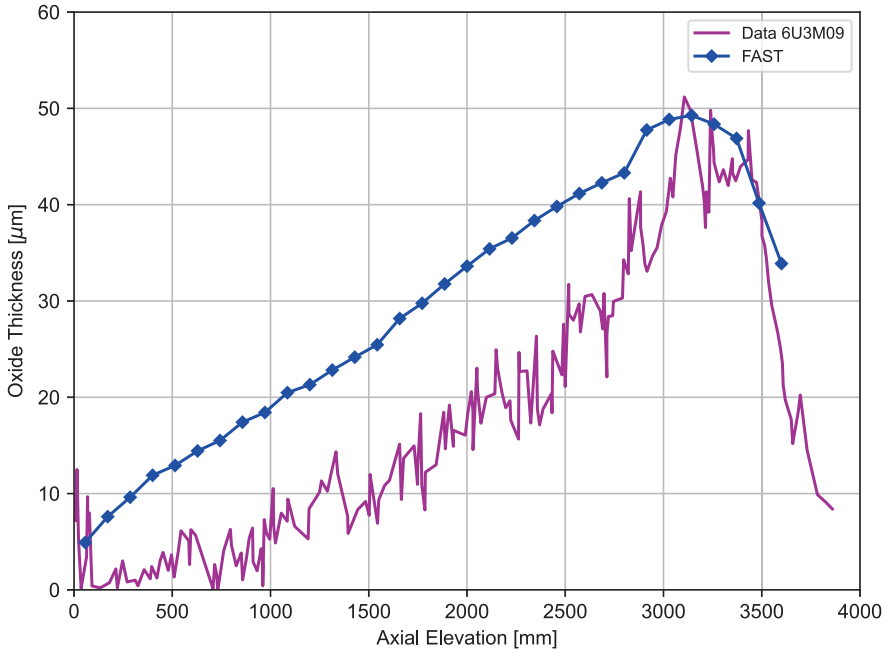

Figure 6-10. Measured and predicted corrosion layer thickness as a function of axial position for North Anna 3-Cycle PWR ZIRLO Rod 6U3M09, 55 GWd/MTU (rod-average)

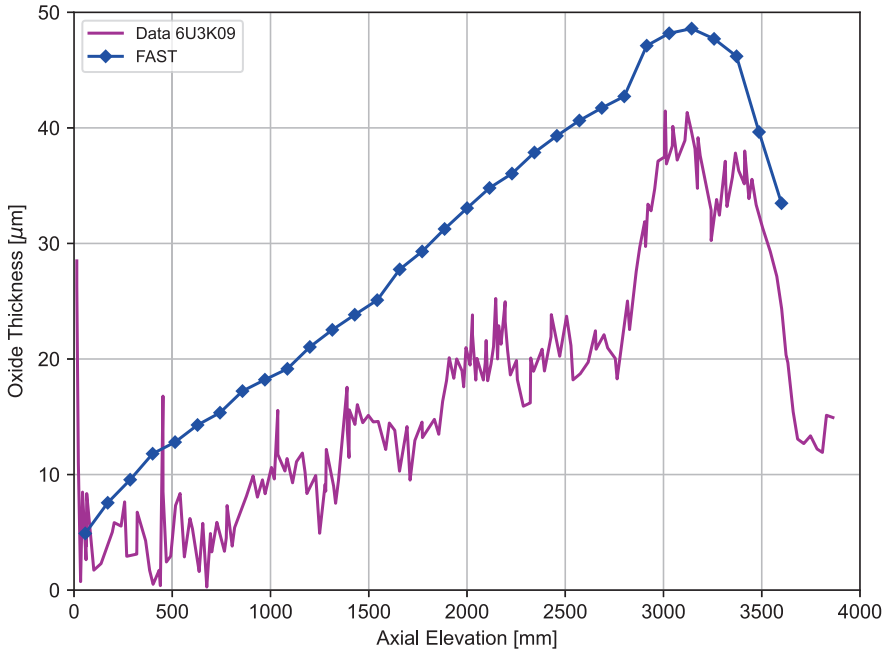

Figure 6-11. Measured and predicted corrosion layer thickness as a function of axial position for North Anna 3-Cycle PWR ZIRLO Rod 6U3K09, 54 GWd/MTU (rod-average)

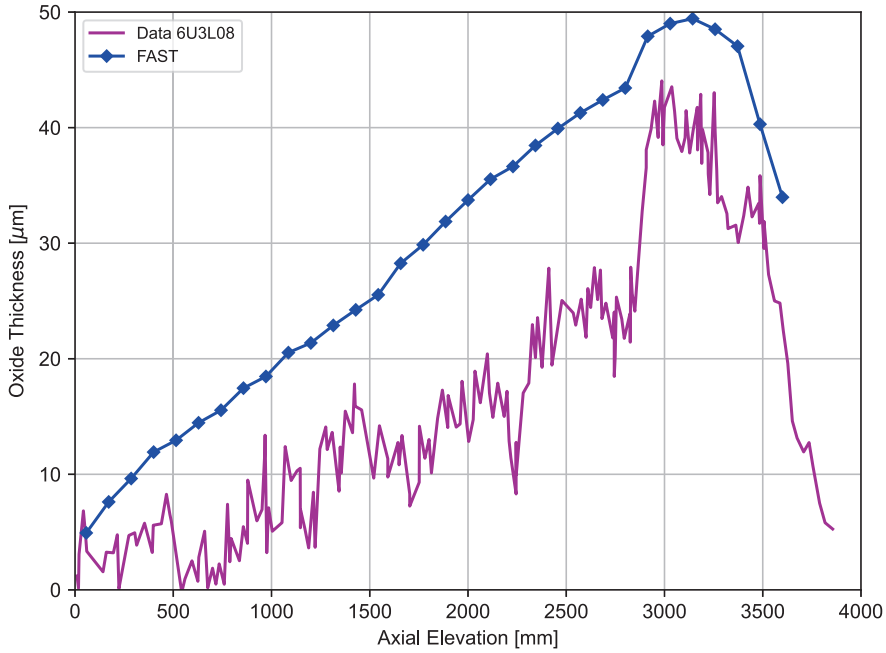

Figure 6-12. Measured and predicted corrosion layer thickness as a function of axial position for North Anna 3-Cycle PWR ZIRLO Rod 6U3L08, 55 GWd/MTU (rod-average)

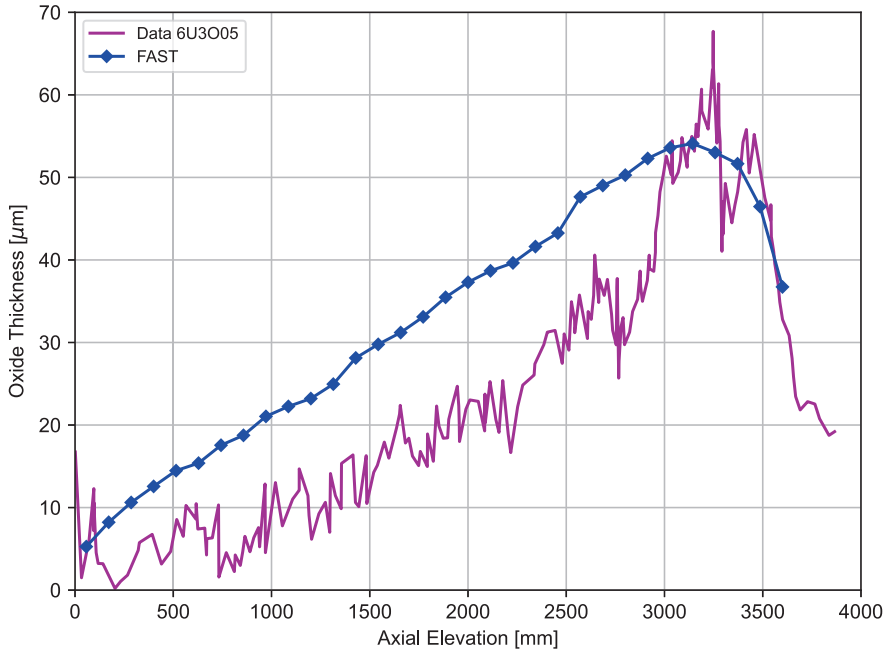

Figure 6-13. Measured and predicted corrosion layer thickness as a function of axial position for North Anna 3-Cycle PWR ZIRLO Rod 6U3O05, 58 GWd/MTU (rod-average)

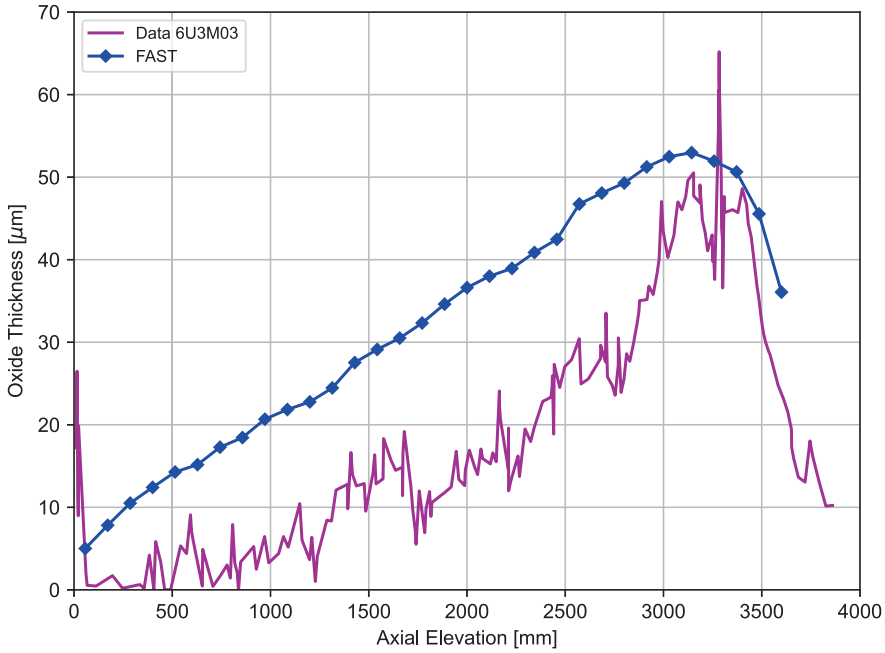

Figure 6-14. Measured and predicted corrosion layer thickness as a function of axial position for North Anna 3-Cycle PWR ZIRLO Rod 6U3M03, 57 GWd/MTU (rod-average)

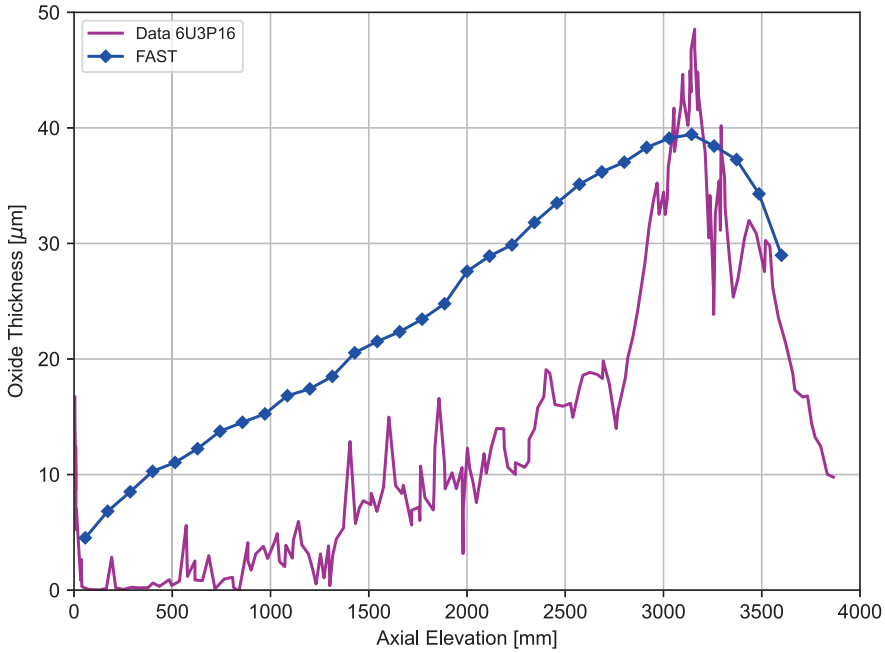

Figure 6-15. Measured and predicted corrosion layer thickness as a function of axial position for North Anna 3-Cycle PWR ZIRLO Rod 6U3P16, 50 GWd/MTU (rod-average)

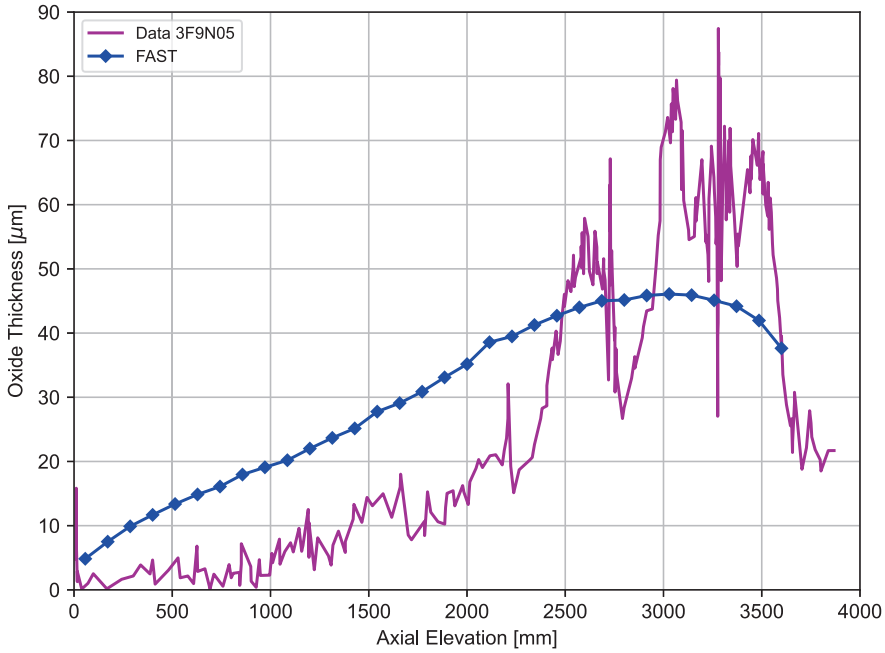

Figure 6-16. Measured and predicted corrosion layer thickness as a function of axial position for North Anna 3-Cycle PWR ZIRLO Rod 3F9N05, 54 GWd/MTU (rod-average)

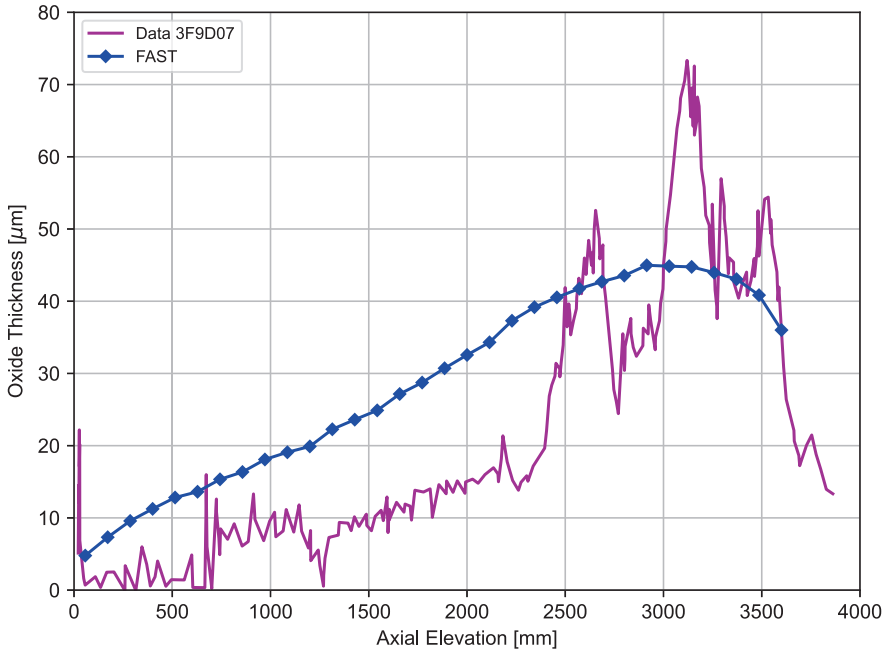

Figure 6-17. Measured and predicted corrosion layer thickness as a function of axial position for North Anna 3-Cycle PWR ZIRLO Rod 3F9D07, 52 GWd/MTU (rod-average)

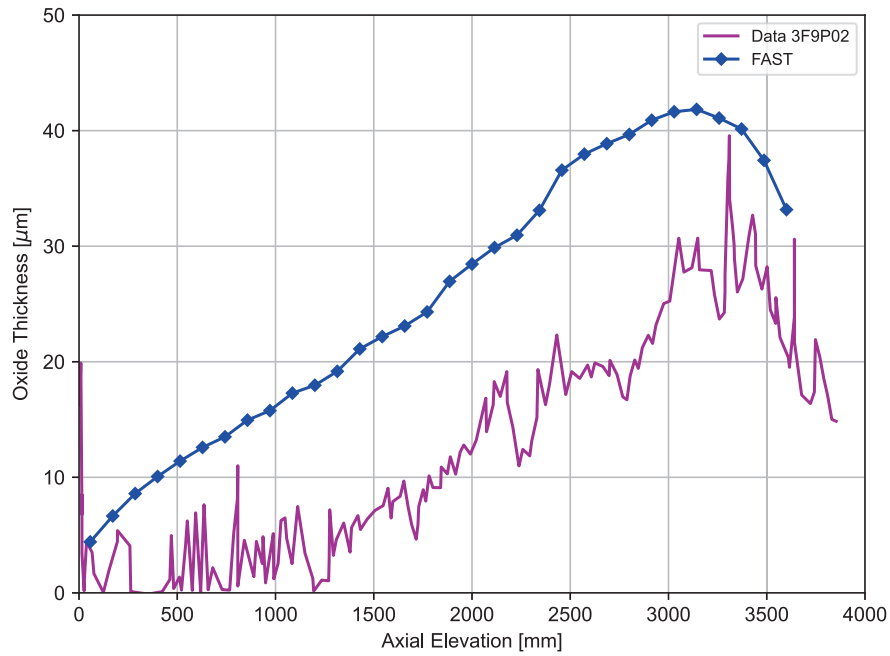

Figure 6-18. Measured and predicted corrosion layer thickness as a function of axial position for North Anna 3-Cycle PWR ZIRLO Rod 3F9P02, 49 GWd/MTU (rod-average)

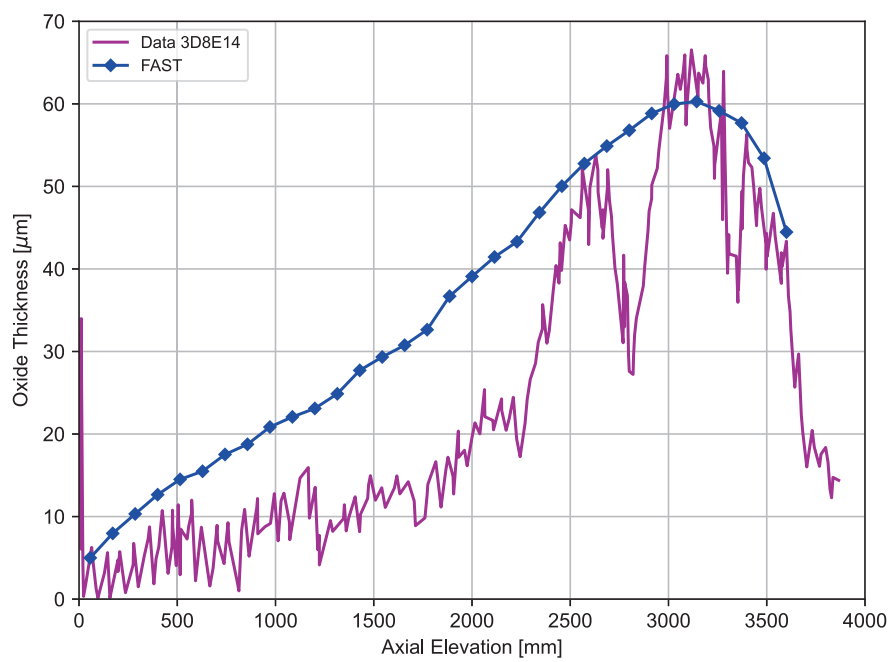

Figure 6-19. Measured and predicted corrosion layer thickness as a function of axial position for North Anna 3-Cycle PWR ZIRLO Rod 3D8E14, 59 GWd/MTU (rod-average)

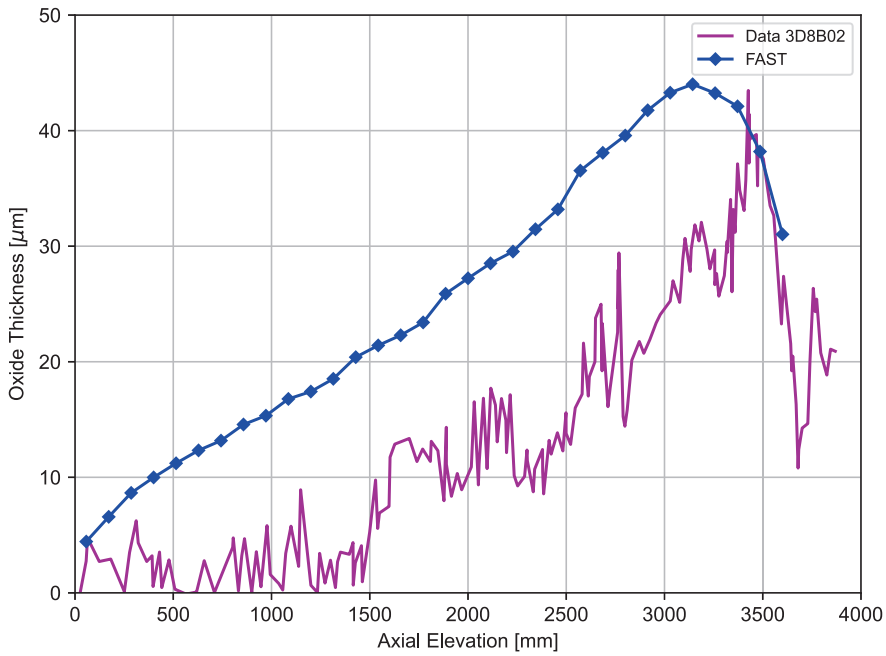

Figure 6-20. Measured and predicted corrosion layer thickness as a function of axial position for North Anna 3-Cycle PWR ZIRLO Rod 3D8B02, 50 GWd/MTU (rod-average)

FAST predicts peak cladding waterside oxidation of ZIRLO4 under PWR conditions with a standard error of 19 μm and an average under-prediction of 9.3 μm.

6.2.4 M5 Corrosion

Figures 6-21 through 6-30 shows the measured and predicted corrosion layer thicknesses as a function of axial position along the rod for the 10 PWR rods with M5 cladding.

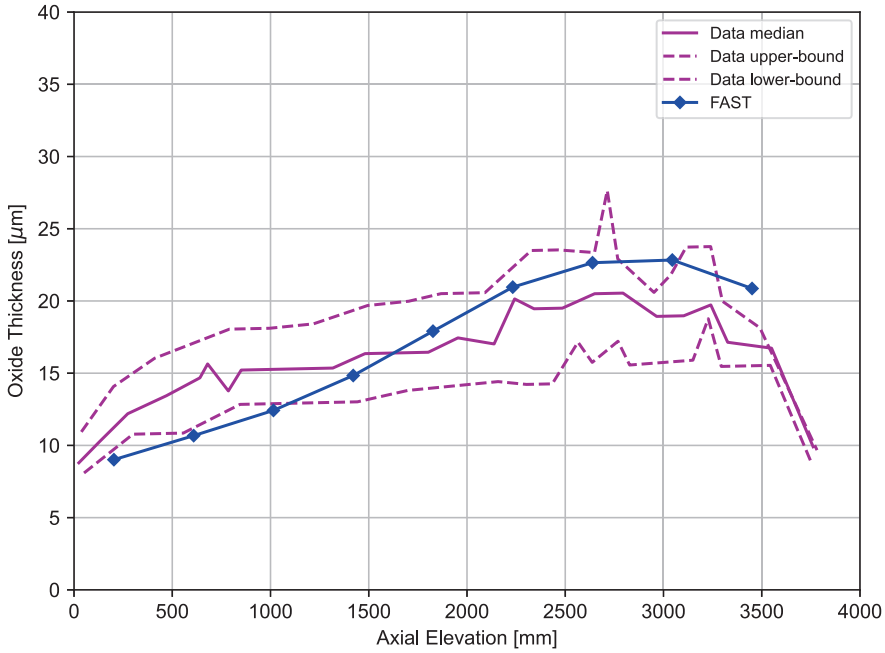

Figure 6-21. Measured and predicted corrosion layer thickness as a function of axial position for Gravelines 5-Cycle PWR M5 Rod N05, 68.1 GWd/MTU (rod-average)

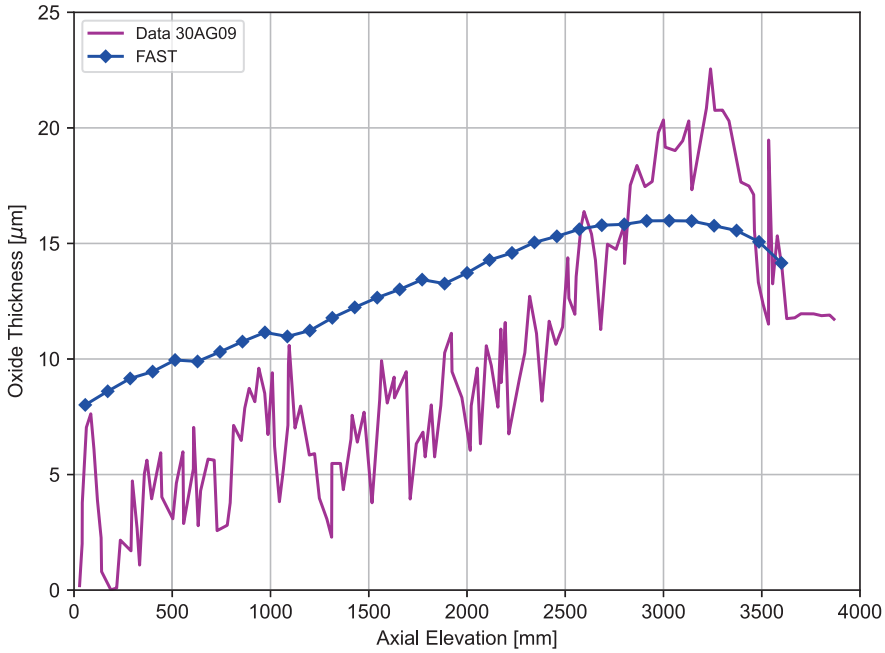

Figure 6-22. Measured and predicted corrosion layer thickness as a function of axial position for North Anna 3-Cycle PWR M5 Rod 30AG09, 54 GWd/MTU (rod-average)

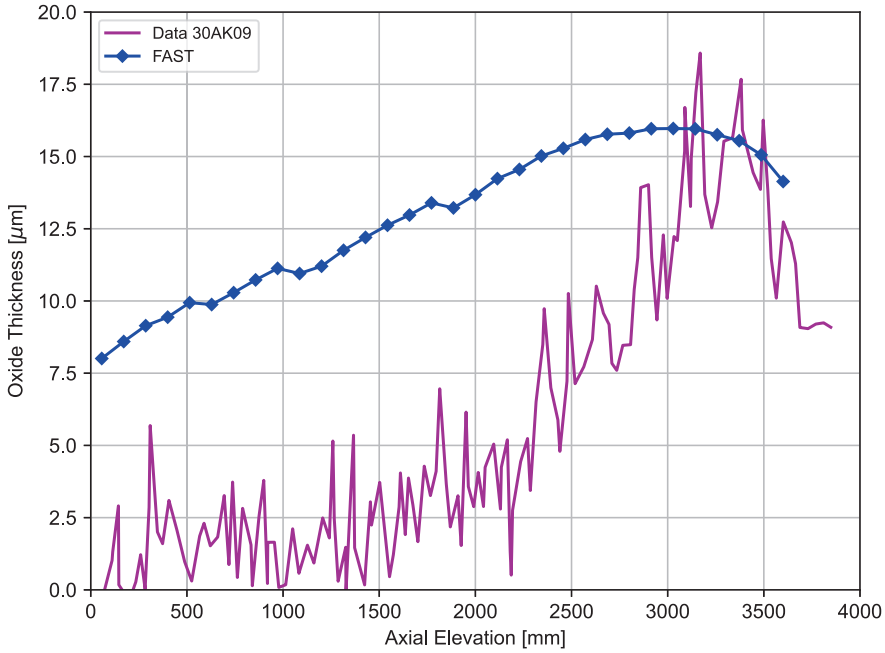

Figure 6-23. Measured and predicted corrosion layer thickness as a function of axial position for North Anna 3-Cycle PWR M5 Rod 30AK09, 53 GWd/MTU (rod-average)

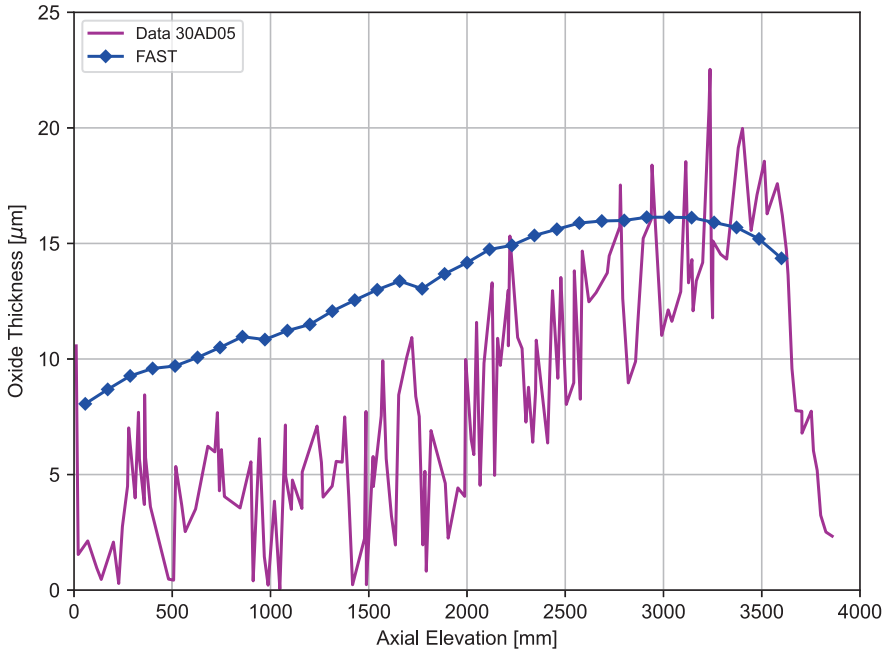

Figure 6-24. Measured and predicted corrosion layer thickness as a function of axial position for North Anna 3-Cycle PWR M5 Rod 30AD05, 54 GWd/MTU (rod-average)

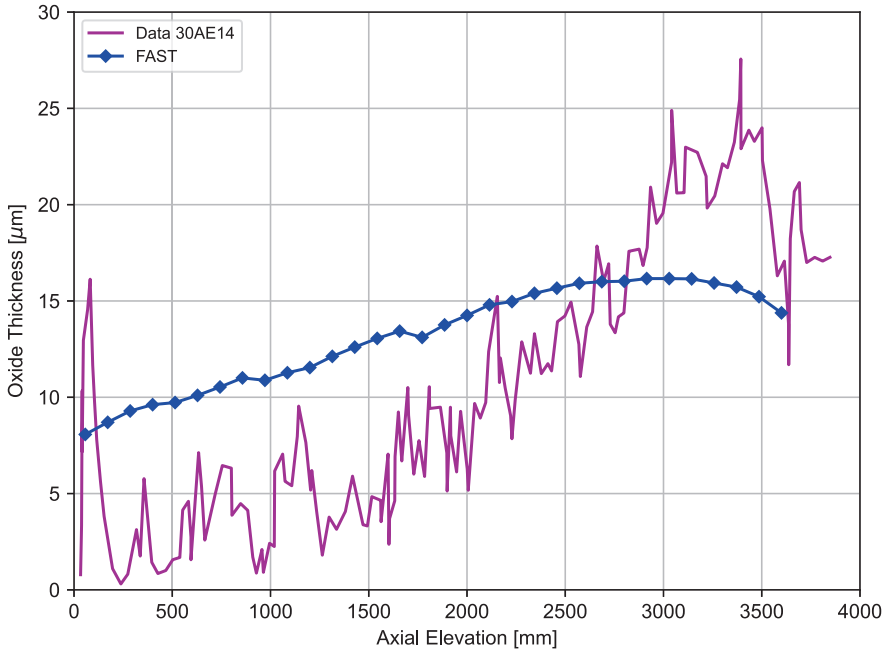

Figure 6-25. Measured and predicted corrosion layer thickness as a function of axial position for North Anna 3-Cycle PWR M5 Rod 30AE14, 54 GWd/MTU (rod-average)

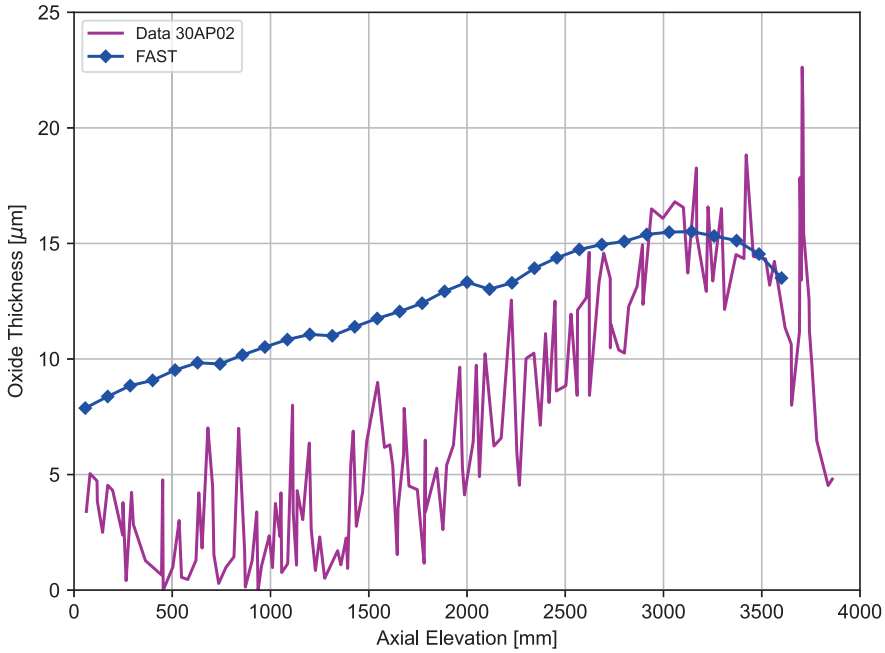

Figure 6-26. Measured and predicted corrosion layer thickness as a function of axial position for North Anna 3-Cycle PWR M5 Rod 30AP02, 49 GWd/MTU (rod-average)

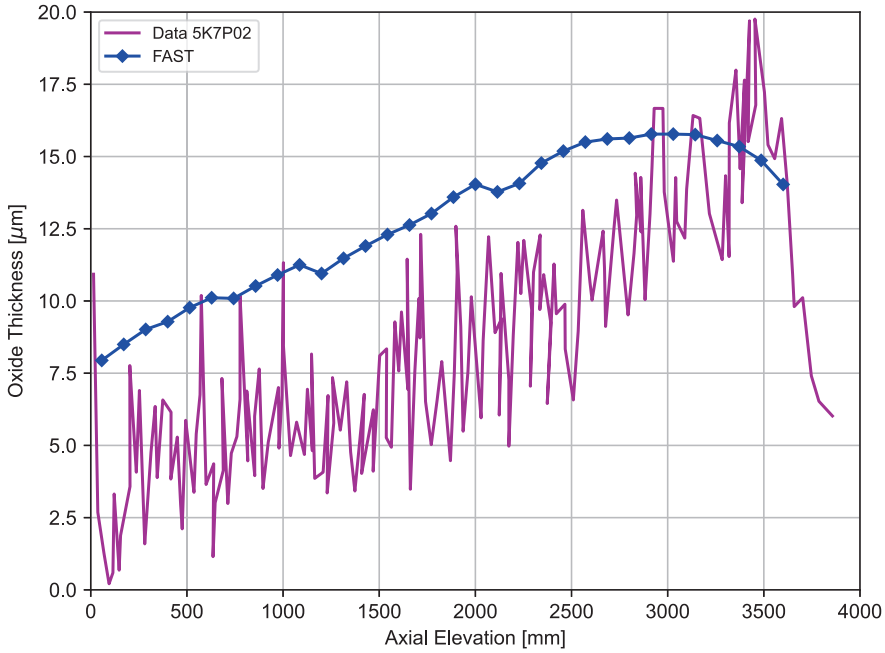

Figure 6-27. Measured and predicted corrosion layer thickness as a function of axial position for North Anna 3-Cycle PWR M5 Rod 5K7P02, 51 GWd/MTU (rod-average)

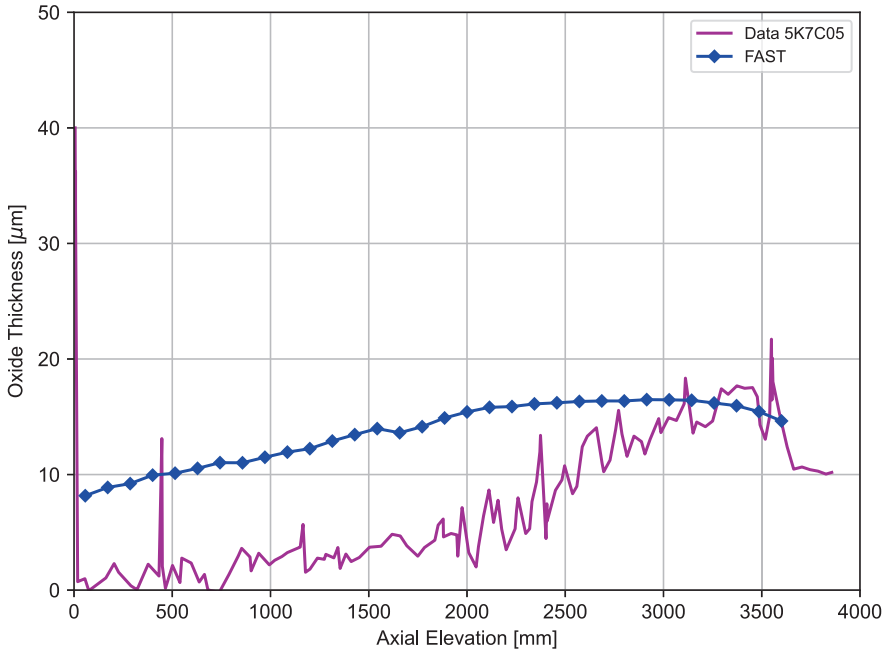

Figure 6-28. Measured and predicted corrosion layer thickness as a function of axial position for North Anna 3-Cycle PWR M5 Rod 5K7C05, 57 GWd/MTU (rod-average)

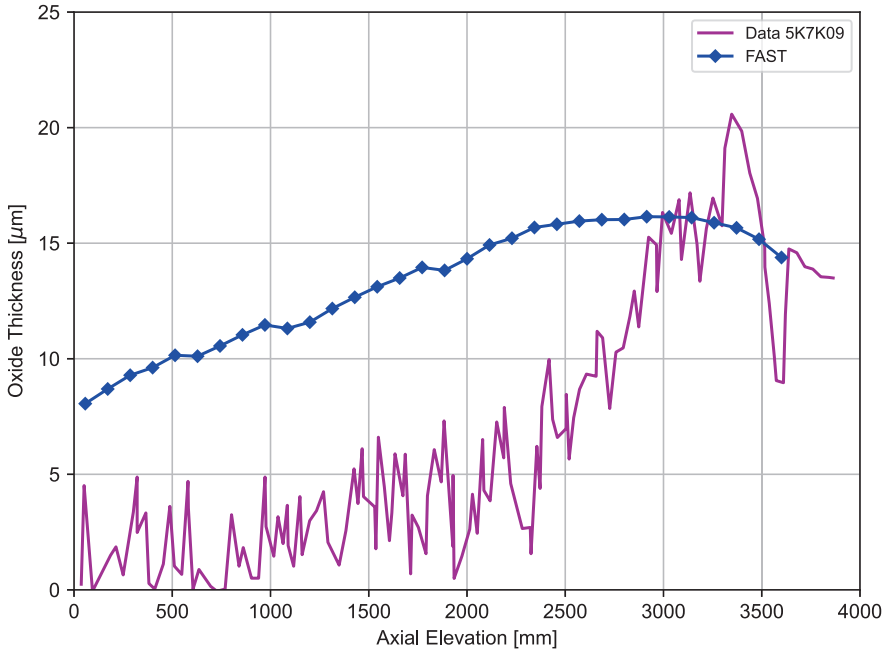

Figure 6-29. Measured and predicted corrosion layer thickness as a function of axial position for North Anna 3-Cycle PWR M5 Rod 5K7K09, 54 GWd/MTU (rod-average)

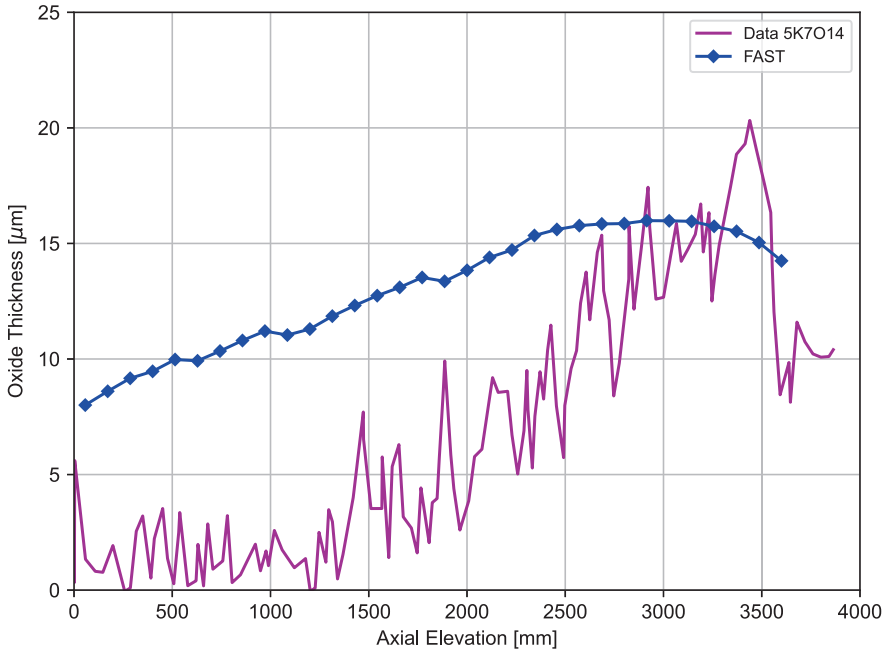

Figure 6-30. Measured and predicted corrosion layer thickness as a function of axial position for North Anna 3-Cycle PWR M5 Rod 5K7O14, 53 GWd/MTU (rod-average)

FAST predicts peak cladding waterside oxidation of M5 under PWR conditions with a standard error of 10 µm and an average under-prediction of 7.1 µm.

6.3 Fuel-Cladding Chemical Interaction

Experimental data from electron probe microanalysis (EPMA) of metal UPuZr rods irradiated in the Experimental Breeder Reactor II (EBR-II) and the Fast Flux Test Facility (FFTF) are available for assessment of fuel-cladding chemical interaction (FCCI), and power histories for these cases are also available (Carmack 2012; Matthews et al. 2017; Yacout et al. 2021). This data takes the form of maximum lanthanide element penetration into the cladding as well as axial height of the examined fuel segment. A set of six fuel rod cases are assessed to cover a variety of fuel rod axial power profiles and burnups:

1. EBR-II fuel rods DP-04, DP-11, DP-70, and DP-75, which are EBR-II fuel rods with burnups of ~10 at.% and peak power at a relatively high axial location that is a feature of the EBR-II geometry.
2. FFTF fuel rod 193045 from the Mechanistic Fuel Failure 3 (MFF-3) experiment with burnup of 12.8 at.%.
3. FFTF fuel rod 195011 from the MFF-5 experiment with burnup of 10.4 at.%.

Figures 6-31 through 6-33 show the comparison between experimental data and the FAST model for these rods. Note that one FAST case is used for the four EBR-II rods due to these rods having similar axial power profiles and burnups from the same experiment.

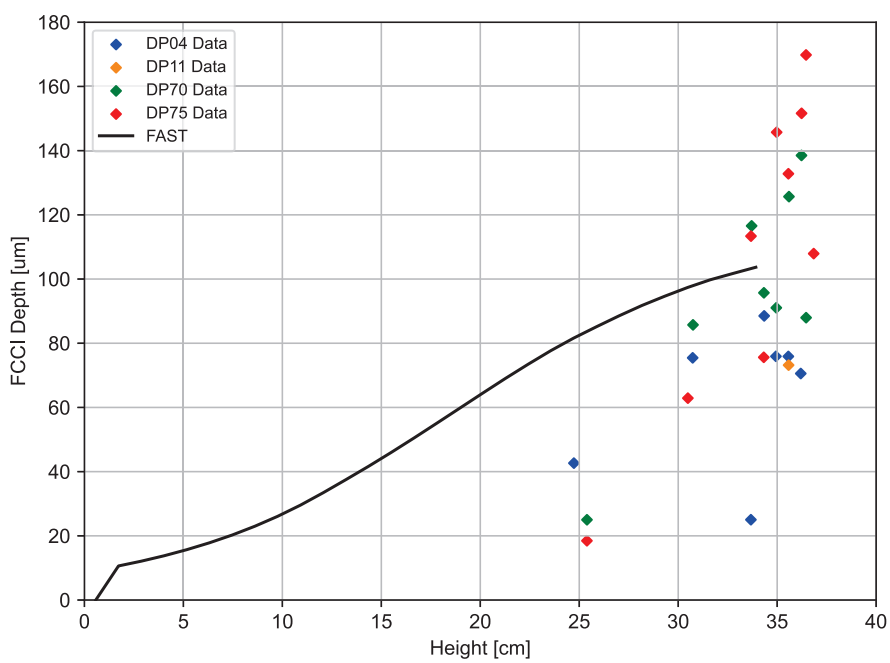

Figure 6-31. Measured and predicted FCCI penetration depth vs. height for EBR-II fuel rod cases (burnups = ~10 at.%)

Figure 6-31 shows data from four fuel rods, two of which (DP-70 and DP-75) featured cladding breaches. Breaches are expected to enhance local FCCI due to ejection of bond sodium carrying fission products through the breach, and for this reason it is difficult to model post-breach FCCI depth. The FAST model appears to be bounding for the unbreached rods (DP-04 and DP-11) as well as for the axial regions of the breached rods away from the breach.

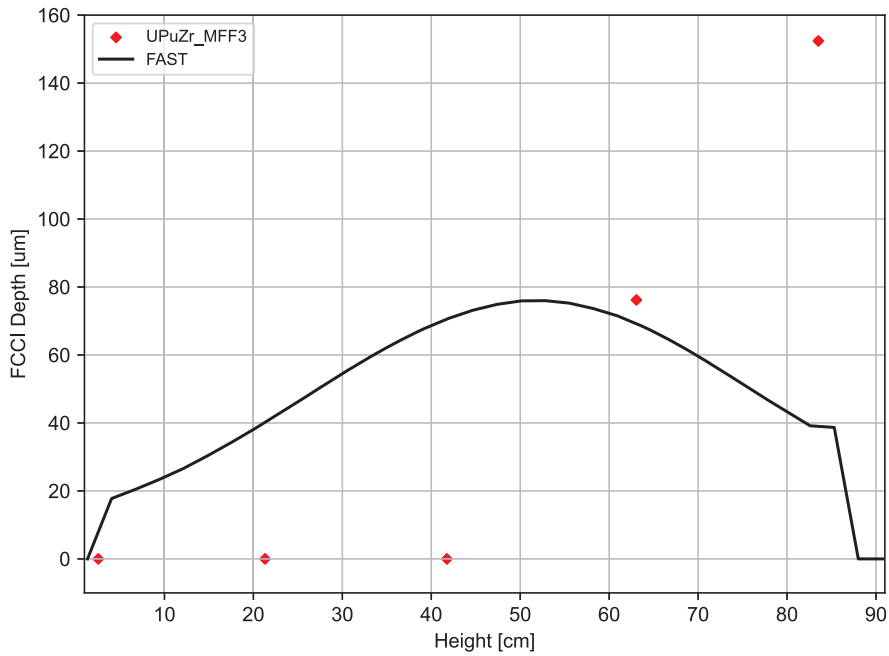

Figure 6-32. Measured and predicted FCCI penetration depth vs. height for FFTF fuel rod 193045 from MFF-3 (burnup = 12.8 at.%)

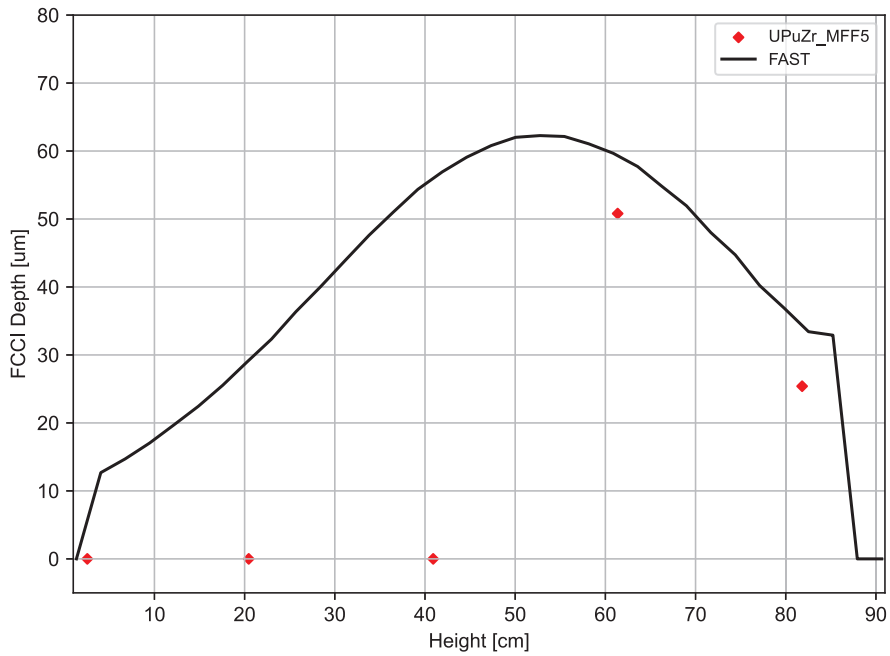

Figure 6-33. Measured and predicted FCCI penetration depth vs. height for FFTF fuel rod 195011 from MFF-5 (burnup = 10.4 at.%)

The FAST model appears to be bounding for the MFF-5 fuel pin but not for the largest height data point in the MFF-3 fuel pin.

This page intentionally blank.

7.0 Cladding Hoop Strain During Power Ramps

7.1 Assessment Cases

The ability of FAST to predict permanent hoop strain during power ramps was originally assessed against a database consisting of 29 power-ramped rods at burnup levels between 18 and 76 GWd/MTU to ramp terminal levels between 30 and 52 kW/m. Some of these rods were held at the ramp terminal level for a significant period of time ($>$ 4 h) while others were held for a very short period of time (between 1 and 30 s). The measured and predicted rod-average permanent hoop strains are shown in Figures 7-1 and 7-2. These figures show that in general FAST over-predicts the measured hoop strain. It was found that, on average, FAST over-predicts cladding permanent strain by 0.07% (absolute) with significant variation between predicted and measured and a standard error of 0.43% (absolute).

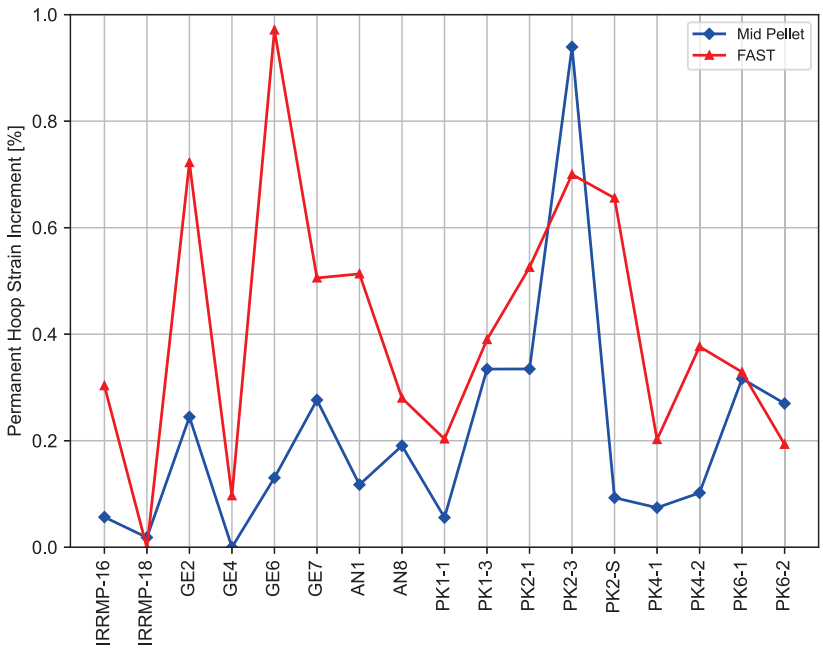

Figure 7-1. Measured and predicted rod-average permanent hoop strain for first half of the assessment database

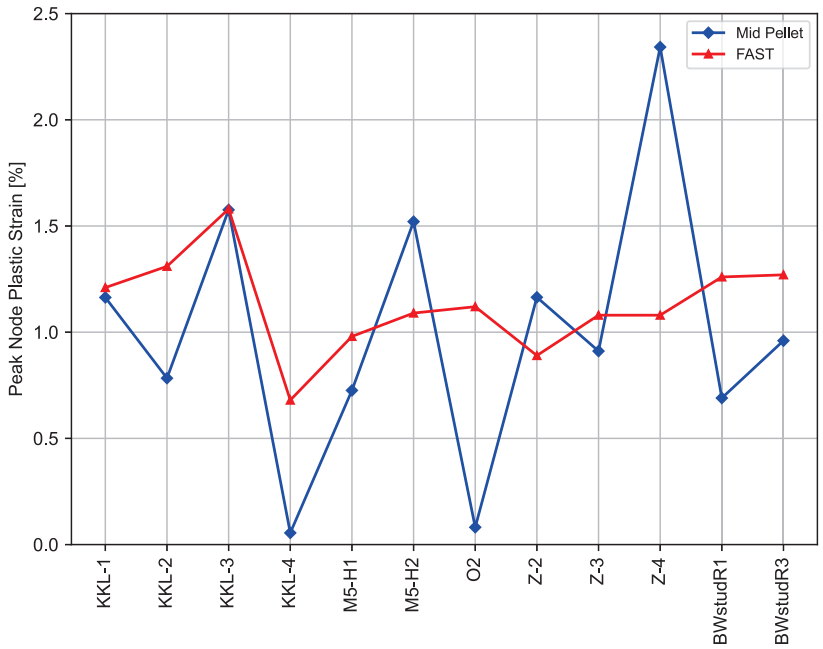

Figure 7-2. Measured and predicted peak node permanent hoop strain for second half of the assessment database

This over-prediction is consistent with the fact that FAST uses a rigid pellet assumption. This means that the pellet is assumed to be significantly stronger than the cladding such that it will not deform, other than the code-assumed accommodation of 50% of the relocation, when it comes in contact with the cladding.

7.2 Comparisons vs. Ramp Terminal Level

Figure 7-3 shows the predicted minus measured permanent hoop strain for all the assessment cases as a function of ramp terminal power level. There does not appear to be any bias in the predictions with increased ramp terminal power level.

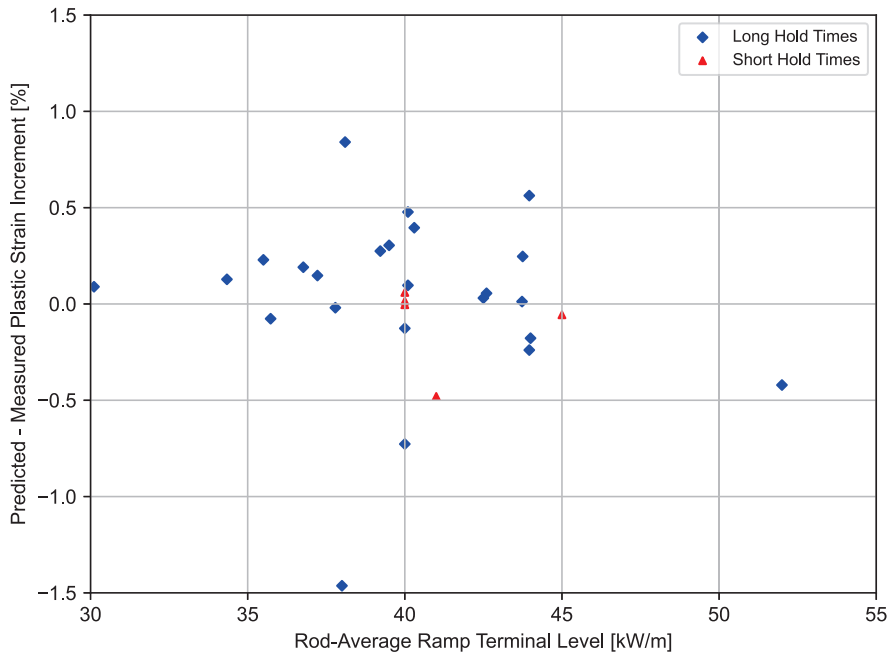

Figure 7-3. Predicted minus measured permanent hoop strain as a function of ramp terminal power level

7.3 Comparisons vs. Burnup

Figure 7-4 shows the predicted minus measured permanent hoop strain for all the assessment cases as a function of burnup. FAST generally provides a good prediction or slight over-prediction of permanent hoop strain up to 76 GWd/MTU.

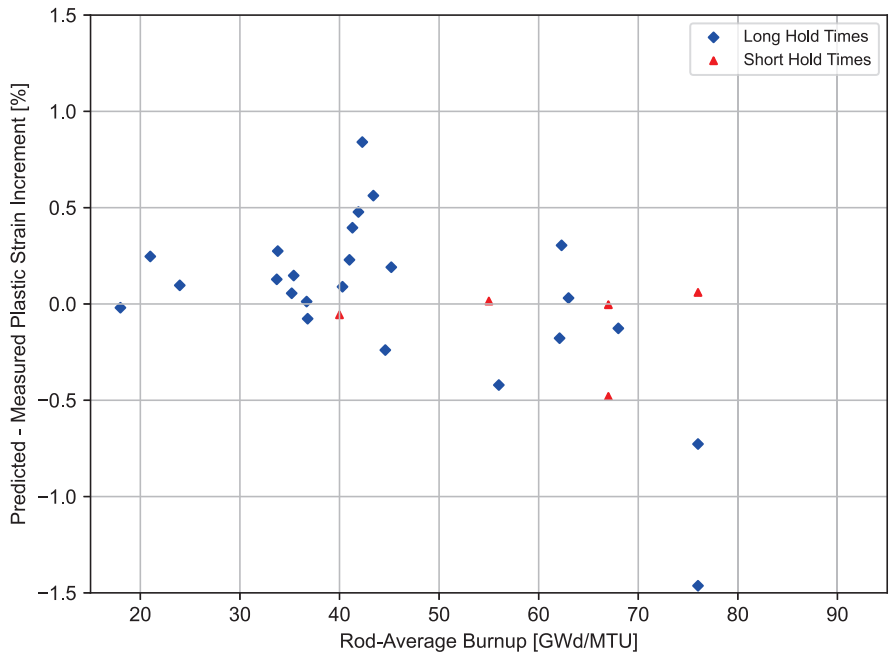

Figure 7-4. Predicted minus measured permanent hoop strain as a function of burnup

The FAST predictions for the ramp test data appear to be predicted well up to 62 GWd/MTU. There is more scatter in the predictions for power ramps above 62 GWd/MTU but other than one ramp test that is significantly under-predicted they also seem to be predicted well.

8.0 Reactivity Initiated Accident Assessment

The RIA assessment cases consist of 32 rods that were refabricated from full-length fuel rods that have been irradiated to burnup levels between 26 and 75 GWd/MTU. The refabricated rods have been taken from PWR, BWR, and VVER fuel rods with Zircaloy-4, Zircaloy-2, ZIRLO, and E-110 cladding and with UO_2 and MOX fuel. The refabricated rods have been tested in the CABRI reactor under flowing sodium, in the NSRR under stagnant room temperature water and stagnant 285 °C water, and in the BIGR reactor under stagnant room temperature water. This assessment database represents a large range of rod designs and reactor conditions.

8.1 Cladding Hoop Strain Predictions

The residual cladding hoop strain prediction during RIA events was assessed using the 12 non-failed UO_2 and MOX rods from the CABRI and NSRR assessment cases. The measured and predicted residual cladding hoop strain values during the RIA transient are shown in Figure 8-1. These values are also listed in 8-1.

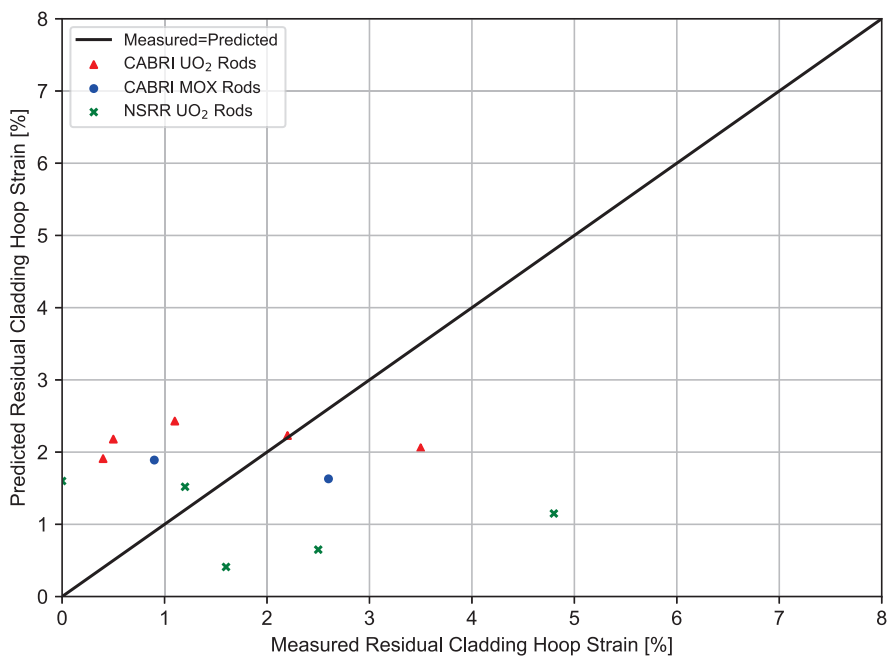

Figure 8-1. FAST-1.2.2 predictions of residual cladding hoop strain for CABRI and NSRR UO_2 and MOX rods

Table 8-1. FAST-1.2.2 predictions of residual cladding hoop strain for CABRI and NSRR UO_2 and MOX rods

Rod	Measured Residual Cladding Hoop Strain (%)	Predicted Residual Cladding Hoop Strain (%)
CABRI NA2	3.5	2.06
CABRI NA3	2.2	2.23
CABRI NA4	0.4	1.91
CABRI NA5	1.1	2.43
CABRI NA6	2.6	1.63
CABRI CIP0-1	0.5	2.18
NSRR FK-1	0.9	1.89
NSRR GK-1	2.5	0.65
NSRR HBO-6	1.2	1.52
NSRR MH-3	1.6	0.41
NSRR OI-2	4.8	1.15
NSRR TS5	0.0	1.60

The non-failed BIGR rods were not used for this assessment because of the large fuel heatup that occurred after the RIA test, which is not modeled in FAST but is expected to cause a large amount of cladding hoop strain due to increased gas pressure and high cladding temperatures.

Figure 8-1 and Table 8-1 show that FAST-1.2.2 provides reasonable predictions of permanent hoop strain for measured strains below 2.2%. There is significant under-prediction of cladding hoop strain for the two NSRR rods with measured uniform strains greater than 2.2%. This may be due to departure from nucleate boiling (DNB) causing local overheating of the rod segments that was not captured by the thermocouples, which are not at the same axial location where DNB occurred (Fuketa et al. 2001).

The overall standard error for the 12 rods is 1.7% strain. If only the cases with strain less than 2.2% are considered, the standard error for the 8 rods is 1.3% strain.

This assessment demonstrates that FAST-1.2.2 predicts reasonable strain for cases with less than 2.2% strain. For cases with greater than 2.2% measured strain, FAST-1.2.2 under-predicts the measured strain, most likely because the code does not accurately predict the initiation of DNB in stagnant water. The determination of DNB in the NSRR or BIGR cores in the small test capsules used for these RIA tests is a very complex problem that requires modeling of the NSRR or BIGR core as well as the individual test capsules with thermal-hydraulic codes. Even with this detailed modeling, the uncertainty in DNB predictions would be relatively large.

8.2 Cladding Failure Predictions

FAST-1.2.2 includes a strain-based failure model (Geelhood et al. 2016) that can be used to predict cladding failure during RIA events. The failure during RIA events was assessed using all 32 UO_2 and MOX rods from the CABRI, NSRR, and BIGR assessment cases. The failure predictions are compared to the observations from the experiments in Table 8-2. Table 8-2 also shows the predicted and reported maximum radially averaged fuel enthalpies and failure enthalpies for those rods predicted to fail. It should be noted that the enthalpies reported are not measured values, but rather are values determined by the experimentalists using a transient fuel performance code similar to FAST-1.2.2 and are therefore code dependent.

Table 8-2. FAST-1.2.2 failure and enthalpy predictions for RIA assessment cases

Test	Measured Failure	Predicted Failure	Reported Enthalpy (cal/g)	Predicted Enthalpy (cal/g)
CABRI NA1	0.074 s	0.078 s	$H_{fail} = 30$ $H_{max} = 114$	$H_{fail} = 46$ $H_{max} = 123$
CABRI NA2	No Failure	No Failure	$H_{max} = 199$	$H_{max} = 56$
CABRI NA3	No Failure	0.082 s	$H_{max} = 124$	$H_{fail} = 74$ $H_{max} = 129$
CABRI NA4	No Failure	No Failure	$H_{max} = 85$	$H_{max} = 88$
CABRI NA5	No Failure	0.080 s	$H_{max} = 108$	$H_{fail} = 66$ $H_{max} = 111$
CABRI NA6	No Failure	No Failure	$H_{max} = 133$	$H_{max} = 157$
CABRI NA7	0.405 s	No Failure	$H_{fail} = 113$ $H_{max} = 138$	$H_{max} = 163$
CABRI NA8	0.5318 s	No Failure	$H_{fail} = 78$ $H_{max} = 98$	$H_{max} = 101$
CABRI NA10	0.456 s	0.010 s	$H_{fail} = 81$ $H_{max} = 98$	$H_{fail} = 16$ $H_{max} = 100$
CABRI CIP0-1	No Failure	0.439 s	$H_{max} = 91$	$H_{fail} = 58$ $H_{max} = 108$
NSRR FK-1	No Failure	No Failure	$H_{max} = 116$	$H_{max} = 123$
NSRR GK-1	No Failure	No Failure	$H_{max} = 93$	$H_{max} = 94$
NSRR HBO-1	Failed	0.201 s	$H_{fail} = 60$ $H_{max} = 73$	$H_{fail} = 50$ $H_{max} = 76$
NSRR HBO-5	Failed	No Failure	$H_{fail} = 76$ $H_{max} = 80$	$H_{max} = 81$
NSRR HBO-6	No Failure	0.208 s	$H_{max} = 85$	$H_{fail} = 58$ $H_{max} = 86$
NSRR MH-3	No Failure	No Failure	$H_{max} = 67$	$H_{max} = 68$
NSRR OI-2	No Failure	No Failure	$H_{max} = 108$	$H_{max} = 109$

Table continued on next page

Table 8-2. FAST-1.2.2 failure and enthalpy predictions for RIA assessment cases (continued)

Test	Measured Failure	Predicted Failure	Reported Enthalpy (cal/g)	Predicted Enthalpy (cal/g)
NSRR TS5	No Failure	No Failure	$H_{max} = 98$	$H_{max} = 100$
NSRR VA1	Failed	0.0078 s	$H_{fail} = 64 \pm 10$ $H_{max} = 133$	$H_{fail} = 40$ $H_{max} = 136$
NSRR VA3	Failed	0.0074 s	$H_{fail} = 82$ $H_{max} = 122$	$H_{fail} = 52$ $H_{max} = 129$
BIGR RT1	No Failure	No Failure	$H_{max} = 142$	$H_{max} = 133$
BIGR RT2	No Failure	No Failure	$H_{max} = 115$	$H_{max} = 106$
BIGR RT3	No Failure	No Failure	$H_{max} = 138$	$H_{max} = 123$
BIGR RT4	No Failure	No Failure	$H_{max} = 125$	$H_{max} = 117$
BIGR RT5	No Failure	No Failure	$H_{max} = 146$	$H_{max} = 134$
BIGR RT6	No Failure	No Failure	$H_{max} = 153$	$H_{max} = 130$
BIGR RT7	No Failure	0.010 s	$H_{max} = 134$	$H_{fail} = 69$ $H_{max} = 128$
BIGR RT8	Failed[1]	0.010 s	$H_{max} = 164$	$H_{fail} = 94$ $H_{max} = 162$
BIGR RT9	Failed[1]	0.041 s	$H_{max} = 165$	$H_{fail} = 119$ $H_{max} = 163$
BIGR RT10	Failed[1]	No Failure	$H_{max} = 164$	$H_{max} = 141$
BIGR RT11	Failed[2]	No Failure	$H_{max} = 188$	$H_{max} = 173$
BIGR RT12	No Failure	No Failure	$H_{max} = 155$	$H_{max} = 159$

[1] These rods have multiple failure locations that appear to be a combination of some locations due to ballooning while others suggest PCMI.

[2] This rod may have failed due to ballooning caused by localized DNB.

It can be seen that FAST predicts the maximum fuel enthalpies well, typically within 10 cal/g.

The PIE results from the BIGR tests (RT-1 through RT-12) indicated that some of the rods may have failed due to highly localized ballooning caused by localized DNB, resulting in a local hot spot and localized ballooning and burst. Of the failed rods, localized ballooning is evident in RT-11, but less evident in RT-8, RT-9, and RT-10. Rods RT-8, RT-9, and RT-10 had multiple failure locations, some of which appear to be due to ballooning while others may be due to pellet/cladding mechanical interaction (PCMI). For example, the RT-8 rod had two failure locations: one at the bottom with large local deformation typical of ballooning and one at the top with much less local deformation, characteristic of PCMI. The RT-10 rod also had characteristic deformation similar to that of RT-8: two failure locations, with the bottom failure having deformation characteristic of ballooning and the top having the less localized deformation characteristic of PCMI. The RT-9 rod had four different failure locations that also appear to demonstrate a combination of ballooning and PCMI. In addition, it seems unlikely that the RT-9 rod could close off gas communication at

four different locations to cause ballooning at each of these locations, especially considering that the RT-9 failure locations are within 1 inch or less of one another.

This assessment demonstrates that FAST-1.2.2 provides a best estimate prediction of cladding failure when the cladding temperature is well known.

8.3 Fission Gas Release Predictions

The FGR predictions during RIA events were assessed using the measured release values from 10 non-failed UO_2 rods from the CABRI and NSRR assessment cases. The code predictions for these tests utilized the grain boundary gas inventory as predicted by the FRAPFGR model in FAST-1.2.2. The grain boundary gas inventory is read in by FAST-1.2.2 and the release model releases this gas when various temperature thresholds are reached (Geelhood, Colameco, et al. 2026). The measured and predicted gas release values during the RIA transient are shown in Figure 8-2 and in Table 8-3. The non-failed BIGR rods were not used for this assessment because of the large fuel heatup that occurred after the RIA test, which is not modeled in FAST but is expected to cause a large amount of FGR. The CABRI MOX rods were not included as there are only two non-failed MOX rods and these were not enough to calibrate an empirical MOX transient FGR model.

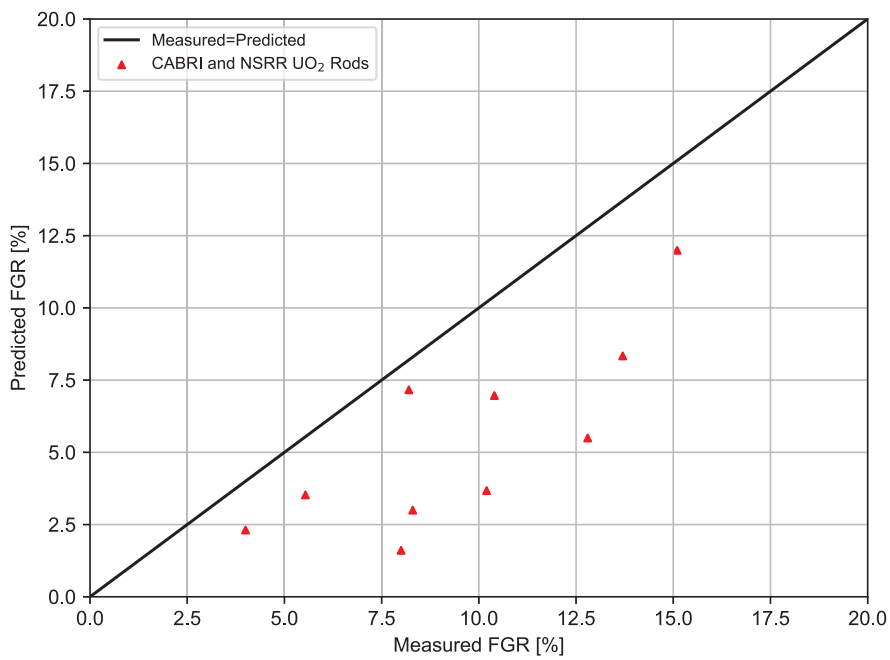

Figure 8-2. FAST-1.2.2 Predictions of RIA FGR for CABRI and NSRR UO_2 Rods

Table 8-3. FAST-1.2.2 predictions of RIA FGR for CABRI and NSRR UO_2 rods

Rod	Measured FGR (%)	Predicted FGR (%)
CABRI NA2	5.54	3.53
CABRI NA3	13.7	8.34
CABRI NA4	8.3	3.00
CABRI NA5	15.1	12.0
NSRR FK-1	8.2	7.16
NSRR GK-1	12.8	5.50
NSRR HBO-6	10.4	6.97
NSRR MH-3	4	2.31
NSRR OI-2	10.2	3.68
NSRR TS5	8	1.61

This assessment demonstrates that FAST-1.2.2 under-predicts UO_2 transient FGR, with a standard error of 5.0% FGR (absolute) and an average under-prediction of 4.2% FGR.

Note: NRC has an empirical transient FGR model for stable and radioactive isotopes for RIA that is a function of burnup and maximum enthalpy only in Regulatory Guide 1.183. This model is not included in FAST-1.2.2. The model may be input using the option to input FGR as a function of time. An option to use this model may be added to future code versions.

9.0 Loss-of-Coolant Accident Assessments

The LOCA assessment cases consist of 18 LOCA test case rods that have been refabricated from various full-length fuel rods that have been irradiated to burnup levels between 0 and 83 GWd/MTU. The refabricated rods have been taken from PWR, BWR, and VVER UO_2fuel rods with Zircaloy-2, Zircaloy-4, ZIRLO, M5, and E-110 cladding. The refabricated rods have been tested in the PBF, TREAT, and Halden reactors under various LOCA scenarios. The LOCA assessment database represents a large range of rod designs and reactor conditions.

FAST-1.2.2 is not intended to predict assembly or core cooling during a LOCA. A systems code such as RELAP5 or TRACE is needed to predict assembly and core coolability during a LOCA for input to FAST. FAST has single-rod coolant models that can be used to predict the cladding temperature and oxidation; however, in some cases the coolant conditions are too complex for these models and cladding surface temperatures calculated with a systems code are input to FAST. The purpose of the FAST code is to predict fuel and cladding temperatures, rod pressures, cladding ballooning, and rupture strains and oxidation based on input from the system codes. The following assessments will provide comparisons to measured rod internal pressures, cladding strains and rupture times, and cladding oxidation.

9.1 Cladding Ballooning, Failure, and Pressure Predictions

The cladding ballooning behavior prediction during LOCA events was assessed using all 18 LOCA assessment cases. FAST predicted the fact of rod rupture correctly in all modeled tests except for three, IFA-650.14 and LOC-11C Rods 2 and 3. For these three cases, FAST predicted rod rupture when there was none observed in the LOCA test.

For the 11 rods predicted correctly to fail, Figure 9-1 shows the relative difference in predicted and measured rupture time vs. average burnup. For these rods, FAST predicts rupture time with a 34% (relative) standard error.

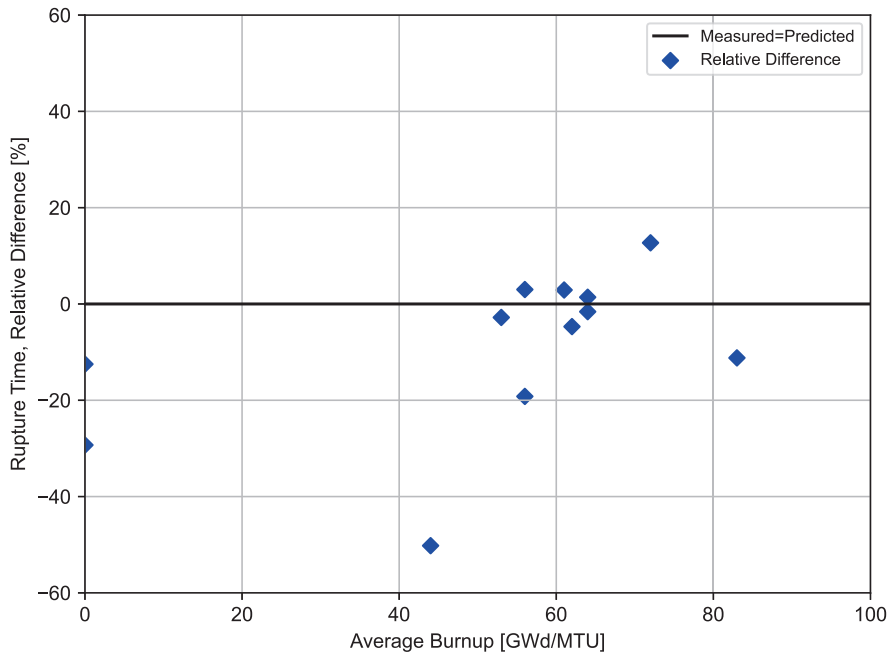

Figure 9-1. Relative difference in predicted and measured ([P-M]/M) rupture time, after start of transient, vs. average burnup for the tests where FAST predicted failure correctly; the FRF-2 measured rupture times were provided as a range.

Figure 9-1 shows that, in general, FAST-1.2.2 predicts failure well for these tests. There are only three cases (IFA-650.14 and LOC-11C Rods 2 and 3) where FAST-1.2.2 predicts failure when none was observed. However, it can be seen that FAST-1.2.2 often predicts failure to occur before it was actually measured. This can also be seen in the rod internal pressure predictions in Figures 9-2 through 9-6. It should be noted that in order to measure the rod internal pressure in these LOCA tests, there is often a rather large gas volume that is not within the heated zone that contains the pressure transducer. FAST-1.2.2 can model an external plenum, but the lower temperature in this gas volume is often not reported. This may lead to larger predicted rod internal pressure values. Larger rod internal pressure values subsequently lead to failure predictions occurring earlier than measured.

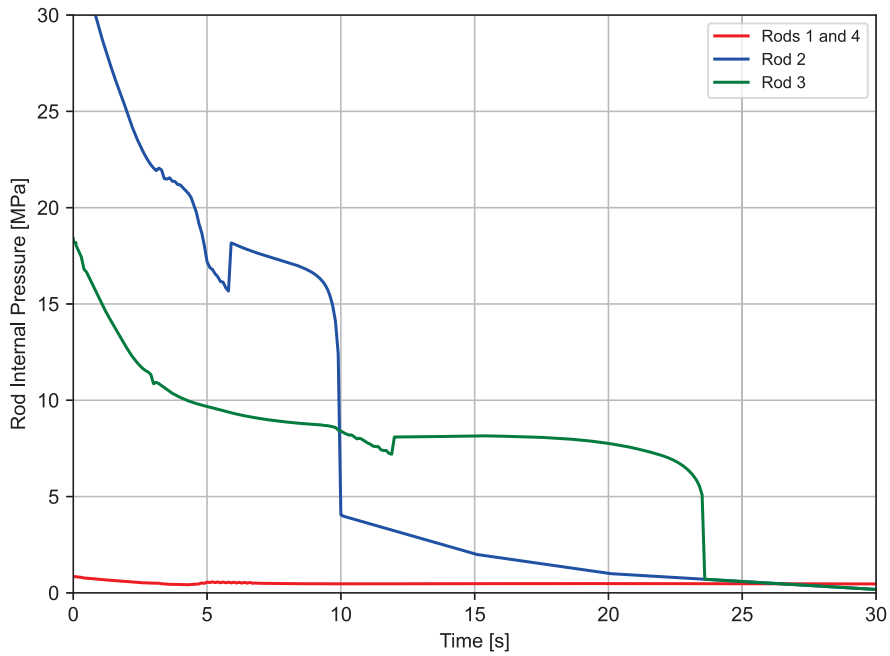

Figure 9-2. FAST-1.2.2 predicted internal pressure for LOC-11C rods. FAST predicted failure for rods 2 and 3. None of the rods were measured to fail and rod internal pressure history was not available for these rods.

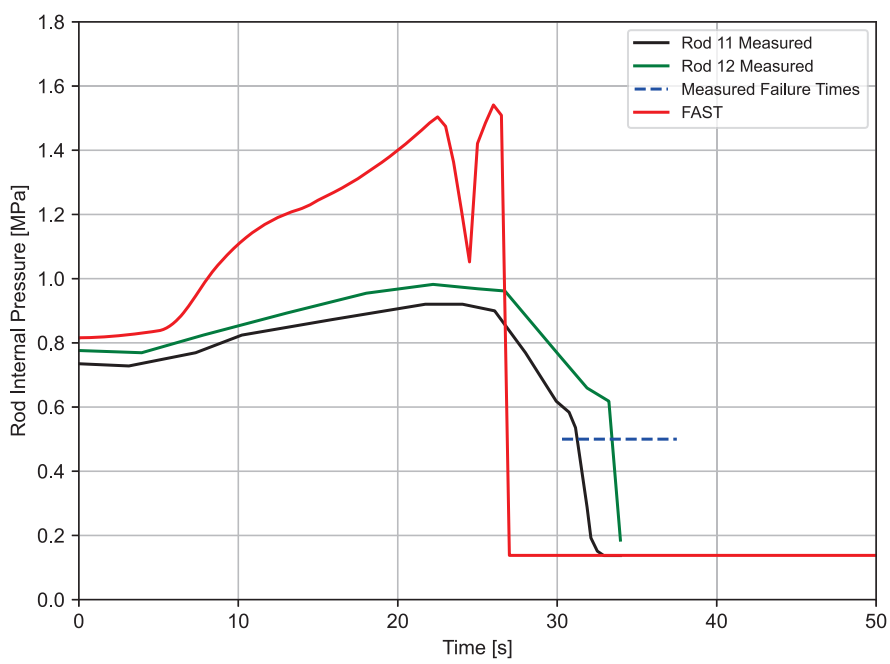

Figure 9-3. FAST-1.2.2 predicted and measured rod internal pressure for TREAT FRF-2 rods. Solid lines show pressure for two rods. Dashed line shows failure time range for all 7 rods.

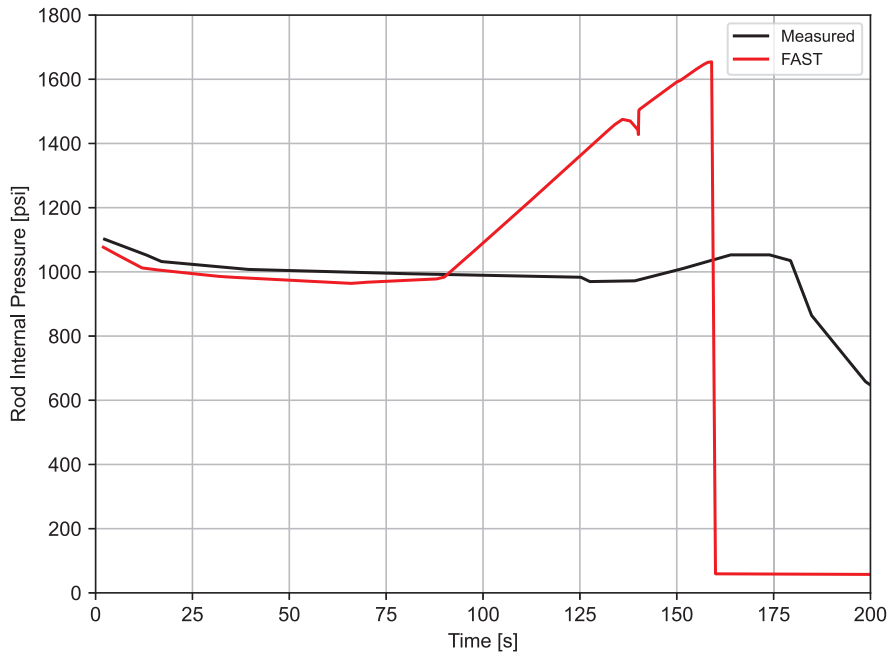

Figure 9-4. FAST-1.2.2 predicted and measured rod internal pressure for IFA-650.5

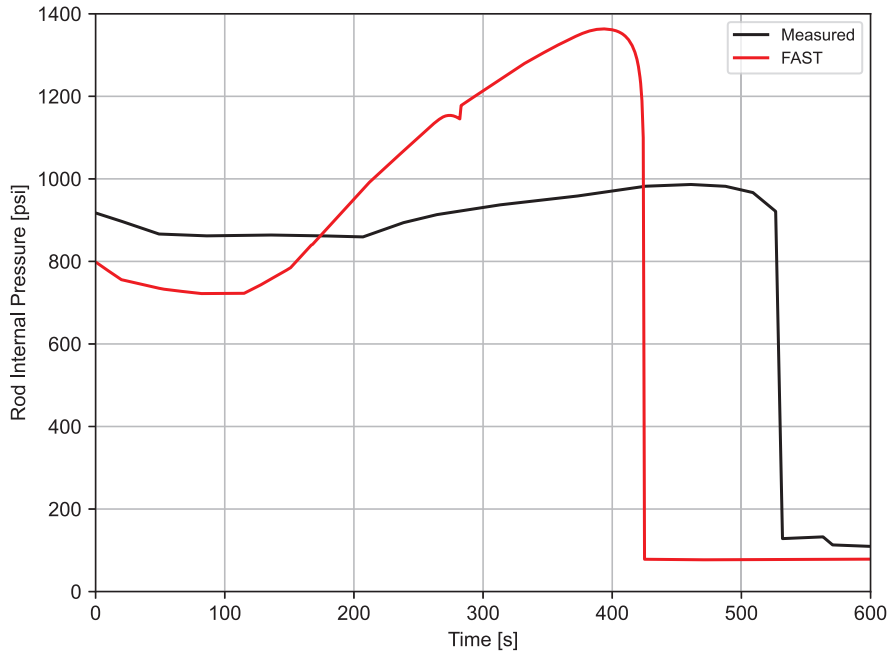

Figure 9-5. FAST-1.2.2 predicted and measured rod internal pressure for IFA-650.6

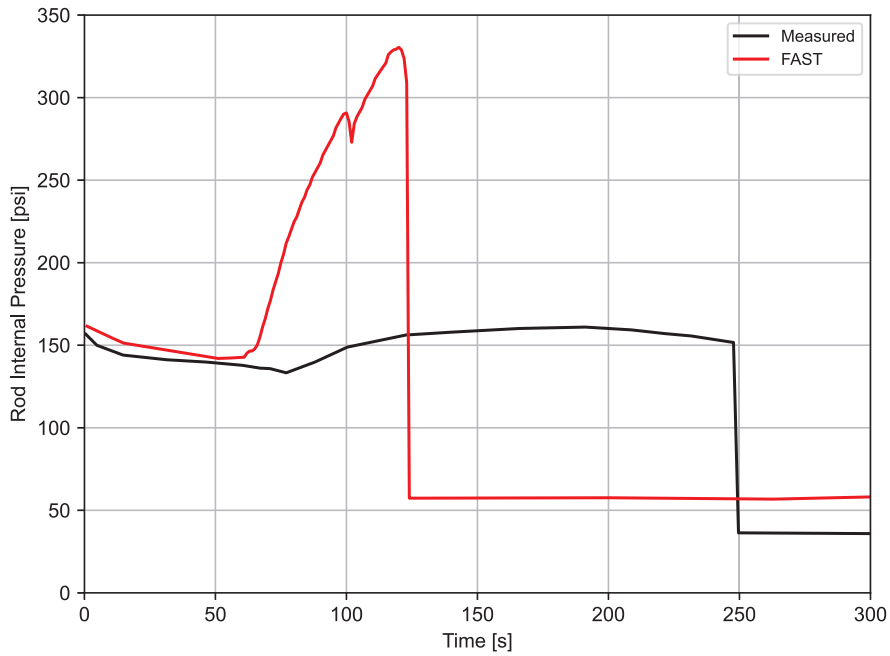

Figure 9-6. FAST-1.2.2 predicted and measured rod internal pressure for IFA-650.7

9.2 Residual Hoop Strain Predictions

The cladding residual hoop strain predictions during LOCA events were assessed using the 15 LOCA assessment cases where residual cladding hoop strain was measured. Table 9-1 shows the measured and predicted peak residual hoop strain for each of these cases. Figure 9-7 shows the absolute difference of measured and predicted hoop strain vs. burnup.

For the failed rods, FAST-1.2.2 both over-predicts (by up to 46.5% strain) and under-predicts (by up to 48% strain) cladding hoop strain. Given the scatter typically observed in burst strain from LOCA burst tests (±50% strain) (Powers and Meyer 1980), this is within the uncertainty of the burst strain.

For the non-failed rods, FAST-1.2.2 over-predicts cladding hoop strain by about 1% strain for the cases that FAST-1.2.2 predicts no failure; for the rods where FAST-1.2.2 predicts failure and none was observed, FAST-1.2.2 both under and over-predicts the hoop strain by up to 33% strain (absolute).

Table 9-1. FAST-1.2.2 predicted and measured peak cladding residual strain following LOCA tests

Case	Measured Peak Residual Hoop Strain	FAST-1.2.2 Peak Residual Hoop Strain
LOC-11C rods 1 and 4	-0.96% and -0.84%	0.02%
LOC-11C rod 2	2.5%	26.1%
LOC-11C rod 3	1.6%	32.6%
TREAT rods 16 and 17	58% and 33%	11.5%
IFA-650.5	16%	19.6%
IFA-650.6	36%	66.7%
IFA-650.7	24%	67.8%

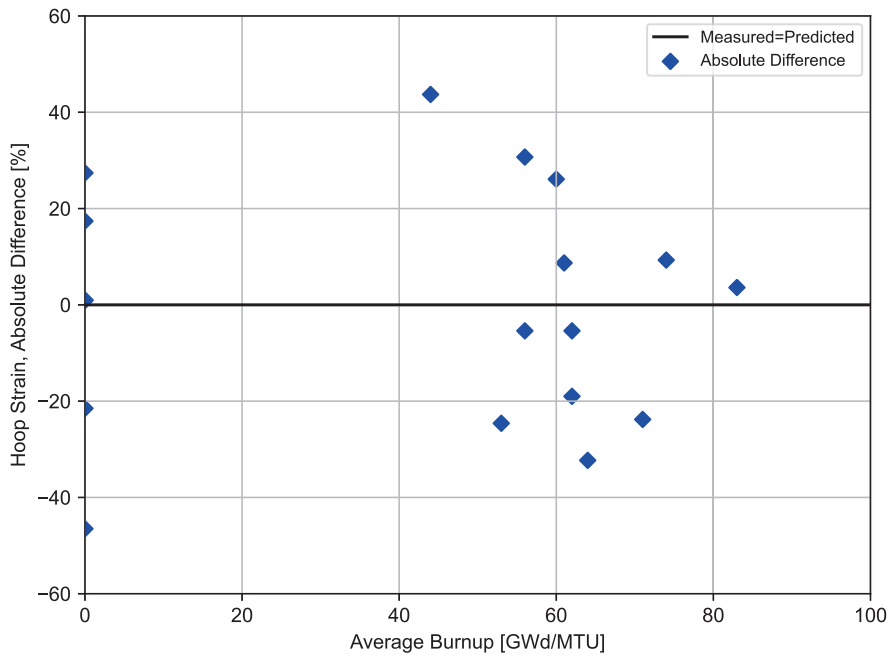

Figure 9-7. Absolute difference in predicted and measured (P-M) hoop strain vs. average burnup; the FRF-2 measured hoop strains were provided as a range.

9.3 Fission Gas Release Predictions

Transient fission gas release (FGR) measurements were provided for four LOCA tests. Figure 9-1 shows the absolute difference in predicted and measured FGR vs. average burnup. For these rods, FAST predicts FGR with a 7.7% (absolute) standard error and an average under-prediction of 1.1% (absolute).

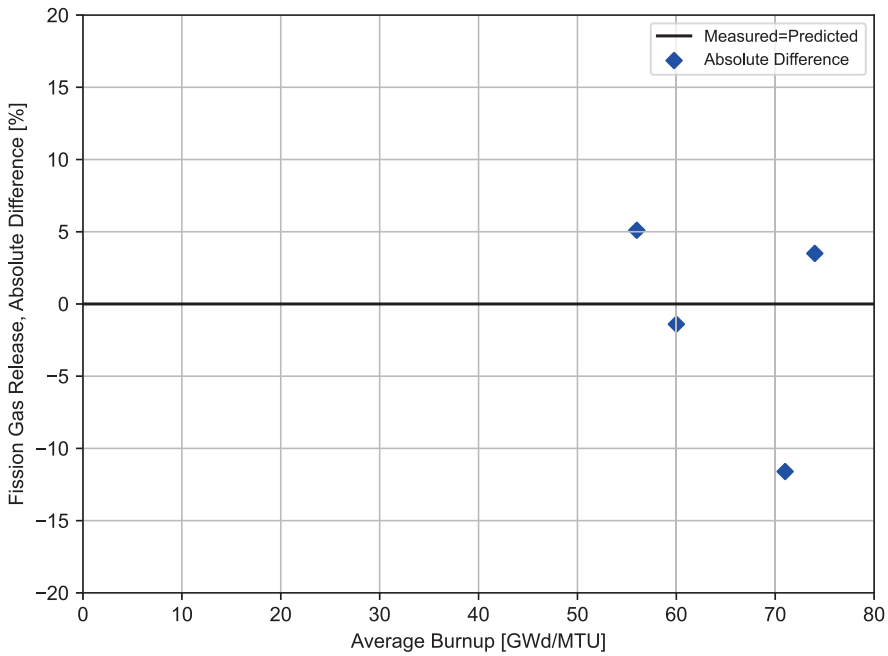

Figure 9-8. Absolute difference in predicted and measured (P-M) FGR vs. average burnup

In general, FAST-1.2.2 predicts FGR well for these tests. The standard error is within the assessed uncertainties for FAST relative to steady-state and power-ramped FGR data (Section 4.0).

This page intentionally blank.

10.0 Conclusions

The FAST steady-state fuel performance code has been assessed against a set of pre-selected data from 227 well characterized fuel rods. The data used for the assessment consisted of measurements of thermal (fuel temperature), FGR, rod internal void volume, cladding corrosion, hoop strain, and rod failure. The fuel rods represent a range of design parameters, including different fuel rod diameters, lengths, gap sizes, fill-gas compositions, fuel types, and cladding types and a wide range of operating conditions with peak LHGRs varying from 8 to 18 kW/ft, rod-average burnups from 0 to 99 GWd/MTU, and FGRs ranging from less than 1% to greater than 50% . The estimates of code thermal and FGR predictive error are based on code comparisons to both the benchmark and independent data sets.

- ***Thermal***: Comparisons were made for BOL UO_2 temperature measurements and UO_2, MOX, and UO_2-Gd_2O_3 temperature measurements as a function of burnup. For the UO_2 BOL temperature measurements, the FAST predictions were within a standard error of 4.6% of measured values and and average bias of 0.14% . For the UO_2 temperature measurements as a function of burnup, the FAST predictions were within a standard error of 6.0% of the measured values. For the MOX temperature measurements as a function of burnup, the FAST predictions were within a standard error of 4.7% of the measured values. For the UO_2-Gd_2O_3 temperature measurements as a function of burnup, the FAST predictions were within a standard error of 5.8% of the measured values and much closer in most cases.

  Typically, a standard error of 3 to 4% is the uncertainty in temperature due to power level uncertainty.

  Overall, FAST gives reasonable predictions (standard error of less than 6%) of fuel centerline temperature for fuel rods with UO_2, MOX, and UO_2-Gd_2O_3 fuel.

- ***Fission Gas Release***: Comparisons were made for the UO_2, MOX, and UO_2-Gd_2O_3 FGR measurements for rods with widely varying power levels and burnups. The UO_2 FGR model was assessed for steady-state conditions and power-ramped rods. For the UO_2 cases, a standard error of 2.32% FGR (absolute) was calculated for the steady-state rods, a standard error of 5.48% FGR (absolute) was calculated for the power-ramped rods when two rods with non-prototypical pellets were removed, and a standard error of 7.6% FGR (absolute) was calculated for the transient rods. These standard errors are considered reasonable.

  For the MOX cases, a standard error of 4.28% FGR (absolute) was calculated for the steady-state rods when the ATR rods with large power uncertainty were removed, and a standard error of 10.0% FGR (absolute) was calculated for the limited number of power-ramped rods that all came from one experimental program. The steady-state standard deviation is considered reasonable. The power-ramped rods were all over-predicted, which is conservative for rod internal pressure and temperature calculations. However, a larger database of MOX power-ramped cases is needed to further assess if this over-prediction is due to a code deficiency. Although there is little data above 62 GWd/MTU, it appears that FAST may under-predict MOX fuel above this burnup level.

  A limited assessment of UO_2-Gd_2O_3 data showed good agreement between measurements and predictions using the UO_2 FGR model in FAST. Based on these comparisons and observations by other researchers it was concluded that the FGR from these rods should be

conservatively bounded with the UO_2 FGR model.

Overall, FAST gives reasonable predictions of FGR for fuel rods with UO_2, MOX, and UO_2-Gd_2O_3 fuel.

- ***Constituent Redistribution***: Comparisons were made for constituent redistribution of U-Zr and U-Pu-Zr metallic fuels. The predictions for the U-Zr cases showed good agreement with the experimental data. The U-Pu-Zr case predictions showed good agreement with the experimental data, but with both under-prediction and over-prediction for the zirconium atom fractions in each phase for two cases.

- ***Internal Void Volume***: Comparisons were made to data from 26 commercial reactor and three test reactor fuel rods. In general, the code over-predicted EOL void volume by an average of 0.085 in^3, a standard error of 14.8% (relative).

- ***Cladding Corrosion***: Comparisons were made to data from two commercial BWR rods with Zircaloy-2 cladding, four commercial PWR rods with Zircaloy-4 cladding, two commercial PWR rods with low-tin Zircaloy-4 cladding, 14 commercial PWR rods with ZIRLO cladding, and 10 commercial PWR rod with M5 cladding. In general, the oxide corrosion predictions are good and tend to bracket the data with the following standard errors:
  - Zircaloy-2: σ =18 µm
  - Zircaloy-4: σ =52 µm
  - Low-Tin Zircaloy-4: σ =96 µm
  - ZIRLO: σ =19 µm
  - M5: σ =10 µm

- ***Fuel-Cladding Chemical Interaction***: Comparisons were made to data from six metallic fuel rods with stainless steel cladding. For the two non-failed rods, FAST bounded FCCI well.

- ***Cladding Hoop Strain***: The original hoop strain assessment cases that were available up to a burnup of around 45 GWd/MTU demonstrated that, on average, FAST slightly over-predicts cladding hoop strain by 0.07% strain. FAST over-predicted all the short hold times cases. Despite this over-prediction, FAST provides reasonable hoop strain predictions up to 62 GWd/MTU.

- ***Reactivity-Initiated Accident***: For RIA scenarios, FAST provided reasonable predictions of permanent hoop strain for measured strains below 2.2%. For cases with greater than 2.2% measured strain, FAST under-predicts the permanent hoop strain by an average of 0.13%. FAST predicted maximum fuel enthalpy well, with some variation in predicting failure of a rod. FAST under-predicted transient FGR (for RIA) with a standard error of 5.0% FGR.

- ***Loss-of-Coolant Accident***: For LOCA scenarios, FAST generally predicts failure well, with an over-prediction of rod internal pressures. For the failed rods, FAST both over-predicted (by up to 46.5% strain) and under-predicted (by up to 48% strain) cladding hoop strain. Given the scatter typically observed in burst strain from LOCA burst tests ($\pm$50%), this is within the uncertainty. For the non-failed rods, FAST over-predicted cladding hoop strain by about 1% strain for the cases where failure was predicted; for cases where failure was predicted and none was observed, FAST over-predicted the hoop strain by up to 33% strain (absolute).

11.0 References

Andersson, R. K., and P. Tejland. 2022. *Integral LOCA Test on Rod 10-O3C1 to Study Fragmentation of ADOPT Fuel.* STUDSVIK/N-22/102. Sweden: Studsvik Nuclear AB.

Arana, I., C. Munoz-Reja, and F. Culbebras. 2012. "Post-Irradiation Examination of High Burnup Fuel Rods from Vandellos II." In *TopFuel Reactor Fuel Performance.* Manchester, United Kingdom: European Nuclear Society.

Bagger, C., H. Carlson, and P. Knudsen. 1978. *Details of Design Irradiation and fission Gas Release for the Danish UO2-Zr Irradiation Test 022.* RISØ-M-2152. Roskilde, Denmark: Risø National Laboratory.

Balfour, M. G. 1982. *BR-3 High Burnup Fuel Rod Hot Cell Program, Final Report, Vol. 1.* WCAP-10238, D0E/ET/34073-1. Pittsburgh, PA: Westinghouse Electric Corporation.

Balfour, M. G., W. C. Chubb, and R. F. Boyle. 1982. *BR-3 High Burnup Fuel Rod Hot Cell Program Vol. 2: Data Summary.* WCAP-10238, DOE/ET/34073-2. Pittsburgh, PA: Westinghouse Electric Corporation.

Barner, J. O., M. E. Cunningham, M. D. Freshley, and D. D. Lanning. 1990. *High Burn up Effects Program Summary Report.* DOE/NE/3406-1, HBEP-61. Richland, WA: Battelle, Pacific Northwest Laboratories.

Baumgartner, J. A. 1984. *BWR Fuel Bundle Extended Burnup Program Technical Progress Report, January 1983 to December 1983.* DOE/ET/34031-17, GEAP-30643. San Jose, CA: General Electric Company.

Beguin, S. 1999. *The Lift-Off Experiment with MOX Fuel Rod in IFA-610.2 Initial Results.* HWR-603. Halden, Norway: OECD Halden Reactor Project.

Blair, P., and J. Wright. 2004. *The IFM/MOX Comparative Test, IFA-651.1: Results after Four Cycles of Irradiation.* HWR-763. Halden, Norway: OECD Halden Reactor Project.

Boulanger, D., M. Lippens, L. Mertens, J. Basselier, and B. Lance. 2004. "High Burnup PWR and BWR MOX Fuel Performance: A Review of BELGONUCLEAIRE Recent Experimental Programs." In *International Meeting on LWR Fuel Performance.* Orlando, FL: American Nuclear Society.

Bradley, E. R., M. E. Cunningham, D. D. Lanning, and R. E. Williford. 1981. *Data Report for the Instrumented Fuel Assembly IFA-513.* NUREG/CR-1838 (PNL-3637). Richland, WA: Pacific Northwest Laboratory.

Buckland, R. J., C. E. Coppin, and C. E. White. 1978. *Experiment Data Report for PBF-LOCA Tests LOC-11b and 11c.* NUREG/CR-0303. Idaho Falls, ID: Idaho National Engineering Laboratory.

Carmack, W. J. 2012. *Temperature and Burnup Correlated FCCI in U-10Zr Metallic Fuel.* INL/EXT-12-25550. Idaho Falls, ID: Idaho National Laboratory.

Chantoin, P. M., E. Sartori, and J. A. Turnbull. 1997. "The Compilation of a Public Domain Database on Nuclear Fuel Performance for the Purpose of Code Development and Validation." In *International Topical Meeting on LWR Fuel Performance,* 515–522. Portland, OR: Americal Nuclear Society.

Claudel, J., and F. Huet. 2001. *Results from the Burnup Accumulation Test with High Exposure (63 MWd/kgHM) Model Fuel (IFA-648).* HWR-651. Halden, Norway: OECD Halden Reactor Project.

Cook, P., B. Christiansen, G. Dassel, E. Matthews, I. Robinson, R. Stratton, C. Walker, and R. Weston. 2003. "Performance of BNFL MOX Fuel." In *TopFuel 2003 Conference.* Würzburg, Germany: Kerntechnische Gesellschaft e. V.

Cook, P., E. Matthews, M. Barker, R. Foster, A. Donaldson, C. Ott, D. Papaioannou, and C. Walker. 2004. "Post-Irradiation Examination and Testing of BNFL SBR MOX Fuel." In *International Meeting on LWR Fuel Performance.* Orlando, FL: American Nuclear Society.

Cook, P., R. Stratton, and C. T. Walker. 2000. "Post Irradation Examination of BNFL MOX Fuel." In *International Topical Meeting on Light Water Reactor Fuel Performance.* Park City, UT: American Nuclear Society.

CSN and ENUSA. 2002. *Characteristics of the ENUSA Rods Irradiated in the Vandellos II Reactor up to 68 GWd/t and Planned to be Used in the CABRI International Programme.* CABRI Water Loop, 2002/34. CABRI International Programme.

Delorme, R., C. H. Valot, L. Fayaette, X. Pujol, I. Aubrun, J. Lamontagne, T. Blay, et al. 2012. "Study of Fission Gas Behaviour and Fuel Restructuration in Irradited $(U,Gd)O_2$ Fuel." In *TopFuel Reactor Fuel Performance.* Manchester, United Kingdom: European Nuclear Society.

Djurle, S. 1985. *Final Report of the Super-Ramp Project.* DOE/ET/34032-1. Washington, D.C.: U.S. Department of Energy.

EPRI. 2014. *High Burnup Dry Storage Cask Research and Development Project: Final Test Plan.* Contract No.: DE-NE-0000593. Palo Alto, CA: Electric Power Research Institute.

Forsberg, K., and A. R. Massih. 1985. "Diffusion theory of fission gas migration in irradiated nuclear fuel UO_2." *Journal of Nuclear Materials* 135 (2–3): 140–148.

Fujii, H., and J. Claudel. 2001. *The Lift-Off Experiments, IFA-610.3 (UO_2), and IFA-610.4 (MOX) Evaluation of In-Pile Measurement Data.* HWR-650. Halden, Norway: OECD Halden Reactor Project.

Fuketa, T., H. Sasajima, and T. Sugiyama. 2001. "Behavior of High-Burnup PWR Fuels with Low-Tin Zircaloy-4 Cladding Under Reactivity-Initiated-Accident Conditions." *Nuclear Technology* 133 (1): 50–62.

Fuketa, T., H. Sasajima, Y. Tsuchiuchi, Y. Mori, T. Nakamura, and K. Ishijima. 1997. "NSRR/RIA Experiments with High Burnup PWR Fuels." In *International Topical Meeting on LWR Fuel Performance.* Portland, OR: American Nuclear Society.

Galloway, J., C. Unal, N. Carlson, D. Porter, and S. Hayes. 2015. "Modeling constituent redistribution in U–Pu–Zr metallic fuel using the advanced fuel performance code BISON." *Nuclear Engineering and Design* 286:1–17. https://doi.org/10.1016/j.nucengdes.2015.01.014.

Geelhood, K., D. Colameco, W. Luscher, C. Goodson, D. F. Wray, T. Zipperer, J. Corson, and J. Whitman. 2026. *FAST-1.2.2: A Computer Code for Thermal-Mechanical Nuclear Fuel Analysis under Steady-state and Transients.* PNNL-39254. Richland, WA: Pacific Northwest National Laboratory.

Geelhood, K., W. Luscher, C. Goodson, J. Wray D. F.and Corson, and J. Whitman. 2026. *MatLib-1.2.2: Nuclear Material Properties Library.* PNNL-39258. Richland, WA: Pacific Northwest National Laboratory.

Geelhood, K. J., and C. E. Beyer. 2008. "Corrosion and Hydrogen Pickup Modeling in Zirconium Based Alloys." In *Water Reactor Fuel Performance Meeting.* Seoul, Korea: Korean Nuclear Society.

———. 2011. "Hydrogen Pickup Models for Zircaloy-2, Zircaloy-4, M5^{TM}, and ZIRLO^{TM}." In *Water Reactor Fuel Performance Meeting.* Chengdu, China.

Geelhood, K. J., W. G. Luscher, and J. M. Cuta. 2016. *FRAPTRAN-2.0: A Computer Code for the Transient Analysis of Oxide Fuel Rods.* PNNL-19400, Vol. 1 Rev. 1. Richland, WA: Pacific Northwest National Laboratory.

Georgenthum, V. 2009. *Influence of test conditions on the PCMI behaviour during RIA based on CIP0-1, VA-1 and VA-3 tests.* Tokai Mura, Japan.

Hirai, M., J. H. Davies, and R. Williamson. 1995. "Diffusivities of fission gas species in UO_2 and $(U,Gd)O_2$ nuclear fuels during irradiation." *Journal of Nuclear Materials* 226 (1–2): 238–251.

Hirschhorn, J., M. Tonks, and C. Matthews. 2021. "A CALPHAD-informed approach to modeling constituent redistribution in Zr-based metallic fuels using BISON." *Journal of Nuclear Materials* 544:152657. https://doi.org/10.1016/j.jnucmat.2020.152657.

Hodge, S. A., L. J. Ott, and F. P. Griffin. 2003. *Implications of the PIE Results for the 40-Gwd/MT-Withdrawal Mox Capsules.* ORNL/MD/LTR-241, Volume 2. Oak Ridge, TN: Oak Ridge National Laboratory.

Hodge, S. A., L. J. Ott, F. P. Griffin, and C. R. Luttrell. 2002. *Implications of the PIE Results for the 30-Gwd/MT-Withdrawal Mox Capsules.* ORNL/MD/LTR-212, Vol. 2, Rev. 1. Oak Ridge, TN: Oak Ridge National Laboratory.

Hoffmann, H., and N. Kraus. 1984. *Fabrication and Characterization Data of BN2 UO_2-Gd_2O_3 Fuel Rod.* GN 84/10. Bruxelles, Belgium: Belgonucleaire.

Jädernaäs, D. 2023. *SCIP-IV Subtask 2.3 - Separate Effects Tests. Intefral LOCA test on the effect of the plenum volume on FFRD. Test VUR1-LOCAplenum or VUR1-LOCA3.* STUDSVIK/N-23/042. Sweden: Studsvik Nuclear AB.

Janvier, J-C, B. de Bernaday de Sigoyer, and R. Delmas. 1967. *Irradiation of Uranium Oxide in Strong Cladding Effect of Initial Diametral Gap on Overall Behavior.* Program CC-7, 1st and 2nd Sections, CEA-R-3358. Paris, France: Commiserat a l'Energie Atomic.

Jeury, F., C. Hee, J. C. Giacalone, and J. Guillot. 2004. *Analysis report of the CABRI CIP0-1 test.* CABRI/WL 2004/55. Fontenay-aux-Roses, France: Institut de Radioprotection et de Sûreté Nucléaire (IRSN).

Jeury, F., C. Hee, J. C. Giacalone, and B. Siri. 2003. *Quick Look report of the CIP0-1 test.* CABRI/WL 2003/41. Fontenay-aux-Roses, France: Institut de Radioprotection et de Sûreté Nucléaire (IRSN).

Jošek, R. 2008a. *LOCA Testing at Halden: The BWR Experiment IFA-650.7.* HWR-906. Halden, Norway: OECD Halden Reactor Project.

———. 2008b. *The High Initial Rating Test IFA-677.1: Final Report on In-Pile Results.* HWR-872. Halden, Norway: OECD Halden Reactor Project.

Kallstrom, R. 2005. *SCIP, Task 0; Ramp Test Results, Final Report.* N-05/154: STUDSVIK-SCIP-42. Sweden: Studsvik Nuclear AB.

Kekkonen, L. 2007a. *LOCA Testing a Halden: The PWR Experiment IFA-650.5.* HWR-839. Halden, Norway: OECD Halden Reactor Project.

———. 2007b. *LOCA Testing a Halden: The VVER Experiment IFA-650.6.* HWR-870. Halden, Norway: OECD Halden Reactor Project.

Klecha, L. 2006. *Comparative Integral Irradiation Test on Gadolinia Fuel (IFA-681).* HWR-832. Halden, Norway: OECD Halden Reactor Project.

Knudsen, P., C. Bagger, H. Carlsen, I. Misfeldt, and M. Mogensen. 1983. *Risø Fission Gas Release Project Final Report.* DOE/ET/34033-1. Washington, D.C.: U.S. Department of Energy.

Koike, H. 2004. *The MOX Fuel Behaviour Test IFA-597.4/.5/.6/.7; Summary of In-Pile Fuel Temperature and Gas Release Data.* HWR-729. Halden, Norway: OECD Halden Reactor Project.

Lanning, D. D. 1986. *Irradiation History and Final Post-Irradiation Data for IFA-432.* NUREG/CR-4717 (PNL-5977). Richland, WA: Pacific Northwest Laboratory.

Lanning, D. D., M. E. Cunningham, J. O. Barner, and E. R. Bradley. 1987. *Qualification of Fission Gas Release Data from Task 2 Rods.* HBEP 25, Final Report. Richland, WA: Pacific Northwest Laboratory.

Larson, J. R., D. R. Evans, and R. K. McCardell. 1978. "Results of the first nuclear blowdown test on single fuel rods (LOC-11 Series in PBF)." In *ENS/ANS International Topical Meeting on Nuclear Power Reactor Safety.* CONF-781022-35. Brussels, Belgium. https://www.osti.gov/servlets/purl/6400249.

Larson, J. R., J. W. Spore, R. K. McCardell, J. M. Broughton, and L. K. Sepold. 1979. *PBF-LOCA Test Series; Test LOC-11 Test Results Report.* NUREG/CR-0618. Idaho Falls, Idaho: Idaho National Engineering Laboratory.

Lorenz, R. A., and G. W. Parker. 1972. *Final Report on the Second Fuel Rod Failure Transient Test of a Zircaloy-Clad Fuel Rod Cluster in TREAT.* ORNL-4710. Oak Ridge, Tennessee: Oak Ridge National Laboratory.

Lysell, G., and S. Birath. 1979. *Hot Cell Post-Irradiation Examination of Inter-Ramp Fuel Rods.* STIR-51. Studsvik, Sweden: Studsvik AB Atomenergi.

Magnusson, P., C. H. Sheng, P. Tejland, and H.-U. Zwicky. 2019. *Post-Irradiation Examinations of Rod 09-OL104.* STUDSVIK/N-16/204, Rev. 1. Sweden: Studsvik Nuclear AB.

Magnusson, P., and P. Tejland. 2023. *Integral LOCA Test on Rod 18-L1M7 with Annular Fuel.* STUDSVIK/N-23/033. Sweden: Studsvik Nuclear AB.

Manley, A. J., P. D. Kennedy, B. C. Scogings, I. Robinson, and J. F.W. Thompson. 1989. *Post Irradiation Examination of Three Rods Comprising Task 3 of the GAIN Programme.* GN 89/50. United Kingdom: United Kingdom Atomic Energy Authority, Windscale Laboratory.

Matsson, I., and J. A. Turnbull. 1998. *The integral fuel rod behaviour test IFA-597.3: Analysis of the measurements.* HWR-543. Halden, Norway: OECD Halden Reactor Project.

Matthews, C., C. Unal, J. Galloway, Jr. D. D. Keiser, and S. L. Hayes. 2017. "Fuel-Cladding Chemical Interaction in U-Pu-Zr Metallic Fuels: A Critical Review." *Nuclear Technology* 198:231–259. https://doi.org/10.1080/00295450.2017.1323535.

Mertens, L., and M. Lippens. 2001. "Study of Fission Gas Release on High Burnup MOX Fuel." In *TopFuel Reactor Fuel Performance.* Stockholm, Sweden: European Nuclear Society.

Mertens, L., M. Lippens, and J. Alvis. 1998. *The FIGARO Programme: The Behaviour of Irradiated MOX Fuel Tested in the IFA-606 Experiment, Description of Results and Comparison with COMETHE Calculation.* HPR 349/30. Halden, Norway: OECD Halden Reactor Project.

Meulemeester, E. de, N. Hoppe, G. de Contenson, and M. Watteau. 1973. "Review of Work Carried out by BELGONUCLEAIRE and CEA on the Improvement and Verification of the COMETHE Computer Code with the Aid of In-Pile Experimental Results." In *BNES International Conference on Nuclear Fuel Performance.* ECS-EEC-73-595. London, United Kingdom.

Mileshina, L., and P. Magnusson. 2019. *Integral LOCA test to study effect of pressure on fuel fragmentation: VUL2 LOCA2.* STUDSVIK/N-18-074. Sweden: Studsvik Nuclear AB.

Mogard, H., U. Bergenlid, S. Djurle, J. A. Gyllander, E. Larsson, G. Lysell, K. Ronnberg G. Saltvedt, and H. Tomani. 1979. *Final Report of the Inter-Ramp Project.* STIR-53. Studsvik, Sweden: Studsvik AB Atomenergi.

Montgomery, R., and B. Bevard. 2023. *Sister Rod Destructive Examinations (FY22).* M2SF-23OR010201024 and ORNL/SPR-2022-2678. Oak Ridge, TN: Oak Ridge National Laboratory.

Montgomery, R., B. Bevard, R. N. Morris, J. Goddard, Jr., S. K. Smith, Jianwei Hu, J. Beale, and B. Yoon. 2018. *Sister Rod Nondestructive Examination Final Report.* SFWD-SFWST-2017-000003, Rev. 1 (M2SF-17OR010201021) and ORNL/SPR-2017/484, Rev. 1 (ORNL/SPR-2018/801). Oak Ridge, TN: Oak Ridge National Laboratory and Electric Power Research Institute.

Morris, R. N., C. A. Baldwin, S. A. Hodge, L. J. Ott, C. M. Malone, and N. H. Packan. 2000. *MOX Average Power Intermediate PIE: 21 GWd/MT Final Report.* ORNL/MD/LTR-199. Oak Ridge, TN: Oak Ridge National Laboratory.

Morris, R. N., C. A. Baldwin, S. A. Hodge, and N. H. Packan. 2001. *MOX Average Power 30 GWd/MT PIE: Final Report.* ORNL/MD/LTR-212, Volume 1. Oak Ridge, TN: Oak Ridge National Laboratory.

Morris, R. N., C. A. Baldwin, and N. H. Packan. 2005. *MOX Test Fuel 50 GWd/MT PIE: Capsule 5 Quick Look.* ORNL/MD/LTR-272. Oak Ridge, TN: Oak Ridge National Laboratory.

Nakamura, T., M. Yoshinaga, M. M. Sobajima, K. Ishijima, and T. Fujishiro. 1994. "Boiling Water Reactor Fuel Behavior at Burnup of 26 GWd/tonne U Under Reactivity-Initiated-Accident Conditions." *Nuclear Technology* 108 (1): 45–59.

Nakamura, T., M. Yoshinaga, M. Takahashi, K. Okonogi, and K. Ishijima. 2000. "Boiling Water Reactor Fuel Behavior Under Reactivity-Initiated-Accident Conditions at Burnup of 41 to 45 GWd/tonne U." *Nuclear Technology* 129 (2): 141–151.

Newman, L. W. 1986. *The Hot Cell Examination of Oconee 1 Fuel Rods After Five Cycles of Irradiation.* DOE/ET/34212-50. Lynchburg, VA: Babcock and Wilcox Company.

Notley, M. J.F., R. DesHais, and J. R. MacEwan. 1967. *Measurements of the Fission Product Gas Pressures Developed in UO_2 Fuel Elements During Operation.* AECL-2662. Chalk River, ON: Atomic Energy of Canada, Ltd.

Notley, M. J.F., and J. R. MacEwan. 1965. *The Effect of UO_2 Density on Fission Product Gas Release and Sheath Expansion.* AECL-2230. Chalk River, ON: Atomic Energy of Canada, Ltd.

Oberländer, B. C., and H. K. Jenssen. 2014. *PIE on the Rod from the LOCA Test IFA-650.14 on High Burn-up BWR Fuel.* HWR-1096. Norway: Institutt for Energiteknikk, OECD Halden Reactor Project.

Ozawa, T. 2004. "Performance of ATR MOX Fuel Assemblies Irradiated to 40 GWd/t." In *International Meeting on LWR Fuel Performance.* Orlando, FL: American Nuclear Society.

Papin, J., B. Cazalis, J. M. Frizonnet, E. Fédérici, and F. Lemoine. 2003. "Synthesis of Cabri-RIA Tests Interpretation." In *The Eurosafe Forum 2003.* Paris, France.

Petiprez, B. 2002. *Ramp Tests with Two High Burnup MOX Fuel Rods in IFA-629.3.* HWR-714. Halden, Norway: OECD Halden Reactor Project.

Powers, D. A., and R. O. Meyer. 1980. *Cladding Swelling and Rupture Models for LOCA Analysis.* NUREG-0630. Washington, D.C.: U.S. Nuclear Regulatory Commission.

Reindl, J., G. Bart, A. Erne, R. Hofer, A. Hermann, R. Restani, and H. U. Zwuicky. 1991. *Destructive Examinations on the BN2, Ge5, and NF17 Fuel Rods 9, 10, 11, 23, 24, and 33 of the GAIN Programme.* GN 91/60. Switzerland: Paul Scherrer Institut.

Rø, E., and G. Rossiter. 2005. *The SBR MOX and UO_2 Comparison Test in Gas Flow Rig IFA-633: An Update of Results.* HWR-0823. Halden, Norway: OECD Halden Reactor Project.

Schrire, D. 2018. *Selected Vattenfall hot cell PIE data for benchmarking of FRAPCON.* Sweden: Vattenfall Nuclear Fuel AB.

Segura, J. C., and C. Bernaudat. 2002. *Fuel Characterization Data and Power History of the Rod which is to be tested in the CARI-WL CIPO-2 Test.* CABRI Water Loop 2002/27. CABRI International Programme.

Shimskey, R. W., M. K. Edwards, J. Geeting, J. R. Allred, S. K. Cooley, R. C. Daniel, R. M. Cox, et al. 2019. *Initial Results of Destructive Examination of Ten Sister Rods at PNNL.* PNNL-28548. Richland, WA: Pacific Northwest National Laboratory.

Smith, G. P., R. C. Pirek, H. R. Freeburn, and D. Schrire. 1994. *The Evaluation and Demonstration of Methods for Improved Nuclear Fuel Utilization.* DOE/ET-34-013-15. Windsor, CT: Combustion Engineering.

Struzik, C. 2004. *REGATE L10, fission gas release and cladding diameter of UO_2 rod during and after a transient at Bu = 47 MWd/kg.* NEA-1696/01. Cadarache, France: Commissariat à l'Energie Atomique.

Sugiyama, T. 2009. "PCMI failure of high burnup fuel under high temperature RIA conditions." In *Fuel Safety Research Meeting.* Tokai Mura, Japan.

Tejland, P., D. Jädernaäs, P. Magnusson, and J. Karlsson. 2022. "SCIP IV - Subtask 2.2 Heating and LOCA test on 07-R2RUP2-2." Presented at SCIPT IV RPG meeting June 2022.

Tejland, P., and C. H. Sheng. 2019a. *Integral BWR H3 overheating test of the fuel rod 12-R1E10.* STUDSVIK/N-19/041. Sweden: Studsvik Nuclear AB.

———. 2019b. *Integral overheating test to study TFGR of the fuel rod 09-0L 1L04.* STUDSVIK/N-19/029. Sweden: Studsvik Nuclear AB.

———. 2019c. *Post-Irradiation Examinations of Rod 12-R1E10.* STUDSVIK/N-18/034. Sweden: Studsvik Nuclear AB.

Thérache, B. 2005. *The High Initial Rating Test, IFA-677.1: Results after First Cycle of Irradiation.* HWR-819. Halden, Norway: OECD Halden Reactor Project.

Tradotti, R. 2014. *LOCA Testing at Halden, the BWR Fuel Experiment IFA 650.14.* HWR-1084. Norway: Institutt for Energiteknikk, OECD Halden Reactor Project.

Turnbull, J. A. 2001. "Concluding Report on Three PWR Rods Irradiated to 90 MWd/kg UO_2 in IFA-519.9: Analysis of Measurements Obtained In-pile and by PIE." In *EHPG-Meeting.* HWR-668. Lillehammer, Norway.

Turnbull, J. A., and R. J. White. 2002. *The Thermal Performance of the Gas Flow Rigs: A Review of Experiments and Their Analyses.* HWR-715. Halden, Norway: OECD Halden Reactor Project.

Tverberg, T., B. Volkov, and J-C Kim. 2005. *Final Report on the UO_2-Gd_2O_3 fuel performance test in IFA-636.* HWR-817. Halden, Norway: OECD Halden Reactor Project.

Tvergerg, T., and M. Amaya. 2001. *Study of Thermal Behaviour of UO_2 and $(U,Gd)O_2$ to High Burnup (IFA-515).* HWR-671. Halden, Norway: OECD Halden Reactor Project.

Wesley, D. A., K. Mori, and S. Inoue. 1994. "Mark BEB Ramp Testing Program." In *International Topical Meeting on Light Water Reactor Fuel Performance,* 343. West Palm Beach, FL.

White, R. J. 1999. *The Re-Irradiation of MIMAS MOX Fuel in IFA-629.1.* HWR-586. Halden, Norway: OECD Halden Reactor Project.

White, R. J., S. B. Fisher, P. M.A. Cook, R. Stratton, C. T. Walker, and I. D. Palmer. 2001. "Measurement and analysis of fission gas release from BNFL's SBR MOX fuel." 288 (1): 43–56.

Wiesenack, W. 1992. "Experimental Techniques and Results Related to High Burn-Up Investigations at the OECD Halden Reactor Project." In *Technical Committee Meeting,* 118–123. IAEA-TECDOC-697. Pembroke, ON.

———. 2015. *Summary and Comparison of LOCA Tests with BWR Fuel in the Halden Reactor Project Test Series IFA-650.* HPR-383. Norway: Institutt for Energiteknikk, OECD Halden Reactor Project.

Wright, J. 2004. *The SBR MOX and UO_2 Comparison Test in Gas Flow Rig IFA-633: Results after Seven Cycles of Irradiation.* HWR-764. Halden, Norway: OECD Halden Reactor Project.

Yacout, A. M., K. Mo, A. Oaks, Y. Miao, T. Sofu, and W. Mohamed. 2021. "FIPD: The SFR metallic fuels irradiation & physics database." *Nuclear Engineering and Design* 380:111225. https://doi.org/10.1016/j.nucengdes.2021.111225.

Yegorova, L., K. Lioutov, N. Jouravkova, O. Nechaeva, A. Salatov, V. Smirnov, A. Goryachev, V. Ustinenko, and I. Smirnov. 2005a. *Experimental Study of Narrow Pulse Effects on the Behavior of High Burnup Fuel Rods with Zr-1%Nb Cladding and UO_2 Fuel (VVER Type) under Reactivity-Initiated Accident Conditions: Program Approach and Analysis of Results.* NUREG/IA-0213, Vol. 1. Moscow, Russia: Nuclear Safety Institute of Russian Research Center Kurchatov Institute.

———. 2005b. *Experimental Study of Narrow Pulse Effects on the Behavior of High Burnup Fuel Rods with Zr-1%Nb Cladding and UO_2 Fuel (VVER Type) under Reactivity-Initiated Accident Conditions: Test Conditions and Results.* NUREG/IA-0213, Vol. 2. Moscow, Russia: Nuclear Safety Institute of Russian Research Center Kurchatov Institute.

Zwicky, H-U. 2024a. *Post-Irradiation Examinations of Rod 09-VUD1.* STUDSVIK/N-24/021. Sweden: Studsvik Nuclear AB.

———. 2024b. *Post-Irradiation Examinations of Rod 09-VUL1.* STUDSVIK/N-24/032. Sweden: Studsvik Nuclear AB.

Zwicky, H-U, and P. Tejland. 2022. *Post-Irradiation Examinations of Rod 10-R2L15.* STUDSVIK/N-22/054. Sweden: Studsvik Nuclear AB.

Zwicky, H.-U., and P. Magnusson. 2019. *Post-Irradiation Examinations of Rod 09-VUL2.* STUDSVIK/M-17/072 Rev. 1. Sweden: Studsvik Nuclear AB.

Appendix A – Description of Assessment Cases

A.1 Steady-State Assessment Cases

A.1.1 Halden IFA-432 Rods

The IFA-432 test (Lanning 1986) was irradiated under a research program on fuel rod steady-state performance sponsored by the NRC from 1974 to 1986. The IFA-432 test assembly was a heavily instrumented, six-rod assembly irradiated in the Halden heavy boiling water reactor (HBWR) from 1975 to 1984. The purpose was to test the long-term steady-state performance of BWR-6 type fuel rods, operated at power levels that were at the upper bound for full-length commercial fuel rods. The fuel pellets were fabricated at Pacific Northwest National Laboratory (PNNL) and shipped to Halden; final rod and assembly fabrication was completed at the Halden site. Destructive examinations of selected rods were carried out at Harwell Laboratories, UK.

The assembly included six instrumented rods and three replaceable non-instrumented spares. Each instrumented fuel rod had a centerline thermocouple in both the top and the bottom end of the fuel column and a pressure transducer to monitor rod internal pressure. The assembly instrumentation included six vanadium self-powered neutron detectors (SPNDs) and one cobalt neutron detector, together with rod elongation sensors at each rod position, coolant thermocouples at the top and bottom of the assembly, and a coolant flow meter (turbine).

The test rods were designed to simulate BWR-6 rod cladding type and radial dimensions, with variations in fuel-cladding gap sizes, fuel types, and fill gas compositions. The fuel rod length was much shorter than full-length (~144 in) commercial reactor rods to fit well within the short length of the Halden reactor core. Fuel rod overall length was 25 in, with an active fuel column length of 22.8 in. The overall void volume was held to 0.5 in^3 (by selection of a ~1 in plenum length at the upper end); this was done to approximate the ratio between fuel volume and void volume found in full-length rods. The cladding for all rods was Zircaloy-2.

Rods 1, 2, and 3 all had typical high-density (95% TD) stable sintered UO_2 fuel pellets and helium fill gas at 1 atm pressure; slight differences in the pellet diameters created variations in fuel-cladding gap size among the rods. Data taken from rod 1 upper and lower thermocouple, rod 2 lower thermocouple, and rod 3 upper and lower thermocouple during the first ramp to power were used in the BOL temperature assessment. Data from the rod 1 lower thermocouple and the rod 3 lower thermocouple were used in the temperature assessment as a function of burnup. It should be noted that much of the helium fill gas was lost from some of these rods during irradiation due to leakage past the thermocouple penetration through the end caps.

A.1.2 Halden IFA-513 Rods

The IFA-513 test fuel assembly (Bradley et al. 1981) was irradiated in the Halden reactor from November 1978 to mid-1981 under a continuation of an NRC program to test the performance of BWR-6 type fuel and the effects of fission gas contamination of the helium fill gas.

Rods 1 and 6 both had typical high density (95% TD) stable sintered UO_2 fuel pellets. Rod 1 had helium fill gas at 1 atm while rod 6 had 23% xenon and 77% helium fill gas at 1 atm. Data taken from rod 1 upper and lower thermocouple and rod 6 upper and lower thermocouple during the first

ramp to power were used in the BOL temperature assessment. Data from the rod 1 upper and lower thermocouple and the rod 6 upper and lower thermocouple were used in the temperature assessment as a function of burnup.

A.1.3 Halden IFA-633 Rods

The IFA-633 test assembly consisted of six instrumented rods (three short binderless route (SBR) MOX fuel rods and three UO_2 rods) irradiated from BOL through a burnup of 31 GWd/MTM. Rod 6 (Wright 2004) was the only MOX rod instrumented with both a fuel centerline thermocouple and a pressure transducer such that temperature and FGR measurements can be compared. Rods 1, 3, and 5 (Rø and Rossiter 2005) were UO_2 rods instrumented with centerline thermocouples and were used to assess the FAST predictions of temperature as a function of LHGR at BOL. This test assembly experienced a power ramp at a burnup of approximately 20 GWd/MTM to achieve fission gas bubble interlinkage. The MOX fuel was fabricated with the SBR process with a grain size of 7.5 microns and was typical of commercial fuel.

Rod 6 was used to assess the FAST temperature predictions for MOX as a function of burnup and the MOX FGR predictions. Rods 1, 3, and 5 were used to assess the FAST temperature predictions for UO_2 as a function of LHGR at BOL.

A.1.4 Halden IFA-677.1 Rods

The high initial rating test, IFA-677.1 (Thérache 2005; Jošek 2008a), was loaded in the Halden reactor in December 2004 and had completed six cycles of irradiation under HBWR conditions as of September 2007, achieving a rig average burnup of 30 GWd/MTU. The single cluster contained six rods supplied by Westinghouse, Framatome ANP, and Global Nuclear Fuel (GNF), all fitted with pressure transducers, fuel centerline thermocouples in both ends, and fuel stack elongation detectors, and with a cladding extensometer for one of the rods. The experiment was aimed at investigating the performance of modern fuels subjected to high initial rating with respect to thermal behavior, dimensional changes (densification and swelling), FGR, and PCMI.

Rod 2 (Framatome ANP), rod 3 (GNF), rod 4 (GNF), and rod 6 (Westinghouse) were all used to assess the BOL UO_2 temperature predictions of FAST as a function of LHGR. In addition, rod 2 was used to assess the UO_2 temperature predictions as a function of burnup up to 32 GWd/MTU.

A.1.5 Halden IFA-562 Rod

The Halden Ultra High Burnup (HUHB) test fuel assembly (IFA-562) (Wiesenack 1992) was initiated by the Halden reactor project to demonstrate the effect of burnup on fuel thermal conductivity. The HUHB configuration of the assembly consisted of six rods, four of which were instrumented with centerline expansion thermometers and two with pressure transducers. The rods were under irradiation in the Halden reactor from September 1989 to 1997. Documented data for fuel center temperatures and linear heat ratings are available to a rod-average burnup of 76 MWd/MTU.

Four rods (rods 15, 16, 17, and 18) contained “expansion centerline thermometers.” These are tungsten (1.8% ZrO) rods that run the full length of the rod on the inside of the pellets and gauge the average center temperature of each rod via thermal expansion of the rod detected by resistance change. Two rods (rods 13 and 14) each contained a pressure transducer for measuring

rod internal pressure. The assembly instrumentation included four SPNDs, three of which were located co-planar at the top of the assembly and one near the bottom to define the thermal neutron flux distribution within the assembly.

The behavior of LHGR and measured temperatures were very similar for all four rods with temperature sensors. One rod (number 18) was selected for comparison to FAST predictions.

A.1.6 Halden IFA-597.3 Rod

The fuel segments for the high-burnup integral rod behavior test IFA-597 (Matsson and Turnbull 1998) were refabricated from fuel rod 33-25065, which was irradiated in the Ringhals 1 BWR in Sweden, for approximately 12 years. The irradiation of this rod and its sibling rod 33-25046 was performed in two stages. During the first irradiation, 1980 to 1986, the rods were part of Ringhals assembly 6477 and an approximate rod-average burnup of 35 GWd/MTU was reached. The rods were then placed into fuel assembly 9902 for a second period of irradiation from 1986 to 1992 in Ringhals 1. The locations of fuel rods 33-25065 and 33-25046 in this assembly were positions 9902/D5 and 9902/E4, respectively. A final rod-averaged burnup of 59 GWd/MTU was achieved. The burnup at the location of the Halden refabricated segments was estimated as 67 GWd/MTU.

Rods 8 and 9 were loaded into positions 2 and 5 in IFA-597.2 (second loading) and irradiated in Halden for some 20 days in July 1995. After a few power ramps, rod 9 failed and the assembly was withdrawn. During this time, useful data were generated on centerline temperature as a function of power.

Rod 9 was removed and replaced by rod 7. The assembly was returned to the reactor as IFA-597.3 (third loading); the irradiation started in January 1997 and continued to May of that year having accrued a further ~2 GWd/MTU. Data obtained included centerline temperature as a function of power and burnup, (rod 8), FGR estimated from the increase in rod internal pressure transducer (rod 8), and clad elongation (rod 7).

The assembly was discharged and transported to Kjeller for PIE. FGRs of 12.6% and 15.8% were measured from puncturing and gas extraction from rods 7 and 8, respectively.

Rod 8 was used to assess the UO_2 temperature and FGR predictions of FAST.

A.1.7 Halden IFA-515.10 Rods

IFA-515.10 (Tvergerg and Amaya 2001) contained hollow rods with centerline thermocouples irradiated up to a burnup of greater than 80 GWd/MTU. Two of the rods contain UO_2 and two of the rods contain 8% gadolinia. However, the gadolinium used in these rods is composed of ^{160}Gd, which is a non-neutron absorbing isotope. In this way, the effect of the thermal conductivity degradation due to gadolinia can be separated from the power reduction that is typically seen in fuel containing gadolinia. For these rods, a special version of FAST was used that does not use the power profiles for neutron-absorbing gadolinia.

Rods A1 and A2 are sibling rods of UO_2 and urania-gadolinia (UO_2-Gd_2O_3), respectively, and experience very similar power histories. This is also true for rods B1 and B2. Halden has reported

that the thermocouples failed in rods A1, A2, and B2 at the burnup indicated on Figures 3-12, 37(b), 38(b).

After this point, the temperature data are no longer valid.

These four rods were used to assess the FAST temperature predictions for UO_2 and UO_2-Gd_2O_3 fuel as a function of burnup.

A.1.8 Halden IFA-681 Rods

IFA-681 (Klecha 2006) consists of six rods that had been irradiated for four cycles, or 340 days, as of 2006. Ongoing irradiation is currently underway in the Halden reactor. The input files for the UO_2 rods (rods 1 and 5) have been extended for six cycles to 507 days. All six of these rods were modeled using FAST. Three of these rods contain solid pellets with hollow pellets at the top end and are equipped with centerline thermocouples in the top pellets. These three rods have UO_2 (rod 1), 2% Gd_2O_3 (rod 2), and 8% Gd_2O_3 (rod 3) pellets.

The other three rods contain all hollow pellets and are equipped with expansion thermometers. These three rods also have UO_2 (rod 5), 2% Gd_2O_3 (rod 4), and 8% Gd_2O_3 (rod 6) pellets, with rod 6 being filled with 50% argon and 50% helium.

For rod 3, there are some over-predictions (50 to 120 °C) in the third and fourth cycles. This may be due to error in the temperature measurement or the estimation of the rod power level. This seems likely because the power level during these cycles is reported to increase from about 21 kW/m to about 25 kW/m, while the temperature is reported to remain constant at about 850 °C. It also seems strange for the power level in this rod to increase during these cycles while the power level in the other rods is constant during these cycles.

These six rods were used to assess the FAST temperature predictions for UO_2 and UO_2-Gd_2O_3 fuel as a function of burnup.

A.1.9 Halden IFA-558 Rods

IFA-558 (Turnbull and White 2002) was an assembly commissioned by Central Electricity Generating Board (later Nuclear Electric) to investigate the effect of hydrostatic restraint on the onset of grain boundary interlinkage, and hence, FGR. The assembly comprised six identical, short BWR type rods, each fitted with a pressure transducer and upper and lower fuel centerline thermocouples. The rods contained 7% enriched hollow pellets supplied by British Nuclear Fuels, Ltd. (BNFL) with a 200 µm cold diametral fuel-to-clad gap. In this way, PCMI effects were minimized, which would otherwise have introduced unwanted uncertainty in the hydrostatic pressure in the fuel pellets.

The assembly was loaded in February 1986 and continued operation successfully until discharge at ~40 GWd/MTU in March 1992. The fuel rods were subsequently sent to AEA Technology for PIE.

During startup, the rods were filled with helium gas at 2 bar pressure. Once the temperatures had stabilized at the prescribed normal operating powers, the pressures of four rods were altered in pairs in such a way as to minimize the spread of temperatures. Subsequently, rods 1 and 2 were

operated at the maximum internal pressure of 40 bar, rods 5 and 6 operated at 20 bar, while rods 3 and 4 remained at 2 bar. These pressures were maintained during all gas flow measurements and were only reduced at cold shutdown for safety reasons. The spread in fuel centerline temperatures during operation at around 35 kW/m for rods 2 through 6 was less than 60 °C, but rod 1 was consistently some 50 °C higher.

Radioactive FGR was measured frequently, particularly in rod 3, and the measurements were used to monitor the onset of grain boundary interlinkage. In addition, all gas swept out of the rods was retained in separate cold traps to measure the activity of ^{85}Kr, which was used to estimate the cumulative release of stable fission gas. This FGR data demonstrated that rod internal pressures up to 40 bar had little effect on FGR.

Rod 6 was used to assess the UO_2 temperature predictions of FAST.

A.1.10 Halden IFA-629.1 Rods

The IFA-629.1 (White 1999) test involved two MOX test rods (rods 1 and 2), but only rod 2 was punctured for FGR measurement such that only this rod will be used for FGR comparison. Both rods are used for the temperature comparison as a function of burnup. The MOX fuel was fabricated using the MIMAS-AUC process by Belgonucleaire (BN). The mother rod for the IFA-629.1 test rods was a full-length PWR MOX rod irradiated for two cycles in the Saint-Laurent PWR, France, with rods 1 and 2 cut as segments from the full-length rod and refabricated into short segments. The rod 2 segment had a burnup of 29 GWd/MTM following commercial irradiation, which was extended to 40 GWd/MTM during the Halden irradiation. The maximum LHGRs in Halden were significant, at 35 to 40 kW/m.

These two rods were used to assess the FAST temperature predictions for MOX as a function of burnup. Rod 2 was used to assess the FAST MOX FGR predictions.

A.1.11 Halden IFA-610 Rods

One segment from four-cycle PWR MOX EdF rod N016 (which was base-irradiated for four cycles in the French Gravelines-4 reactors to a burnup of approximately 55 MWd/kgM) was re-fabricated and instrumented for use in the sequential IFA-610.2,4 cladding liftoff experiments (Beguin 1999; Fujii and Claudel 2001). The rod was tested under simulated PWR conditions in a pressurized water loop within the Halden reactor. The rod was connected to a gas supply system, and temperature measurements were made in both helium and argon fill gases at varying pressures. Fuel temperature data from helium gas fill periods were used to assess the FAST temperature predictions.

The rod was base-irradiated at nominal LHGRs for ~1500 days. The final burnup for the segment was 54.5 MWd/kgM. The rod was instrumented with a fuel center thermocouple and a rod elongation sensor. Internal gas pressure was varied throughout the ~100 −day IFA-610.2 test to investigate the threshold for cladding liftoff. The LHGR level during the IFA-610.2 test was steady at about 14 to 15 kW/m, and LHGR at the thermocouple was about 13.5 to 14 kW/m.

In IFA-610.4, the LHGRs were similar at the beginning and drifted downward to 12.5 and 12.0 kW/m for rod-average and thermocouple location, respectively (Fujii and Claudel 2001). The test dura-

tion was similar to that of IFA-610.2 (100 days); however, after 50 days, questions of potential thermocouple degradation were raised, and code data comparison was only conducted over the first 50 days of the test.

These two experiments were used to assess the FAST temperature predictions for MOX as a function of burnup.

A.1.12 Halden IFA-648.1 Rods

The IFA-648.1 irradiation (Claudel and Huet 2001) was simply a burnup extension at low LHGR for two refabricated instrumented segments from Gravelines-4 four-cycle PWR MOX rods, one segment each from rods N12 and P16. The irradiation was carried on at low LHGR under simulated PWR conditions in a pressurized water loop within the Halden reactor. The rods were then power-ramped in the follow-on IFA-629.3 test to investigate FGR and rod elongation behavior.

The other rods were base-irradiated at nominal LHGRs for ~1200 days. The final burnup for the rods N12 and P16 were 57 and 53 MWd/kgM, respectively. The two rods were instrumented differently upon refabrication. Rod 1 carried a fuel center thermocouple and a rod elongation sensor. Rod 2 carried a fuel center thermocouple and a pressure transducer. The LHGRs were kept deliberately low to accumulate more burnup without inducing FGR.

These two rods were used to assess the FAST temperature predictions for MOX as a function of burnup.

A.1.13 Halden IFA-629.3 Rods

Following base irradiation in a commercial PWR and further irradiation in Halden, two rods were further irradiated from 62 GWd/MTU to 68 to 72 GWd/MTU. The MOX fuel was fabricated using the MIMAS (micronized master blend) process. The documentation does not mention whether the UO_2 was fabricated using the ammonium diuranate (ADU) or ammonium uranyl carbonate (AUC) process, but it is likely that the AUC process was used because the fuel was fabricated in the early 1990s. The MOX rods in IFA-629.3 (Petiprez 2002) were irradiated for four cycles in the Gravelines-4 PWR; after this period, two experimental rods were refabricated from the full-length rods, refilled with helium, and loaded in the IFA 648.1 rig to accumulate more burnup at low powers and no additional gas release. Following irradiation in IFA-648.1, rod 6 was punctured and refilled with helium and the two rods were irradiated in IFA-629.3. These rods were irradiated up to a final burnup of 68 and 72 GWd/MTM and discharged for PIE. The measured gas release values for these rods have been obtained by puncture meas

These two rods were used to assess the FAST temperature predictions for MOX as a function of burnup and the MOX FGR predictions.

A.1.14 Halden IFA-606 Rod

The IFA-606 test assembly (Mertens et al. 1998; Mertens and Lippens 2001) consisted of four refabricated rod segments from a full-length PWR MOX rod irradiated in the Beznau-1 reactor, Switzerland, at nominal LHGRs to a burnup of 50 MWd/kgM. The MOX fuel was fabricated using the MIMAS-AUC process by BN. Two test rods were instrumented with a fuel thermocouple and a

pressure transducer, and irradiated under Halden conditions for approximately 30 days at elevated LHGR in “Phase 2” of the test, to determine FGR behavior. The code-data comparisons presented are for only rod 2 that measured FGR by rod puncture, with a 12.5 micron grain size.

The fuel rod segment was instrumented with a pressure transducer and a fuel centerline thermocouple. The rod was base-irradiated at nominal LHGRs for ~1500 days. The rod segment reached a burnup of 49.5 GWd/MTM during commercial operation, with additional 30 days of irradiation in Halden for a total burnup of 50.6 GWd/MTM.

This rod was used to assess the FAST temperature predictions for MOX as a function of burnup and the MOX FGR predictions.

A.1.15 Halden IFA-636 Rods

IFA-636 (Tverberg et al. 2005) contained both hollow pellets with centerline thermocouples and solid pellets irradiated up to a burnup of 25 GWd/MTU. FAST was used to model two of the rods from this assembly. These rods contained 8% gadolinia of the type typically used in power reactors. Centerline temperature data from IFA-636 rod 2 (hollow pellets) was used to compare to FAST predictions.

Centerline temperature from IFA-636 rod 4 (solid rod) was estimated by Halden based on measurements from IFA-636 rod 2. These estimates were used to compare to FAST predictions. These estimates may have more error than those for rod 2 due to both power uncertainties and uncertainties in estimating rod 4 temperature from rod 2 data.

These two rods were used to assess the FAST temperature predictions for UO_2-Gd_2O_3 fuel as a function of burnup.

A.1.16 BR-3 Rods

The DOE sponsored high-burnup irradiation of five well-characterized PWR-type test rods (Balfour 1982; Balfour et al. 1982) in the BR-3 reactor, located in Mol, Belgium, to demonstrate the feasibility of extending commercial fuel rod burnup and thereby help to minimize radioactive waste disposal. These rods were fabricated by Westinghouse Corporation, whose staff also oversaw the PIEs. The PIE on the rods was carried out in the BR-2 hot cell facility at the Mol site. The rods were of basic PWR radial dimensions. Goal peak burnups exceeded 70 GWd/MTU.

The test rods were designed to simulate Westinghouse PWR (15x15) rod cladding type and radial dimensions, with variations in fuel enrichment and rod position providing variations in power history. The fuel rod length was much shorter than the full-length (~144 in) commercial reactor rods and fit well within the short length of the BR-3 reactor core. The fuel rod overall length was 44 in with an active fuel column length of 38.4 in.

Six rods were selected for comparison with FAST FGR predictions: 24-I-6, 36-I-8, 111-I-5, 28-I-6, 30-I-8, and 332. Three of these rods were also selected for comparison with FAST void volume predictions: 24-I-6, 36-I-8, and 111-I-5.

A.1.17 Zorita Rod

Four fuel assemblies were initially irradiated in Zorita cycles 1 and 2. A total of 41 of the fuel rods in each assembly were removable, and 16 of these rods per assembly had high enrichment (4.08 to 6.6 wt% ^{235}U) to achieve high linear power levels and burnups. One of these rods, rod 332 (Balfour et al. 1982), with high enrichment that was irradiated up to 57 GWd/MTU, was selected as an FGR assessment case for FAST.

A.1.18 BNFL BR-3 Rods

Battelle, Pacific Northwest Laboratories administered the international group-sponsored High Burnup Effects Program (HBEP), which continued from 1978 to 1990. The objective of the HBEP was to determine the effects of extended burnup on fuel rod performance, especially FGR. A variety of test rods and commercial power reactor rods were irradiated and examined under the HBEP, including two PWR assemblies (366 and 373) (Lanning et al. 1987; Barner et al. 1990) containing PWR-type test rods irradiated in a single assembly in the BR-3 test reactor in Mol, Belgium. Both of these assemblies experience high power, and the rods showed significant FGR.

One rod from each assembly (rod DE from 373 and rod 5-DH from 366) was selected to be part of the UO_2 FGR assessment cases for FAST.

A.1.19 DR-3 Rods

Test 022 comprised three UO_2-Zr test fuel pins which were irradiated in the DR-3 reactor at Risø, Denmark, at 7.2 MPa (70 atm) system pressure (Bagger et al. 1978). A burnup of approximately 42 GWd/MTU was accumulated at heat loads in the range of 35 to 53 kW/m. Fission gas analysis for two of the pins (PA29-4 and M2-2C) showed that the releases were 49 and 36% .

The three almost identical test fuel pins had 12.6 mm sintered UO_2 pellets of 2.28% enrichment in 128 mm long stacks. The cladding was cold-worked and stress-relieved Zircaloy-2 tubing of approximately 0.55 mm wall thickness which had been autoclaved on both sides. The diametral pellet-clad clearance was 0.24 mm, and the pins were backfilled with 0.1 MPa (1 atm) helium.

These two rods were used to assess the FAST UO_2 FGR predictions.

A.1.20 NRX Rods

Several sets of UO_2 fuel rods were irradiated in a pressurized water loop in the NRX reactor in Chalk River, Canada (Meulemeester et al. 1973; Notley et al. 1967). The goal of these tests was to measure the gas pressures inside the rods, with the following objectives:

- To determine the effects of fuel density on gas pressure and FGR.
- To determine the effects of element power output variations on gas pressure and FGR.
- To obtain data to test the predictions of a model for calculating the variation of gas pressure with power output.

After irradiation, the rods were dimensioned and punctured for fission gas analysis. Samples from the rods were also analyzed for chemical burnup. Five of these rods were selected as UO_2 FGR assessment cases for FAST because they provide FGR data at low burnups (<11 GWd/MTU) while the other FGR assessment data were at burnups greater than 20 GWd/MTU. Rods CBR, CBY, and CBP were irradiated together to 2.7 GWd/MTU in 85 days. Rod LFF was irradiated to 3.3 GWd/MTU in 108 days. Rod EPL-4 was irradiated to 10.4 GWd/MTU in 100 days.

A.1.21 EL-3 Rods

Sixteen cartridges, each containing two rods, were irradiated in the EL-3 reactor, France, for a varying number of cycles to achieve burnups from 3 to 12 GWd/MTU. The aspects of the rods studied in this project were:

- Macroscopic appearances: crack network, material movement, and dimensional changes
- Microscopic appearances: re-crystallization, pore redistribution, and new phases
- Migration of fission products: stable gases released by the fuel and distribution of solid fission products

Each cartridge was constructed of Zircaloy-2 and consisted of two separate stages, each containing a stack of UO_2 fuel 123 mm high at each end, and in the central joint, space was provided for cobalt flux indicators. Each stage contained a chromel-alumel thermocouple located in the center of the stack. The cartridges were then filled with helium.

After irradiation, the rods were dimensioned and punctured for fission gas analysis. Gamma scans were done as well as a radiochemical analysis. The rods 4110-AE2 and 4110-BE2 (Janvier et al. 1967) were used to assess the UO_2 FGR predictions of FAST.

Both rods 4110-AE2 and 4110-BE2 contained fuel pellets with an as-fabricated density of 10.52 g/cm^3. AE2 ran at a power of 17.6 kW/ft while BE2 ran at a power of 17.8 kW/ft. Rods 4110-AE2 and 4110-BE2 were maintained throughout life at constant average LHGRs of 17.6 and 17.8 kW/ft, respectively. Both ran with a flat axial power profile. The input LHGRs were a flat 17.6 and 17.8 kW/ft, with a few steps to get up to power.

These two rods were used to assess the FAST UO_2 FGR predictions at burnups less than 15 GWd/MTU.

A.1.22 FUMEX 6f and 6s Rods

Two rods were base-irradiated in the Halden HBWR at low power to 55 GWd/MTU. Each of these rods was then refabricated to include pressure transducers and run at higher power while the pressure was being monitored. These rods, FUMEX 6s and FUMEX 6f (Chantoin et al. 1997) were included as FAST UO_2 FGR assessment cases.

A.1.23 Halden IFA-429 Rod

The IFA-429 test fuel assembly (Turnbull 2001) was initiated by NRC-Research and designed and fabricated by Idaho National Laboratory (with fuel pellet fabrication by PNNL) to demonstrate

the effect of burnup, power level, and fuel grain size on fuel thermal behavior and FGR. The assembly consisted of 18 original short rods, arranged in three clusters of 6 rods each, and 15 non-instrumented spare and replacement rods. Rod DH is a replacement rod that was re-instrumented with a pressure transducer after it had attained about 30 GWd/MTU burnup at relatively low LHGR; the rod was then irradiated in IFA-519 at much higher and variable LHGR as part of a load-follow test, and eventually attained a peak burnup of 99 GWd/MTU. The FGR for this rod was obtained by puncture during PIE. It should be noted that the puncture data provided much higher release values than were estimated from the pressure transducer measurements because the rod pressures had exceeded the measurement capabilities of the pressure transducer.

A.1.24 Arkansas Nuclear One Unit 2 PWR Rod

DOE sponsored a program with ABB Combustion Engineering and Energy Operations, Inc. to improve the use of PWR fuel. The scope of this project was to develop more efficient fuel management concepts and an increase in the burnup of discharged fuel.

Two 16x16 lead test assemblies were irradiated in the Arkansas Nuclear One-Unit 2 reactor (ANO-2). This is a PWR that operates at 2815 MWt. One of the assemblies, D039, was irradiated for three cycles and achieved a burnup of 33 GWd/MTU. The other assembly, number D040, was irradiated for five cycles and achieved a burnup of 52 GWd/MTU.

Rod TSQ002 (Smith et al. 1994), irradiated in assembly D040, was of standard CE 16x16 design and contained solid UO_2. Assembly D040 was irradiated from 1979 to 1988 in ANO-2, cycles two through six. It accumulated 52 GWd/MTU assembly-average burnup. Rod TSQ002 accumulated an end-of-life (EOL) rod-average burnup of 56.1 GWd/MTU. The rod-average LHGR varied from 2.75 to 6.95 kW/ft, with the higher values near BOL.

This rod was used to assess the FAST UO_2 FGR predictions, the EOL void volume predictions and the Zircaloy-4 corrosion predictions.

A.1.25 Oconee PWR Rod

DOE sponsored a long-term, multi-organizational program on the performance of LWR fuel rods during operation to extend burnups. As part of that program, Babcock and Wilcox (B&W) 15x15-type PWR fuel assemblies were irradiated to 3, 4, and 5 cycles in the Oconee PWR, operated by Duke Power Company. One assembly, 1D45, completed five cycles of irradiation in June 1983, having achieved an assembly average burnup of 50 GWd/MTU during 1553 effective full-power days.

Several rods from the assembly were non-destructively and destructively examined in the B&W hot cells. This document summarizes the design and operating parameters for one rod, number 15309 (Newman 1986). Fuel density and microstructure, rod growth, cladding oxidation/hydriding, and diametral strain data are available for this rod together with FGR measurement via rod puncture and plenum gas analysis. The FGR for this low-powered rod was $<1\%$; but the cladding oxidation, growth, and diametral strain were significant.

The rods were standard 15x15 full-length PWR rods. The rod initially had a rod-average LHGR of 7 to 8 kW/ft; however, this decreased to ~4 kW/ft by EOL. The axial power profile flattened early

and remained relatively flat throughout life.

This rod was used to assess the FAST UO_2 FGR predictions, the EOL void volume predictions and the Zircaloy-4 corrosion predictions.

A.1.26 Halden IFA-651 Rods

The IFA-651.1 rig (Blair and Wright 2004) contained six fuel rod segments. Three of these rod segments contained inert matrix fuel and three rod segments contained MOX fuel. The MOX rods (rods 1, 3, and 6) were modeled with FAST. Rod 1 MOX fuel was fabricated using an SBR that results in a relatively homogeneous distribution of the PuO_2 compared to MOX fabricated using the MIMAS process. Rods 3 and 6 were fabricated at Paul Scherrer Institute using a two-stage attrition milling process developed by the Korean Atomic Energy Research Institute. Micrographs provided appear to demonstrate that this process provides a homogenous distribution of PuO_2 similar to that observed in the SBR process.

These rods were irradiated for four cycles in the Halden reactor to a rod-average burnup between 20 and 23 GWd/MTM. PIE showed that the fuel in rods 1 and 6 had an in-reactor densification of 2% , while the fuel in rod 3 had an in-reactor densification of 1% . These values have been entered into the code as input parameters. The measured gas release values used for model verification have been estimated from pressure measurements and are subject to greater uncertainty than measurements made by rod puncture.

These three rods were used to assess the FAST temperature predictions for MOX as a function of burnup and the MOX FGR predictions.

A.1.27 Advanced Test Reactor WG-MOX Rods

Oak Ridge National Laboratory has reported base-irradiation LHGR histories and post-irradiation FGR for seven fuel pins irradiated in the ATR (Morris et al. 2000; Morris et al. 2001; Morris et al. 2005; Hodge et al. 2002; Hodge et al. 2003). These pins were irradiated in stainless steel capsules. Several pins were withdrawn for PIE after Phases II, III, and IV, after the pins had accumulated 21, 30, and 40 to 50 GWd/MTM, respectively. The fuel used in these pins was fabricated using weapons-grade (WG) plutonium with a process similar to MIMAS. Fuel produced from WG plutonium differs from commercial MOX fuel in two ways. First, the WG MOX has greater amounts of ^{239}Pu, and second, WG MOX contains small amounts of gallium.

The measured gas release values for these rods have been obtained by puncture measurement.

These three rods were used to assess the FAST MOX FGR predictions.

A.1.28 Gravelines-4 PWR Rods

The Halden Project has reported base-irradiation LHGR histories and post-irradiation (rod puncture) FGR for three full-length PWR MOX rods from Gravelines-4 reactor, France, which were subsequently sectioned to produce test rods for various instrumented tests (Beguin 1999; Fujii and Claudel 2001; Claudel and Huet 2001; Petiprez 2002). These commercial rods did not expe-

rience LHGRs in excess of 25 kW/m or temperatures in excess of 1500 K, resulting in measured FGR below 5% .

These three full-length commercial rods were used to assess the FAST MOX FGR predictions.

A.1.29 Beznau-1 M504 Rods

The M504 program (Cook et al. 2003; Cook et al. 2004) consisted of four MOX rods irradiated in assembly M504 for four cycles in the Beznau-1 PWR reactor. The MOX fuel was fabricated using the SBR process, which results in a relatively homogenous distribution of the PuO_2. These rods were irradiated up to a burnup between 37 and 43 GWd/MTM. The measured gas release values are relatively low and have been obtained from puncture measurements that have less uncertainty than those estimated from pressure measurements.

These four rods were used to assess the FAST MOX FGR predictions.

A.1.30 Beznau-1 M308 Rod

In the M308 program (Boulanger et al. 2004), segmented MOX rods were irradiated in the Beznau reactor up to peak burnups of 55 to 60 GWd/MTM. The MOX fuel was fabricated using the MIMAS–AUC process by BN, which results in larger PuO_2 particle sizes than the SBR process. Sufficient detail on the power history and measured FGR was provided for Segment 2, such that this segment was modeled using FAST. Only the cladding inner and outer diameters were provided for this segment; however, since these values were identical to the cladding inner and outer diameters for a Westinghouse 15x15 fuel rod, it was assumed the rest of the rod dimensions were the same as for a Westinghouse 15x15 fuel rod.

This rod was used to assess the FAST MOX FGR predictions

A.1.31 Halden IFA-597.4/.5/.6/.7 Rods

IFA-597.4, 5, 6, and 7 (Koike 2004) contained two MOX rods, containing fuel that was fabricated with the MIMAS-ADU process. Rod 10 contained mostly solid pellets, with a few hollow pellets at the top of the stack to accommodate the fuel centerline thermocouple. Rod 11 contained all hollow pellets. These rods were irradiated for four cycles in the Halden reactor to a burnup between 35 and 37 GWd/MTM. The power history at the thermocouple position was provided for both rod 10 and rod 11. To determine the rod-average LHGR, for rod 10, the power history was increased by the ratio of average power to power at the top of the rod, and the ratio of the volume of a solid pellet to the volume of a hollow pellet. For rod 11, the power history was increased by only the ratio of average power to power at the top of the rod. For these pellets, the out-of-pile re-sintering tests of 24 hours at 1700 °C showed a density increase of 0.46% . However, based on in-pile free volume and pressure measurements, it was determined that the maximum densification was 0.8% for rod 10 and 1.4% for rod 11. These measured values were used in the FAST input files.

The measured gas release values used for the FAST assessment have been estimated from pressure measurements and are subject to greater uncertainty than measurements made by rod puncture.

These two rods were used to assess the FAST temperature predictions for MOX as a function of burnup and the MOX FGR predictions.

A.1.32 FUGEN Rods

The MOX fuel assembly, E09 (Ozawa 2004), was irradiated for 10 cycles in the Japanese advanced thermal reactor, Fugen. This assembly reached the highest assembly average burnup of 38 GWd/MTM. The rods in this assembly were arranged in a circular pattern consisting of three concentric rings. The power history was approximately the same for all rods in a given ring. However, the power histories given for each ring did not provide the rod-average burnup that was measured in the pellets via gamma scanning. This discrepancy is most likely due to uncertainty in the linear heat rates that were provided. To model these cases, the power histories that were supplied were increased by a factor so the burnup calculated using these histories would be equivalent to the measured burnup.

The pellet stack consisted of pellets with varying plutonium concentration in different axial regions. The top and bottom areas contained more plutonium than the central region. Since it is not possible to specify the plutonium concentration at various axial regions along the pellet stack in FAST, two cases were run. In the first case, the plutonium concentration for the middle section was used for the entire rod, and in the second case, the plutonium concentration for the top and bottom sections was used for the entire rod. This allowed the effect of plutonium concentration on FGR to be seen. Plutonium concentration had very little impact on the predicted FGR ($<$5% relative).

The measured gas release values for these rods have been obtained by puncture measurement on several rods from each ring.

These three rods were used to assess the FAST MOX FGR predictions.

A.1.33 Monticello BWR Rod

A DOE program was completed in 1985 in which nine 8x8 fuel assemblies in the Monticello BWR were taken to high burnup (up to 45.6 MWd/MTM assembly average), and the rods were periodically examined non-destructively and sampled for destructive examinations (Baumgartner 1984). Four of the assemblies went for the “full term” from cycle 3 through cycle 9 from May 1974 to September 1982.

All of these rods have fully annealed Zircaloy-2 cladding. One of these rods, rod A1 from assembly MTB99 was used in the Zircaloy-2 corrosion assessment for FAST.

A.1.34 TVO-1 BWR Rod

Battelle, Pacific Northwest Laboratories administered the international group-sponsored HBEP, which continued from 1978 to 1990. The objectives of the HBEP were to determine the effects of extended burnup on fuel rod performance, especially FGR. A variety of test rods and commercial power reactor rods were irradiated and examined under the HBEP, including nine full-length 5- and 6-cycle rods from the TVO-1 BWR in Finland (Barner et al. 1990). One of these rods was used to assess the corrosion performance of FAST for Zircaloy-2: rod number H8/36-6 from 5-cycle fuel assembly 6116.

The rod occupied position H8, which was the control blade corner position. The rod-average burnup at EOL was 44.6 GWd/MTU, with a peak value (confirmed by chemical burnup analysis) of 50.9 GWd/MTU. The rod-average LHGR varied between 12 and 24 kW/m (3.3 to 7.6 kW/ft), but large variations in the peak-to-average LHGR ratio occurred due to control blade movements.

A.1.35 Vandellos PWR ZIRLO Rods

A joint Spanish and Japanese effort irradiated a large number of full-length fuel rods for five cycles in the Spanish PWR Vandellos 2 (CSN, ENUSA 2002). The rods were clad with ZIRLO and Mitsubishi Developed Alloy (MDA). Two of the ZIRLO rods (A06 and A12) have been modeled with FAST to assess the performance of the ZIRLO corrosion model to high burnup.

A.1.36 Gravelines-5 PWR M5 Rod

One high-burnup rod was taken from the French reactor Gravelines-5 and refabricated for the RIA test CIP0-1, performed in the CABRI reactor, France (Segura and Bernaudat 2002). This rod, N05, was clad with M5. Before refabrication, rod N05 was examined and the oxide layer thickness was measured. This full-length commercial rod has been modeled with FAST to assess the performance of the M5 corrosion model to high burnup.

A.1.37 GAIN UO_2-Gd_2O_3 Rods

The GAIN Programme, which was an international program lead by Belgonucleaire, irradiated four rods with two different doping concentrations. Rods 301 and 302 were doped with 3wt% Gd while rods 701 and 702 were doped with 7wt% Gd. All four rods were irradiated in BR3 for four cycles, but rod 701 was removed for transient tests between cycles in BR2 (Hoffmann and Kraus 1984; Manley et al. 1989; Reindl et al. 1991). FGR measurements were obtained from each rod.

A.1.38 North Anna Sibling Rods

The sibling rods are part of the High Burnup Spent Fuel Data Project sponsored by the US Department of Energy Office of Nuclear Energy. This project aims to “provide confirmatory data for model validation and potential improvement, provide input to future spent nuclear fuel (SNF) dry storage cask design, support license renewals and new licenses for Independent Fuel STorage Installations (ISFSIs), and support transportation licensing for high burnup SNF” (EPRI 2014). 32 high burnup (>45 GWd/MTU) fuel assemblies irradiated at North Anna were loaded into a NRC-licensed storage cask and after at least 10 years, the cask will be opened and the fuel examined and tested to provide confirmation of laboratory data.

25 sibling rods were removed from fuel assemblies–nine rods from the cask-loaded assemblies and 16 from similar high burnup assemblies–and shipped to Oak Ridge National Laboratory (ORNL) for detailed nondestructive examination (Montgomery et al. 2018); oxide measurements were made. 10 of these rods were then sent to PNNL; both ORNL and PNNL performed destructive examination on the sibling rods (Montgomery and Bevard 2023; Shimskey et al. 2019) to measure FGR and void volumes.

A.2 Power-Ramp Assessment Cases

A.2.1 Ramped HBEP Obrigheim/Petten Rods

The HBEP was an international, group-sponsored program administrated by Battelle Pacific Northwest Laboratory from 1979 to 1989 (Barner et al. 1990). The objective was to investigate the impact of extended burnup on fuel rod performance, especially FGR. A total of 81 rods of both BWR and PWR types were irradiated and examined under the program, with rod-average burnups ranging up to 69 GWd/MTU and peak pellet burnups up to 83 GWd/MTU.

Under Task 2 of the program, full-length segmented rods were irradiated in commercial power reactors and then subjected to power ramps in test reactors. The rod segments comprised “rodlets” that were individual short-length fuel rods, mated end-to-end to form the full-length rods. Following irradiation to a variety of burnup levels, the rods were disassembled into the individual rodlets, and the rodlets were ramp-tested in test reactors. The peak LHGRs in these ramps ranged from 35 to 50 kW/m, and hold times ranged from 48 to 196 hours. The FGR during bumping was a function of the peak LHGRs and ranged from 10 to 45% . The pre-bump LHGRs ranged from 15 to 35 kW/m, as confirmed by calibrated nondestructive ^{85}Kr activity determinations for the plenum gas, and the pre-bump FGRs were generally low (1 to 5%).

Two PWR-type ramped rodlets were chosen for comparison to FAST predictions. Both were fabricated by Kraftwerk Union (KWU), irradiated in the same fuel assembly in the Obrigheim PWR, Germany, and then power-ramped to approximately the same peak LHGR (41 to 43 kW/m) in the JRC-Petten test reactor, the Netherlands. Rodlet D200 attained 25 GWd/MTU burnup in one reactor cycle at LHGRs of 25(2) kW/m. Rodlet D226 attained 45 GWd/MTU by further irradiation in the same assembly for two more cycles, with LHGR generally decreasing with time from 25 kW/m at BOL to $\sim$17 kW/m during the final cycle. The fuel in these rods resulted in high fuel densification $<$2.5% TD and high open porosity that is atypical of today’s fuel. Comparisons of the FGR data from these power-ramped rods to other power-ramped data with lower densification and open porosity fuel typical of today’s fuel suggests that these FGR data are higher than observed from today’s fuel. As a result, the FAST code tended to under-predict this data, which is not surprising.

The post-bump FGR is greater for the higher-burnup rodlet D226 than for rodlet D200 (44 vs. 38%), despite D226 having a smaller as-fabricated fuel cladding gap. The pre-ramp FGRs, based on ^{85}Kr activity in the plenums, were very similar: 4.2 and 6.6% , respectively. Therefore, the net FGR during ramping is greater for rodlet D226, and this was attributed to burnup effects. This rodlet pair thus provides a test of the burnup effects inherent in FAST.

A.2.2 Super-Ramp Rods

The Super-Ramp Project was an international, group-sponsored program involving base-irradiation of segmented full-length BWR and PWR rods in various power reactors, followed by ramp-testing of the rod segments in the Studsvik R-2 test reactor in Sweden (Djurle 1985). The project’s purpose was to establish the failure threshold for rods of varying types and burnup, and some rod segments did fail during high-power ramp testing. Rod segments that did not fail, however, gave data on FGR and cladding permanent hoop strain during EOL power transients.

Three rod segments were selected as FGR assessment cases and nine rod segments were se-

lected as cladding hoop strain assessment cases. These were all non-failed PWR rod segments, which had been base-irradiated in the Obrigheim PWR for three cycles up to a burnup of 34 to 37 GWd/MTU. The segments were then ramp-tested in the Studsvik reactor to ramp terminal levels as high as 43 kW/m. The FGRs and residual cladding hoop strain were measured following the ramp test.

The segmented PWR rods were designed in basic conformance with KWU's 15x15 PWR fuel design. The general design specifications are given in Table A15.1. The fuel segment length was short, 39 cm overall and 31.5 cm active fuel length, to match well within the ~1 m active length of the Studsvik reactor core. The diametral fuel-cladding gap was 145 microns (5.7 mils). The fuel pellet density is 95% TD, and the standard KWU densification test is only 2.2 hours at 1700 °C rather than the 24 hour densification test at 1700 °C required by the NRC as a measure of maximum densification. Therefore, the quoted maximum densification for this fuel "none" may be low, and it may be as great as 1% TD–the latter figure is used as FAST input.

A.2.3 Inter-Ramp Rods

The Studsvik Inter-Ramp Project objective was to investigate the mechanical failure threshold for BWR 8x8 type fuel rods. Short rodlets with standard BWR 8x8 dimensions and components were fabricated by ABB/Atom specifically for the project and were base-irradiated to ~20 GWd/MTU at low LHGRs before EOL ramping at rapid rate to high LHGRs to probe for cladding failure. Hold times at the ramp terminal (LHGR) level were 24 hours for non-failed rods. For the non-failed rods, post-ramp FGR was determined by rod puncture.

Two of the non-failed, ramp-tested Inter-Ramp rods, numbers 16 and 18 (Mogard et al. 1979; Lysell and Birath 1979), were selected for FGR and cladding permanent hoop strain assessment.

Twenty short 21 in rodlets were fabricated for the test, with nominal 8x8 BWR fuel rod characteristics, and there were some departures from these characteristics. Rods 16 and 18 were both "nominal rods" with 6 mil diametral gaps, 1 atm helium fill, and 95% TD solid, dished fuel pellets. The rods were irradiated in approximate BWR coolant conditions in pressurized loops within the Studsvik reactor. Rods 16 and 18 operated for ~550 days at LHGRs ranging from 20 to 40 kW/m and achieved burnups of 21 and 18 GWd/MTU, respectively.

Rods 16 and 18 were then preconditioned for 24 hours at 29 and 25 kW/m, respectively, and then ramped at a rate of ~70 W/m per second to terminal levels (maximum peak LHGR values) of 48 and 41 kW/m, respectively, where they were each held for 24 hours, during which the coolant was monitored for added radioactivity (indicating rod failure). Neither rod failed. Therefore, puncture and FGR determinations were feasible, and were performed.

A.2.4 Ramped Halden/DR-2 Rods

The Risø Fission Gas Release Project was an international, group-sponsored program administrated by Risø Laboratories, from 1980 to 1981. The objective was to investigate the impact of extended burnup and EOL power ramping on FGR in BWR-type fuel rods. This was done by performing power-bumping tests in the DR-2 reactor (Denmark) on 9 of the 14 rods irradiated in test fuel assembly IFA-148. This assembly was operated in the Halden reactor, Norway, from 1968 to 1979. The power ramps featured 24-hour hold periods at the peak power level, with the peak

power level varied among the tests. These tests were supplemented by nondestructive examinations before and after the bumping irradiations, rod puncturing/gas analysis on all tested rods, and detailed destructive examinations on selected rods.

Three of the bumped rods were selected as FAST FGR assessment cases: rods F7-3, F9-3, and F14-6 (Knudsen et al. 1983), which had rod-average burnups of 35, 33, and 27 GWd/MTU, respectively. The analyses of plenum gas ^{85}Kr activity before and after bumping were performed, and these were calibrated against the post-bump rod puncture results to yield an estimate of the net FGR caused by the power bumping. Thus, these cases provide the opportunity to assess the transient power induced short-term FGR predictions of the FAST FGR model.

The IFA-148 assembly contained a total of 14 short BWR-type test rodlets, with 7 rods each in two clusters (upper and lower clusters). The fuel pellets were 5% enriched sintered urania, with some variations in density and grain size. These two assessment cases, the nominal grain size and the fuel pellet densities, are equal (13 to 16 micron grain size and density of 93.4% TD, with a 0.6% increase upon resinter). The rods were initially filled with 1 atm helium fill gas.

A.2.5 Risø-3 Ramped Rods

The Risø National Laboratory in Denmark has carried out three irradiation programs of slow ramp and hold tests, so called “bump tests,” to investigate FGR and fuel microstructural changes. The third and final project, which took place between 1986 and 1990, bump-tested fuel re-instrumented with both pressure transducers and fuel centerline thermocouples.

The innovative technique used for refabrication involved freezing the fuel rod to hold the fuel fragments in position before cutting and drilling away the center part of the solid pellets to accommodate the new thermocouple.

The fuel used in the project was from IFA-161 irradiated in the Halden BWR to 52 GWd/MTU, GE BWR fuel irradiated in Quad Cities 1 and Millstone 1 from 23 to 45 GWd/MTU, and ANF PWR fuel irradiated in Biblis A (Germany) to 43 GWd/MTU. All these rods were subsequently ramped in the DR-3 reactor.

Four of the GE BWR rods (GE2, GE4, GE6, and GE7) (Chantoin et al. 1997) and two of the ANF rods (AN1 and AN8) (Chantoin et al. 1997) were selected to assess the FAST predictions of UO_2 FGR and cladding hoop strain.

A.2.6 B&W Rods Ramped at Studsvik

Three well-characterized 1.10 m long rodlets that had been irradiated to burnups slightly greater than 62 GWd/MTU in ANO-1 were ramp tested in the Studsvik R2 experimental reactor (Wesley et al. 1994). Peak power levels of 39.5, 42.0, and 44.0 kW/m and a 12 hour hold time were selected for these tests. No failures were experienced during testing and no incipient cracks were detected in the cladding during the post-ramp examinations. The FGR after the ramp was measured. Two of these rods (rods 1 and 3) were used in the assessment of the FAST UO_2 FGR predictions.

A.2.7 Regate Rod

This Regate experiment (Struzik 2004) deals with the study of FGR and fuel swelling during power transient at medium burnup. The rod was base-irradiated in the Gravelines-5 PWR and then re-irradiated in the test reactor SILOE in Grenoble, France. Since the rod was initially a segmented rod, the refabrication process prior to loading in the test is minor. In particular, the rod was not purged of its fission gases following refabrication.

The segmented rod consisted of UO_2 fuel with 4.5% enrichment. It was irradiated up to 47 GWd/MTU. In the SILOE reactor, the rod was given a conditioning power step of 195 W/cm for 48 hours and then was ramped at 10 W/cm/min and held at 385 W/cm for 90 minutes. This rod is particularly valuable for examining FGR for power ramps of short time duration because the other power ramped UO_2 rods used for FAST assessment were for hold times of 4 hours or greater.

This rod was used as part of the FAST UO_2 FGR assessment.

A.2.8 Beznau-1 M501 Rods

Two MOX rods were irradiated for three cycles in the Beznau-1 PWR up to a rod-average burnup between 34 and 37 GWd/MTM. The MOX fuel was fabricated using SBR that results in a relatively homogenous distribution of the PuO_2. One of these rods had a high plutonium enrichment (5.54 wt%) and one had a medium plutonium enrichment (3.72 wt%). After this, eight rodlets were refabricated from these two rods. Rodlets HR-1 to HR-4 (White et al. 2001; Cook et al. 2000; Cook et al. 2003; Cook et al. 2004) were refabricated from the high-enrichment rod, number 4463, and rodlets MR-1 to MR-4 (White et al. 2001; Cook et al. 2000; Cook et al. 2003; Cook et al. 2004) were refabricated from the medium enrichment rod, number 7612. These rodlets were ramp tested in the Petten high flux reactor. The ramp consisted of a 60 hour hold time at a preconditioning level followed by a ramp to a higher level with a hold of 12 hours for all the rodlets except MR-4, which was only held at the higher level for 20 minutes. It should be noted that the preconditioning and ramp power levels listed in the documents are the peak node powers. These values have been divided by the peak-to-average ratio to determine the rod-average power levels for these ramp tests.

These eight rodlets were used to assess the FAST MOX FGR predictions.

A.2.9 Studsvik Cladding Integrity Project Ramped Rods

The Studsvik Cladding Integrity Program (SCIP) has subjected 10 test rods to power ramp testing (Kallstrom 2005). Each test rod was subjected to a designated type of ramp test, which included staircase, short hold, long hold, and two-step power ramp tests. Each test rod was fabricated from a rodlet sectioned from a previously irradiated father rod.

Four ramp test rods were made by refabricating rodlets from BWR father rods that had been irradiated in Kernkraftwerk, Leibstadt. These test rods were labeled KKL-1, KKL-2, KKL-3, and KKL-4 and were irradiated to approximately 63, 67, 56, and 40 MWd/mtU average rodlet burnup, respectively. Before ramp testing, each rod was conditioned for a designated period of time and LHGR. The first ramp test, KKL-1, was aimed at defining the ramp terminal level where rod failure would occur. The rod was subjected to a staircase ramp, and after six steps of 5 kW/m with a 1 hour

hold time between steps, the rodlet failed after 40 minutes at an LHGR of 42 kW/m. To determine if the failure, which was caused by an outside-in crack, was dependent on burnup, a similar test was performed on KKL-3. A staircase ramp consisting of eight steps at 5 kW/m with a 1 hour hold time between steps was performed up to 52 kW/m. After holding for 12 hours at 52 kW/m, no failure was observed in KKL-3. Ramp tests of the other two rods, KKL-2 and KKL-4, were aimed at studying the geometric changes during a power transient and their dependence on burnup. The rods, KKL-2 and KKL-4, were held at 41 and 45 kW/m for 30 and 5 seconds, respectively. Neither KKL-2 or KKL-4 failed during ramp testing.

Two ramp test rods, M5-H1 and M5-H2, were fabricated from the same father rod, which had been irradiated in Ringhals 4 PWR and used to study the influence of holding time on geometric changes. The rods, M5-H1 and M5-H2, had been irradiated to a rodlet-average burnup of 67 and 68 MWd/kgU, respectively, and conditioned for a designated period of time and LHGR prior to ramp testing. During the short hold and long hold ramp tests, holding times of 5 seconds and 12 hours were used on M5-H1 and M5-H2, respectively, at an LHGR of 40 kW/m. Neither rod failed during the ramp test.

Ramp testing was performed on rod O2 (55 MWd/kgU burnup) to study geometric changes and PCI. Rod O2 had been previously irradiated in the BWR Oskarshamn 2 to an average rodlet burnup of 55 MWd/kgU. A short hold ramp test was performed by holding rod O2 at an LHGR of 45 kW/m for 30 seconds. Rod O2 did not fail during the ramp test.

Ramp test rods Z-2, Z-3, and Z-4 had each been irradiated to 76 MWd/kgU. Rods Z-3 and Z-4 were irradiated in the PWR North Anna while rod Z-2 was irradiated in the PWR Vandellos. Rod Z-3 was intended to study the hydrogen embrittlement by ramping the rod to an LHGR of 40 kW/m for a 5 second hold. However, failure occurred at an LHGR of 39 kW/M, which prevented the short hold ramp test from being completed. Rods Z-2 and Z-4 were intended to study delayed hydrogen cracking (DHC), and were subjected to two-step power ramp tests. Rod Z-2 was initially ramped to an LHGR of 35 kW/m and held for 6 hours before being ramped to an LHGR of 40 kW/m and held for an additional 6 hours. Rod Z-4 was initially ramped to 33 kW/m and held for 6 hours before being ramped to 38 kW/m and held for an additional 6 hours. The rods, Z-2 and Z-4, did not fail during the two-step power ramp.

These 10 rods were used to assess the FAST predictions of cladding hoop strain.

A.3 Transient Assessment Cases

A.3.1 Reactivity Insertion Accident Assessment Cases

A.3.1.1 CABRI Tests

The CABRI rodlets were taken from commercial rods that were base irradiated in various commercial PWRs. After base irradiation and refabrication, the rodlets were subjected to an RIA pulse in the CABRI reactor with 280 °C flowing sodium (Papin et al. 2003; Georgenthum 2009; Jeury et al. 2003; Jeury et al. 2004). The following describes the modeling approach and assumptions used to model these tests with FAST-1.2.2.

The as-fabricated dimensions for each rodlet were taken from the data sheet for the father rod.

When modeling the base irradiation of a rod that will later be cut into a segment to be tested, it is necessary to model the base irradiation on the short segment only.

The power history given for each father rod was used for the base irradiation. This power history was uniformly scaled by a constant factor to achieve the measured burnup for the rodlet. The axial power profile was assumed to be flat over the length of the rodlet based on a flat axial gamma scan.

The coolant pressure and mass flow rate were taken as typical values for the commercial reactor in which each rodlet was irradiated. The coolant inlet temperature for modeling the rodlet should be greater than the reactor inlet temperature due to heatup along the length below the rodlet. To model the base irradiation accurately, the inlet temperature was set such that the average predicted end of life oxide thickness was close to the measured value while still being a reasonable value for the span from which the rodlet was taken.

When the rodlets were refabricated, they were refilled with a different gas composition and pressure.

The provided RIA power history was used for the LHGR. The axial power profile from the final thermal balance was used as the axial power profile during the RIA test.

Measured cladding surface temperature histories were available for several axial locations during each of the CABRI tests. To model the coolant conditions, the rod was divided into several zones and the measured temperature histories for each of the axial elevations were set to the coolant temperature in each of these axial zones. To force the code to use the same coolant temperature and cladding surface temperature, a large cladding-to-coolant heat transfer coefficient (352222 Btu/ft^2−hr−°F) was set in the code as recommended in the FAST input instructions.

A.3.1.2 NSRR Cold Capsule Tests

The NSRR cold capsule tests were taken from commercial rods that were base irradiated in various commercial PWRs. After base irradiation and refabrication, the rodlets were subjected to an RIA pulse in the NSRR in a capsule with 20 °C stagnant water (Nakamura et al. 2000; Fuketa et al. 1997; Nakamura et al. 1994; Georgenthum 2009; Sugiyama 2009). The following describes the modeling approach and assumptions used to model these tests with FAST-1.2.2.

The as-fabricated dimensions for each rodlet were taken from the data sheet for the father rod. When modeling the base irradiation of a rod that will later be cut into a segment to be tested, it is necessary to model the base irradiation on the short segment only.

The power history given for each father rod was used for the base irradiation. This power history was uniformly scaled by a constant factor to achieve the measured burnup for the rodlet. The axial power profile was assumed to be flat over the length of the rodlet based on a flat axial gamma scan over the length of the rodlet.

The coolant pressure and mass flow rate were taken as typical values for the commercial reactor in which each rodlet was irradiated. The coolant inlet temperature for modeling the rodlet should be greater than the reactor inlet temperature due to heatup along the length below the rodlet. To model the base irradiation accurately, the inlet temperature was set such that the average predicted end

of life oxide thickness was close to the measured value while still being a reasonable value for the span from which the rodlet was taken.

When the rodlets were refabricated, they were refilled with a different gas composition and pressure.

The provided RIA power history was used for the LHGR. A flat power profile was assumed due to the short rodlet length in NSRR.

Cladding surface temperature histories were available from thermocouple measurements at several axial locations during most of these tests (GK-1, FK-1, HBO-1, HBO-5, HBO-6, MH-3, OI-2, and TS-5). To model the coolant conditions, the rod was divided into several zones and the measured cladding temperature histories for each of the axial elevations were set as the coolant temperature in each of these axial zones. To force the code to use the same coolant temperature and cladding surface temperature, a large cladding-to-coolant heat transfer coefficient (352222 Btu/ft^2−hr−°F) was set in the code as recommended in the FAST input instructions.

For test VA-1, no cladding surface temperature measurements were made. To model the coolant conditions, the recommendations from the FAST input instructions for stagnant water were used. The water temperature and pressure were set at constant values of 20 °C and 0.1 MPa, respectively. The cladding-to-coolant heat transfer coefficient was set at the recommended value of 5 Btu/ft^2−hr−°F for stagnant water.

A.3.1.3 NSRR Hot Capsule Test

The NSRR hot capsule test was taken from a commercial rod that was base irradiated in a commercial PWR. After base irradiation and refabrication, the rodlet were subjected to an RIA pulse in the NSRR in a capsule with 285 °C stagnant water (Georgenthum 2009; Sugiyama 2009).

The modeling approach and assumptions used to model this test in FAST was identical to the approach and assumptions used for the NSRR cold capsule tests, except that cladding surface temperature histories were not available. To model the coolant conditions, the recommendations from the FAST input instructions for stagnant water were used. The water temperature and pressure were set at constant values of 285 °C and 6.8 MPa, respectively. The cladding-to-coolant heat transfer coefficient was set at the recommended value of 5 Btu/ft^2−hr−°F for stagnant water.

A.3.1.4 BIGR Tests

Two full-length VVER-440 rods irradiated to 60 GWd/MTU and four full-length VVER-1000 rods irradiated to 48 GWd/MTU were sectioned and refabricated into rodlets, and then subjected to a rapid energy pulse in the BIGR reactor, similar to what is experienced during an RIA. These tests were carried out in a sealed capsule within the BIGR reactor. The rodlets were submerged in room temperature water but the capsule was not completely filled with water, allowing the water to boil. The purpose of these tests was to determine the RIA failure threshold at each burnup level (Yegorova et al. 2005a, 2005b).

To determine the failure threshold, the rodlets were all subjected to pulses that were about 3 ms wide at half peak. For the VVER-1000 rods irradiated to 48 GWd/MTU, eight rodlets were tested

with peak fuel enthalpies between 115 cal/g and 188 cal/g. Based on these tests, the failure threshold was determined to be between 155 cal/g and 164 cal/g. For the VVER-440 rods irradiated to 60 GWd/MTU, four rodlets were tested with peak fuel enthalpies between 125 cal/g and 165 cal/g. Based on these tests, the failure threshold was determined to be between 134 cal/g and 164 cal/g.

VVER rods use E-110 cladding. The only information provided about the base irradiation power history was the cycle lengths and the average LHGR at beginning and end of cycle for each rodlet. A power history for each rodlet was created by interpolating between the LHGRs provided. Since all of the rodlets used in these tests were taken at axial locations away from the end of the father rods, the axial power distribution over the length of the rodlet is assumed to be uniform. Axial gamma scans confirm this assumption.

For each rod, the reactor coolant conditions were provided, in particular the coolant pressure, inlet temperature, and mass flux. The coolant pressure and mass flux were input directly. However, since the rodlets were taken from axial locations above the core base plate, the given inlet temperature for full-length rods was lower than the temperature at the bottom of each rodlet. Measurements were provided for oxide thickness and hydrogen content taken from cladding areas close to each rodlet. Based on these measurements, the coolant inlet temperature used in the FAST calculations was selected such that the code predicted a hydrogen content level consistent with the measurement. The selected inlet temperature is less than the typical outlet temperature for a PWR and is therefore a reasonable assumption. Since the PCMI failure threshold used to predict cladding failure during a RIA in FAST is a function of hydrogen content, it is important that the correct cladding hydrogen content is also predicted.

When the rodlets were refabricated, they were refilled with a different gas composition and pressure.

For each test, a plot of the core average power was provided as well as the total energy deposited. To determine the LHGR to be input, the core average power was scaled by a factor such that the integral of the LHGR curve was equal to the total energy deposited. The axial power distribution during the RIA tests was assumed to be constant for all of these cases. This assumption is supported by measurements from neutron detectors along the length of the rodlet.

The initial coolant conditions in the test capsule were stagnant water at room temperature and atmospheric pressure. To model the coolant conditions, the recommendations from the FAST input instructions for stagnant water were used. The water temperature and pressure were set at constant values of 20 °C and 0.1 MPa, respectively. The cladding-to-coolant heat transfer coefficient was set at the recommended value of 5 Btu/ft^2−hr−°F for stagnant water.

A.3.2 Loss-of-Coolant Accident Assessment Cases

A.3.2.1 PBF LOC-11C Tests

LOCA testing was conducted in the Power Burst Facility (PBF) as part of the Thermal Fuels Behavior Program for the NRC. The PBF was designed primarily for performing very-high-power excursions and consists of a driver core in a water pool and a pressurized-water test loop capable of providing a range of test conditions. The central test space operates as a neutron flux trap that permits high power densities in tested fuel rods relative to the active core. An in-pile tube fits in

this central flux trap region and contains the test assemblies.

In the LOC-11 test series, four PWR-type, unirradiated fuel rods were subjected to cladding temperatures similar to those expected for the highest powered PWR rods during blowdown and heatup of a 200%, double-ended cold leg break. The test sequence was heatup, power calibration, preconditioning, decay heat buildup, blowdown and quench, and cool down. Three sequential tests were run: LOC-11A, -11B, and -11C. The LOC-11C test was intended to result in peak cladding temperatures of approximately 1030 K. There was no indication of fuel rod failure in any of the three tests (Buckland et al. 1978; Larson et al. 1979).

Instrumentation for each rod in the LOC-11C test included four thermocouples for cladding surface temperature, cladding centerline temperature, cladding axial elongation, and plenum temperature and pressure. The effect of fuel rod pressurization was demonstrated with the two 0.1 MPa (1 atm) rods (rods 1 and 4) having diameter decreases and the two pressurized rods (rod 3: 2.41 MPa (24 atm) and rod 2: 4.8 MPa (48 atm)) having ballooning at the axial mid-plane where cladding temperatures were highest.

For the PBF LOC-11 assessment cases, the FAST input coolant temperature history was based on the measured cladding temperature histories. The four test rods for LOC-11C were irradiated in flowing steam following the scram that initiated the transient. Initial cladding temperatures were approximately 620 K and increased to peaks of approximately 950 K to 1050 K.

Cladding outer surface temperatures were measured on all four test rods at elevations of 0.53 m and 0.61 m, and all four rods showed similar temperature behavior during the transient. The input cladding/coolant temperature history for FAST was developed as follows.

First, an initial cladding temperature of 620 K was assumed along the full-length of the rods based on a FAST calculation that showed minimal axial variation in cladding outer surface temperature before the transient. Next, cladding temperatures were assumed to remain constant for the first two seconds of the transient. The input coolant temperature history was then a lineal approximation of the measured cladding temperatures. The history at 0.5 m approximated the measurements at 0.53 m; the history at 0.3 m and 0.6 m approximated the measurements at 0.61 m; and the history at the top of the fuel column (1.0 m) was assumed to be approximately 75 K less than the measured history at 0.61 m.

A.3.2.2 TREAT FRF-2 Test

The FRF-2 test was the second seven-rod bundle irradiated in the Transient Reactor Test Facility (TREAT). Power was increased to 71.6 kW/m for 20 s during steam cooling. The irradiation was performed to evaluate code simulations of fuel rod heat capacity by comparing predicted and measured cladding temperatures during beginning-of-life adiabatic heatup (Lorenz and Parker 1972).

The TREAT reactor is a solid, graphite-moderated, air-cooled reactor capable of steady-state operation at 0.1 MW or transient operation of 1000 MW−s. Removal of heat from the reactor is the limiting factor for operation. The core has an active height of 48 in with a central, vertical test hole for materials testing. The LOCA test was performed in a water loop.

Instrumentation for the test included cladding surface thermocouples on two rods, rod gas pressure for two rods, and coolant conditions. The test rods were examined after irradiation and cladding strain measurements were obtained. Peak cladding temperatures were 2400 °F to 2450 °F. The rods failed by rupture from 30 s to 37 s when cladding temperatures were between 2200 °F to 2400 °F.

Three principal gas volumes are important to the measured gas pressures for rods 11 and 12 in this test: the fuel and gap pressure, the plenum pressure, and an external pressure cell. Primarily because of the external pressure cell, gas pressures did not increase as much as would have been expected had the rods been sealed systems. For the FAST calculation, it is important to note that 65 % of the gas volume stayed at relatively low temperatures during the transient. Accounting for these volumes and temperature differences in the FAST calculation is discussed further below.

For the TREAT FRF-2 assessment case, the FAST input coolant temperature history was based on the measured cladding temperature histories. The seven test rods for FRF-2 were irradiated in a flowing steam/helium mixture during the transient. To achieve the desired peak cladding temperature of approximately 2400 °F, rod-average power level up to approximately 11 kW/ft were induced during the transient. Cladding outer surface temperatures were measured on two rods (rods 12 and 13) at elevations of 11 in, 14 in, 15 in and 19 in below the top of the rods. The pre-transient cladding axial temperature profile was approximately constant at 335 °F.

The input cladding temperature history for FAST was developed as follows. Cladding temperatures did not begin to increase until approximately 7 s into the transient. At that point, cladding temperature increased at an average rate of approximately 80 °F/s until about 30 s to 35 s, when temperatures reached a maximum and then began to decrease. It is assumed that cladding temperatures linearly increased from 335 °F at 7 s to the measured peak cladding temperatures at 35 s, then decreased by 50 °F/s from 35 s to 50 s of the transient.

As discussed above, there were three principal gas volumes in the experimental setup which affected the interpretation of the gas pressure data. To model this with FAST, the coolant temperature was forced to a low value at the top of the rod to simulate the exterior gas volume that was kept at a low temperature.

A.3.2.3 IFA-650.5 Test

The IFA-650.5 rod was taken from a commercial PWR rod that was base irradiated for six cycles up to a burnup of 83.4 GWd/MTU for the segment. After base irradiation and refabrication, the rodlet was subjected to LOCA testing in the Halden reactor (Kekkonen 2007a). The following describes the modeling approach and assumptions used to model this test with FAST.

The dimensions for IFA-650.5 were taken from the data sheet for the father rod. The active fuel length of the rodlet was 480 mm. The total void volume for the test was 15 cm^3. From this value, a plenum length could be calculated; however, a portion of this void volume was outside the reactor core at a lower temperature. This external volume was not modeled in FAST because the temperature profile was not available; it was included in the rod plenum value. This led to an over-prediction of rod pressure because of the assumption that all the gas is at an elevated temperature, when in reality some of the gas was at a lower temperature.

Cycle-average power levels are given for the father rod. These power levels were adjusted to give the measured segment burnup when used as constant values for the length of each cycle. The axial power profile was assumed to be flat over the length of the rodlet.

The radial rod dimensions were the same as that of a 15x15 PWR rod. The axial length was that of the test segment. The rod internal pressure, coolant pressure, and coolant mass flow rate were all taken as standard 15x15 PWR values. The coolant inlet temperature was adjusted up from the standard 15x15 PWR value to simulate the segment being taken from the sixth span of the rod. The predicted oxide thickness (66 µm) and hydrogen content (360 ppm to 510 ppm) mean, 80 µm maximum) and hydrogen content (650 ppm), which indicates the base irradiation input was representative of the actual base irradiation. For the transient portion of the test, a constant power history of 2.4 kW/m was input, as well as the provided axial power profile of IFA-650.5.

The coolant conditions for the test were atypical of LWR LOCA conditions, and consisted of a fuel rod within a heated tube. Water was evacuated from this tube to start the test, spray was eventually applied, and the reactor was scrammed to end the test. Rather than attempt to model these conditions, FAST was set up to use measured cladding surface temperatures as the temperature boundary condition. Cladding surface temperature histories were available for two axial locations during this test. The rod was divided into two zones and the temperature histories for each of the two axial elevations were set as the coolant temperature in each of these axial zones. To force the code to use the same coolant temperature and cladding surface temperature, a large cladding-to-coolant heat transfer coefficient (352222 Btu/ft^2−hr−°F) was input.

A.3.2.4 IFA-650.6 Test

The IFA-650.6 rod was taken from a commercial VVER rod that was base irradiated in Loviisa NPP (in Finland) for four cycles up to a burnup of 55.5 GWd/MTU for the segment. After base irradiation and refabrication, the rodlet was subjected to LOCA testing in the Halden reactor (Kekkonen 2007b). The following describes the modeling approach and assumptions used to model this test with FAST.

The dimensions for IFA-650.6 were taken from the data sheet for the father rod. The active fuel length of the rodlet was 480 mm. The total void volume for the test was 16 cm^3 to 18 cm^3. From these values, a plenum length could be calculated. The power history for the IFA-650.6 father rod was used for the base irradiation and the axial power profile was assumed to be flat over the length of the rodlet, based on a flat axial gamma scan.

The radial rod dimensions were the same as that of a VVER-1000 rod. The axial length was that of the test segment. The rod internal pressure, coolant pressure, and coolant mass flow rate were all taken as standard VVER-1000 values. The coolant inlet temperature was adjusted up from the standard VVER-1000 value to simulate the segment being taken from the second span of the rod. The predicted oxide thickness (8 µm) and hydrogen content (48 ppm to 50 ppm) were close to the measured oxide thickness (5 µm) and hydrogen content (44 ppm), which indicates the base irradiation input was representative of the actual base irradiation. For the transient portion of the test, a constant power history of 1.3 kW/m was input, as well as the provided axial power profile of IFA-650.6.

The coolant conditions for the test were atypical of LWR LOCA conditions, and consisted of a

fuel rod within a heated tube. Water was evacuated from this tube to start the test, spray was eventually applied, and the reactor was scrammed to end the test. Rather than attempt to model these conditions, FAST was set up to use measured cladding surface temperatures as the temperature boundary condition. Cladding surface temperature histories were available for two axial locations during this test. The rod was divided into two zones and the temperature histories for each of the two axial elevations were set as the coolant temperature in each of these axial zones. To force the code to use the same coolant temperature and cladding surface temperature, a large cladding-to-coolant heat transfer coefficient (352222 Btu/ft^2−hr−°F) was input.

A.3.2.5 IFA-650.7 Test

The IFA-650.7 rod was taken from a commercial BWR rod that was base irradiated in Kernkraftwerk Leibstadt (KKL) for three cycles up to a burnup of 44.3 GWd/MTU for the segment. After base irradiation and refabrication, the rodlet was subjected to LOCA testing in the Halden reactor (Jošek 2008a). The following describes the modeling approach and assumptions used to model this test with FAST.

The dimensions for IFA-650.7 were taken from the data sheet for the father rod. The active fuel length of the rodlet was 480 mm. The total void volume for the test was 17 cm^3 to 18 cm^3. From this value, a plenum length could be calculated. The power history for the IFA-650.7 father rod was used for the base irradiation and the axial power profile was assumed to be flat over the length of the rodlet, based on a flat axial gamma scan.

The rod internal pressure, coolant pressure, and coolant mass flow rate were all taken as standard 10x10 Westinghouse BWR values. The predicted oxide thickness (17 µm) and hydrogen content (70 ppm) were close to the measured oxide thickness (4.4 µm) and hydrogen content (44 ppm), which indicates the base irradiation input was representative of the actual base irradiation. For the transient portion of the test, a constant power history of 3.4 kW/m was input, as well as the provided axial power profile of IFA-650.7.

The coolant conditions for the test were atypical of LWR LOCA conditions, and consisted of a fuel rod within a heated tube. Water was evacuated from this tube to start the test, spray was eventually applied, and the reactor was scrammed to end the test. Rather than attempt to model these conditions, FAST was set up to use measured cladding surface temperatures as the temperature boundary condition. Cladding surface temperature histories were available for two axial locations during this test. The rod was divided into two zones and the temperature histories for each of the two axial elevations were set as the coolant temperature in each of these axial zones. To force the code to use the same coolant temperature and cladding surface temperature, a large cladding-to-coolant heat transfer coefficient (352222 Btu/ft^2−hr−°F) was input.

This page intentionally blank.

Pacific Northwest National Laboratory

902 Battelle Boulevard
P.O. Box 999
Richland, WA 99352
1-888-375-PNNL (7665)

www.pnnl.gov